Systemic design of hybrid and electric powertrains

Adham Kaloun

N° d'ordre: **413**

CENTRALE LILLE

THESE

Présentée en vue
d'obtenir le grade de

DOCTEUR

En

Spécialité : Génie électrique

Par

Adham Kaloun

DOCTORAT DELIVRE PAR CENTRALE LILLE

Titre de la thèse:

Conception de chaînes de traction hybrides et électriques par optimisation sur cycles routiers

Systemic design of hybrid and electric powertrains

Soutenue le vendredi 4 décembre 2020 devant le jury d'examen :

Président du jury	Bruno SARENI	PU - Université de Toulouse
Rapporteure	Florence OSSART	PU - Sorbonne Université
Rapporteur	Emmanuel VINOT	CR HDR - Université Gustave Eiffel
Examinateur	Benoît DELINCHANT	PU - Université de Grenoble Alpes
Examinateur	Salvy BOURGUET	MCF - Université de Nantes
Directeur de thèse	Stéphane BRISSET	PU - Centrale Lille
Co-directeur de thèse	Maxime OGIER	MCF - Centrale Lille
Examinatrice	Mariam AHMED	Dr. Ing. - Valeo
Invité	Robin VINCENT	Ing. - Valeo

Thèse préparée dans le Laboratoire L2EP
Ecole Doctorale SPI 072 (Université de Lille, Artois, ULCO, UVHC, Centrale Lille)

"*Trust, but verify.*"

Russian Proverb

Preface

This work is a CIFRE industrial collaboration research project between the L2EP laboratory and automotive supplier Valeo. Thus, I would like to start by showing my appreciation to both Valeo and L2EP for their trust and for giving me the necessary tools to go well beyond the initial goals that were defined.

I would also like to extend my warmest thanks to Prof. Dr. Florence Ossart and Dr. Emmanuel Vinot for the quality of their reports and the relevance of their remarks, Prof. Dr. Bruno Sareni for his excellent organization, and Prof. Dr. Benoît Delinchant and Dr. Salvy Bourguet for agreeing to be part of the jury.

Numerous people have contributed to the success of this project in different ways and it is mandatory to give thanks where thanks are due. First of all, I would like to thank my supervisor, Prof. Dr. Stéphane Brisset, and my co-supervisor, Dr. Maxime Ogier, for their efficient oversight and for giving me full autonomy during the course of the project.

Furthermore, I am grateful for Dr. Mariam Ahmed for her exceptional guidance and contribution to this work, and both Robin Vincent and Maxime Reynouard for their supervision and valuable scientific input.

Finally, I am thankful for the amazing support and patience of my family, mentors, close friends and life partner over the course of this demanding and highly rewarding journey.

Contents

Introduction

A worldwide campaign for better energy efficiency has been gaining an ever-increasing momentum over the last decades, motivated by the need to tackle the negative impact of human activities on the entirety of the ecosystem. With transportation being one of the major sources of emissions, the way goods and people move will change drastically over the upcoming years by a combination of policy and technico-economical reasons, leaning towards more environmentally friendly vehicles.

Providing better fuel economy with lower emissions compared to conventional vehicles, hybrid electric vehicles (HEVs) are one of the most promising solutions. Optimal design of electrified powertrains is the key to unlock their full potential. The design task focuses on developing products of high quality satisfying various specifications and requirements at the lowest cost possible. Meanwhile, the optimization process will help the designer gain a competitive edge by selecting the solution leading to the lowest fuel consumption values. The main aim of this thesis is to develop fast and reliable design optimization methodologies.

Given the huge leap in computing power, modeling seems like the most convenient option to compare between different solutions and evaluate their fuel economy. However, hybrid vehicles are complex systems whose fuel saving potential depends on multiple factors such as their architecture and the sizing of their components.

Thus, designing HEVs is a transverse and multidisciplinary approach that poses several challenges: on one hand, a thorough understanding of the functioning of the components is required in order to integrate the main phenomena impacting its results. This calls for professionals from various fields with different skill-sets, tools and models. On the other hand, a global vision over the system for extended periods of time such as homologation cycles while considering the interactions between the components of the drive-train is needed as well to assess its performance. In fact, optimizing the powertrain components separately does not guarantee that once assembled, they will form an optimal system due to their strong interactions. However, system supervision throughout the conception phase is difficult when considering a company's structure, where multiple teams, each dedicated to the study of a specific component of the system or a particular physical behaviour, have limited exchanges.

In addition to this, the system's fuel consumption depends on its control: various possibilities can be selected to deliver the required torque to the wheels during the driving cycle, due to the presence of multiple mechanical energy sources and a reversible storage capacity. This increases the complexity of the system and adds thousands of decision variables to the global optimization problem. It then becomes impossible to find a solution in reasonable delays by just applying an all-at-once approach.

Hence, this thesis work centers primarily around reducing the complexity of the opti-

mization study, evaluating the system's performance and proposing efficient systemic design methodologies for the optimal sizing of hybrid powertrains. These approaches should also be adapted to an industrial setting. In order to present the work that was carried out to achieve these objectives, this manuscript is divided into four chapters.

Chapter 1 expands on the scope of the research project by detailing its background, objectives and challenges. Afterwards, the thesis work is confronted to other relevant projects. Strategies that were undertaken to overcome the barriers specific to the optimization of complex systems are dissected. Different possibilities are then investigated to reduce the required calculation time when searching for a system-optimal solution without compromising global accuracy: optimal control methods, cycle reduction techniques and decomposition-based strategies. Frameworks aimed at solving Plant/Controller optimization problems, to which the HEV case study belongs to, are explored as well.

Chapter 2 then starts by presenting the general formulation of this class of problems before implementing the most interesting leads found previously. These are then assessed over the hybrid railway power substation test-case first, as it provides a reference solution and is much easier and faster to evaluate compared to the HEV case study. This enables a thorough preliminary analysis of the implemented methods, allow for the improvement of the most efficient strategies as well as lead to the development of novel alternative design strategies.

The hybrid powertrain optimization problem is detailed afterwards in Chapter 3. The application scope and an overview of the system model are given before presenting the optimization variables considered in this project. After selecting a suitable level of system granularity, the component models are disclosed. The methods adopted to generate the required data quickly while maintaining a high level of model accuracy are presented as well. Next, the command and design constraints are listed before formulating the optimal design problem.

Finally, the most promising design approaches developed in the previous chapters are compared in Chapter 4. A compact vehicle equipped with a parallel hybrid powertrain is selected, even though the proposed design strategies can be applied for other hybrid architectures and systems. The comparison between the various approaches considers different criteria such as computation time and cost reduction. Once an optimal approach is identified, the robustness of the optimal solution as well as the impact of additionnal design constraints are discussed.

Chapter 1

Context and state of the art

Contents

Introduction

This chapter introduces the environmental, economic and scientific context of the research project along with its objectives. The main challenges of systemic design such as the importance of considering the other components, the different physical phenomena, the design cycle and the compromise on time/precision when modelling the system are also discussed.

The research work is positioned afterwards using the research lab as reference first, before comparing it to other relevant projects, nationally and internationally, related to the theme

of systemic design. Since the hybrid powertrain's fuel efficiency depends on its use, the main possibilities offered for the integration of driving cycles, either through power management or cycle reduction, are presented.

The fourth part is then specifically dedicated to the exploration of the coupling between design and controller optimizations, and how the previous techniques can be incorporated during system optimization. Finally, the last section investigates other decomposition methods, applied for a wider range of problems, that are aimed at reducing the complexity of systemic design problems and assesses their suitability for hybrid powertrain optimization.

1.1 Context of the research project

1.1.1 Air pollution consequences

Human activities are the major cause of air pollution. To support an ever-growing population, projected to reach 8 billion in 2024 [1], increased energy production, mobility and supporting industries are needed. This results in higher levels of harmful emissions in the atmosphere, especially in large urban areas [2].

Even though there is much to be learned about the health consequences of air pollution, experts have unanimously linked them to numerous neurological, cardiovascular and respiratory diseases, as well as cancer and birth defects [3, 4, 5]. Toxic air pollutants, and gas emissions in general, also damage Fauna, Flora and bodies of water. The last decade has been marked with growing concerns over the adverse environmental and ecological effects these emissions have, such as acid rain, haze, depletion of the ozone layer and global climate change (GCC) [3, 6, 7].

Different indicators can be observed to grasp the magnitude of climate change around the world [8], urging an immediate global response. The clearest of which is the continuous temperature rise on Earth's surface, as shown in Figure 1.1.

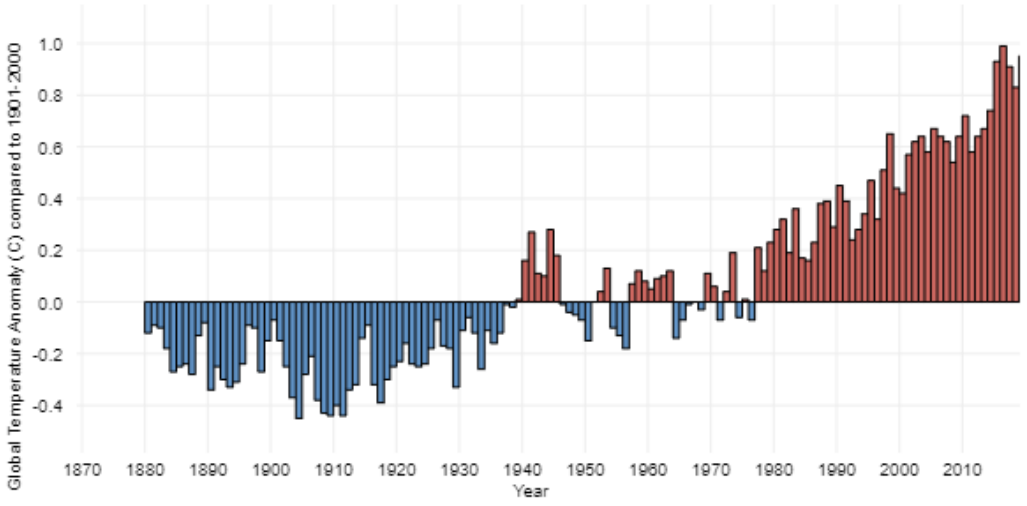

Figure 1.1: History of the global surface temperature since 1880 [9]

Thus, it can be understood that Earth's surface temperature has increased by 1.5 degrees over the 20^{th} century. This might seem as negligible, but these small temperature variations can lead to disastrous changes in the environment, since it preserved stable temperatures during the planet's recent history.

In fact, the consequences of climate change are already perceptible: mass extinctions of thousands of plant and animal species, longer drought periods, a huge increase in the number of tropical storms and forest fires, and the rise of sea levels, as depicted in Figure 1.2. The damage caused by climate change will only increase and become more severe, as the Intergovernmental Panel on Climate Change has alerted [2]. In order to avoid irreversible damage to the ecosystem and insurmountable threats to human survival, environmental agencies worldwide warn that the mean global temperature rise should be maintained well under 2 degrees over the next century [10].

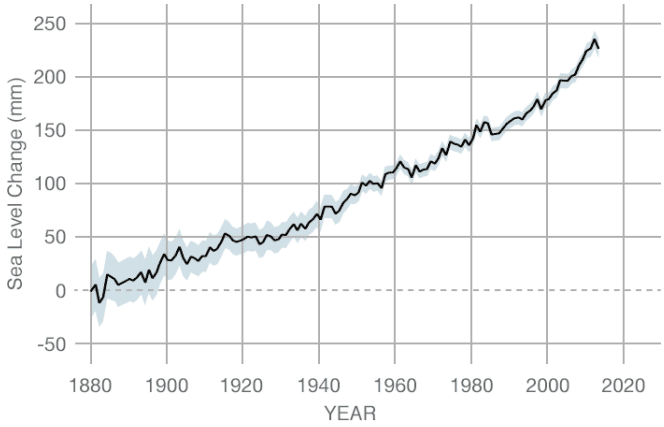

Figure 1.2: Evolution of the global mean sea level ([8], data retrieved from [11])

1.1.2 Greenhouse gas emissions

GCC is mainly driven by higher concentrations of greenhouse gases. These gases absorb and emit the sun's radiant energy, reflected by Earth's surface, within the infrared range. This is referred to as the greenhouse effect.

The 5 main greenhouse gases are: water vapor (H_2O), carbon dioxide (CO_2), methane (CH_4), nitrous oxyde (N_2O) and hydrofluorocarbons (HFC). Water vapor is the most abundant, fluctuating between 0.4% and 4% of the atmospheric volume, while all the other gases combined take up only 0.1% [12]. It has been proven that human activities only directly impact the concentration of the latter. However, when studying greenhouse gases, it is much wiser to discuss their global warming potential (GWP, [12]) rather than only focus on their volume proportions.

The GWP index compiles the lifetime of the gases in the atmosphere, the amount of energy absorbed and emitted per kilogram and their concentrations to determine how they contribute to GCC. The GWP of the main greenhouse gases has been estimated in the short term, designated as a period under 20 years, and the long term, spanning over a century, as shown in Figure 1.3 .

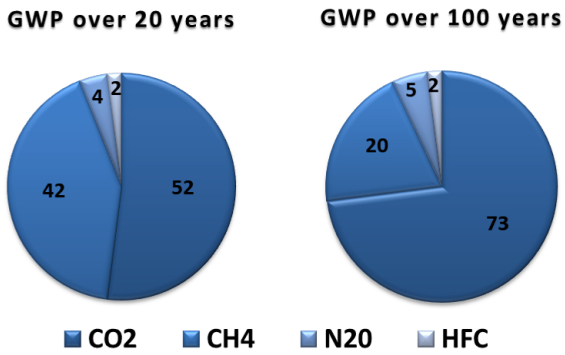

Figure 1.3: Global warming potential of greenhouse gases (Data retrieved from [9])

Despite its low radiative properties compared to other greenhouse gases, with 1 kg of CH_4 absorbing and emitting radiant energy as much as 28 kg of CO_2 for example, CO_2 contributes the most to climate change because of its much higher levels in the atmosphere. In 2018 for example, global CO_2 emissions have reached 37.4 Gt [12].

In order to achieve different temperature rise targets, Representative Concentration Pathways (RCP) are studied to set limits of emissions for different greenhouse gases [10, 12]. This introduces a "Carbon Budget", that shows the maximum amount of CO_2 emissions to keep temperature from rising above a certain target. Figure 1.4 presents the carbon budget to stay below the 2 degrees target, as part of the RCP2.6 pathway.

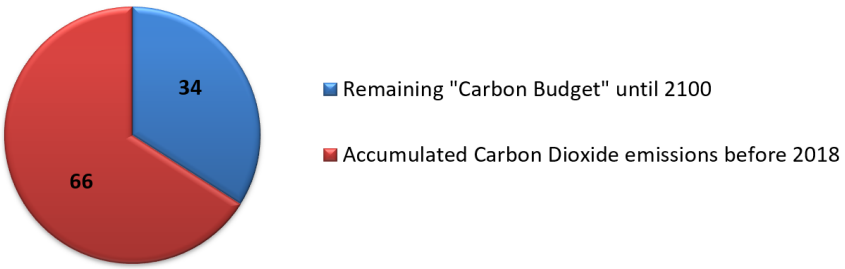

Figure 1.4: Carbon Budget for RCP2.6 [12]

This leads in turn to the study of how different sectors worldwide contribute to the release of carbon dioxide, in order to conceive a global plan of action. Emissions from different human activities are illustrated in Figure 1.5. The main emitters are energy production (mostly coal-fired power), transport (passenger vehicles and heavy-duty trucks) and industrial activities.

1.1.3 Decarbonization and policy

To follow the RCP2.6 pathway, aggressive decarbonization policies need to be taken and enforced to drastically reduce emissions from the main emitting sectors in the upcoming years. Governments worldwide should cut overall emissions in half by 2050 if they want to keep on track.

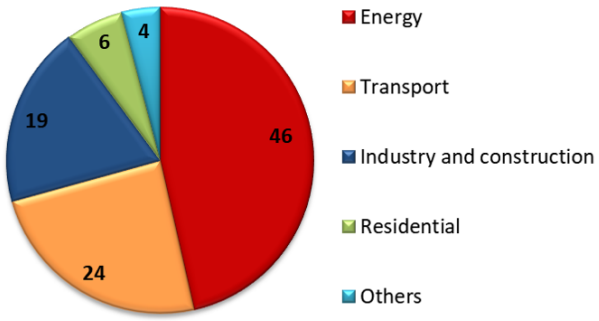

Figure 1.5: Worldwide CO_2 emissions by sector in 2016 [2]

As of now, global efforts have been made towards this goal: coal and oil fired power plants are being gradually substituted with cleaner energy. Processes to generate heat either in residential areas or industrial factories are being progressively electrified [13]. Furthermore, the way goods and people move will change drastically over the upcoming years by a combination of policy and technico-economical reasons.

In the EU for example, mandatory emission reduction targets for new cars are set [14, 15]. Original Equipment Manufacturers (OEMs) who are not aligning with these targets are fined important penalty payments. As of 2019, the penalty is 95 € per gCO_2/km target exceedance.

Between 2015 and 2019, the new european car fleet had to meet a target of 130 gCO_2/km. Data compiled of the average emissions in 2018, showed the average emissions of new passenger cars circulating to be of 120 gCO_2/km [16], indicating the effectiveness of the implemented policy. From 2020 onwards, the average CO_2 emissions of the EU's new car fleet needs to remain under 95 g/km. From 2025 on, a 15 % emissions reduction target from the 2021 starting points is set, before imposing a further 37.5 % reduction from 2030 on.

As of September 2018, the EU also put into force a new testing protocol: the WLTP, which stands for the Worldwide Harmonised Light Vehicle Test Procedure, to measure these emissions, replacing the New European Driving Cycle (NEDC) process. The main goal of the WLTP is to reduce the gap between test results and realistic vehicle usage, found with the NEDC procedure [17, 18]. This is observed directly on the driving cycles used to assess vehicle performance for each of these processes, presented in Figure 1.6 . The World Harmonized Light Vehicles Test cycles (WLTC), ranked according to the automobile's power-to-mass ratio, are characterized by longer distances and duration, higher maximum and average speeds, more dynamic phases and stronger accelerations/decelerations when compared to NEDC test cycles.

Another goal of the WLTP is to harmonize test procedures on a global level for better comparison between vehicle emissions using a common benchmark [19]. Besides lab testing, the WLTP adds another component for vehicle homologation, the Real Driving Emissions test (RDE), to measure emissions and pollutant particles under real on-road conditions [20]. Different incentives have been put into place as well to encourage the emergence and investment in innovative technologies [15]. These include eco-innovation and super credits,

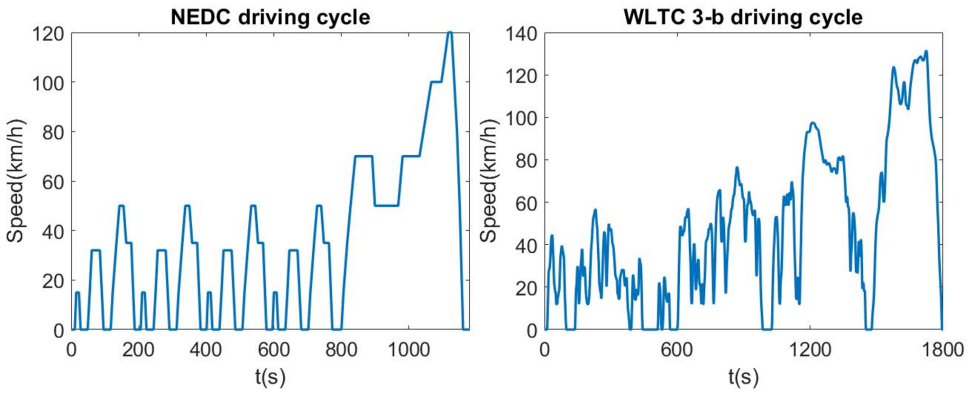

Figure 1.6: NEDC and WLTC 3-b driving cycles

and the possibility for car manufacturers to group together, referred to as manufacturer pools, working jointly to develop cheaper and more fuel efficient cars, eventually leading to less carbon emissions.

1.1.4 Automotive strategies

Improving the vehicle's characteristics such as the drag coefficient for enhanced aerodynamics, the rolling resistance of tyres in addition to more efficient aftertreatment systems have helped OEMs reach earlier emission targets. However, in order to meet stricter limits in the future, the automotive industry needed to shift towards more profound changes such as powertrain electrification.

Electrification of the powertrain refers to both electric vehicles (EVs) and hybrid electric vehicles (HEVs). EVs are equipped with one or multiple electric motors as the sole source of mechanical power in the powertrain and an electric energy storage, mainly electrochemical batteries or fuel cell systems. HEVs on the other hand combine several energy sources, one of which is thermal and the other one electric [21]. Thus, hybrid powertrains usually include an internal combustion engine (ICE) and an electric motor (EM), as shown for instance in Figure 1.7.

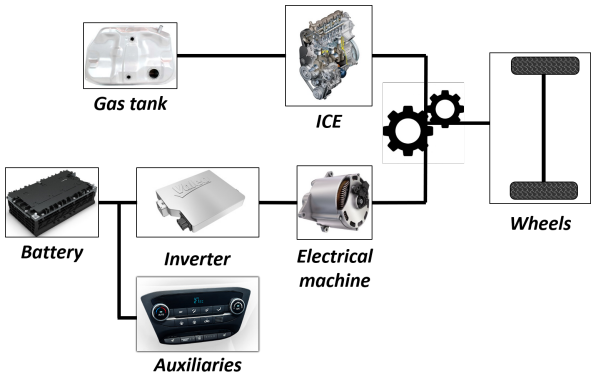

Figure 1.7: Example of a parallel hybrid powertrain

With an estimated global fleet of 1.5 billion cars and around 30 million new commercial

vehicle sales every year [22], the automotive market has been witnessing a steady rise of the share of EVs and HEVs [23, 24], as shown in Figure 1.8. In fact, most automakers are now focusing on electrification: all new Volvo cars are now equipped with an electric motor [25], Honda announced two thirds of their global sale will be from electrified vehicles in 2030 [26] while hybrid cars accounted for 52% of Toyota's 2019 sales, the world's largest car manufacturer [27]. Recent figures also show that HEVs in general are the most appealing choice for millenials, fueling the projections for a more important increase in greener vehicles [28]. All these reasons have led to renewed interest in the study of powertrain hybridization.

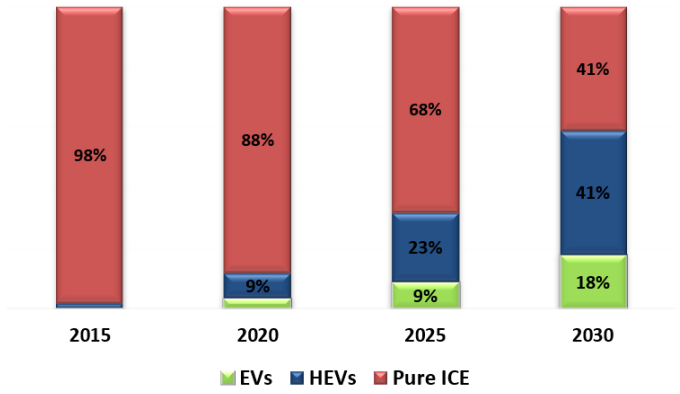

Figure 1.8: Global EV/HEV share and forecast (Data retrieved from [24])

1.1.5 Hybrid families

HEVs are categorized following their degree of hybridization, directly linked to their electrical power output [21, 29]. Micro-hybrids (μHEVS) are the closest to conventional vehicles, with an additional small electric motor that does not require extra battery capacity (12 V). The electric motor is mainly used for engine Stop-Start (STT), to help cut the engine's pumping losses at vehicle stops (direct CO_2 emissions reduction of 3∼5% due to fuel consumption) and increase the lifetime of starters. They can also be used as alternators, known as Starter-Generators.

On the other hand, with an increased battery capacity (48 V), embedded power electronics and a higher-rated electric motor (10∼30 kW), mild hybrids (MHEVs) allow for more flexibility. The electric motor assists the engine in Boost mode in order to use the latter more efficiently or provide all of the required mechanical power in ZEV (Zero Emissions Vehicle) mode, albeit for a limited range. The battery can be recharged afterwards either by retrieving part of the vehicle's kinetic energy (Regen mode) or by converting the ICE's mechanical output power with the electric machine (Generation mode). In this way, MHEVs enable lower fuel consumption, hence lower carbon emissions (direct CO_2 emissions reduction of 15∼20% due to fuel consumption). They also allow for engine downsizing to achieve even better fuel consumption gains. The different possible operation modes are presented in Figure 1.9.

Full Hybrids (FHEVs) and Plug-in hybrids (PHEVs) are equipped with a larger energy storage system and a more powerful EM. This allows to extend the range of use of ZEV and

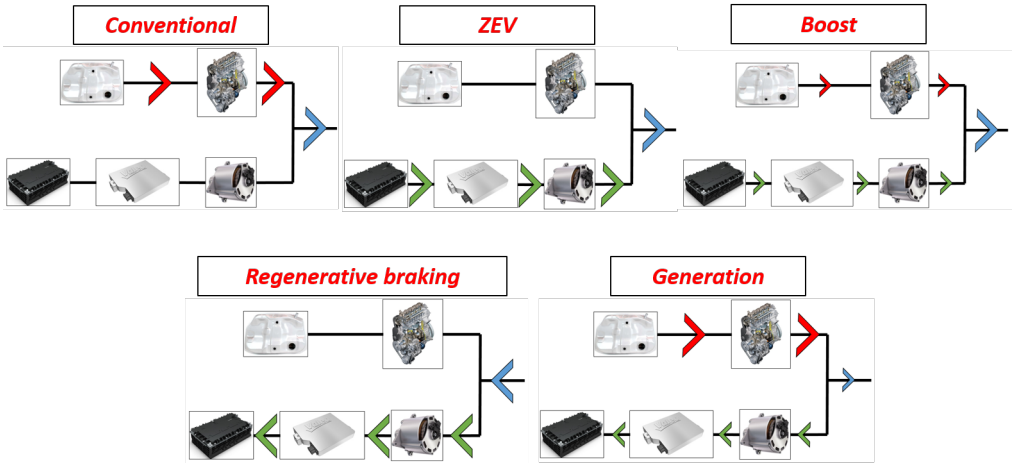

Figure 1.9: Different operation modes of a parallel hybrid powertrain (blue: power flow from the wheels, red: power flow from the thermal power source, green: power flow from the electrical power source)

Regen modes considerably (longer distances over 60 km and at higher speeds), leading to greater direct CO_2 emissions reduction (>30%). The difference between PHEVs and FHEVs is that PHEVs are fitted with bigger batteries that can be recharged directly from the grid, leading to higher levels of fuel economy. The main types of HEVs are summarized in Figure 1.10.

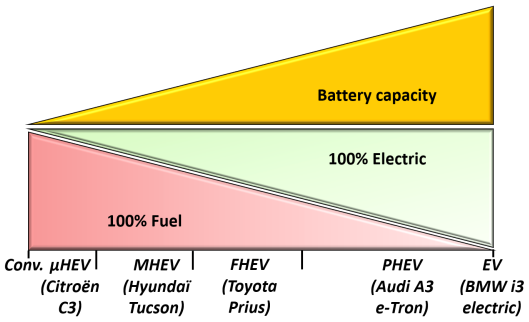

Figure 1.10: HEV classification and examples

Thus, OEMs have a large portfolio of vehicle hybridization solutions to choose from. However, to meet future emission targets, they need to further exploit the concept of hybridization. This can only be achieved by the complex task of improving the overall efficiency of the hybrid powertrain.

1.2 Importance of systemic design and work positioning

1.2.1 Scientific issues

The research work is focused on the optimal design of parallel hybrid powertrains, presented in Figure 1.7. The design task centers around developing a product meeting a specific set

of standards and requirements at the lowest cost possible. Improving the overall efficiency of the hybrid powertrain in terms of fuel consumption, and thus carbon emissions, will also be paramount in this project.

From an industrial point of view, in the early stages of conception, design teams were small with a single supervisor having a global vision of the project and being able to take the most important decisions. With the increasing complexity of designed systems, it was necessary to develop systems' studies, also known as systemics [30, 31, 32].

If systemics has experienced a significant leap forward since the 1990s, it is still difficult to implement into a company structure, where there are different teams using distinct tools and models, each dedicated to the study of a specific component of the system or a particular physical behaviour of the latter. This type of organization leads to limited exchanges during the design process, reducing the efficiency of the designed system.

In fact, optimizing each component separately while neglecting the different system interactions leads to suboptimal solutions. A simple case to illustrate this would be to consider two devices in series with a shared parameter, as shown in Figure 1.11 (the injected current for example in the case of two transformers connected in series).

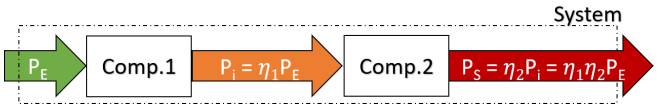

Figure 1.11: System of two components in series

The performance of each of these components is shown in Figure 1.12 as a function of this common variable. The system's efficiency, defined as the product of the yields of both components, is presented as well. It can be concluded that in order to achieve the best performance from a system's point of view, a different value for the variable x must be selected other than those needed for the optimal performance of either components individually.

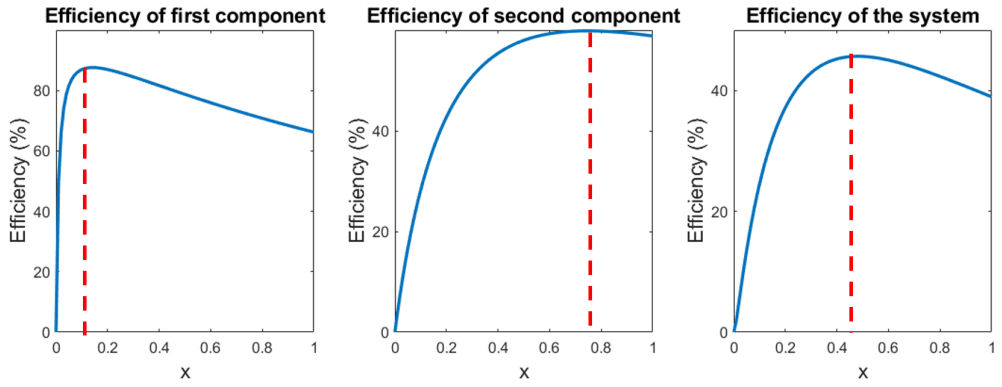

Figure 1.12: Efficiency curves as a function of the selected variable (optima defined by red lines)

This is all the more true for the studied system, given the number of components in a hybrid powertrain. Higher fuel economy and cost reduction are expected when considering more components during the optimization process, as depicted in Figure 1.13.

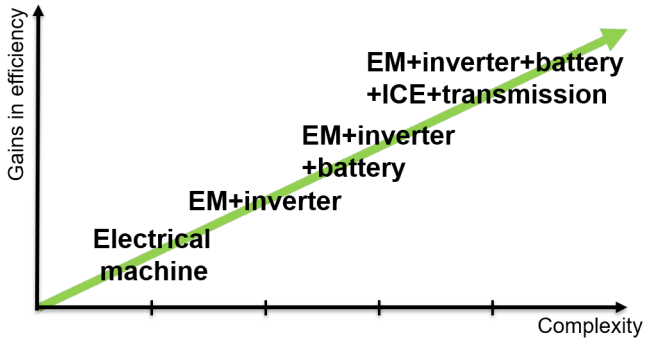

Figure 1.13: Evolution of expected gains as a function of the design process complexity

More importantly, a large number of optimization variables needs to be considered at once. In fact, the presence of two mechanical power sources, the engine and the electric machine, that exploit different resources and the use of reversible energy storage (the battery) raises the difficulty of determining how these components should operate in the most efficient way possible.

Thus, the power split, as shown in Figure 1.14, and other powertrain control parameters such as the selected gear, must be optimized for each time step in order to minimize fuel consumption throughout the drive-cycle. Integrating driving cycles, such as the Artemis Urban , which is displayed in Figure 1.15 and is discretized to 1000 time steps, means thousands of additionnal control variables need to be considered.

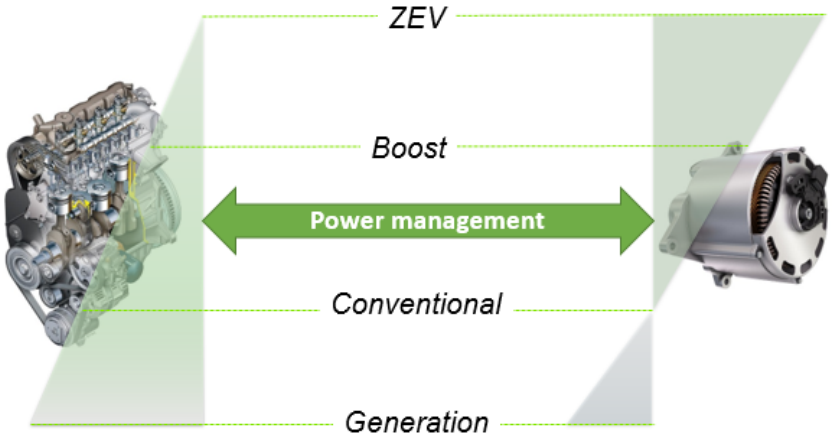

Figure 1.14: Power management problem in HEVs

On the other hand, solving the control/design optimization problems sequentially mostly leads to suboptimal results, as this has been confirmed mathematically [33] and using various numerical and experimental demonstrations [34, 35, 36, 37, 38]. Finding and imposing physical design variables before moving on to optimizing the control reduces design flexibility as well. In some cases, a design that meets system objectives and requirements may not

be found using this approach [39].

In this sense, both problems are coupled and integrated approaches, where the synergy between physical and control design decisions is exploited, should be applied. This allows for the selection of the powertrain with the best fuel saving potential instead of just comparing powertrains based on fuel economy values over a fixed, often suboptimal, control strategy.

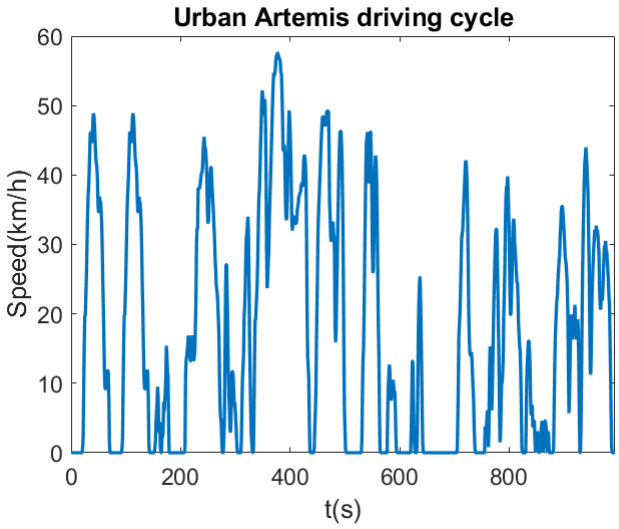

Figure 1.15: Artemis Urban driving cycle

Additionally, the presence of different discipline transients of varying orders of magnitude, listed in Figure 1.16, leads to the use of separate models and computer tools. This raises the challenge on how to couple them afterwards while keeping the design methodology straightforward.

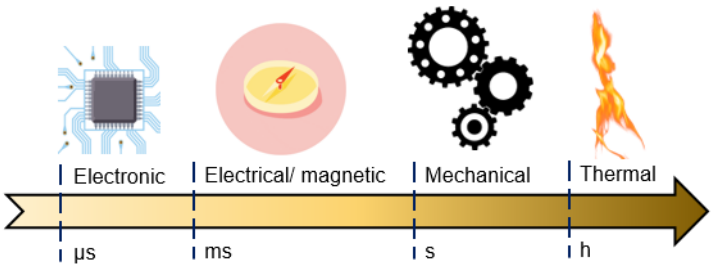

Figure 1.16: Transients of various physical phenomena

There is also a wide range of models to choose from, classified according to different criteria such as model orientation (inverse or direct), portability (communication with other models/tools) and more importantly the degree of finesse/granularity. While a more accurate representation is always preferred, finer models are more expensive in terms of computational resources and calculation time. Figure 1.17 presents some of the different possibilities explored to simulate the electromagnetic behaviour of the electric machine.

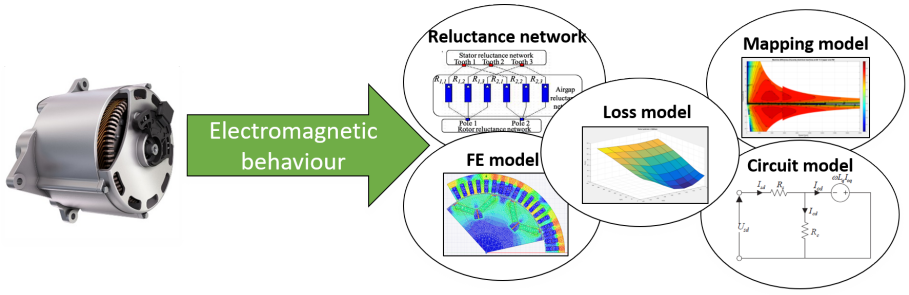

Figure 1.17: Possible models to simulate the electromagnetic behaviour of the EM

Furthermore, the performance of each component is estimated on mission profiles and/or road cycles of several minutes, thus requiring thousands of simulations of the hybrid drive model. Using a 2D finite element (FE) model for the electric machine and analytic models for the rest of the powertrain components means the system model requires nearly 1 min for each evaluation at a specific operation point/time step. If for instance, the cycle presented in Figure 1.15 is selected for hybrid powertrain optimization, a fuel consumption value can only be obtained after 16 hours of calculations.

Optimization algorithms are based on a large number of system evaluations to assess the behaviour of the utility function. This number increases exponentially with the number of variables considered, leading to the impossibility of finding an optimal solution in a reasonable time or even difficulties converging when thousands of variables are considered at once. This is referred to as the curse of dimensionality [40].

It is therefore necessary to develop new design methodologies to reduce the complexity of the optimization problem by decomposing the studied system, other than apply an all-at-once approach where control and design variables are considered simultaneously.

1.2.2 Lab positioning of the research project

Hybrid powertrain optimization falls within the scope of several research projects led by L2EP to improve the efficiency of energy conversion systems. In fact, systemic design projects were launched more than two decades ago at the research lab, mainly focusing on the optimization of electric machines as components in larger systems. Three axes were developed and are summarized in Figure 1.18 (adapted for the HEV application).

The multi-component axis seeks to establish high-performance methods to take into account the various interactions within the system, while respecting the constraints of the industrial environment. The work carried out by [41] and [42] on railway traction application aims to reduce system specifications to the component level (Target Cascading). [43] and [44] applied other methods to decompose an optimization problem into several coupled subproblems that are easier to solve (Collaborative Optimization and Benders Decomposition methods).

Other techniques have been proposed to couple the different physics (multi-disciplinary axis), based on the relaxation of the consistency between the different disciplines. [45] compares the main possible approaches in order to improve the autonomy of electric vehicles.

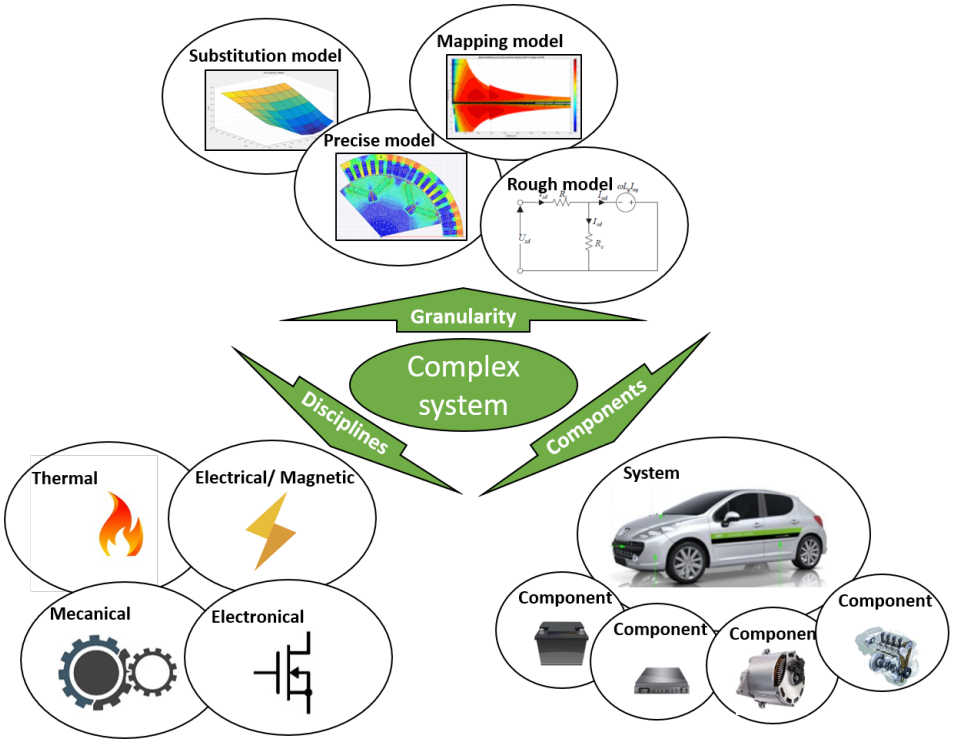

Figure 1.18: Decomposition axes for complex systems

Moreover, a significant part of the L2EP's work on systemic issues focuses on the multiple possibilities offered to improve the design models (multi-granularity axis): for example, the investigation of much faster substitution models, such as the Kriging models adopted by [46] for railway applications.

Another possibility is to reduce the operation cycle to a few representative points, in order to use finer models while achieving significant gains in calculation times. For [47], it has been possible to accelerate the optimization of electric machines for the production of green energy using the barycenter method.

Finally, there are also space mapping techniques that aim to use two models of the same component, such as a coarse model for optimization and a finer model for output correction for example. Several variants based on the same principle were used in the laboratory, notably by [48] and [49] for transformer optimization.

However, for the HEV sizing problem, more sophisticated approaches need to be implemented, as the optimization problem is much more complex. The added complexity is due to the necessity of optimizing the powertrain's command, which has not arised in the previous applications.

1.2.3 National positioning of the research project

Of course, considering the system interactions during the design process has been implemented in other projects by different research centers in France. Important volumes of work focused on implementing Plant/Controller optimization approaches to a wide variety

of problems. These methodologies allow the decomposition of the main problem into coupled sizing and control optimization problems.

[50] applied a simplified rule-based strategy to assess the fuel consumption of different hybrid vehicle designs, using the latter as the minimization criterion for the sizing problem. The use of suboptimal command strategies however does not guarantee a system optimum.

A different iterative approach was used by [51] to solve the eco-sizing problem of a fly-back converter destined for residential applications. [52] on the other hand, implemented the bi-level strategy, to design a micro-grid approach where the command optimization problem is nested within the sizing problem. This approach also enabled the optimization of a wave generator farm [53].

The bi-level approach has been widely used for hybrid vehicle optimization as well: [54] and [55] applied it to optimize the design of an electric machine inside an HEV, while [29] implemented it to select the best hybrid powertrain architecture for a specific cycle. [54] and [29] used dynamic programming while [55] relied on Pontryagin's Minimum Principle to find the optimal command at each time step of the design cycle.

Other possibilities for Plant/Controller optimization have not been investigated thoroughly however. These require a more in-depth study on how to still achieve system optimality while keeping the methodology fast and robust.

1.2.4 Global positioning of the research project

Numerous ongoing research projects worldwide are related to systemic design in electrical engineering. Laboratories around the globe have developed software for the sizing of renewable energy installations such as HOMER [56], RAPSim [57] and PVsyst [58]. The efficiency of the installation in each case is evaluated for different configurations using a power management strategy, not requiring an a priori knowledge of the selected design cycle.

Greater diversity has been found as well for the optimization of hybrid vehicles: [59] relied on the iterative scheme to develop an analytical target cascading approach; [60, 61] managed to apply the simultaneous approach by adjusting parameters of a simplified rule-based strategy and design parameters using genetic algorithms; [62, 63, 64, 65, 66, 67, 68, 69] implemented the bi-level scheme using dynamic programming to optimize power management and various algorithms for the sizing problem (Sequential Quadratic Programming, genetic algorithms, Particle Swarm Optimization and DIviding RECtangles).

As such, numerous possibilities can be explored to solve the studied problem, with the bi-level framework being the most popular strategy. A comparison between the different optimization strategies, conducted on a common benchmark, is also necessary to evaluate their advantages and disadvantages. This will help with the task of selecting which method fits best within the scope of the project.

Multidisciplinary design optimization as well as cycle reduction techniques can also be coupled with Plant/Controller optimization frameworks for example in a bid to reduce the problem's complexity even further.

1.3 Integration of design cycles

1.3.1 Power management

In a conventional vehicle for example, pressing the accelerator pedal corresponds directly to a fuel injection demand, supplied to the combustion engine, providing mechanical torque afterwards. Intuitively, the driver regulates the speed of the vehicle by pressing or releasing the accelerator pedal.

If the driver acts in a similar manner for a hybrid vehicle, management laws need to be developed to improve the powertrain's performance. In fact, for each operation point, which can be represented by a torque demand and a given vehicle speed, different "discrete" hybrid modes are possible (as presented in Figure 1.9). These modes are then translated into an infinite number of possibilities when using the vehicle, depending on the selected power split between the engine and the electric motor.

This choice is then oriented in order to achieve the best possible savings in fuel consumption, the major aim of hybridization, while considering the battery storage constraints. These are referred to as real-time power management strategies or online control strategies, implemented within the vehicle's hybrid control unit (HCU).

There is an abundant literature for the diverse strategies that have been developped on the matter. Rule-based strategies are the first ones to be studied and remain the easiest to deploy [21, 50, 70]. They generally rely on the levels of the battery charge and requested power/torque as inputs to switch between the different hybrid modes, as shown for instance in Figure 1.19. These strategies are still the most widely used methods in today's hybrid car fleet.

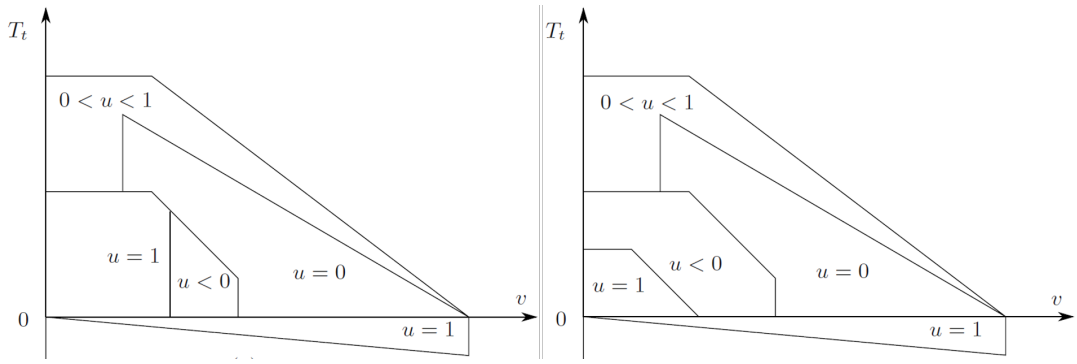

Figure 1.19: Rule-based strategy proposed by [21]: T_t is the requested torque, v the vehicle's speed and u the power-split ratio between the EM and ICE. The map on the right is for when the battery's state of charge is high, and the map on the left is for when it is low

Fuzzy logic controllers [71, 72, 73, 74] have also been suggested as well as the use of trained Neural Networks [75, 76]. These methods have shown they are only as efficient when the driving cycle remains close to the learning base used for their development.

Other techniques such as convex optimization [77] have managed to improve fuel efficiency through simplification of the powertrain model. The most efficient strategies however remain those derived from optimal control theory such as λ-Control [78, 79], Equivalent

Consumption Minimization Strategy (ECMS, [80]), Loss Minimization Strategy (LMS, [81]), Stochastic Dynamic Programming (SDP, [82]) and model predictive control [72, 83].

Thus, the above-mentioned strategies allow the ECU to find adequate commands quickly without the need to know for certain the future behaviour of the vehicle. On the other hand, it is clear that the absolute minimum of fuel consumption can only be achieved by knowing the speed cycle in advance. For instance, if the driver is aggressively decelerating in the near future, the potential electrical energy to be recovered through regenerative braking can be injected much earlier into the electric motor to reduce the load on the combustion engine, leading to better fuel efficiency.

These are referred to as optimal control strategies in the sense that the minimum fuel consumption provided, subject to the assumptions made, is the absolute minimum taking into account a maximum number of parameters, including some that are difficult to know in reality such as the evolution of the vehicle speed in this case.

In the context of this research project, the comparison between the different powertrains should be based on this value. This limits the impact of the control strategy's bias and prevent controller conditioning, leading to suboptimal solutions for the global optimization problem. For this reason, the focus is mainly shifted towards optimal control strategies in this work.

1.3.2 Optimal control strategies

The purpose of optimal control strategies is to determine the system control that minimizes the fuel consumption over the whole driving cycle, which is known in advance. The battery's state of charge (SoC) at the end of the driving cycle needs to be close to its initial value, as it is a requirement in hybrid vehicle homologation, referred to as the charge-sustaining condition. This defines the optimal control problem whose solution takes much longer to find as when compared to real-time strategies. For this reason, calculations generally need to be executed offline, which explains why optimal control methods are referred to as offline strategies.

Several authors relied on meta-heuristic methods to solve the optimal control problem: [84] used the simulated annealing method while [85] applied a particle swarm algorithm to coordinate the powertrain control strategy. [86] on the other hand turned to Marco Dorigo's method (ant colonies) to deduce the optimal command.

The main drawback of these strategies is the excessive number of model evaluations, which increases exponentially with the number of variables involved. Since the latter increases with the number of time steps considered, application of these strategies is only limited to short cycles.

Deterministic optimization algorithms have also been tested on numerous occasions. For instance, [54] used sequential quadratic programming (SQP) on short driving cycles. This limitation is due to non-convergence problems for longer driving cycles (over 200 time steps), especially in the absence of convexity or problem linearization options.

If the current homologation procedure is considered, the control needs to be optimized over the WLTC 3-b cycle (Figure 1.6). This cycle lasts 30 minutes and is discretized to the second, leading to thousands of control variables. Different techniques that are not limited

to a reduced number of variables should then be explored. [60] optimized parameters of a rule-based strategy for example with genetic algorithms, as shown in Figure 1.20, as a solution.

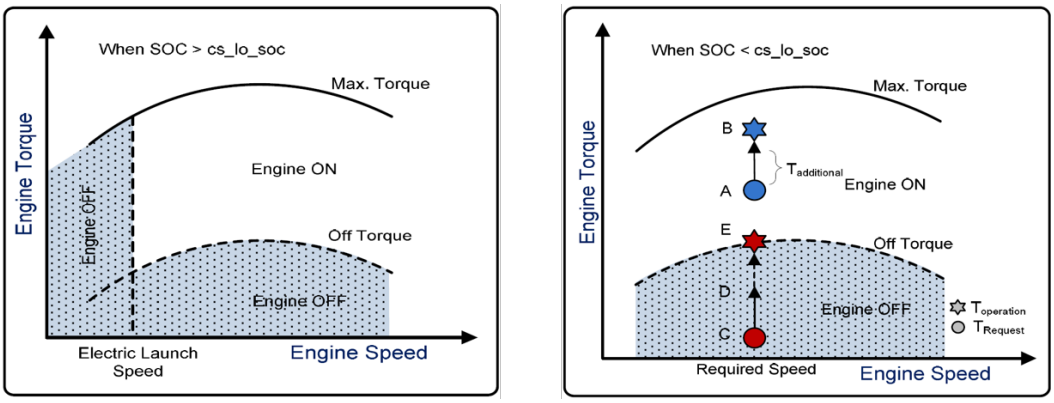

Figure 1.20: Rule-based strategy proposed by [60]

The most commonly used approaches for optimal power management however remain those deriving from the Calculus of Variations as in Pontryagin's Minimum Principle (PMP, [29, 55, 87, 88, 89]) and those based on solving the Hamilton-Jacobi-Bellman equation (HJB, [40]) like dynamic programming (DP, [90, 91, 92]).

PMP solves a dual problem with the same solution as the initial problem. The dual problem is simplified by introducing a Lagrange multiplier. Optimal command is found afterwards at each time step through a much simpler minimization problem.

Along with its simple implementation, PMP's main advantage is that the total calculation time is only linear with the number of steps. One of the main drawbacks of PMP however is the minimization process, often leading to local optima, as well as the difficulty of taking other constraints into account, such as the limitations of the powertrain components.

Meanwhile, DP's process can be easily explained through Bellman's principal, illustrated in Figure 1.21: if the optimal trajectory from point A to point B minimizing a certain cost function passes through a third point C, then the portion of the path from C to B is optimal as well considering the same cost function.

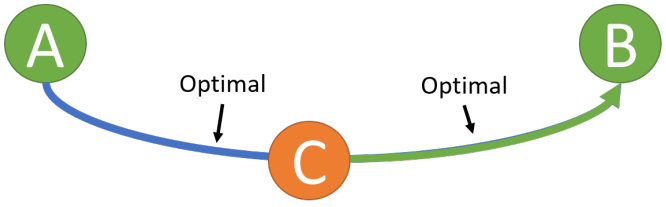

Figure 1.21: Example illustrating Bellman's principle

In simple terms, DP comes down to decomposing the original control optimization prob-

lem throughout the entire cycle into easier-to-solve subproblems, where the command is only optimized from a given state at a given time step until the end of the driving cycle, and storing the solution every time so that each subproblem is only solved once. However, building an end to end solution in reasonable times using this procedure is only feasible by discretizing the number of possible state values at each time step and passing through these later on.

When an adequate discretization is selected, a solution is always provided. Moreover, the required time only evolves, similarly to PMP, in a linear fashion with respect to the number of time steps considered. Nevertheless, improving the solution naturally requires a higher number of discrete values, as this leads to a greater number of paths to explore. This in turn results in exponentially higher calculation times, the main disadvantage of DP.

Both PMP and DP have been frequently compared in literature, achieving close performance in terms of fuel consumption and computation time [83, 87]. As such, they should be confronted later on with each other for the studied application. These strategies are explored in greater detail in Chapter 2.

1.3.3 Cycle reduction

Once a control strategy is selected, how the machine is used at each time step is imposed. Optimizing the design over the entire rolling cycle means taking into account hundreds (or even thousands) of operation points for each considered component (as shown in Figure 1.22). Hence, a direct sizing approach using cycle performance as criteria will not find an optimal solution in a reasonable time.

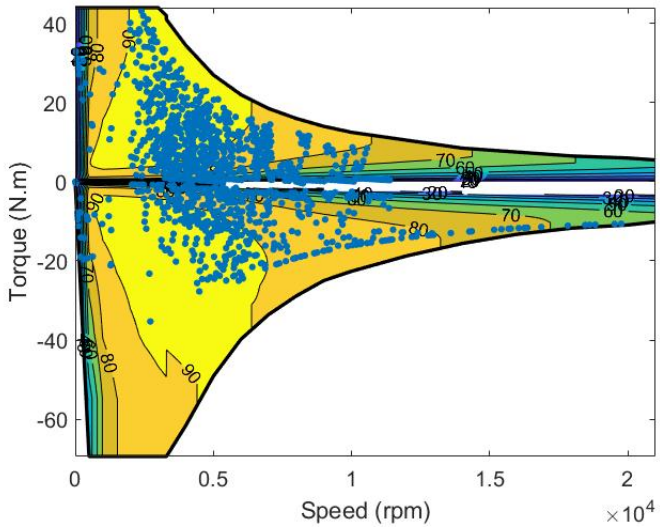

Figure 1.22: Example of EM's efficiency mapping and its operation points over WLTC 3-b

One of the possibilities would be to substitute the machine performance over the cycle to simply evaluating its performance over a reduced number of representative points. In order to achieve acceptable accuracy, various methods have been proposed in the literature and applied to numerous fields including the automotive industry such as the sizing of renewable

energy farms, data mining, railway applications, etc.

The single point method is the most widely used in the industry and is based on expert rules to determine a unique critical point to be optimized during the conception process.

On the other hand, [93] proposed the Random Sampling method where a reduced number of points is randomly selected from the initial pool of operation points using a statistical law. This method can be used to halve the initial number of points without a significant loss in precision [94]. However, its use for an even further reduction (less than a dozen points of interest) remains to be explored.

The histogram method has also been used. It is based on the statistical distribution of operational points into different intervals. The centre of each interval is then considered for the calculation of losses over the cycle, as illustrated in Figure 1.23 for the example of electric machine design. [47] used this method for the sizing of micro wind turbines. It is clear nevertheless that this method is only suited to other applications with correlated outputs (correlation between torque and speed in the case of the studied application).

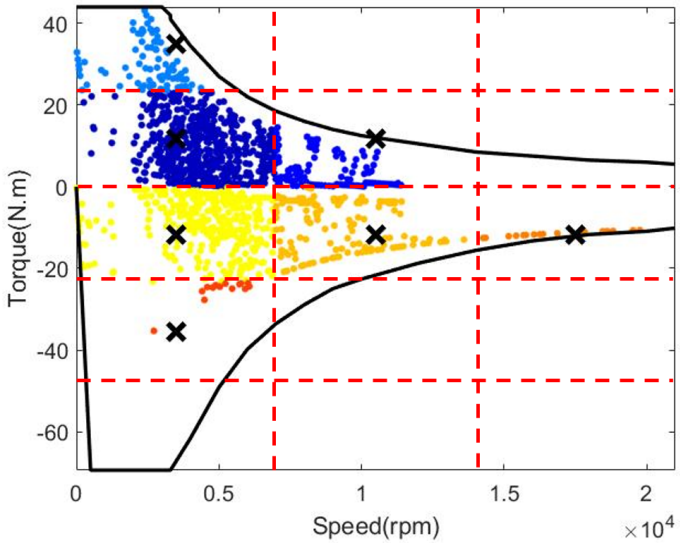

Figure 1.23: Application of the histogram method. The center of each interval is highlighted.

Meanwhile, [45, 95, 96] relied on the barycenters method to find the optimal design of an electric machine for electric vehicles. The method relies, in a similar manner as the histogram method, in dividing the torque-speed characteristic of the machine into several zones. The operation points within each area are then reduced to their barycenters, as presented in Figure 1.24.

Different alternatives have been suggested afterwards to estimate the machine's cycle losses, from the values calculated at the selected barycenters. In [45], the losses are weighted to the number of operation points in each interval while [95] proposed a different formula for each type of machine losses, based on the hypothesis of torque/current and speed/voltage correlations.

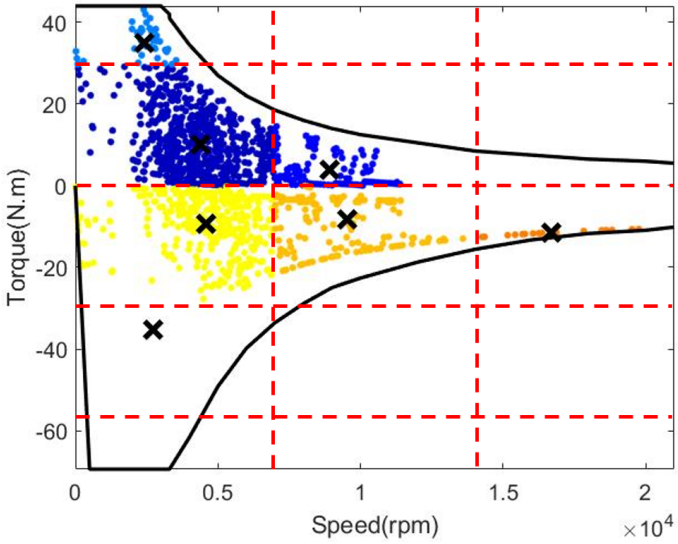

Figure 1.24: Application of the barycenters method. The barycenters are highlighted.

Another method worth exploring, mainly used in data science to reduce the size of information to be analyzed, is Clustering [97]. It refers to a statistical operation that divides a group of variables into a limited number of "clusters" or segments. In contrast with the barycenter or histogram method, these clusters are not defined in advance. This approach seeks to assemble objects sharing similar characteristics, with the intention of achieving internal homogeneity (similarity within the same cluster) and external heterogeneity (distinction between different clusters), as seen in Figure 1.25.

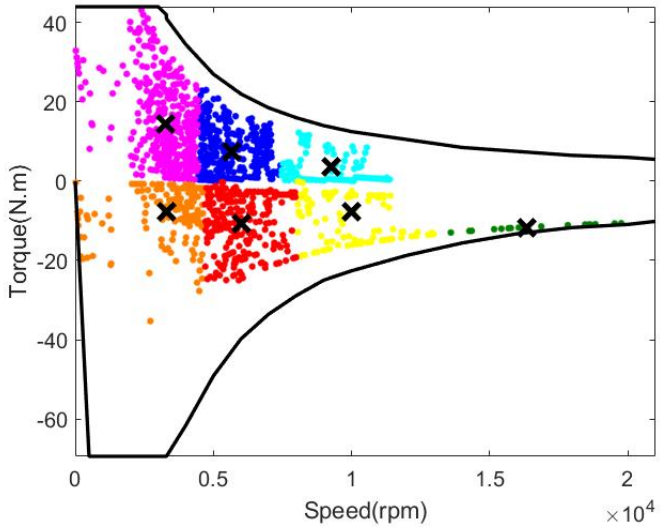

Figure 1.25: Application of the Clustering technique. The centroïds of each cluster are highlighted.

Several algorithms are called upon to achieve this division, such as the k-means or k-medoïd method. The centres of these clusters, called centroïds, represent the points of interest to be retained for the rest of the study. For electric machine sizing, the two variants presented to estimate the machine's performance through the barycenters method can be adapted for Clustering as well.

As such, these techniques differ in their implementation and their adaptability to the conception problem. Another important criteria to consider in hybrid powertrain design is the number of interest points required to achieve acceptable accuracy, which directly impacts the overall calculation time of the optimization process. Since literature on the comparison between these methods is scarce, an assessment over the common benchmark of the hybrid powertrain application is required.

1.4 Plant/Controller optimization

It is necessary to remember that when road cycles are taken into account during the sizing of the powertrain, the problem addressed has a double complexity: powertrain design optimization is based on fuel consumption, which is in turn strongly impacted by the powertrain control strategy, as explained in the previous section.

Thus, the hybrid powertrain optimization problem, as studied in this work, belongs to the Plant/Controller optimization class of problems. This type of optimization problems can be solved using different schemes: sequentially, iteratively, using a bi-level approach or simultaneously.

The sequential approach is where the design is optimized first for a certain control strategy, before optimizing the command afterwards, as depicted in Figure 1.26. It is the simplest to implement amongst the four studied approaches and the most intuitive, explaining its wide use in the industry. Still, it does not guarantee system optimality, as demonstrated by [33].

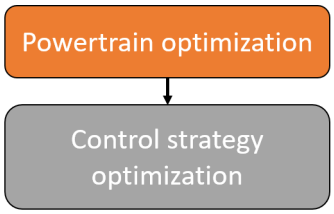

Figure 1.26: Sequential approach applied for hybrid powertrain optimization.

The iterative approach on the other hand improves the solution of the sequential method by reoptimizing the design following significant changes in the controller's command, before reiterating again until convergence. System optimality is afforded in this manner for certain cases [98]. Application on the studied problem is shown in Figure 1.27.

Meanwhile, the bi-level approach, also referred to as nested approach, finds the optimal control for each proposed design by the top level algorithm, as presented in Figure 1.28. The objective is to select the powertrain with the best possible fuel gains at the end of the optimization loop. In this way, the required optimality conditions can still be ensured [33].

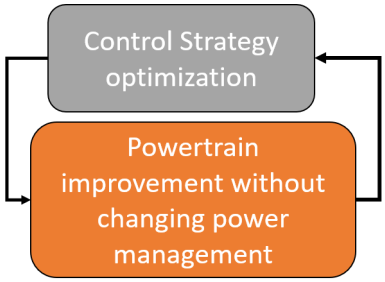

Figure 1.27: Iterative approach applied for hybrid powertrain optimization.

Thus, both the iterative and bi-level approaches allow for the partitioning of the original problem into design and control optimization problems. By doing so, optimal control strategies, presented in the previous section, can be used to efficiently solve the controller optimization problem and greatly reduce the complexity of the complete problem.

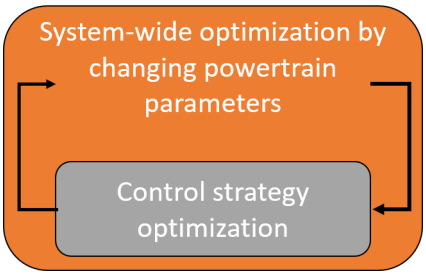

Figure 1.28: Bi-level approach applied for hybrid powertrain optimization.

However, if the nested approach is exploited extensively, implementations of the iterative scheme are quite rare. The latter should be analyzed further as different alternatives can be explored. One of the proposed options relies on the coupling with cycle reduction techniques, presented in section 1.3.3, as shown in figure 1.29. This can lead to faster iterations and the ability to use higher fidelity models.

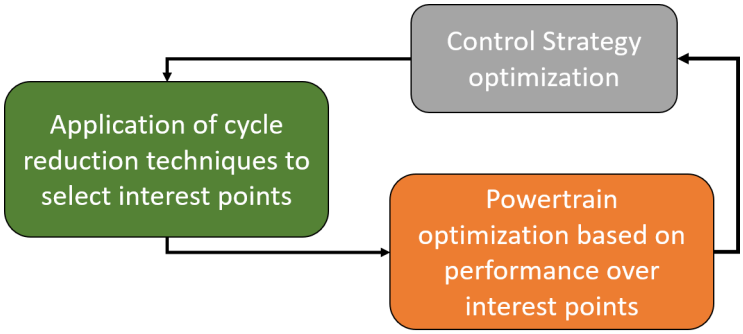

Figure 1.29: Iterative approach alternative applied for hybrid powertrain optimization.

Finally, the simultaneous approach solves the global optimization problem directly by finding the optimal control and design variables simultaneously. While this method always guarantees a system optimum as it considers all of the variables at once, it requires a much

higher number of resources to be allocated and has limited applications [45]. [54] finds non-convergence problems when using the simultaneous approach for a large number of decision variables. This forces him to only apply it on short missions.

The simultaneous scheme can also be applied in different ways. For example, [60, 61] have both considered the design and parameters of a rule-base strategy at once when optimizing hybrid powertrains. This allows to reduce the number of total variables and overcome the main disadvantage of the original approach. This alternative, shown in Figure 1.30, would lead to near-optimal results when coupled with highly efficient rule-based strategies.

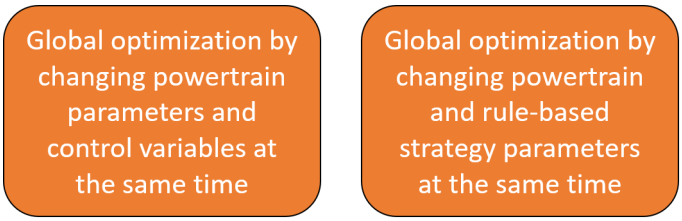

Figure 1.30: Left : Simultaneous approach for hybrid powertrain optimization - Right: Studied alternative based on the simultaneous approach

Choosing the most appropriate strategy depends on the type of application and requires additional analysis. A thorough comparison between these approaches and alternatives is required on the studied application. Detailed implementations of each one of these frameworks are presented in Chapter 2. A complete study, assessing their performance afterwards based on computation time, reliability, robustness and accuracy, will follow afterwards.

1.5 Multidisciplinary Design Optimization

1.5.1 Decomposition-based strategies

Systemic design of the hybrid powertrain can also rely on the methods developed in Multidisciplinary Design Optimization (MDO). As the name suggests, this field uses optimization methods to solve design problems incorporating several disciplines.

MDO aims at structurally reducing the complexity and calculation time of the optimization. Thus, the main subject of MDO is the description of the problem itself. Once the problem is reformulated using an MDO approach, it is solved using one or multiple solvers based on different optimization algorithms.

A distinction is made between monolithic strategies requiring a single optimization block, and distributed strategies with several optimizers exchanging variables and constraints between them. These are explored in sections 1.5.2 and 1.5.3 respectively.

1.5.2 Monolithic optimization

Four possible approaches can be cited for monolithic optimization: MultiDisciplinary Feasible (MDF), Individual Discipline Feasible (IDF), Simultaneous Analysis and Design (SAND) and All-At-Once (AAO).

The MDF approach is the most intuitive of these, linking the different disciplines until convergence at each model evaluation. The IDF strategy on the other hand aims to reduce computation time by integrating new variables and constraints into the optimization to ensure model consistency and eliminate internal loops.

Figure 1.31 illustrates the difference between both implementations, applied to solve the following problem based on a model with two coupled disciplines:

$$\min_{\boldsymbol{x}} \quad f(\boldsymbol{x}, \boldsymbol{y}) \tag{1.1a}$$

$$\text{subject to} \quad \boldsymbol{g}(\boldsymbol{x}, \boldsymbol{y}) \leq 0 \tag{1.1b}$$

$$\boldsymbol{h}(\boldsymbol{x}, \boldsymbol{y}) = 0 \tag{1.1c}$$

$$\boldsymbol{y_1} = \boldsymbol{y_1}(\boldsymbol{x}, \boldsymbol{y_2}) \tag{1.1d}$$

$$\boldsymbol{y_2} = \boldsymbol{y_2}(\boldsymbol{x}, \boldsymbol{y_1}) \tag{1.1e}$$

where $\boldsymbol{x}$ refers to the optimization variables while $\boldsymbol{y}$ represents the outputs of the coupled discipline models. f, $\boldsymbol{g}$ and $\boldsymbol{h}$ are the objective function, inequality and equality constraints respectively. When applying the IDF method, $\boldsymbol{y'}$ is added with additionnal constraints aimed at reducing the gap between these values and $\boldsymbol{y}$.

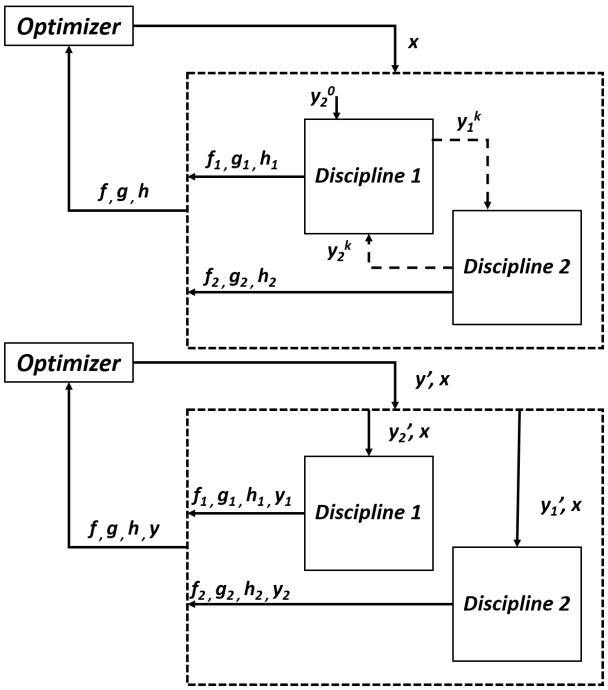

Figure 1.31: Top: MDF process, bottom: IDF process

[99] compares the different methods that are cited on a railway application and finally finds that the MDF strategy is the most robust (with a higher convergence rate) for a runtime close to the IDF strategy. [45] reaches similar conclusions and finds negligible differences as well in execution time between these two strategies. MDF is implemented and assessed on the hybrid powertrain application when considering the interaction between the different

energy domains involved in the adopted models.

On the other hand, the SAND approach seeks to bring back the consistency equations (physical equations describing the disciplinary model) as constraints managed by the chosen optimizer. Meanwhile, the AAO approach goes even further than SAND by breaking down any iterative procedure within the same behavioural model. All the implicit unknowns of the problem become optimization variables for the main optimizer. Both these approaches are therefore not possible when black box models are used, as it is often the case in this work.

1.5.3 Distributed optimization

Distributed or multi-level optimization techniques seek to break down an optimization problem into subproblems that are easier to solve with multiple solvers that can be launched in parallel. Several of these strategies have been developed over the last few decades. The ones most commonly found are Analytical Target Cascading (ATC), Collaborative Optimization (CO) and Bi-Level Integrated System Synthesis (BLISS).

ATC starts from the system specifications to deduce the subsystem requirements and the requirements of their components as well. The optimization is carried out separately afterwards. In addition to the shared variables $\boldsymbol{y^U}$, the system imposes target values $\boldsymbol{R^U}$ to be achieved by the subsystems (descending phase). These later return the feedback outputs $\boldsymbol{R^L}$ and new values $\boldsymbol{y^L}$ (ascending phase). This process is presented in Figure 1.32.

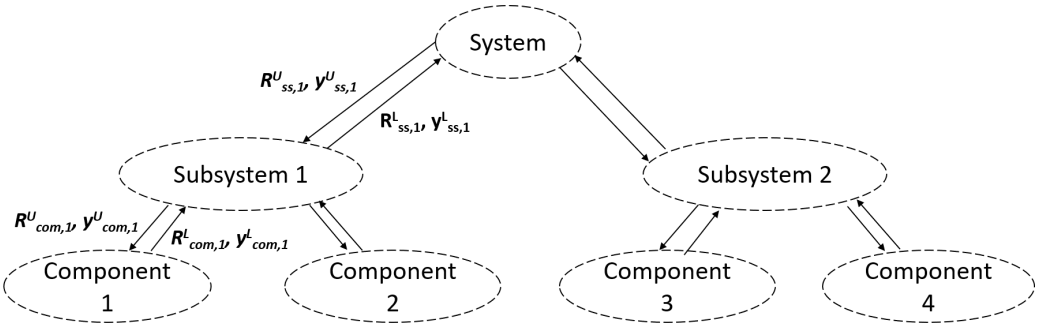

Figure 1.32: ATC process

The following optimization problem is launched first on the top level to deduce the targets for the subsystems:

$$\min_{\boldsymbol{x_{sys}}, \boldsymbol{y_{ss}}, \boldsymbol{R_{ss}}, \epsilon_R, \epsilon_y} \quad \|\boldsymbol{R_{sys}} - \boldsymbol{T_{sys}}\| + \epsilon_R + \epsilon_y \tag{1.2a}$$

$$\text{subject to} \quad \boldsymbol{R_{sys}} = \boldsymbol{f}(\boldsymbol{x_{sys}}, \boldsymbol{R_{ss}}) \tag{1.2b}$$

$$\sum_{j \in N_{ss}} \|\boldsymbol{R_{ss,j}} - \boldsymbol{R_{ss,j}}^{\mathbf{L}}\| \leq \epsilon_R \tag{1.2c}$$

$$\sum_{j \in N_{ss}} \|\boldsymbol{y_{ss,j}} - \boldsymbol{y_{ss,j}}^{\boldsymbol{L}}\| \leq \epsilon_y \tag{1.2d}$$

$$\boldsymbol{g_{sys}}(\boldsymbol{x}, \boldsymbol{y}) \leq 0 \tag{1.2e}$$

$$\boldsymbol{h_{sys}}(\boldsymbol{x}, \boldsymbol{y}) = 0 \tag{1.2f}$$

where $\boldsymbol{x_{sys}}$ refers to the local system design variables, while $\boldsymbol{T_{sys}}$ and $\boldsymbol{R_{sys}}$ represent correspondingly the system's target and response. $\boldsymbol{R_{ss}}$ and $\boldsymbol{y_{ss}}$ are the subsystems response and shared variables respectively whilst ϵ_{R} and ϵ_{y} are added tolerances to be minimized. $\boldsymbol{g_{sys}}$ and $\boldsymbol{h_{sys}}$ are the system's inequality and equality constraints whereas N_{ss} refers to the number of subsystems.

Subsystem level optimization problems afterwards seeks to minimize the gap between the target values and their responses. They also impose the new constraints on the variables shared at the higher levels. For instance, optimization problem for subsystem j is expressed as:

$$\min_{\boldsymbol{x_{ss,j}},\boldsymbol{y_{ss,j}},\boldsymbol{y_{com}},\boldsymbol{R_{com}},\epsilon_{\mathrm{R}},\epsilon_{\mathrm{y}}} \quad \|\boldsymbol{R_{ss,j}} - \boldsymbol{R_{ss,j}}^{\mathbf{U}}\| + \|\boldsymbol{y_{ss,j}} - \boldsymbol{y_{ss,j}}^{\mathbf{U}}\| + \epsilon_{\mathrm{R}} + \epsilon_{\mathrm{y}} \tag{1.3a}$$

$$\text{subject to} \quad \boldsymbol{R_{ss,j}} = \boldsymbol{f}(\boldsymbol{x_{ss,j}}, \boldsymbol{y_{ss,j}}, \boldsymbol{R_{com}}) \tag{1.3b}$$

$$\sum_{k \in N_{\mathrm{com,j}}} \|\boldsymbol{R_{com,k}} - \boldsymbol{R_{com,k}}^{\mathbf{L}}\| \leq \epsilon_{\mathrm{R}} \tag{1.3c}$$

$$\sum_{k \in N_{\mathrm{com,j}}} \|\boldsymbol{y_{com,k}} - \boldsymbol{y_{com,k}}^{\mathbf{L}}\| \leq \epsilon_{\mathrm{y}} \tag{1.3d}$$

$$\boldsymbol{g_{ss,j}}(\boldsymbol{x_{ss,j}}, \boldsymbol{y_{ss,j}}, \boldsymbol{R_{com}}) \leq 0 \tag{1.3e}$$

$$\boldsymbol{h_{ss,j}}(\boldsymbol{x_{ss,j}}, \boldsymbol{y_{ss,j}}, \boldsymbol{R_{com}}) = 0 \tag{1.3f}$$

where $\boldsymbol{x_{ss,j}}$ refers to the local subsystem design variables, while $\boldsymbol{R_{com}}$ and $\boldsymbol{y_{com}}$ are the components response and shared variables respectively. $\boldsymbol{g_{ss,j}}$ and $\boldsymbol{h_{ss,j}}$ are the subsystem's inequality and equality constraints whereas $N_{\mathrm{com,j}}$ refers to the number of components of the considered subsystem.

Finally, the optimization problems on the component level can be defined and solved. The optimization problem for component k for example is formulated as:

$$\min_{\boldsymbol{x_{com,k}},\boldsymbol{y_{com,k}}} \quad \|\boldsymbol{R_{com,k}} - \boldsymbol{R_{com,k}}^{\mathbf{U}}\| + \|\boldsymbol{y_{com,k}} - \boldsymbol{y_{com,k}}^{\mathbf{U}}\| \tag{1.4a}$$

$$\text{subject to} \quad \boldsymbol{R_{com,k}} = \boldsymbol{f}(\boldsymbol{x_{com,k}}, \boldsymbol{y_{com,k}}) \tag{1.4b}$$

$$\boldsymbol{g_{com,k}}(\boldsymbol{x_{com,k}}, \boldsymbol{y_{com,k}}) \leq 0 \tag{1.4c}$$

$$\boldsymbol{h_{com,k}}(\boldsymbol{x_{com,k}}, \boldsymbol{y_{com,k}}) = 0 \tag{1.4d}$$

where $\boldsymbol{x_{com,k}}$ refers to the component design variables while $\boldsymbol{g_{com,k}}$ and $\boldsymbol{h_{com,k}}$ are the selected component's equality and inequality constraints.

In this way, an iteration of the ATC is completed and this process is repeated as long as unacceptable deviations are found (iterative framework). This decomposition therefore seeks to take advantage of the hierarchical structure of companies, where each team have their own tools and methods to solve their corresponding subproblem, justifying the industrial interest in such approaches.

This method should then be used when there is a need to optimize multiple physical components with strong interactions [100]. Since the design endeavour in this work focuses primarily on the electric machine component, this approach will not be explored any further.

CO on the other hand proposes a principle that can be used for a wider range of optimization problems, based on the decomposition of the optimization problem into several subproblems with a reduced number of variables making them easier to solve. This structure promotes disciplinary autonomy while maintaining interdisciplinary compatibility (nested framework).

The aim is to optimize the objective function of the main problem by acting on the global design variables and the coupling variables between each discipline. At the level of each discipline, a different optimization problem is solved, by varying the local design variables while interdisciplinary constraints ensure overall consistency between the different subproblems.

The basic implementation of CO is shown in Figure 1.33, with F being the global cost function, $\boldsymbol{G}$ the consistency constraints, $\boldsymbol{z}$ the optimization variables of the initial problem, that is split into multiple subproblems. $\boldsymbol{z^*}$ are the imposed values at the subproblem level of the variables $\boldsymbol{z}$, (whose deviation from $\boldsymbol{z}$ must remain small) and $\boldsymbol{y}$ the shared variables between the different subproblems. $\boldsymbol{g_i}$ and $\boldsymbol{h_i}$ respectively define the constraints of inequality and equality specific to each subproblem.

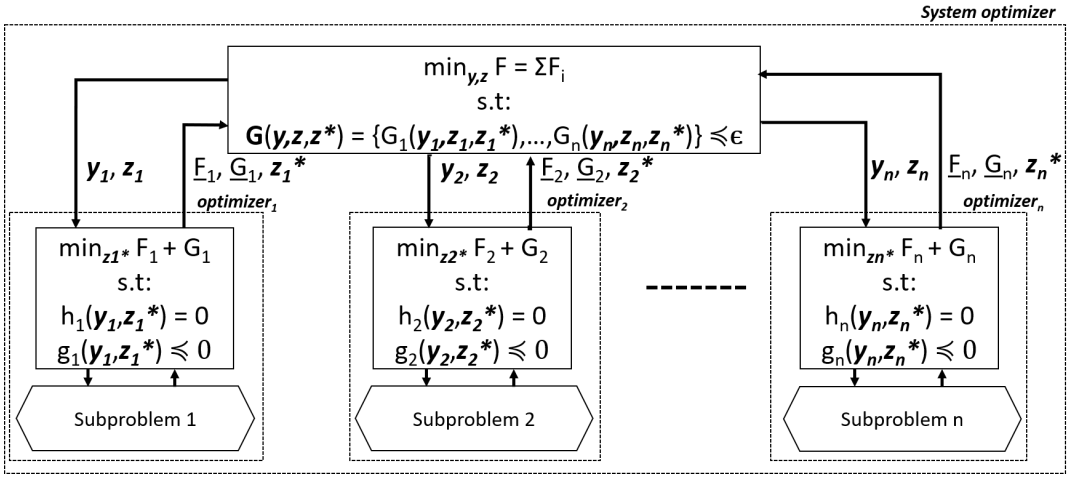

Figure 1.33: CO process

In this way, CO can be implemented for example afterwards to decompose the driving cycle into smaller portions, with a reduced number of variables. This allows for the application of meta-heuristic and deterministic optimization whose use is only limited on short missions, as explained previously.

One of the major drawbacks of CO however is the need to add the consistency constraints, which allow the coordination between the different subproblems. These can lead to slow convergence or even non-convergence issues. Some authors have thought of easing these constraints to facilitate convergence [101, 102], while others have adapted the CO approach to propose new strategies such as BLISS [103].

The BLISS method adopts the same bi-level structure as CO, and tries to better estimate the local variables for each subproblem based on a multidisciplinary analysis conducted by the optimizer at the system level. More advanced versions were later proposed, such as the BLISS2000 strategy, mainly used in aerospace engineering, which relies on substitution

models to speed up calculations.

Finally, it needs to be noted that while several dynamic systems have been designed using MDO approaches, the established MDO formulations, including those that are presented here, are largely based on static system analysis, and do not address the temporality of some variables explicitly.

If they can be adapted for different systemic design problems with a large number of variables, Plant/Controller optimization frameworks, that have been specifically developed to solve design problems where system performance is directly linked to the way it is used, need to be prioritized in this work.

It is also worth mentioning that Plant/Controller design approaches can be included in the definition of MDO as well, as they integrate the link between the design and control disciplines. This has prompted various authors to attribute them to a new branch of MDO referred to as Multidisciplinary Dynamic System Design Optimization (MDSDO) [39].

Conclusion

Electrification of the powertrain is part of a worldwide campaign for more energy efficiency that has been gaining an ever-increasing momentum over the last decades, driven by the need to reduce the negative impact of human activities on its ecosystem. However, meeting more stringent emission limits means car manufacturers need to optimize their powertrains for better fuel economy.

The design of hybrid powertrains is a complex task which calls for experts from various fields. On one hand, the presence of two different mechanical energy sources, the engine and the electric machine, raises the difficulty of choosing the best power split between both, amongst other control parameters. This is then translated to thousands of additionnal control decisions to be considered.

If meta-heuristic and deterministic optimization can only be applied on short missions, DP and PMP, based on optimal control theory, are developped specifically for control optimization over long drive-cycles. These strategies are analyzed, improved and confronted further in Chapter 2. CO is explored as well, to overcome the limitations of optimization algorithms by decomposing long driving cycles into more manageable portions.

On the other hand, the fuel saving potential of hybrid powertrains greatly depends on both their use and the sizing of their components interdependently. As such, a sequential approach can not guarantee a system optimum and only integrated frameworks need to be considered.

Plant/Controller optimization frameworks are explored in this case. The direct simultaneous approach is limited by the large number of variables present, which explains the need to find other alternatives of this scheme. One proposition requiring deeper analysis is to reduce the number of control variables by imposing a rule-based strategy whose parameters are optimized.

Meanwhile, the bi-level and iterative approaches reduce the complexity of the optimization problem using interdisciplinary partitioning while attempting to guarantee system op-

timality. If the bi-level approach was used extensively in literature, insufficient research surrounds the application of the iterative scheme, requiring further studies. This scheme can be improved as well by adopting cycle reduction techniques to enable faster iterations. These methods are presented afterwards in greater detail once the global optimization problem is properly formulated.

Furthermore, since meeting project deadlines leaves only a small window for system optimization, different monolithic and multilevel decomposition methods have been investigated as well to reduce the calculation time without compromising global accuracy. The MDF strategy for instance is applied afterwards to couple between the different disciplines impacting the performance of the hybrid powertrain.

Chapter 2

Systemic design approaches on drive-cycle

Contents

Introduction

This chapter presents both the discrete and continuous formulations of the optimal energy problem, as well as the formulation of the Plant/Controller optimization problems, to which the systemic design of the hybrid powertrain problem belongs. The different optimization variables and constraints are considered and the criteria for the optimal solution is introduced.

In order to compare the strategies introduced in Chapter 1, a simpler and fast benchmark which provided a reference solution is required before applying the most promising methods on the HEV case study. Thus, the hybrid railway power substation problem (HRPS) is presented afterwards, using the same formalism established for control and design optimization problems.

The direct use of optimization algorithms to solve the optimal control problem, as well as the implementation of Collaborative Optimization to reduce the calculation burden are investigated. Optimal control laws, including Dynamic Programming and Pontryagin's Minimum Principle, are also detailed in the third section of the chapter. The latter are developped specifically to handle the large number of command variables when solving the optimal control problem. These control methods are then applied and assessed for the HRPS power management before being implemented for system optimization using Plant/Controller decomposition frameworks.

In this regard, three design optimization approaches are explored and tested later on: the simultaneous, bi-level and iterative frameworks. These methods are compared on the HRPS problem in terms of precision and calculation time. The optimal solution's proximity to the reference solution is evaluated as well as its distance from the initial point to allow for deeper analysis of their convergence.

The last section of this chapter presents other possible approaches for systemic design optimization. These strategies are also based on the studied Plant/Controller frameworks and can be used as alternatives to improve their performance when applied for more complex systems using heavy models, such as the hybrid powertrain.

2.1 Optimal control and design problems formulation

The objective of the hybrid powertrain power management problem is to minimize the fuel consumption of a vehicle over a specific driving cycle by optimizing its command variables. Since the hybrid powertrain is a dynamic system, state variables are introduced as well. This defines an optimal control problem, which is expressed as:

$$\begin{aligned}
\underset{\boldsymbol{u}}{\text{minimize}} \quad & \int_{t_0}^{t_\mathrm{f}} L(\boldsymbol{x}(t), \boldsymbol{u}(t), t)dt && \text{(2.1a)}\\
\text{subject to} \quad & \boldsymbol{x}'(t) = \boldsymbol{f}(\boldsymbol{d}, \boldsymbol{x}(t), \boldsymbol{u}(t), t) && \text{(2.1b)}\\
& \boldsymbol{x}(t_0) = \boldsymbol{x_0} && \text{(2.1c)}\\
& \boldsymbol{x}(t_\mathrm{f}) = \boldsymbol{x_\mathbf{f}} && \text{(2.1d)}\\
& \boldsymbol{g}(\boldsymbol{x}(t), \boldsymbol{u}(t), t) \leq 0 && \text{(2.1e)}\\
& \boldsymbol{h}(\boldsymbol{x}(t), \boldsymbol{u}(t), t) = 0 && \text{(2.1f)}\\
& \boldsymbol{x}(t) \in [\boldsymbol{x_{\min}}(t), \boldsymbol{x_{\max}}(t)] && \text{(2.1g)}\\
& \boldsymbol{u}(t) \in [\boldsymbol{u_{\min}}(t), \boldsymbol{u_{\max}}(t)] && \text{(2.1h)}
\end{aligned}$$

where $\boldsymbol{u}$ and $\boldsymbol{x}$ refer to the command and state variables respectively. The controller's cost is calculated as an integral of the cost functional L between the initial time step t_0 and the final time step t_f.

$\boldsymbol{f}$ is the evolution function of the state variables while $\boldsymbol{g}$ and $\boldsymbol{h}$ are respectively the inequality and equality command constraints. $\boldsymbol{x_0}$ and $\boldsymbol{x_\mathbf{f}}$ are the state variable values at t_0

and t_f respectively. All the introduced variables are limited by their lower and upper bounds.

However, in order to solve the problem numerically, the design cycle is discretized following a time step Δt. Δt is selected considering the system dynamics impacting the cost function the most, such as the mechanical transient when considering the HEV application for instance as opposed to the thermal or electronic transient.

The discretized optimization problem is then expressed as:

$$\begin{aligned}
\underset{\boldsymbol{u}}{\text{minimize}} \quad & \sum_{t_0}^{t_\mathrm{f}-\Delta t} L(\boldsymbol{x}(t), \boldsymbol{u}(t), t)\Delta t && \text{(2.2a)}\\
\text{subject to} \quad & \boldsymbol{x}(t+\Delta t) = \boldsymbol{f}(\boldsymbol{x}(t), \boldsymbol{u}(t), t)\Delta t + \boldsymbol{x}(t) && \text{(2.2b)}\\
& \boldsymbol{x}(t_0) = \boldsymbol{x_0} && \text{(2.2c)}\\
& \boldsymbol{x}(t_\mathrm{f}) = \boldsymbol{x_\mathbf{f}} && \text{(2.2d)}\\
& \boldsymbol{g}(\boldsymbol{x}(t), \boldsymbol{u}(t), t) \leq 0 && \text{(2.2e)}\\
& \boldsymbol{h}(\boldsymbol{x}(t), \boldsymbol{u}(t), t) = 0 && \text{(2.2f)}\\
& \boldsymbol{x}(t) \in [\boldsymbol{x_{\min}}(t), \boldsymbol{x_{\max}}(t)] && \text{(2.2g)}\\
& \boldsymbol{u}(t) \in [\boldsymbol{u_{\min}}(t), \boldsymbol{u_{\max}}(t)] && \text{(2.2h)}
\end{aligned}$$

The main aim of hybrid powertrain optimization is to find the design parameters that minimize both the cost of the hybrid powertrain along with its fuel consumption, while considering the fact that its fuel efficiency is impacted by its use.

As such, the studied optimization problem belongs to the Plant/Controller optimization class of problems, whose general formulation is expressed as:

$$\begin{aligned}
\underset{\boldsymbol{d},\boldsymbol{u}}{\text{minimize}} \quad & J(\boldsymbol{d}, \boldsymbol{u}) = \alpha Inv(\boldsymbol{d}) + \beta \sum_{t_0}^{t_\mathrm{f}-\Delta t} L(\boldsymbol{d}, \boldsymbol{x}(t), \boldsymbol{u}(t), t)\Delta t && \text{(2.3a)}\\
\text{subject to} \quad & \boldsymbol{x}(t+\Delta t) = \boldsymbol{f}(\boldsymbol{d}, \boldsymbol{x}(t), \boldsymbol{u}(t), t)\Delta t + \boldsymbol{x}(t) && \text{(2.3b)}\\
& \boldsymbol{x}(t_0) = \boldsymbol{x_0}(\boldsymbol{d}) && \text{(2.3c)}\\
& \boldsymbol{x}(t_\mathrm{f}) = \boldsymbol{x_\mathbf{f}}(\boldsymbol{d}) && \text{(2.3d)}\\
& \boldsymbol{g}(\boldsymbol{d}, \boldsymbol{x}(t), \boldsymbol{u}(t), t) \leq 0 && \text{(2.3e)}\\
& \boldsymbol{h}(\boldsymbol{d}, \boldsymbol{x}(t), \boldsymbol{u}(t), t) = 0 && \text{(2.3f)}\\
& \boldsymbol{k}(\boldsymbol{d}) \leq 0 && \text{(2.3g)}\\
& \boldsymbol{l}(\boldsymbol{d}) = 0 && \text{(2.3h)}\\
& \boldsymbol{x}(t) \in [\boldsymbol{x_{\min}}(\boldsymbol{d}, t), \boldsymbol{x_{\max}}(\boldsymbol{d}, t)] && \text{(2.3i)}\\
& \boldsymbol{u}(t) \in [\boldsymbol{u_{\min}}(\boldsymbol{d}, t), \boldsymbol{u_{\max}}(\boldsymbol{d}, t)] && \text{(2.3j)}\\
& \boldsymbol{d} \in [\boldsymbol{d_{\min}}, \boldsymbol{d_{\max}}] && \text{(2.3k)}
\end{aligned}$$

where J represents the total cost function to minimize. Optimization variables are split into the design variables $\boldsymbol{d}$ and command variables $\boldsymbol{u}$. J is expressed as the sum of both the plant's cost Inv, directly linked to the design parameters, and the controller's cost defined earlier. α and β are the weights added to both terms of the cost function and are adjusted in regards to the objective of the optimization. α takes a zero value for example when the controller cost is the only one that is considered. $\boldsymbol{k}$ and $\boldsymbol{l}$ refer correspondingly to the

inequality and equality design constraints.

In the absence of constraints, $\boldsymbol{d^*}$ and $\boldsymbol{u^*}$ define a local minimum $\boldsymbol{s^*}$ if:

$$J(\boldsymbol{s}) \geq J(\boldsymbol{s^*}) \quad \forall \boldsymbol{s} \in \boldsymbol{N}(\boldsymbol{s^*}) \tag{2.4}$$

where $\boldsymbol{N}(\boldsymbol{s^*})$ is a neighborhood of $\boldsymbol{s^*}$ and a subdomain of the cost function's feasible domain of definition $\boldsymbol{D}$. A necessary condition to verify in this case is:

$$\nabla J(\boldsymbol{s^*}) = 0 \tag{2.5}$$

This condition is sufficient if J is a convex function. On the other hand, $\boldsymbol{s^*}$ is a global minimum if expression 2.6 is valid:

$$J(\boldsymbol{s}) \geq J(\boldsymbol{s^*}) \quad \forall \boldsymbol{s} \in \boldsymbol{D} \tag{2.6}$$

As such, a global optimum is a local optimum as well. Meanwhile, when a local optimum is found, global optimality is only guaranteed if the problem is convex. When considering constrained optimization problems however, the following equations, known as Karush-Kuhn-Tucker (KKT) conditions and based on the method of Lagrange multipliers, must be satisfied [104]:

$$\nabla J(\boldsymbol{s^*}) + \sum_{i=1}^{m} \lambda_{\mathrm{i}} \nabla ineq_{\mathrm{i}}(\boldsymbol{s^*}) + \sum_{j=1}^{n} \mu_{\mathrm{j}} \nabla eq_{\mathrm{j}}(\boldsymbol{s^*}) = 0 \tag{2.7a}$$

$$\lambda_{\mathrm{i}} = 0 \; and \; ineq_{\mathrm{i}}(\boldsymbol{s^*}) < 0 \; d \; i = 1, .., m \tag{2.7b}$$

$$or \quad \lambda_{\mathrm{i}} > 0 \; and \; ineq_{\mathrm{i}}(\boldsymbol{s^*}) = 0 \quad i = 1, .., m \tag{2.7c}$$

where $\boldsymbol{ineq}$ and $\boldsymbol{eq}$ refer to all the inequality and equality constraints while $\boldsymbol{\lambda}$ and $\boldsymbol{\mu}$ are added Lagrange multipliers.

Gradient-based algorithms such as Sequentially Quadratic Programming (SQP) stop if a local optimum is found. This is determined by evaluating the above KKT conditions. While the latter only define first-order necessary optimality conditions, additional tests based on the hessian values, can be used to prove that a local minimum is obtained [105]. Various techniques are employed afterwards, such as multi-start in which numerous initial solution guesses spread out in the search space are used for algorithm initialization, to help find the global optimum.

Meta-heuristic algorithms on the other hand rely on different stopping criteria such as function and optimization variables relative difference between successive iterations or a maximum number of algorithm iterations [106].

Aside from its optimality, a solution's robustness needs to be assessed as well, since the optimization problem is solved in a deterministic way while the industrial processes applied when manufacturing introduce various parameter uncertainties. This is explored in greater detail on Chapter 4.

2.2 Hybrid railway power substation application

The hybrid railway power substation (HRPS) optimization problem, based on the work in [44], is used afterwards to compare between several control strategies and system-wide op-

timization approaches.

These facilities can satisfy parts of their electrical energy consumption through the use of renewable energies, combined with energy storage devices to tackle the related intermittency issues. The studied HRPS for example, shown in Figure 2.1, is equipped with wind turbines and solar panels as well as batteries.

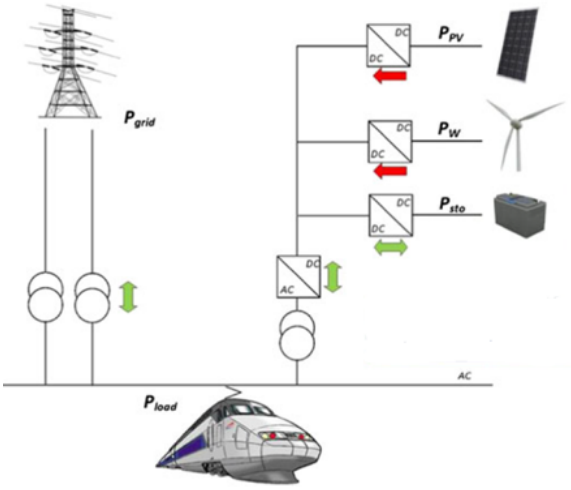

Figure 2.1: HRPS design problem [44].

To maximize the efficiency of the facility, the size of its components (solar panels, wind turbines, storage capacity,...) have to be properly designed while considering their usage over a long period of time. The use of the storage devices also has an important impact on the energy bill, especially when the daily evolution of electricity prices and seasonal changes are considered. The time step for this study is equal to 10 minutes.

The HRPS optimization problem, is then expressed as:

$$\underset{E_{\max},P_{\max},S_{\mathrm{PV}},S_{\mathrm{W}},E_{\mathrm{ini}},\boldsymbol{P_{\mathrm{sto}}},\boldsymbol{P_{\mathrm{grid}}}}{\text{minimize}} \quad Inv(E_{\max},P_{\max},S_{\mathrm{PV}},S_{\mathrm{W}}) + \sum_{t_0}^{t_{\mathrm{f}}-\Delta t} C_{\mathrm{grid}}(P_{\mathrm{grid}}(t),t)\Delta t \tag{2.8a}$$

$$\text{subject to} \quad P_{\mathrm{grid}}(t) = P_{\mathrm{sto}}(t) + P_{\mathrm{load}}(t) - S_{\mathrm{PV}}P_{\mathrm{irr}}(t) - S_{\mathrm{W}}P_{\mathrm{wind}}(t) \tag{2.8b}$$

$$E_{\mathrm{sto}}(t+\Delta t) = P_{\mathrm{sto}}(t)\Delta t + E_{\mathrm{sto}}(t) \tag{2.8c}$$

$$E_{\mathrm{sto}}(t_0) = E_{\mathrm{ini}} \tag{2.8d}$$

$$E_{\mathrm{sto}}(t_{\mathrm{f}}) = E_{\mathrm{ini}} \tag{2.8e}$$

$$E_{\mathrm{sto}}(t) \in [0, E_{\max}] \tag{2.8f}$$

$$E_{\max} \in \mathbb{R}^+, P_{\max} \in \mathbb{R}^+, S_{\mathrm{PV}} \in \mathbb{R}^+, S_{\mathrm{W}} \in \mathbb{R}^+ \tag{2.8g}$$

$$P_{\mathrm{sto}}(t) \in [-P_{\max}, P_{\max}], P_{grid}(t) \in \mathbb{R} \tag{2.8h}$$

with $E_{\max}$ representing the energy storage capacity in J, $P_{\max}$ the maximum input/output power to the batteries in W, S_{PV} the surface of the solar panels in m^2, S_{W} the swept surface

of the wind turbines in m^2 and E_{ini} the energy initially stored in the batteries in J.

$\boldsymbol{P_{\text{load}}}$ is the consumed power, while $\boldsymbol{P_{\text{grid}}}$, $\boldsymbol{P_{\text{sto}}}$, $\boldsymbol{P_{\text{PV}}}$ and $\boldsymbol{P_{\text{W}}}$ represent the power flow from the grid, the batteries, the installed solar panels and wind turbines respectively in W. C_{grid} refers to the energy cost function. $\boldsymbol{P_{\text{wind}}}$ is the available wind power in W/m^2 while $\boldsymbol{P_{\text{irr}}}$ is the solar irradiance in W/m^2. $\boldsymbol{E_{\text{sto}}}$ is the energy stored in the batteries in J.

In this case study, the HRPS investment cost is linear, as expressed in 2.9:

$$Inv(E_{\max}, P_{\max}, S_{\text{PV}}, S_{\text{W}}) = C^{\text{E}}{}_{\text{sto}} E_{\max} + C^{\text{P}}{}_{\text{sto}} P_{\max} + C_{\text{PV}} S_{\text{PV}} + C_{\text{W}} S_{\text{W}} \tag{2.9}$$

where $C^{\text{E}}{}_{\text{sto}}$, $C^{\text{P}}{}_{\text{sto}}$, C_{PV} and C_{W} are the fixed costs related to $E_{\max}$, $P_{\max}$, S_{PV} and S_{W} respectively.

As for the energy cost, a piece-wise linear pricing system is adopted, which depends on the direction of the power flow from the grid. By decomposing $\boldsymbol{P_{\text{grid}}}$ into power received from the grid $\boldsymbol{P_{\text{grid}}}^{+}$ and power sent to the grid $\boldsymbol{P_{\text{grid}}}^{-}$, the energy cost can be expressed as:

$$C_{\text{grid}}(P_{\text{grid}}(t), t) = C^{+}{}_{\text{grid}}(t) P_{\text{grid}}{}^{+}(t) + C^{-}{}_{\text{grid}}(t) P_{\text{grid}}{}^{-}(t) \tag{2.10}$$

The cost components applied above satisfy the following:

$$C^{+}{}_{\text{grid}}(t) > C^{-}{}_{\text{grid}}(t) \tag{2.11}$$

This then means that, if an optimal solution is found, logically either $P_{\text{grid}}{}^{-}(t)$ or $P_{\text{grid}}{}^{+}(t)$ are equal to zero at time step t. This is crucial as the power flow needs to remain in one direction per time step.

Thus, the total cost function is linearized. Since the constraints are linear as well, the complete HRPS problem is linearized. An all-at-once linear programming (LP) optimization algorithm such as dual-simplex is used to accurately find the global optimum of the HRPS problem.

On the other hand, it is clear that the HRPS problem falls in the same category as hybrid powertrain optimization of the Plant/Controller class of problems. The optimization problem is reformulated as in 2.3, with $\boldsymbol{d}$, $\boldsymbol{u}$ and $\boldsymbol{x}$ referring to ($E_{\max}$, $P_{\max}$, S_{PV}, S_{W}, E_{ini}), $\boldsymbol{P_{\text{sto}}}$ and $\boldsymbol{E_{\text{sto}}}$ respectively:

$$\min_{\boldsymbol{d},\boldsymbol{u}} \quad J(\boldsymbol{d}, \boldsymbol{u}) = Inv(\boldsymbol{d}) + \sum_{t_0}^{t_{\text{f}}-\Delta t} C_{\text{grid}}(u(t) + P_{load}(t) - d_3 P_{irr}(t) - d_4 P_{\text{wind}}(t), t)\Delta t \tag{2.12a}$$

$$\text{s.t.} \quad x(t + \Delta t) = u(t)\Delta t + x(t) \tag{2.12b}$$

$$x(t_0) = d_5 \tag{2.12c}$$

$$x(t_{\text{f}}) = d_5 \tag{2.12d}$$

$$d_5 - d_1 \leq 0 \tag{2.12e}$$

$$x(t) \in [0, d_1] \tag{2.12f}$$

$$u(t) \in [-d_2, d_2] \tag{2.12g}$$
$$\boldsymbol{d} \in {\mathbb{R}_+}^5 \tag{2.12h}$$

with:

$$Inv(\boldsymbol{d}) = {C^{\mathrm{E}}}_{\mathrm{sto}} d_1 + {C^{\mathrm{P}}}_{\mathrm{sto}} d_2 + C_{\mathrm{PV}} d_3 + C_{\mathrm{W}} d_4 \tag{2.13}$$

If the design variables are imposed, the HRPS optimal control problem can be defined as well:

$$\min_{\boldsymbol{u}} \quad \sum_{t_0}^{t_\mathrm{f}-\Delta t} C_{\mathrm{grid}}(u(t) + P_{\mathrm{load}}(t) - d_3 P_{\mathrm{irr}}(t) - d_4 P_{\mathrm{wind}}(t), t)\Delta t \tag{2.14a}$$
$$\text{s.t.} \quad x(t + \Delta t) = u(t)\Delta t + x(t) \tag{2.14b}$$
$$x(t_0) = E_{\mathrm{ini}} \tag{2.14c}$$
$$x(t_\mathrm{f}) = E_{\mathrm{ini}} \tag{2.14d}$$
$$x(t) \in [0, E_{\max}] \tag{2.14e}$$
$$u(t) \in [-P_{\max}, P_{\max}] \tag{2.14f}$$

The HRPS application is investigated before hybrid powertrain optimization for various reasons: on one hand, this case study introduces, similarly to the HEV optimization problem, a large number of variables. on the other hand, its system model is much faster to evaluate and, as explained earlier, the global optimum is easily found through problem linearization. This solution is used as a reference to draw a first comparison between the control and sizing strategies presented in the following sections.

2.3 Optimal control strategies

Controller optimization is addressed first before discussing system-wide optimization. Thus, this section mainly focuses on the optimal control methods introduced in Chapter 1 that can be used to solve problem 2.2: direct optimization, CO, PMP and DP. Comparison over a common benchmark, the HRPS case study, is established afterwards to select the most adequate methods to implement when studying the hybrid powertrain application.

2.3.1 Direct Optimization

Different methods exist to solve the optimal control problem, with direct optimization, either by implementing meta-heuristic or non-linear programming (NLP) algorithms, still being a viable option. The SQP methods, seen as more accurate and efficient when compared to other non-linear programming methods over large optimization problems [107], are applied afterwards.

The SQP methods solve a sequence of optimization subproblems at different solution guesses. The optimization subproblems are based on a quadratic approximation of the Lagrangian function and linearization of the problem's inequality constraints allowing them to be solved using quadratic programming algorithms. Once they are solved, the current solution guess is updated. If a local optimum is not found (first-order optimality conditions) and the stopping thresholds described in the previous section are not crossed, a new

solution guess is proposed using a line search procedure and the previous process is repeated.

On the other hand, it should still be expected that a large number of optimization variables impacts the convergence of the algorithm and lead to prohibitive calculation times. This eventually restricts their use on short design cycles of a few hundred time steps only. For longer cycles, it is imperative to implement more adequate methods.

2.3.2 Collaborative Optimization

Decomposition techniques such as CO can be applied in a bid to reduce the number of variables handled by direct optimization solvers: the optimization problem between time steps t_0 and t_f is split into N optimal control problems calculating J_i over shorter design cycles. The cycle corresponding to J_i is limited by time steps t_i and $t_{\mathrm{i}+1}$, with t_N equal to t_f.

The equivalent optimal control problem, representing the top optimization problem, is expressed as:

$$\underset{\boldsymbol{x_1},\ldots,\boldsymbol{x_N}}{\text{minimize}} \quad \sum_{i=0}^{N-1} J_\mathrm{i}(\boldsymbol{x_\mathbf{i}}, \boldsymbol{x_{\mathbf{i+1}}}) \tag{2.15a}$$

$$\boldsymbol{x_\mathbf{N}} = \boldsymbol{x_\mathbf{f}} \tag{2.15b}$$

$$\boldsymbol{x_\mathbf{i}} \in [\boldsymbol{x_{\mathbf{min}}}(t_\mathrm{i}), \boldsymbol{x_{\mathbf{max}}}(t_\mathrm{i})] \tag{2.15c}$$

While J_i is calculated by solving the following subproblem:

$$J_\mathrm{i}(\boldsymbol{x_\mathbf{i}}, \boldsymbol{x_{\mathbf{i+1}}}) \quad = \min_{\boldsymbol{u}} \sum_{t_\mathrm{i}}^{t_{\mathrm{i}+1}} L(\boldsymbol{x}(t), \boldsymbol{u}(t), t)\Delta t \tag{2.16a}$$

$$\text{subject to} \quad \boldsymbol{x}(t+\Delta t) = \boldsymbol{f}(\boldsymbol{x}(t), \boldsymbol{u}(t), t)\Delta t + \boldsymbol{x}(t) \tag{2.16b}$$

$$\boldsymbol{x}(t_\mathrm{i}) = \boldsymbol{x_\mathbf{i}} \tag{2.16c}$$

$$\boldsymbol{x}(t_{\mathrm{i}+1}) = \boldsymbol{x_{\mathbf{i+1}}} \tag{2.16d}$$

$$\boldsymbol{g}(\boldsymbol{x}(t), \boldsymbol{u}(t), t) \leq 0 \tag{2.16e}$$

$$\boldsymbol{h}(\boldsymbol{x}(t), \boldsymbol{u}(t), t) = 0 \tag{2.16f}$$

$$\boldsymbol{x}(t) \in [\boldsymbol{x_{\mathbf{min}}}(t), \boldsymbol{x_{\mathbf{max}}}(t)] \tag{2.16g}$$

$$\boldsymbol{u}(t) \in [\boldsymbol{u_{\mathbf{min}}}(t), \boldsymbol{u_{\mathbf{max}}}(t)] \tag{2.16h}$$

This decomposition should consider the limitations of the solvers for both problems. The use of NLP algorithms for example leads to convergence difficulties for a large number of variables at the top problem and subproblem levels. Even though it provides solutions for much longer cycles compared to the direct use of optimization algorithms, the use of CO is still restricted to cycles of thousands of variables and motivates the study of algorithms based on optimal control theory instead, such as Pontryagin's Minimum Principle (PMP) and Dynamic Programming (DP).

2.3.3 Pontryagin's Minimum Principle

The main idea behind the PMP approach is to solve the dual problem of the optimal control problem. This is achieved by introducing the augmented Lagrangian for the evolution constraint using a co-state value $\boldsymbol{\lambda}$. For the continuous formulation, it is defined as:

$$\bar{J}(\boldsymbol{x}, \boldsymbol{u}, \boldsymbol{\lambda}) = \int_{t_0}^{t_\mathrm{f}} L(\boldsymbol{x}(t), \boldsymbol{u}(t), t)dt + \int_{t_0}^{t_\mathrm{f}} \boldsymbol{\lambda}(t)(\boldsymbol{f}(\boldsymbol{x}(t), \boldsymbol{u}(t), t) - \boldsymbol{x}'(t))dt \tag{2.17a}$$

$$= \int_{t_0}^{t_\mathrm{f}} L(\boldsymbol{x}(t), \boldsymbol{u}(t), t)dt + \int_{t_0}^{t_\mathrm{f}} \boldsymbol{\lambda}(t)\boldsymbol{f}(\boldsymbol{x}(t), \boldsymbol{u}(t), t)dt - \int_{t_0}^{t_\mathrm{f}} \boldsymbol{\lambda}(t)\boldsymbol{x}'(t)dt \tag{2.17b}$$

$$= \int_{t_0}^{t_\mathrm{f}} (L(\boldsymbol{x}(t), \boldsymbol{u}(t), t) + \boldsymbol{\lambda}(t)\boldsymbol{f}(\boldsymbol{x}(t), \boldsymbol{u}(t), t))dt - \int_{t_0}^{t_\mathrm{f}} \boldsymbol{\lambda}(t)\boldsymbol{x}'(t)dt \tag{2.17c}$$

The hamiltonian H is introduced:

$$\bar{J}(\boldsymbol{x}, \boldsymbol{u}, \boldsymbol{\lambda}) = \int_{t_0}^{t_\mathrm{f}} H(\boldsymbol{x}(t), \boldsymbol{u}(t), \boldsymbol{\lambda}(t), t)dt - \int_{t_0}^{t_\mathrm{f}} \boldsymbol{\lambda}(t)\boldsymbol{x}'(t)dt \tag{2.18}$$

Integration by parts is applied afterwards, resulting in:

$$\bar{J}(\boldsymbol{x}, \boldsymbol{u}, \boldsymbol{\lambda}) = \int_{t_0}^{t_\mathrm{f}} H(\boldsymbol{x}(t), \boldsymbol{u}(t), \boldsymbol{\lambda}(t), t) + \boldsymbol{\lambda}'(t)\boldsymbol{x}(t)dt - \boldsymbol{\lambda}(t_\mathrm{f})\boldsymbol{x}(t_\mathrm{f}) + \boldsymbol{\lambda}(t_0)\boldsymbol{x}(t_0) \tag{2.19}$$

Finally, partial derivation of equation 2.19 with respect to $\boldsymbol{u}$ leads to:

$$\frac{\partial \bar{J}}{\partial \boldsymbol{u}}(\boldsymbol{x}, \boldsymbol{u}, \boldsymbol{\lambda}) = \int_{t_0}^{t_\mathrm{f}} \frac{\partial H}{\partial \boldsymbol{u}}(\boldsymbol{x}(t), \boldsymbol{u}(t), \boldsymbol{\lambda}(t), t)dt \tag{2.20}$$

It has been demonstrated that if ($\boldsymbol{x}^*$, $\boldsymbol{u}^*$, $\boldsymbol{\lambda}^*$) is a stationary point of the augmented Lagrangian, then it is also a stationary point for the optimal control problem under the evolution constraint of the state variables $\boldsymbol{x}$ [88]. It is then concluded from 2.17 that the solution to the optimal power management problem needs to verify the following constraint:

$$\int_{t_0}^{t_\mathrm{f}} \frac{\partial H}{\partial \boldsymbol{u}}(\boldsymbol{x}^*(t), \boldsymbol{u}^*(t), \boldsymbol{\lambda}^*(t), t)dt = 0 \tag{2.21}$$

When applying the same reasoning detailed earlier using specific control functions before projecting Equation 2.21 [108], the following condition is found:

$$\frac{\partial H}{\partial \boldsymbol{u}}(\boldsymbol{x}^*(t), \boldsymbol{u}^*(t), \boldsymbol{\lambda}^*(t), t) = 0 \tag{2.22}$$

The above condition is generalized when H is not differentiable with respect to $\boldsymbol{u}$:

$$\boldsymbol{u}^*(t) = \underset{\boldsymbol{u}}{\operatorname{argmin}} \quad H(\boldsymbol{x}^*(t), \boldsymbol{u}, \boldsymbol{\lambda}^*(t), t) \tag{2.23}$$

And thus optimal command can be found as a solution to a simpler minimization problem at each time step. The constraints over the initial and final values are validated by selecting the appropriate values for $\boldsymbol{\lambda}$. The PMP approach is summarized in Figure 2.2.

Furthermore, partial derivation of equation 2.18 with respect to $\boldsymbol{x}$ leads to:

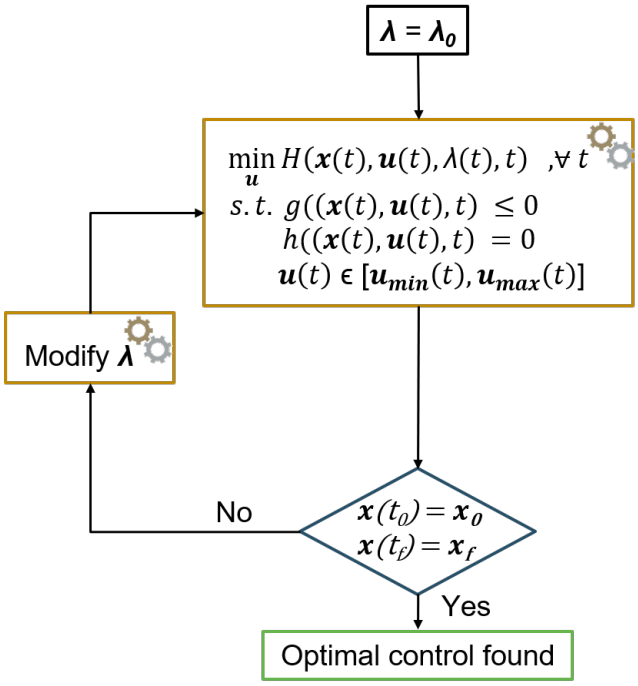

Figure 2.2: PMP process

$$\frac{\partial \bar{J}}{\partial \boldsymbol{x}}(\boldsymbol{x}, \boldsymbol{u}, \boldsymbol{\lambda}) \quad = \int_{t_0}^{t_f} \frac{\partial H}{\partial \boldsymbol{x}}(\boldsymbol{x}(t), \boldsymbol{u}(t), \boldsymbol{\lambda}(t), t) + \boldsymbol{\lambda}'(t) dt \tag{2.24}$$

This imposes the following condition on the evolution of $\boldsymbol{\lambda}$:

$$\boldsymbol{\lambda}'(t) = -\frac{\partial H}{\partial \boldsymbol{x}}(\boldsymbol{x}^*(t), \boldsymbol{u}^*(t), \boldsymbol{\lambda}^*(t), t) \tag{2.25}$$

If H is independent of $\boldsymbol{x}$, for instance in applications where the cost functional and the evolution function do not depend on the state variables such as those presented in this work, then $\boldsymbol{\lambda}$ has a fixed value throughout the design cycle. Finding $\boldsymbol{\lambda}$ in this case can be based on a simpler process such as dichotomy.

One of the main deficiencies of PMP however remains the fact that the different constraints on the control variables are not carefully considered, since they require the addition of other co-state values to be determined as well, further complexifying the process. As such, the optimal control must be found inside the admissible region of $\boldsymbol{u}$ and not on its boundaries [109] to achieve control optimality.

2.3.4 Dynamic Programming

The DP algorithm adopts a distinct approach by introducing the cost-to-go function V. $V(\boldsymbol{x},t)$ represents the minimum cost required to get from state value $\boldsymbol{x}$ at time step t to reach the imposed value $\boldsymbol{x_f}$ at the last time step. $V(\boldsymbol{x},t)$ is also, according to Bellman's principle, a solution to the following problem:

$$V(\boldsymbol{x}, t) = \min_{\boldsymbol{u_i}} \quad V(\boldsymbol{x}(t+\Delta t), t+\Delta t) + L(\boldsymbol{x}, \boldsymbol{u_i}, t)\Delta t \tag{2.26a}$$

$$\text{subject to} \quad \boldsymbol{x}(t+\Delta t) = \boldsymbol{f}(\boldsymbol{x}, \boldsymbol{u_i}, t)\Delta t + \boldsymbol{x}(t) \tag{2.26b}$$

$$\boldsymbol{g}(\boldsymbol{x}, \boldsymbol{u}_\text{i}, t) \leq 0 \tag{2.26c}$$

$$\boldsymbol{h}(\boldsymbol{x}, \boldsymbol{u}_\text{i}, t) = 0 \tag{2.26d}$$

$$\boldsymbol{x}(t+\Delta t) \in [\boldsymbol{x_{min}}(t+\Delta t), \boldsymbol{x_{max}}(t+\Delta t)] \tag{2.26e}$$

$$\boldsymbol{u}_\text{i} \in [\boldsymbol{u_{min}}(t), \boldsymbol{u_{max}}(t)] \tag{2.26f}$$

Using a backwards approach, this problem can be solved either using an optimization algorithm or by assessing different values for the command limited by its lower and upper bounds. This is repeated for different discrete values of the state variables.

The discretization, called mesh, defines the grid $\boldsymbol{D_x}$, representing the set of discrete values for the state variables at each time step. The discretization should allow for $\boldsymbol{x_0}$ and $\boldsymbol{x_f}$ to belong to the grid at their respective time steps.

The values previously found for the cost-to-go function and optimal commands are stored in matrices of the same size as the mesh. In this way, their values at time step $t+\Delta t$ can be exploited at time step t without the need to recalculate them.

Thus, the dynamic programming algorithm can be summed up as followed:

Algorithm 1: Dynamic Programming algorithm

```
V(x_f, t_f) = 0;
V(x ≠ x_f, t_f) = +∞;
for t = t_f-Δt to t_0 by -Δt do
    for x_i ∈ D_x(t) do
        Find V(x_i, t) by solving 2.26;
        Store V(x_i, t);
        Store optimal command u_i at t;
    end
end
```

The optimal cost and command for the complete cycle using the selected mesh are stored at the grid point defined by ($\boldsymbol{x_0}$,t_0).

The mesh should be defined adequately when applying DP. On one hand, a finer mesh improves the quality of the solution. On the other hand, smaller discretization steps lead to longer calculation times and require important storage capacity.

Since the cost-to-go and optimal command values are only stored at grid points defined by ($\boldsymbol{x}(t+\Delta t)$,$t+\Delta t$) when solving problem 2.26 at time step $t+\Delta t$, a common approximation is to interpolate their values if $\boldsymbol{x}(t+\Delta t) \notin \boldsymbol{D_x}(t+\Delta t)$ when solving the same problem at time step t.

A more accurate and faster approach would be to select only command values allowing for passage throughout the grid points. A separate function $\boldsymbol{b}$ can be added for example such as to find the "cheapest" command to reach different state variable values at two successive time steps.

The DP algorithm is improved in the following way:

Algorithm 2: Improved dynamic programming algorithm

$V(\boldsymbol{x_f}, t_f) = 0$;
$V(\boldsymbol{x} \neq \boldsymbol{x_f}, t_f) = +\infty$;
for $t = t_f$-Δt *to* t_0 *by* -Δt **do**
  for $x_i \in \boldsymbol{D_x}(t)$ **do**
    $V(\boldsymbol{x_i}, t) = +\infty$;
    for $x_{i+1} \in \boldsymbol{D_x}(t+\Delta t)$ **do**
      $\boldsymbol{u_i} = \boldsymbol{b}(\boldsymbol{x_i}, \boldsymbol{x_{i+1}}, t)$;
      if $\boldsymbol{u_i} \in [\boldsymbol{u_{min}}(t), \boldsymbol{u_{max}}(t)]$, $\boldsymbol{g}(\boldsymbol{x_i}, \boldsymbol{u_i}, t) \leq 0$, $\boldsymbol{h}(\boldsymbol{x_i}, \boldsymbol{u_i}, t) = 0$ and
       $V(\boldsymbol{x_i}, t) > V(\boldsymbol{x_{i+1}}, t+\Delta t) + L(\boldsymbol{x_i}, \boldsymbol{u_i}, t)\Delta t$ **then**
        $V(\boldsymbol{x_i}, t) = V(\boldsymbol{x_{i+1}}, t+\Delta t) + L(\boldsymbol{x_i}, \boldsymbol{u_i}, t)\Delta t$;
        Store $\boldsymbol{u_i}$ as best command;
      end
    end
    Store $V(\boldsymbol{x_i}, t)$;
    Store best command as optimal command from $(\boldsymbol{x_i}, t)$;
  end
end

If $\boldsymbol{L}$ is independent with respect to the state variables and the values for $\boldsymbol{b}$ are only impacted by $\Delta \boldsymbol{x}$, it is recommended to use a uniform mesh and store the possible values for $\boldsymbol{L}$ in an array at each time step to be used afterwards for faster calculation times.

On the other hand, better solutions require a finer meshing, which increases the number of possible paths to explore. However, the time complexity is quadratic to the mesh. One of the solutions that are proposed in this work to drastically reduce calculation time is the application of an adaptive meshing process, displayed in Figures 2.3 and 2.4.

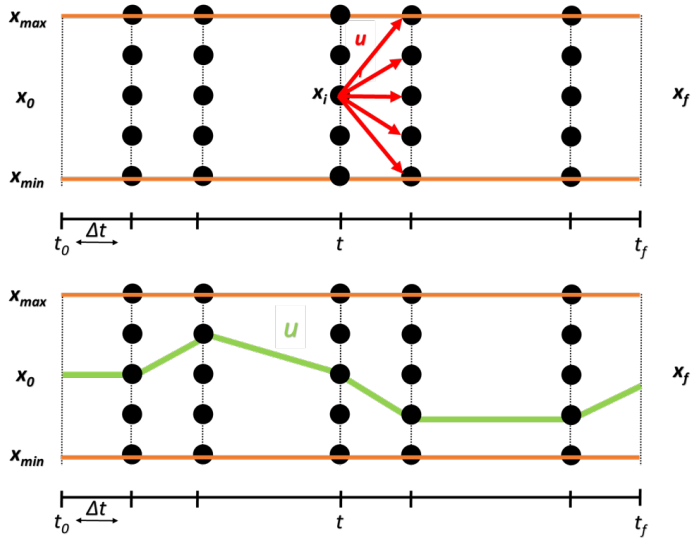

Figure 2.3: First part of an iteration of the adaptive meshing process. The black dots represent the grid points and the green line the optimal solution with the current mesh

This process starts with an initial solution found using a coarse mesh, presented as an

evolution of the state variables. The DP process is reconducted afterwards, while this time limiting the range of the state variables around the previously found values, modifying the shape of the grid. This allows for the use of finer meshing by limiting the number of grid points present in the updated grid, as shown in Figure 2.4.

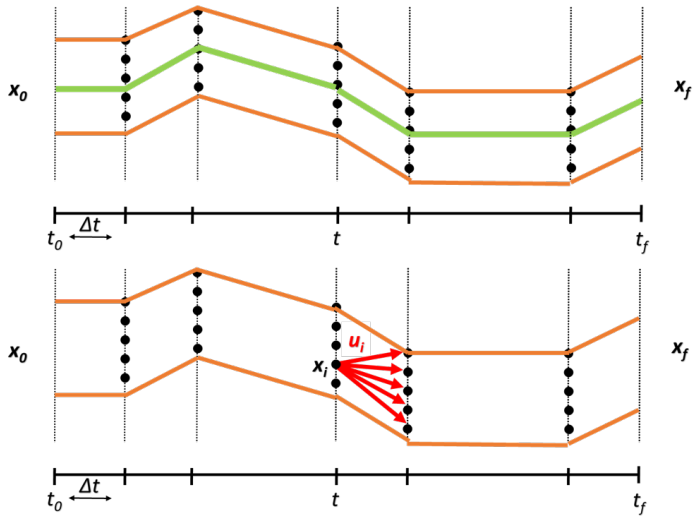

Figure 2.4: Second part of an iteration of the adaptive meshing process. The green line represents the previous solution, the orange line the new grid limits and the black dots the updated grid points

This process is then reiterated for either a fixed number of loops or based on a specific criterion such as the relative evolution of the optimal cost. The Dynamic Programming with Adaptive Meshing (DPAM) algorithm is summarized in the following way:

Algorithm 3: DPAM algorithm

for $l = 1$ *to* num_{loops} **do**
  Update $\boldsymbol{D}_{\mathbf{x}}$;
  Launch Algorithm 2;
end

2.3.5 Link between PMP and DP

DP's Hamilton-Jacobi-Bellman (HJB) equation is expressed as:

$$V(\boldsymbol{x}(t),t) = \min_{\boldsymbol{u}(t)} \quad V(\boldsymbol{x}(t+\Delta t),t+\Delta t) + L(\boldsymbol{x}(t),\boldsymbol{u}(t),t)\Delta t \tag{2.27}$$

The value of $\boldsymbol{x}(t+\Delta t)$ can be replaced using the evolution equation:

$$V(\boldsymbol{x}(t),t) = \min_{\boldsymbol{u}(t)} \quad V(\boldsymbol{f}(\boldsymbol{x}(t),\boldsymbol{u}(t),t)\Delta t + \boldsymbol{x}(t),t+\Delta t) + L(\boldsymbol{x}(t),\boldsymbol{u}(t),t)\Delta t \tag{2.28}$$

Replacing the cost-to-go function in the right side with its first Taylor polynomial leads to:

$$V(\boldsymbol{x}(t),t) = \min_{\boldsymbol{u}(t)} V(\boldsymbol{x}(t),t) + \frac{\partial V}{\partial x}(\boldsymbol{x}(t),t)\boldsymbol{f}(\boldsymbol{x}(t),\boldsymbol{u}(t),t)\Delta t + \frac{\partial V}{\partial t}(\boldsymbol{x}(t),t)\Delta t + L(\boldsymbol{x}(t),\boldsymbol{u}(t),t)\Delta t \tag{2.29}$$

The equation is then simplified as:

$$\min_{\boldsymbol{u}(t)} \quad \frac{\partial V}{\partial x}(\boldsymbol{x}(t),t)\boldsymbol{f}(\boldsymbol{x}(t),\boldsymbol{u}(t),t) + \frac{\partial V}{\partial t}(\boldsymbol{x}(t),t) + L(\boldsymbol{x}(t),\boldsymbol{u}(t),t) = 0 \tag{2.30}$$

Since V is independent of the command value, the equation is further simplified as:

$$\frac{\partial V}{\partial t}(\boldsymbol{x}(t),t) + \min_{\boldsymbol{u}(t)} \quad \frac{\partial V}{\partial x}(\boldsymbol{x}(t),t)\boldsymbol{f}(\boldsymbol{x}(t),\boldsymbol{u}(t),t) + L(\boldsymbol{x}(t),\boldsymbol{u}(t),t) = 0 \tag{2.31}$$

Finally, finding the optimal command value at time step t comes down to minimizing a term similar to the PMP's hamiltonian defined as:

$$H(\boldsymbol{x}(t),\boldsymbol{u}(t),\boldsymbol{\lambda}(t),t) = L(\boldsymbol{x}(t),\boldsymbol{u}(t),t) + \boldsymbol{\lambda}(t)\boldsymbol{f}(\boldsymbol{x}(t),\boldsymbol{u}(t),t) \tag{2.32}$$

with the value of the co-state value λ expressed as:

$$\boldsymbol{\lambda}(t) = \frac{\partial V}{\partial x}(\boldsymbol{x}(t),t) \tag{2.33}$$

In this way, it is proven that both DP's and PMP's processes converge, although these control strategies are applied differently. Similar results should then be expected when implementing both these methods for control optimization, and any deviations that are observed should be investigated and justified.

2.3.6 Comparison and analysis

The different studied methods are compared afterwards over the HRPS control optimization problem and LP is used in this case to provide a reference solution. NLP is tested at first by applying the SQP version included in Matlab's Optimization Toolbox [110].

Two different variants of CO are assessed afterwards, by decomposing the design cycle into either one day or half-day long cycles and are referred to as CO1 and CO2 respectively. The optimizers for both the top-level problem and for the subproblems use the SQP algorithm as well. Independent optimizations on the subproblem level are executed in parallel for faster iterations.

Furthermore, DP and DPAM are both investigated. The use of the improved versions for both algorithms requires the definition of function $\boldsymbol{b}$ described earlier. For the HRPS problem, this function is simply defined as:

$$b(x_{\mathrm{i}}, x_{\mathrm{i+1}}, t) = \frac{x_{\mathrm{i+1}} - x_{\mathrm{i}}}{\Delta t} \tag{2.34}$$

The selected time step for the optimization problem is set at 10 minutes. In this case, a design cycle spanning one day can be discretized into 144 time steps. Comparison is done

afterwards on cycles of increasing length with 1 day increments. An order of magnitude similar to a typical drive-cycle is reached for a 5-day design cycle. The different methods are compared in terms of computation time CT in seconds and relative deviation to the optimal cost D found with LP. The results are summarized in Table 2.1 and shown in Figure 2.5.

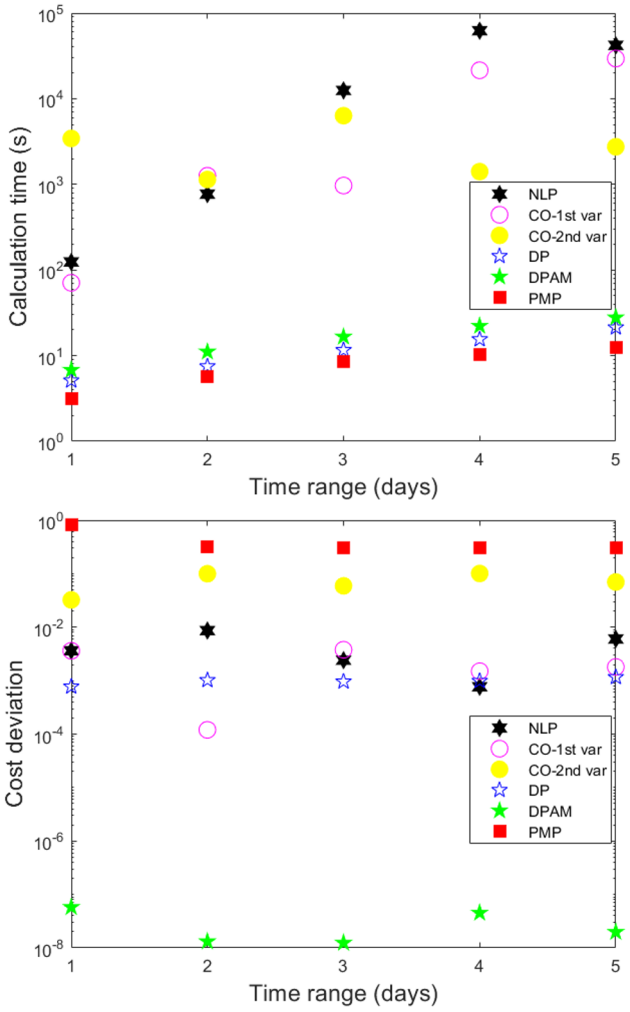

Figure 2.5: Comparison of control methods to solve the HRPS command optimization problem

	NLP		CO1		CO2		DP		DPAM		PMP	
TS	CT	D	CT	D	CT	D	CT	D	CT	D	CT	D
1 day	12.4	3.62e-3	13.8	3.62e-3	3.44e3	3.24e-2	5.12	7.74e-4	6.80	5.79e-8	3.14	8.09e-1
2 days	76.9	8.63e-3	1.26e3	1.20e-4	1.14e3	1.00e-1	7.48	1.02e-3	11.1	1.32e-8	5.64	3.13e-1
3 days	1.25e4	2.41e-3	9.69e2	3.78e-3	6.34e3	5.93e-2	11.6	9.60e-4	16.6	1.24e-8	8.45	3.11e-1
4 days	6.23e4	7.67e-3	2.15e4	1.50e-3	1.41e3	1.01e-1	15.5	9.85e-4	22.2	4.52e-8	10.2	3.09e-1
5 days	4.20e4	6.00e-3	2.95e4	1.80e-3	2.75e3	6.98e-2	21.3	1.16e-3	27.8	1.98e-8	12.4	3.08e-1

Table 2.1: Control strategy comparison

NLP finds good results but comes with high computation times, growing exponentially with the number of variables. Non convergence issues are expected for a larger number of variables.

CO1 is a more adequate method, having the same level of precision while being faster than NLP. The first variant finds the best compromise of both alternatives between fast optimizations on the subproblem level and the number of variables at the top level optimizer. Nevertheless, CO still finds difficulty providing solutions at reasonable times as well.

Providing gradient information of the cost and constraint functions allows for better convergence for both NLP and CO methods. However, this information is only available when adopting analytical models, and thus it cannot be generalized to other cases such as the studied hybrid powertrain optimization.

Meanwhile, PMP is the fastest but leads to poor results, as a necessary condition for finding the optimal control using this method is not met on this application. In fact, the hamiltonian is expressed as:

$$H(x(t), u(t), t) = C_{\text{grid}}(u(t) + P_{\text{load}}(t) - d_3 P_{\text{irr}}(t) - d_4 P_{\text{wind}}(t)) + \lambda(t)u(t) \tag{2.35}$$

As mentioned earlier, since H is independent with respect to $\boldsymbol{x}$, λ is a constant. Hence, the hamiltonian is a piece-wise linear function with respect to $\boldsymbol{u}$. Depending on the value of λ, the optimal control value is often either found at the upper or lower bounds. This is referred to as "Bang-Bang" command [111]. As explained before, optimal command being found at the boundaries only leads to sub-optimal solutions when using PMP.

Finally, DP and DPAM manage to find command values with small cost deviations and low calculation times. Their computation time is linear with the length of the cycle while their precision remains steady. Similar conclusions are observed for longer design cycles spanning over two weeks. Moreover, DPAM manages to find the optimal solution with much greater accuracy at comparable times to DP. For these reasons, DPAM is selected as the HRPS control strategy when implementing systemic design approaches.

2.4 Systemic design approaches

In the previous chapter, different systemic design approaches are introduced. The coupling between the optimization of the design and control problems allowed for the exploration of the main Plant/Controller frameworks, classified as the simultaneous, bi-level, iterative and sequential approaches.

The sequential approach is not considered in this research project since, while following a similar scheme to the iterative approach, it cannot, unlike the latter, lead to a system optimum. The remaining approaches are detailed further and compared on the HRPS application later on.

2.4.1 Simultaneous approach

The simultaneous framework, representing the most direct approach, consists in solving the optimization problem 2.3 directly either by using non-linear programming algorithms such as SQP or meta-heuristic methods like genetic algorithms.

However, this leads to a large number of optimization variables to consider at once mainly because of the command variables involved, limiting their use to system optimization problems over small design cycles.

2.4.2 Bi-level approach

As shown in Figure 2.6, when adopting the bi-level approach, also called nested approach, at each iteration of a top level problem, an optimization subproblem is solved to calculate the optimal controller cost $C(\boldsymbol{d})$ for the selected design variables $\boldsymbol{d}$.

The top problem defined in 2.36 focuses on finding only the optimal design variables, leading to less convergence issues as opposed to the previously defined simultaneous approach.

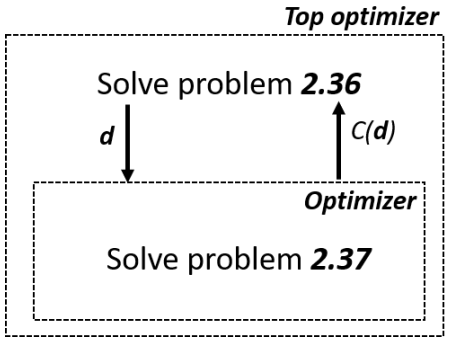

Figure 2.6: Bi-level framework

$$\underset{\boldsymbol{d}}{\text{minimize}} \quad \alpha Inv(\boldsymbol{d}) + C(\boldsymbol{d}) \tag{2.36a}$$

$$\text{subject to} \quad \boldsymbol{k}(\boldsymbol{d}) \leq 0 \tag{2.36b}$$

$$\boldsymbol{l}(\boldsymbol{d}) = 0 \tag{2.36c}$$

$$\boldsymbol{d} \in [\boldsymbol{d_{\min}}, \boldsymbol{d_{\max}}] \tag{2.36d}$$

Meanwhile, $C(\boldsymbol{d})$ is calculated by solving an optimal control problem defined by 2.37, similar to the one expressed in 2.2. This results in slower iterations at the top level as compared to function evaluations when using the simultaneous approach.

$$C(\boldsymbol{d}) = \min_{\boldsymbol{u}} \quad \beta \sum_{t_0}^{t_\mathrm{f}-\Delta t} L(\boldsymbol{d}, \boldsymbol{x}(t), \boldsymbol{u}(t), t)\Delta t \tag{2.37a}$$

$$\text{subject to} \quad \boldsymbol{x}(t+\Delta t) = \boldsymbol{f}(\boldsymbol{d}, \boldsymbol{x}(t), \boldsymbol{u}(t), t)\Delta t + \boldsymbol{x}(t) \tag{2.37b}$$

$$\boldsymbol{x}(t_0) = \boldsymbol{x_0}(\boldsymbol{d}) \tag{2.37c}$$

$$\boldsymbol{x}(t_\mathrm{f}) = \boldsymbol{x_\mathbf{f}}(\boldsymbol{d}) \tag{2.37d}$$

$$\boldsymbol{g}(\boldsymbol{d}, \boldsymbol{x}(t), \boldsymbol{u}(t), t) \leq 0 \tag{2.37e}$$

$$\boldsymbol{h}(\boldsymbol{d}, \boldsymbol{x}(t), \boldsymbol{u}(t), t) = 0 \tag{2.37f}$$

$$\boldsymbol{x}(t) \in [\boldsymbol{x_{\min}}(\boldsymbol{d}, t), \boldsymbol{x_{\max}}(\boldsymbol{d}, t)] \tag{2.37g}$$

$$\boldsymbol{u}(t) \in [\boldsymbol{u_{\min}}(\boldsymbol{d}, t), \boldsymbol{u_{\max}}(\boldsymbol{d}, t)] \tag{2.37h}$$

Another advantage of using this framework is the possibility to implement different and more adequate optimizers for the design and control problems. Thus, faster calculation times and convergence of the solution can be achieved while preserving the robustness of the approach.

2.4.3 Iterative approach

The iterative scheme goes further than the bi-level approach by completely separating both the design and control optimization blocks, as seen in Figure 2.7.

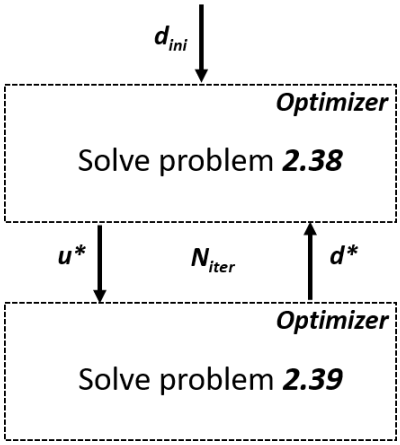

Figure 2.7: Iterative framework

At first, the design variables $\boldsymbol{d^*}$ are initialized to values $\boldsymbol{d_{ini}}$. The iterative framework then starts by solving the control optimization problem, expressed as:

$$\boldsymbol{u^*} = \underset{\boldsymbol{u}}{\operatorname{argmin}} \quad \beta \sum_{t_0}^{t_f-\Delta t} L(\boldsymbol{d^*}, \boldsymbol{x}(t), \boldsymbol{u}(t), t)\Delta t \tag{2.38a}$$

$$\text{subject to} \quad \boldsymbol{x}(t+\Delta t) = \boldsymbol{f}(\boldsymbol{d^*}, \boldsymbol{x}(t), \boldsymbol{u}(t), t)\Delta t + \boldsymbol{x}(t) \tag{2.38b}$$

$$\boldsymbol{x}(t_0) = \boldsymbol{x_0}(\boldsymbol{d^*}) \tag{2.38c}$$

$$\boldsymbol{x}(t_f) = \boldsymbol{x_f}(\boldsymbol{d^*}) \tag{2.38d}$$

$$\boldsymbol{g}(\boldsymbol{d^*}, \boldsymbol{x}(t), \boldsymbol{u}(t), t) \leq 0 \tag{2.38e}$$

$$\boldsymbol{h}(\boldsymbol{d^*}, \boldsymbol{x}(t), \boldsymbol{u}(t), t) = 0 \tag{2.38f}$$

$$\boldsymbol{x}(t) \in [\boldsymbol{x_{min}}(\boldsymbol{d^*}, t), \boldsymbol{x_{max}}(\boldsymbol{d^*}, t)] \tag{2.38g}$$

$$\boldsymbol{u^*}(t) \in [\boldsymbol{u_{min}}(\boldsymbol{d^*}, t), \boldsymbol{u_{max}}(\boldsymbol{d^*}, t)] \tag{2.38h}$$

Once the optimal command variables are found, the control strategy is fixed and the design variables are updated when solving the following design optimization problem:

$$\boldsymbol{d}^{*} = \underset{\boldsymbol{d}}{\operatorname{argmin}} \quad J(\boldsymbol{d}) = \alpha Inv(\boldsymbol{d}) + \beta \sum_{t_0}^{t_\mathrm{f}-\Delta t} L(\boldsymbol{d}, \boldsymbol{x}(t), \boldsymbol{u}^{*}(t), t)\Delta t \tag{2.39a}$$

$$\text{subject to} \quad \boldsymbol{x}(t+\Delta t) = \boldsymbol{f}(\boldsymbol{d}, \boldsymbol{x}(t), \boldsymbol{u}^{*}(t), t)\Delta t + \boldsymbol{x}(t) \tag{2.39b}$$

$$\boldsymbol{x}(t_0) = \boldsymbol{x_0}(\boldsymbol{d}) \tag{2.39c}$$

$$\boldsymbol{x}(t_\mathrm{f}) = \boldsymbol{x_\mathbf{f}}(\boldsymbol{d}) \tag{2.39d}$$

$$\boldsymbol{g}(\boldsymbol{d}, \boldsymbol{x}(t), \boldsymbol{u}^{*}(t), t) \leq 0 \tag{2.39e}$$

$$\boldsymbol{h}(\boldsymbol{d}, \boldsymbol{x}(t), \boldsymbol{u}^{*}(t), t) = 0 \tag{2.39f}$$

$$\boldsymbol{k}(\boldsymbol{d}) \leq 0 \tag{2.39g}$$

$$\boldsymbol{l}(\boldsymbol{d}) = 0 \tag{2.39h}$$

$$\boldsymbol{x}(t) \in [\boldsymbol{x_{\min}}(\boldsymbol{d}, t), \boldsymbol{x_{\max}}(\boldsymbol{d}, t)] \tag{2.39i}$$

$$\boldsymbol{u}^{*}(t) \in [\boldsymbol{u_{\min}}(\boldsymbol{d}, t), \boldsymbol{u_{\max}}(\boldsymbol{d}, t)] \tag{2.39j}$$

$$\boldsymbol{d} \in [\boldsymbol{d_{\min}}, \boldsymbol{d_{\max}}] \tag{2.39k}$$

This describes the first iteration of the iterative scheme, which is repeated as long as cost improvements are found when updating both the design and control variables or for a maximum number of iterations N_{iter}. It is imperative to include the controller cost when solving the design problem in order to ensure the consistency and convergence of this approach.

Finally, this scheme, as it is also the case for the bi-level framework, allows for the implementation of optimal control strategies to solve the separate control problem. This can then greatly improve the time required by this approach and ensure its convergence.

2.4.4 Comparison and analysis

In order to compare the proposed system design approaches, the HRPS design problem is studied over a cycle length of two weeks. The total number of decision variables in this case is equal to 2021. This allows to achieve the same level of complexity as the HEV optimization problem over the WLTC 3-b cycle (1800 time steps). The grid costs are recalculated as to achieve an order of magnitude for the energy cost similar to a life cycle exploitation of the HRPS, estimated at 20 years.

DPAM and LP are both applied alternatively for power management when implementing the bi-level and iterative frameworks. This helps assess the impact of the power management strategy on the convergence of the approaches and optimal solutions.

The design variables are optimized using SQP. The design variables are also normalized based on imposed upper and lower bounds to improve the convergence speed of the algorithm. A pool of 100 design configurations, generated from Sobol's Quasirandom Sequence [112] to fill the search space in a highly uniform manner, is used afterwards to initialize the algorithm for each approach. This allows for a better assessment of the convergence when analyzing the different approaches.

Moreover, the design optimization constraints for the iterative approach are simplified by only considering the maximum and minimum values of the imposed command variables. For example, $P_{\max}$ simply needs to verify the following conditions:

$$P_{\max} > max(\boldsymbol{u}) \tag{2.40a}$$

$$P_{\max} > -min(\boldsymbol{u}) \tag{2.40b}$$

Table 2.2 compiles the best results that are found, with $\mathcal{SM}$, $\mathcal{BL}$ and $\mathcal{IT}$ referring to the simultaneous, bi-level and iterative approaches respectively. CT refers to the calculation time in seconds while D refers to the deviation with the optimal cost provided by LP.

$\mathcal{SM}$		$\mathcal{BL}$ + LP		$\mathcal{BL}$ + DPAM		$\mathcal{IT}$ + LP		$\mathcal{IT}$ + DPAM	
CT	D	CT	D	CT	D	CT	D	CT	D
Non convergence		32.6	5.68e-9	1.94e4	8.53e-10	8.39	1.13e-3	1.30e3	1.39-3

Table 2.2: Systemic design strategies comparison

As expected, the simultaneous approach fails to converge due to the large number of optimization variables considered. The bi-level and iterative approaches on the other hand have managed to find solutions at small cost deviations and reasonable calculation times. Thus, only the bi-level and iterative approaches are analyzed further.

Bi-level approach analysis

The bi-level approach requires longer calculation times when DPAM is used compared to LP. The power management strategy however did not impact the accuracy of this approach, as precise results are found in both cases. This is justified by DPAM's small cost deviations of around 10^{-8} when confronted to LP.

The distance between the proposed solution at each optimization calculation and its initial design (DistI) is evaluated, as well as the distance between said solution and the HRPS reference solution found through problem linearization (DistR).

These indicators are analyzed to verify if this approach is viable. While smaller values for DistR are sought after, meaning the solutions found by the approach converge towards the global optimum values, smaller values for DistI on the other hand mean the approach is unable to look at other configurations in the feasible domain outside the initial point's neighborhood to improve the total cost.

Similar tendencies, observed in Table 2.3, are found when implementing either LP or DPAM for power management of the bi-level approach.

Table 2.3: Bi-level approaches convergence analysis, focusing on the number of solutions whose distance from the initial point (DistI) or reference (DistR) is under a specified value for the different design variables

	$\mathcal{BL}$ + LP					$\mathcal{BL}$ + DPAM				
DistI	$E_{\max}$	$P_{\max}$	S_{PV}	S_{W}	E_{ini}	$E_{\max}$	$P_{\max}$	S_{PV}	S_{W}	E_{ini}
$\leqslant$1	100	100	100	100	100	100	100	100	100	100
$\leqslant$0.1	20	8	10	9	15	30	23	20	21	66
$\leqslant$0.01	1	0	1	0	1	12	14	14	13	51
$\leqslant$1e-3	0	0	1	0	1	10	14	14	13	46
$\leqslant$1e-4	0	0	1	0	1	8	10	12	10	42
$\leqslant$1e-5	0	0	1	0	1	4	5	8	4	39
$\leqslant$1e-6	0	0	1	0	1	4	4	4	3	35

DistR										
⩽1	100	100	100	100	100	100	100	100	100	100
⩽0.1	98	98	100	100	61	38	84	88	82	18
⩽0.01	98	98	100	100	24	15	83	85	81	7
⩽1e-3	97	97	100	100	19	10	83	85	81	6
⩽1e-4	92	97	100	100	16	8	83	85	81	6
⩽1e-5	88	97	100	100	13	6	82	83	81	6
⩽1e-6	79	95	100	100	10	5	81	83	78	4

Table 2.3: Bi-level approaches convergence analysis, focusing on the number of solutions whose distance from the initial point (DistI) or reference (DistR) is under a specified value for the different design variables - continued

It is deduced that both applications of the bi-level approach have good convergence rates for the different variables. However, the convergence of $\mathcal{BL}$+LP is better. $\mathcal{BL}$+DPAM's convergence can be improved by enhancing the accuracy of DPAM, requiring finer meshing.

For the first variant, by not considering parameter E_{ini} as it has a negligible impact in this problem, a high convergence rate of 79% is achieved. Furthermore, only a limited number of proposed solutions remain in the same neighborhood as the algorithm's initialization, which goes to prove the robustness of the bi-level approach.

Iterative approach analysis

The previous convergence analysis is conducted on the iterative approach as well. Table 2.4 compiles the results that are found:

	$\mathcal{IT}$ + LP					$\mathcal{IT}$ + DPAM				
DistI	$E_{\max}$	$P_{\max}$	S_{PV}	S_{W}	E_{ini}	$E_{\max}$	$P_{\max}$	S_{PV}	S_{W}	E_{ini}
⩽1	100	100	100	100	100	100	100	100	100	100
⩽0.1	40	100	10	9	42	46	100	10	9	36
⩽0.01	32	100	1	0	3	37	100	1	0	6
⩽1e-3	32	100	1	0	2	32	100	1	0	4
⩽1e-4	32	100	1	0	1	30	98	1	0	1
⩽1e-5	32	96	0	0	1	30	98	1	0	1
⩽1e-6	32	95	0	0	1	30	98	1	0	1
DistR										
⩽1	100	100	100	100	100	100	100	100	100	100
⩽0.1	27	9	100	100	25	27	9	100	100	22
⩽0.01	2	0	100	100	16	2	0	100	100	12
⩽1e-3	0	0	100	100	12	0	0	100	100	9
⩽1e-4	0	0	100	100	12	0	0	100	100	9
⩽1e-5	0	0	100	100	12	0	0	100	100	9
⩽1e-6	0	0	100	100	12	0	0	100	100	9

Table 2.4: Iterative approaches convergence analysis, focusing on the number of solutions whose distance from the initial point (DistI) or reference (DistR) is under a specified value for the different design variables

If similar conclusions to the bi-level strategy are made for the iterative approach when considering S_{PV} and S_{W}, the same cannot be said when observing $E_{\max}$ and $P_{\max}$. This can be explained in part by analyzing the impact of command constraints on design optimization.

Optimization of the command determines the values for $\boldsymbol{E_{sto}}$ and $\boldsymbol{P_{sto}}$ that are constrained between the upper and lower bounds, delimited by $E_{\max}$ and $P_{\max}$. The design optimization conducted afterwards will then logically seek to lower the values of $E_{\max}$ and $P_{\max}$ as much as possible with respect to their constraints due to their impact on the cost for a fixed command.

These constraints are in turn directly linked to the values of $\boldsymbol{E_{sto}}$ and $\boldsymbol{P_{sto}}$ found previously. This is repeated at each iteration, resulting in only smaller values for these design variables. It can be concluded that while the approach still converges for this application, the search direction is imposed for these variables as opposed to S_{PV} and S_{W}. Relaxing the command constraints during controller optimization can help solve this issue.

A new iterative approach, referred to as $\mathcal{IT}_{\mathrm{Imp}}$, is implemented in this regard. This approach is based on the same scheme as the iterative framework without imposing command constraint 2.38.e. This is applied for all iterations except the last one to ensure that the obtained solution is consistent.

Table 2.5 presents the results of this approach, and compares them to the first application of the iterative approach.

$\mathcal{IT}$ + LP		$\mathcal{IT}$ + DPAM		$\mathcal{IT}_{\mathrm{Imp}}$ + LP		$\mathcal{IT}_{\mathrm{Imp}}$ + DPAM	
CT	D	CT	D	CT	D	CT	D
8.39	1.13e-3	1.30e3	1.39-3	3.58	2.563e-16	1.97e3	6.24e-4

Table 2.5: Comparison between the different iterative strategies

The iterative approach with relaxed command constraints finds better solutions compared to the initial implementation of the iterative scheme. The precision found for the solution is similar to that of the bi-level approach. Indicators DistI and DistR are recalculated as well. The different results are shown in Table 2.6.

Table 2.6: Iterative approach with relaxed command constraints approaches convergence analysis, focusing on the number of solutions whose distance from the initial point (DistI) or reference (DistR) is under a specified value for the different design variables

	$\mathcal{IT}_{\mathrm{Imp}}$ + LP					$\mathcal{IT}_{\mathrm{Imp}}$ + DPAM				
DistI	$E_{\max}$	$P_{\max}$	S_{PV}	S_{W}	E_{ini}	$E_{\max}$	$P_{\max}$	S_{PV}	S_{W}	E_{ini}
$\leqslant$1	100	100	100	100	100	100	100	100	100	100
$\leqslant$0.1	16	9	10	9	100	11	9	10	9	64
$\leqslant$0.01	1	0	1	0	100	0	0	1	0	50
$\leqslant$1e-3	0	0	1	0	100	0	0	1	0	32
$\leqslant$1e-4	0	0	1	0	100	0	0	1	0	7
$\leqslant$1e-5	0	0	1	0	100	0	0	1	0	2
$\leqslant$1e-6	0	0	1	0	100	0	0	1	0	1

DistR										
⩽1	100	100	100	100	100	100	100	100	100	100
⩽0.1	22	100	100	100	10	3	100	100	100	11
⩽0.01	12	100	100	100	2	3	100	100	100	2
⩽1e-3	12	100	100	100	1	3	100	100	100	1
⩽1e-4	12	100	100	100	1	3	100	100	100	1
⩽1e-5	12	100	100	100	1	3	100	100	100	1
⩽1e-6	12	100	100	100	1	3	100	100	100	1

Table 2.6: Iterative approach with relaxed command constraints approaches convergence analysis, focusing on the number of solutions whose distance from the initial point (DistI) or reference (DistR) is under a specified value for the different design variables - continued

It can be observed that the convergence for the design variables has greatly improved. However, the convergence rate for all values towards the global optimum is still not as high as when applying the bi-level approach. When measured for all design variables except for E_{ini}, it is estimated at 12% as opposed to 79% when using the bi-level strategy. It is deduced that the iterative framework, while it can lead to the global optimum, is still more sensitive to its design variable initialization compared to the bi-level approach.

2.5 Alternative design approaches

Other systemic design approaches can be proposed as well that do not fall within the mentioned Plant/Controller schemes. During this research project, three different alternatives are proposed and are adapted for the HEV design problem.

The main idea behind each one of these strategies is to overcome the unreasonable delays and convergence difficulties that occur when implementing the system optimization frameworks explored earlier and using heavy black box models. To achieve this, these strategies focus on altering the design optimization problem while applying the guidelines of the selected systemic design scheme, as explained afterwards.

While these methods are aimed at improving the calculation time and robustness of the Plant/Controller frameworks, they can lead to suboptimal solutions to the main optimization problem expressed in 2.3. Under certain conditions however, these methods can still guarantee a global optimum.

2.5.1 Approach based on the simultaneous scheme: $\mathcal{A}_1$

The main limitation when applying the simultaneous approach is the presence of a large number of variables. Different alternatives can be proposed to overcome this challenge.

One option, referred to as $\mathcal{A}_1$ in this work, is to reduce the number of command variables by introducing a control strategy $\boldsymbol{R}$ which is adjusted using a smaller number of parameters $\boldsymbol{p}$.

The optimization problem solved in this case is expressed as:

$$\underset{\boldsymbol{d},\boldsymbol{p}}{\text{minimize}} \quad J(\boldsymbol{d},\boldsymbol{R}(\boldsymbol{p})) = \alpha Inv(\boldsymbol{d}) + \beta \sum_{t_0}^{t_\mathrm{f}-\Delta t} L(\boldsymbol{d},\boldsymbol{x}(t),\boldsymbol{R}(\boldsymbol{p},t),t)\Delta t \tag{2.41a}$$

$$\text{subject to} \quad \boldsymbol{x}(t+\Delta t) = \boldsymbol{f}(\boldsymbol{d},\boldsymbol{x}(t),\boldsymbol{R}(\boldsymbol{p},t),t)\Delta t + \boldsymbol{x}(t) \tag{2.41b}$$

$$\boldsymbol{x}(t_0) = \boldsymbol{x_0}(\boldsymbol{d}) \tag{2.41c}$$

$$\boldsymbol{x}(t_\mathrm{f}) = \boldsymbol{x_\mathbf{f}}(\boldsymbol{d}) \tag{2.41d}$$

$$\boldsymbol{g}(\boldsymbol{d},\boldsymbol{x}(t),\boldsymbol{R}(\boldsymbol{p},t),t) \leq 0 \tag{2.41e}$$

$$\boldsymbol{h}(\boldsymbol{d},\boldsymbol{x}(t),\boldsymbol{R}(\boldsymbol{p},t),t) = 0 \tag{2.41f}$$

$$\boldsymbol{k}(\boldsymbol{d}) \leq 0 \tag{2.41g}$$

$$\boldsymbol{l}(\boldsymbol{d}) = 0 \tag{2.41h}$$

$$\boldsymbol{x}(t) \in [\boldsymbol{x_{\min}}(\boldsymbol{d},t), \boldsymbol{x_{\max}}(\boldsymbol{d},t)] \tag{2.41i}$$

$$\boldsymbol{R}(\boldsymbol{p},t) \in [\boldsymbol{u_{\min}}(\boldsymbol{d},t), \boldsymbol{u_{\max}}(\boldsymbol{d},t)] \tag{2.41j}$$

$$\boldsymbol{d} \in [\boldsymbol{d_{\min}}, \boldsymbol{d_{\max}}] \tag{2.41k}$$

Global optimality is guaranteed if the control strategy $\boldsymbol{R}$ always leads to the optimal cost of the controller for a specific set of parameters $\boldsymbol{p}$ when updating the design variables. A high performance rule-based strategy can be expected to lead to similar results as well when implemented.

2.5.2 Approach based on the bi-level scheme: $\mathcal{A}_2$

Likewise, several options can be explored to improve the use of the bi-level scheme. One of these possibilities, addressed as $\mathcal{A}_2$, consists in adopting substitution models at the top level to enable faster iterations.

Since both the total cost and constraints functions for design optimization generally require long calculation times, they can be replaced with polynomial models for example. The top problem of the bi-level approach is then simplified in this way:

$$\underset{\boldsymbol{d}}{\text{minimize}} \quad J_\mathrm{s}(\boldsymbol{d}) \tag{2.42a}$$

$$\text{subject to} \quad \boldsymbol{k_s}(\boldsymbol{d}) \leq 0 \tag{2.42b}$$

$$\boldsymbol{l_s}(\boldsymbol{d}) = 0 \tag{2.42c}$$

$$\boldsymbol{d} \in [\boldsymbol{d_{\min}}, \boldsymbol{d_{\max}}] \tag{2.42d}$$

where J_s is the simplified cost function, and $\boldsymbol{g_\mathbf{s}}$ and $\boldsymbol{h_\mathbf{s}}$ are the functions replacing $\boldsymbol{g}$ and $\boldsymbol{h}$ respectively.

The use of substitution models also increases the optimization's robustness in the sense that they do not fail for some design configurations, which can be the case when adopting more complex models. For instance, issues related to mesh generation can be encountered for some machine designs when using FE models. In contrast, a significant loss in precision is to be expected as well as running the risk of producing physically incoherent outputs.

2.5.3 Approach based on the iterative scheme: $\mathcal{A}_3$

Finally, $\mathcal{A}_3$ is another alternative proposed for the iterative scheme. It is based on the substitution of the utility function J in the design optimization problem 2.39 with an equivalent

function J_e.

This variant will then deliver the same solution as the first iterative approach when the following condition is valid for all system controls:

$$\underset{\boldsymbol{d}}{\operatorname{argmin}} \quad J(\boldsymbol{d}) \quad = \quad \underset{\boldsymbol{d}}{\operatorname{argmin}} \quad J_e(\boldsymbol{d}) \tag{2.43}$$

This strategy is used to improve the optimization's calculation time by adopting faster functions, improve the robustness of the original approach when providing easier to evaluate functions and/or increase the model's precision. This is possible in our case by coupling cycle reduction techniques and the direct use of FE models for hybrid powertrain optimization, as it is detailed further in Chapter 4.

Conclusion

Solving the hybrid powertrain optimization problem using the Plant/Controller optimization formulations allows for the investigation of multiple possibilities to find a system-optimal solution. The most promising frameworks, the bi-level and iterative schemes, decompose the coupled system design and controller optimizations. More adequate algorithms are implemented to solve each of these problems.

If different techniques are explored for controller optimization, such as direct optimization and CO, the most commonly applied approaches remain those deriving from the Calculus of Variations as in PMP and those based on solving HJB equation like DP. Proposed improvements such as DPAM help reduce calculation times while improving the solution to the optimization problem.

The HRPS problem, belonging to the same class of problems as drive-cycle HEV optimization, is then studied. Since this problem is based on piece-wise linear models, faster computation times are obtained and a reference solution is easily provided through linear optimization. This explains why it is better suited as an early benchmark to compare the different proposed control strategies and systemic design frameworks before selecting the most promising approaches for the main research project.

For power management optimization, NLP and CO manage to find precise solutions, but their long calculation times and non convergence issues encountered for long design cycle restrict their use on only small cycles. PMP is also found to be inadequate for HRPS controller optimization as the optimal command is at the specified boundaries, and while NLP and CO are not considered for the remainder of this study, PMP still needs to be further investigated on other applications. On the other hand, DP and DPAM prove to be efficient strategies with the latter providing the best results in reasonable calculation times. DPAM was selected for HRPS power management and will be applied as an efficient hybrid powertrain optimal control strategy afterwards as well.

Systemic design approaches are implemented afterwards. The simultaneous approach is applied at first but it does not converge towards an optimal solution due to the presence of a large number of variables. Meanwhile, the bi-level approach provides precise results when adopting both LP and DPAM for power management and has a high convergence rate but requires long calculation times. In contrast, the iterative approach is 10 times faster but leads to sub-optimal results and lower convergence rates. This is mainly due to the impact

of the command constraints which, when relaxed, lead to greater accuracy and improved performance. Both these frameworks are compared further on the HEV optimization problem. Other alternative strategies ($\mathcal{A}_1$, $\mathcal{A}_2$ and $\mathcal{A}_3$), based on these frameworks and seeking to overcome their main limitations, will be implemented and applied as well.

Chapter 3

Hybrid Electric Vehicle application

Contents

Introduction

In this chapter, the hybrid powertrain optimization problem is explained in greater detail. At first, the application scope as well as an overview of the system model are given before presenting the design, command and state variables afterwards.

A second part is dedicated to the presentation of the powertrain's components models which consider the impact of the different optimization variables, with special emphasis given to the EM model as the main adjustable element of the optimization applications.

The command and design constraints are enumerated later on, allowing for the hybrid powertrain design optimization problem, as well as the hybrid vehicle power management problem, to be defined.

3.1 System presentation

In this work, a C-segment vehicle equipped with a parallel hybrid powertrain is considered. This means it incorporates an ICE and an EM, both of which can provide, either simultaneously or separately, the required torque to the wheels. The different modes presented in Chapter 1 are possible in this case: Regenerative braking (Regen), ZEV, conventional, Boost and Generation. The different components of the powertrain are shown in Figure 3.1.

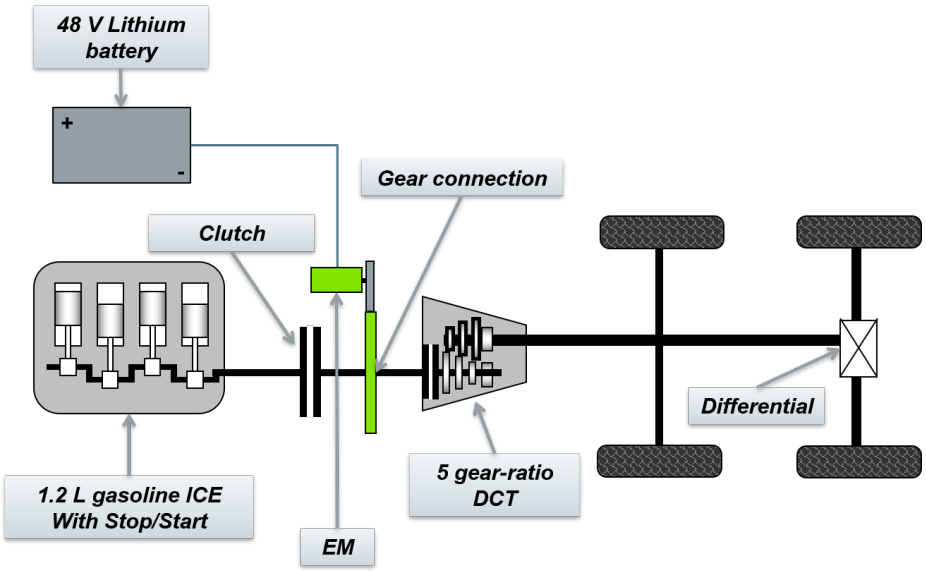

Figure 3.1: Studied powertrain

The engine, a 1.2-liter gasoline ICE, is equipped with a starter. When the vehicle is in motion, the clutch between the ICE and EM allows for the ICE to be turned off while the EM ensures the traction or regenerative braking. Fuel consumption in low efficiency areas and unnecessary pumping losses during braking as well as standstill are eliminated.

The EM block on the other hand, referring to both the machine and its inverter, is always connected to the transmission shaft via a gear set and is powered by a 48 V Lithium battery. For this work, a permanent magnet synchronous machine (PMSM), commonly applied for electric mobility [113, 114, 115, 116], is considered. This machine is shown in Figure 3.2.

The hybrid powertrain optimization problem shall consider either a specific driving cycle or a set of drive-cycles to evaluate the vehicle's performance, discretized at time step Δt. In this research project, the machine, its inverter as well as its gear connection are optimized. Thus, design variables $\boldsymbol{d}$ are introduced and will refer to parameters linked to these powertrain components. The design of the other HEV elements remains the same and is conserved during the optimization process.

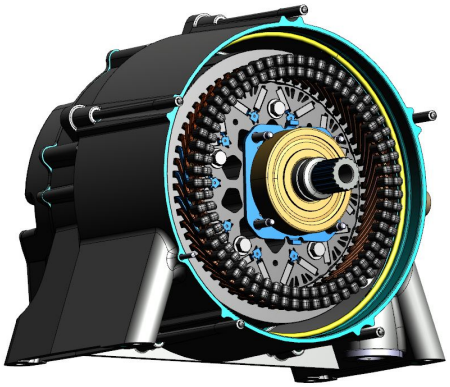

Figure 3.2: Example of studied PMSM

The system block, shown in Figure 3.3, enables the calculation of the instantaneous fuel consumption $\boldsymbol{L}$, expressed in g/s. It considers, in addition to the driving cycle speed $\boldsymbol{v}$, expressed in m/s, the impact of the battery's state of charge, the engine's starter command and the gear switching. By adopting the same term definitions as in Chapter 2, $\boldsymbol{x}$ has three components: the state of charge of the battery (SoC), the selected gear and the state of the engine.

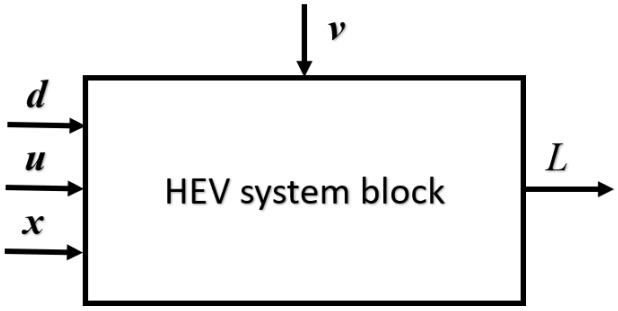

Figure 3.3: System block.

$\boldsymbol{u}$, the command variable, is directly linked to the variations of $\boldsymbol{x}$ and as a result also has three components ($\boldsymbol{u_1}$: ΔSoC/Δt, $\boldsymbol{u_2}$: gear switch, $\boldsymbol{u_3}$: starter command). Thus, the evolution function $\boldsymbol{F}$ only depends on the command variable and corresponds to the identity function $\boldsymbol{Id}$, while considering the discrete/continuous nature of each variable. $\boldsymbol{x}$ is then directly deduced from $\boldsymbol{u}$:

$$x_1(t+\Delta t) = u_1(t)\Delta t + x_1(t) \tag{3.1a}$$
$$x_2(t+\Delta t) = u_2(t) + x_2(t) \tag{3.1b}$$
$$x_3(t+\Delta t) = u_3(t) + x_3(t) \tag{3.1c}$$

The system model assumes isothermal conditions for all powertrain components and data is provided by Valeo's simulation platform. A global overview of the system block is presented in Figure 3.4. This figure summarizes how the different component blocks interact.

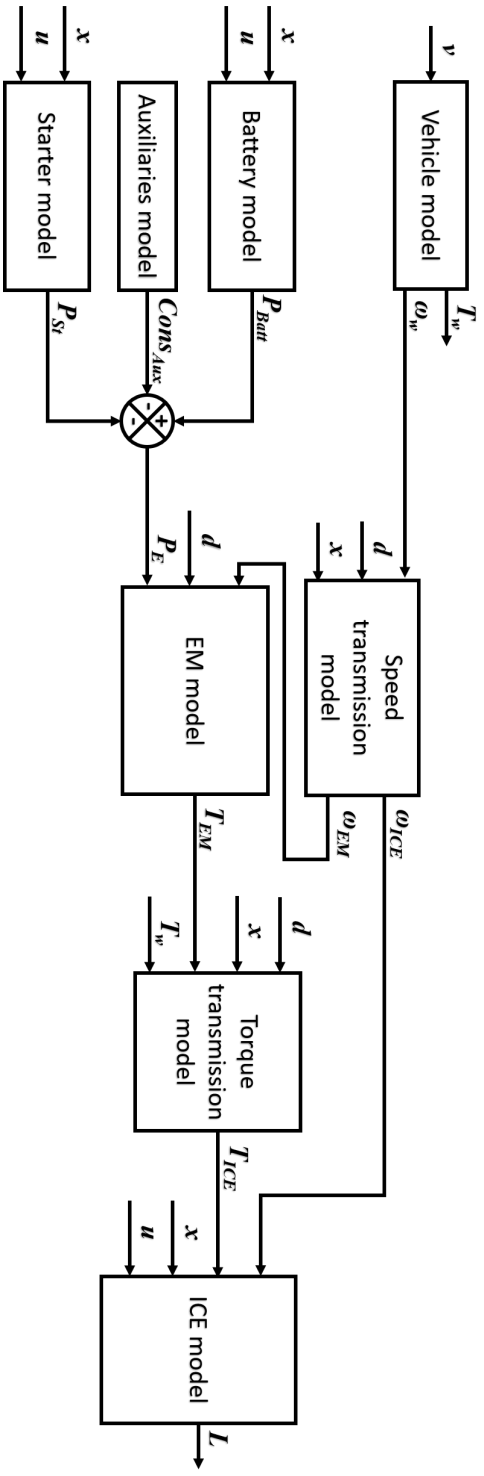

Figure 3.4: System block A0 level

The powertrain provides the required torque at the wheels $\boldsymbol{T_w}$, expressed in N.m, at each instant, to negate the driving resistances applied to the vehicle when it is moving and to achieve the required speed $\boldsymbol{v}$. $\boldsymbol{T_w}$ is given by the vehicle model, which considers the vehicle parameters and its speed. The wheel speed $\boldsymbol{\omega_w}$ in rpm is also an output of this model as shown in Figure 3.4.

The speed transmission model links the rotation speeds of the EM and ICE to $\boldsymbol{\omega_w}$, referred to as $\boldsymbol{\omega_{EM}}$ and $\boldsymbol{\omega_{ICE}}$ in rpm. This model is impacted by the selected gear and hence $\boldsymbol{x}$, as well as the design parameters.

The EM model considers the machine parameters as well as the provided electrical power $\boldsymbol{P_E}$ in W and the value for $\boldsymbol{\omega_{EM}}$, to deliver the mechanical torque $\boldsymbol{T_{EM}}$ in N.m.

The balance between the power provided by the powertrain and the power required at the wheels needs to be satisfied at every instant. Along these lines, a torque transmission model is used to calculate the torque to be delivered by the ICE from the values of $T_{\mathrm{EM}}(\mathrm{t})$, $T_{\mathrm{w}}(\mathrm{t})$, and as it is the case with the speed transmission model, based on $\boldsymbol{d}$ and $\boldsymbol{x}$ as well.

The fuel consumption is then evaluated using both the torque provided by the engine and its speed as inputs. The ICE block is displayed in Figure 3.8 with the cost functional $\boldsymbol{L}$ referring directly to the fuel consumption value. This value is also impacted by the engine's state as well as gear shifting, since the latter leads to non negligible mechanical losses to be considered.

On another note, the electrical power balance needs to be addressed as well. This is expressed by the following equation:

$$P_{\mathrm{Batt}}(t) = P_{\mathrm{E}}(t) + P_{\mathrm{St}}(t) + Cons_{\mathrm{Aux}}(t) \tag{3.2}$$

where $\boldsymbol{P_{Batt}}$ is the battery's output power in W, retrieved from the battery's model block.

Meanwhile, $\boldsymbol{Cons_{Aux}}$ represents the consumption of the different vehicle auxiliaries such as the lights, wipers and engine control unit throughout the cycle in W. This value is directly deduced from the auxiliaries model, as presented in Figure 3.4.

$\boldsymbol{P_{St}}$ on the other hand refers to the electric consumption in W of the starter used for restarting the engine when it is turned off and is a direct output of the starter block.

The previously mentioned variables are subject to multiple constraints, related to the limitations of their respective powertrain components, as well as the powertrain requirements for this application. Once these constraints as well as the cost function are defined, the design optimization problem is determined.

3.2 Vehicle representation

For the vehicle model, a backward approach is adopted: the target speed, imposed by the driving cycle, is always achieved and no speed regulation or driver model is considered.

On the other hand, the mechanical energy released by the two powertrain motors is not fully converted into kinetic energy that can be used by the vehicle to move. In fact, some

of this energy is drained by different driving resistances when it is in motion.

These forces are split into: $\boldsymbol{F_A}$ the aerodynamic drag, $\boldsymbol{F_R}$ the rolling resistance, $\boldsymbol{F_P}$ the vehicle's weight and $\boldsymbol{F_C}$ the contact force with the road surface. These forces, expressed in N, are shown in Figure 3.5.

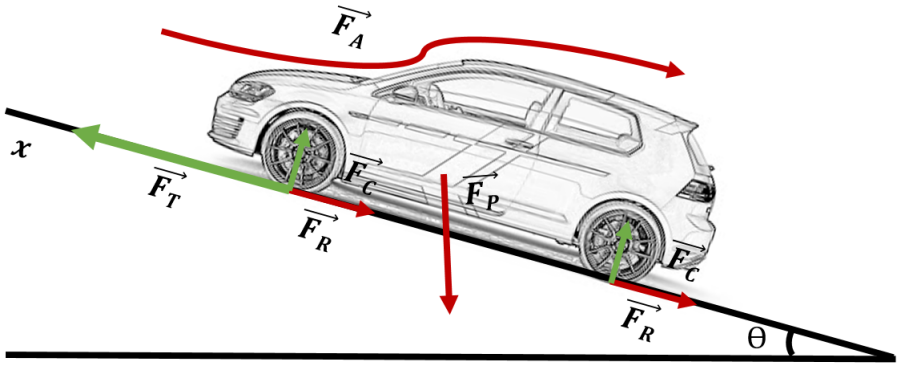

Figure 3.5: External driving resistances

When brakes are applied, the braking force $\boldsymbol{F_B}$ is considered as well. Projection on the longitudinal axis leads to the following dynamic equation:

$$Mv'(t) = F_{\mathrm{T}}(t) - F_{\mathrm{P}}(t)sin(\Theta(t)) - F_{\mathrm{R}}(t) - F_{\mathrm{A}}(t) - F_{\mathrm{B}}(t) \tag{3.3}$$

where M is the mass of the vehicle in kg and $\boldsymbol{\Theta}$ the slope angle in rad. $\boldsymbol{F_P}$ is expressed as:

$$F_{\mathrm{P}}(t) = Mg \tag{3.4}$$

where g is the acceleration of gravity, equal to 9.81 m/s^2 in this work.

Meanwhile, $\boldsymbol{F_R}$ makes it possible to quantify the losses linked to the vehicle's contact with the ground. This force, referred to as the rolling resistance, is essentially due to the deformation of the tyres in contact with the road surface [117] and is generally expressed as:

$$F_{\mathrm{R}}(t) = MgC_{\mathrm{R}} + Mgk_{\mathrm{R}}v(t) \tag{3.5}$$

where C_{R} and k_{R} are the rolling characteristics of the selected tyres, with k_{R} in s/m. This expression is only valid when the vehicle is in motion without any tyre slip. $\boldsymbol{F_R}$ is equal to zero when the car is at full stop.

The aerodynamic drag is considered as well. This force, which is the primary reason for fuel consumption at high speeds, is impacted by the vehicle's frontal surface and global

shape, as well as the latitude and weather conditions amongst other factors [118]. In the context of this project however, $\boldsymbol{F_A}$ is defined as:

$$F_{\mathrm{A}}(t) = 0.5\rho_{\mathrm{Air}} S C_{\mathrm{x}} {v_{\mathrm{r}}}^2 \tag{3.6}$$

where ρ_{Air} is the air density, equal in this application to 1.2 kg/m^3, S is the projected frontal surface in m^2 and C_{x} the drag coefficient. $\boldsymbol{v_r}$ is the relative speed of the wind in the opposite direction of vehicle motion in m/s. It should be noted that several authors tend to combine both the rolling resistance and aerodynamic drag into one term referred to as the global friction force [29, 54].

This model holds true in on-road conditions as well as during laboratory tests. In fact, numerous measures are applied to ensure similar findings between the two settings, like the addition of roller benches connected to air blowing systems [119, 120]. Thus, the same model can be used for both RDE assessment as well as laboratory evaluation of the consumption over specific driving cycles.

In case of indoor test settings, $\boldsymbol{v_r}$ is equal to $\boldsymbol{v}$ and the slope $\boldsymbol{\Theta}$ is equal to zero. When brakes are not applied and no slip is considered, the traction force is then equal to:

$$F_{\mathrm{T}}(t) = M\frac{v(t+\Delta t) - v(t)}{\Delta t} + MgC_{\mathrm{R}} + Mgk_{\mathrm{R}}v(t) + 0.5\rho S C_{\mathrm{x}} v^2(t) \tag{3.7}$$

Based on this, the torque to be provided to the wheels is equal to:

$$T_{\mathrm{w}}(t) = rF_{\mathrm{T}}(t) \tag{3.8}$$

where r is the wheel radius in m. The wheel rotation speed is deduced as well:

$$\omega_{\mathrm{w}}(t) = \frac{60}{2\Pi}\frac{v(t)}{r} \tag{3.9}$$

3.3 Powertrain components

3.3.1 Battery

The battery adopts a simplified circuit model using an internal resistance $\boldsymbol{IR}$ connected in series with an open circuit voltage $\boldsymbol{OCV}$, as displayed in Figure 3.6. The battery is also characterized with a finite capacity C_{Batt} in A.s and current limit I_{max} in A for both charge and discharge. This leads to the following requirement on the command values:

$$\frac{-100 I_{\mathrm{max}}\Delta t}{C_{\mathrm{Batt}}} \leq u_1(t) \leq \frac{100 I_{\mathrm{max}}\Delta t}{C_{\mathrm{Batt}}} \tag{3.10}$$

To limit premature battery ageing, the usage of the battery is restricted between 30 % and 70 % of its total charge, which implies the following condition on the state of charge:

$$30 \leq x_1(t) \leq 70 \tag{3.11}$$

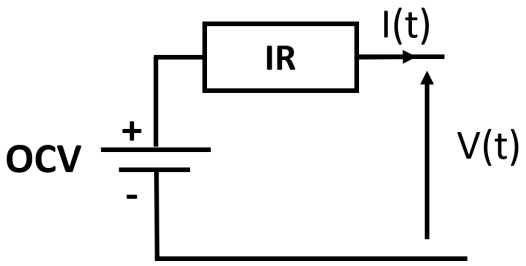

Figure 3.6: Battery circuit model. $\boldsymbol{I}$ and $\boldsymbol{V}$ are the battery's current and voltage respectively

In this range, $\boldsymbol{IR}$ and $\boldsymbol{OCV}$ values vary by less than 5% as seen in Figure 3.7. They are assumed to be independent of the SoC afterwards. Their mean values over this range, referred to as MIR and $MOCV$ in Ω and V respectively, are selected to simplify the battery model for control applications later on.

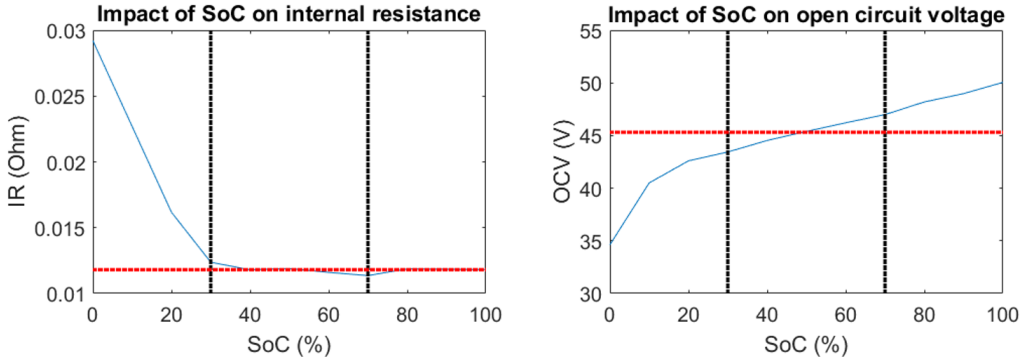

Figure 3.7: Battery parameters evolution with respect to its SoC. The black lines delimit the recommended operation region and the red line highlights the mean value

The faradaic yield, which considers the losses related to the occurrence of secondary reactions, inducing leakage currents at the electrodes that do not participate in electrochemical storage, is neglected, since the battery is based on Li-ion technology [121].

The battery's output current is then expressed as:

$$I(t) = -C_{\text{Batt}} \frac{u_1(t)}{100} \tag{3.12}$$

Finally, the battery's output power is calculated as:

$$P_{\text{Batt}}(t) = V(t)I(t) = (MOCV - MIR\ I(t))I(t) \tag{3.13}$$

$\boldsymbol{P_{\text{Batt}}}$ is split afterwards between the EM, the engine's starter and the vehicle auxiliaries.

3.3.2 Auxiliaries

The auxiliary power consumption, linked to the use of fans, windshield wipers and window lifters amongst other vehicle equipment, is considered. A constant consumption value $Cons$

in W, drawn from the vehicle's 12 V on-board network, is used to approximate this power supply.

In order to comply with the charge sustaining constraint, the auxiliary power supply is compensated by the 48 V network. This network is powered by the 48 V battery and is connected to the on-board network using a DC-to-DC converter with constant efficiency η_{DC}. The auxiliary consumption is then calculated using the following equation:

$$Cons_{\mathrm{Aux}}(t) = \frac{Cons}{\eta_{\mathrm{DC}}} \tag{3.14}$$

3.3.3 Electric machine

The electric machine is at the core of the optimization application. Thus, more emphasis is given to this component as this subsection details the selected machine architecture, then presents the design variables considered before explaining how the different inputs and models are integrated inside the EM block.

Permanent Magnet synchronous machine

Synchronous machines (SM) are a type of alternative current (AC) machines whose shaft movement is synchronised with the frequency of the supply current. These machines, like any other rotating electric motor, consist of a rotating part called a rotor and a fixed part named stator. The rotor can be located inside the stator, as it is the case in this study, or externally.

The stator consists of an outer frame and a core with windings inserted in slots, that serve as multiphase AC electromagnet. This gives the stator the ability to generate a rotating magnetic field which follows the oscillations of the supply currents.

The most common designs use three-phase windings. Six-phase windings, consisting of two offset three-phase windings at 30-degrees phase shift, are also used and are considered in this study since they allow for better vibro-acoustic performance and higher power rating. SM can also be equipped with distributed or concentrated windings, with Delta or Wye connections [122].

Meanwhile, the rotor can adopt different solutions to produce a constant magnetic field. In the case of PMSMs, permanent magnets, which are materials with high coercive force, are used. Different possibilities are offered for the rotor design in this case and are presented in Figure 3.8.

For this research project, the machine adopts a V-shape inserted magnet configuration (VI-PMSM), as seen in Figure 3.8. This rotor design is suggested as the most efficient and with the highest torque density when compared to other PMSM rotor types [123].

The working of the PMSM is then simply based on the interaction of the rotating magnetic field generated by the stator with the magnetic field of the rotor. This then creates an electromagnetic torque on the rotor's axis and the rotor poles rotate in synchronicity with the stator's magnetic field.

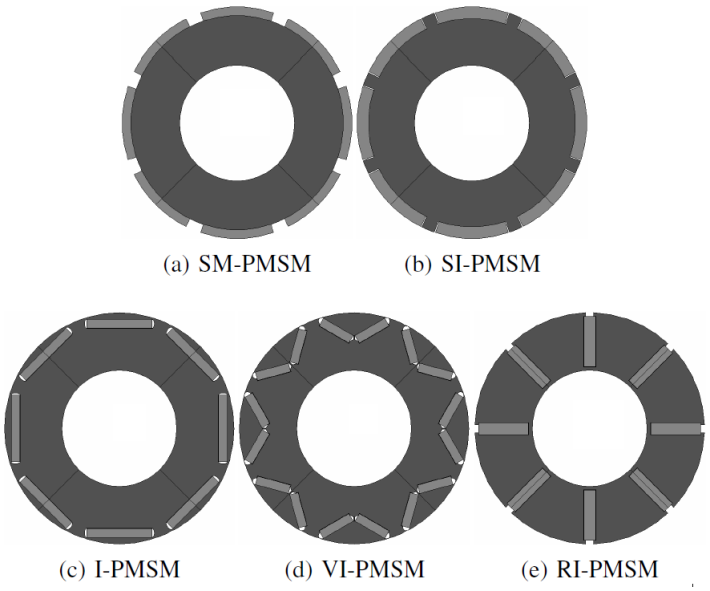

Figure 3.8: Main permanent-magnet excited rotor types [123]. SM: Surface mounted - SI: Surface inserted - I: Inserted - VI: V inserted - RI: Radially inserted

Inverter

Since the studied machine is connected to a battery, the use of an inverter is required. This device converts the direct current (DC) power supply to an alternating current (AC) power supply of variable magnitude and frequency.

In order to do so, the inverter of the studied hybrid powertrain uses 6 MOS field effect transistors (MOSFET) (12 when using a six-phase configuration), connected to form a three-phase full bridge converter architecture, as shown in Figure 3.9. This inverter, coupled with the power supply and a control system [124], produces currents of the desired characteristics pulsating through the different phase windings.

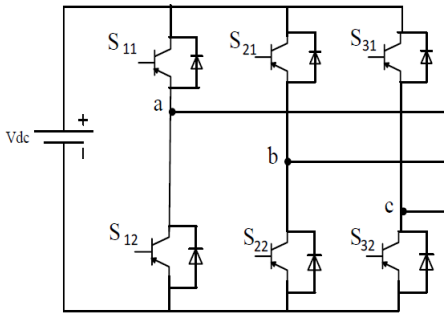

Figure 3.9: Three-phase full bridge inverter

If the output waveforms of ideal inverters should be sinusoidal, the waveform of practical inverters are non-sinusoidal and contain undesirable distortions, also known as harmonics. This is directly linked to the applied switching strategy. In this work, two switching strategies

are used: Pulse Width Modulation (PWM) and Full Wave (FW). The PWM strategy is selected for less output harmonic content while the FW strategy allows for less switching losses and higher current magnitudes.

EM losses

In order to evaluate the mechanical torque of the machine for a certain electrical power input, the machine losses $Losses_{\mathrm{EM}}$ need to be defined. In this study, they are expressed as:

$$Losses_{\mathrm{EM}} = Losses_{\mathrm{Mech}} + Losses_{\mathrm{Joule}} + Losses_{\mathrm{Iron}} + Losses_{\mathrm{Inverter}} \tag{3.15}$$

with $Losses_{\mathrm{Mech}}$, $Losses_{\mathrm{Joule}}$, $Losses_{\mathrm{Iron}}$ and $Losses_{\mathrm{Inverter}}$ referring to the mechanical, Joule, iron and inverter losses respectively in W.

Since the selected machine is water-cooled at the external surface of the stator, and due to the shape of the rotor, the machine's mechanical losses are mainly due to friction occurring at the bearings. $Losses_{\mathrm{Mech}}$ is then equal to:

$$Losses_{\mathrm{Mech}} = T_{\mathrm{d}}\omega_{\mathrm{EM}} + K_{\mathrm{f}}{\omega_{\mathrm{EM}}}^2 \tag{3.16}$$

where T_{d} and K_{f} are experimentally deduced coefficients expressed in W/rpm and W/rpm^2 respectively.

The stator winding is supposed to be a balanced and direct system. Under the first order harmonic approximation, the currents injected in a three-phase machine for example are expressed as:

$$i_{\mathrm{a}}(t) = Isin(2\Pi ft + \phi) \tag{3.17a}$$

$$i_{\mathrm{b}}(t) = Isin(2\Pi ft + \phi + \frac{2\Pi}{3}) \tag{3.17b}$$

$$i_{\mathrm{c}}(t) = Isin(2\Pi ft + \phi - \frac{2\Pi}{3}) \tag{3.17c}$$

where I is the current magnitude in A and ϕ the current phase in rad. The Joule losses are calculated as a a sum of the DC and AC Joule losses. The former, also known as copper losses, can be expressed as:

$$Losses_{\mathrm{DC}} = k_{\mathrm{Dist}} N_{\mathrm{ph}} R_{\mathrm{s}} \frac{I^2}{2} \tag{3.18}$$

where R_{s} is the winding phase resistance in Ω and N_{ph} the number of winding phases. k_{Dist} is an added coefficient to consider the impact of current harmonics on the Joule losses, which depends on the inverter strategy.

Meanwhile, AC Joule losses occur when using large section conductors with dimensions that are larger than the skin depth and when the EM operates at high frequency [125, 126]. In this work, the following model is proposed:

$$Losses_{\mathrm{AC}} = (A_{\mathrm{AC}}(H_{\mathrm{con}}, L_{\mathrm{con}}){\omega_{\mathrm{EM}}}^2 + B_{\mathrm{AC}}(H_{\mathrm{con}}, L_{\mathrm{con}})\omega_{\mathrm{EM}})Losses_{\mathrm{Joule}} \tag{3.19}$$

where H_{con} and L_{con} are the height and width of the conductor respectively in mm. A_{AC} and B_{AC} are response surfaces based on simulation results obtained for various values of H_{con} and L_{con}. Deviations of less than 5% are achieved using this model as compared to the results of high fidelity models.

Iron losses are considered as well and are linked to the active parts of the machine being subjected to changing magnetic fields. This induces microscopic and macroscopic currents leading to energy losses in the ferromagnetic materials [127]. These losses are decomposed into hysteresis losses $Losses_{\text{Hys}}$, eddy currents losses $Losses_{\text{EC}}$ and excess losses $Losses_{\text{Exc}}$.

Different methods are found in literature to calculate these terms such as analytic formulas [128, 129], hysteresis [130, 131] and loss surface models [132]. They generally require the knowledge of the magnetic flux density distribution in the iron core of the designed machine, which then leads to the use of Finite Element (FE) software to guarantee precise results.

Meanwhile, analytic models are used to describe the inverter losses. These are due to the non ideal MOSFET characteristics and are decomposed into conduction losses and switching losses during the turn-on/turn-off period [133, 134]. The inverter losses are then deduced using the following expression for a Wye machine winding configuration:

$$Losses_{\text{Inverter}} = N_{\text{MOS}}((R_{\text{DS-on}} + R_{\text{D-bound}})\frac{I^2}{2} + f_{\text{Sw}}k_{\text{Sw}}MOCVI) \tag{3.20}$$

where N_{MOS} is the number of MOSFETs in the inverter, f_{Sw} is the switching frequency in kHz while $R_{\text{DS-on}}$, $R_{\text{D-bound}}$ and k_{Sw} are the selected MOSFET device characteristics referring to the on-resistance in Ω, the bounding resistance in Ω and the switching losses coefficient respectively.

In case of a Delta connection, $Losses_{\text{Inverter}}$ is calculated using the following expression:

$$Losses_{\text{Inverter}} = N_{\text{MOS}}((R_{\text{DS-on}} + R_{\text{D-bound}})\frac{3I^2}{2} + f_{\text{Sw}}k_{\text{Sw}}MOCV\sqrt{3}I) \tag{3.21}$$

Thus, it can be understood that the machine losses not only depend on the power supply and operation point of the machine, but also on its different design parameters, which are adjusted during the optimization process. This requires, as well as for the assessment of other machine outputs, the use of high granularity models to achieve an acceptable level of accuracy.

Parametric model

In this study, we have defined 27 machine parameters to give the highest degree of design flexibility. The parametric model is based on the study of various VI-PMSM projects and computer aided designs (CAD). The number of pole pairs p and the number of slots per pole N_{slot} can be modified as well as other geometrical design parameters shown in Figure 3.10.

The selected model uses distributed winding and considers 4 additionnal winding parameters that can be adjusted: the number of series and parallel conductors, referred to as N_{series} and N_{parallel} respectively, the nature of the winding connection Wnd_{Con} and the number of winding phases N_{ph}. Furthermore, an additional inverter degree of freedom is

considered for the studied optimization problem: $Speed_{\mathrm{FWM}}$. The latter refers to the machine's rotational speed as of which the inverter switches from a PWM to a FW strategy.

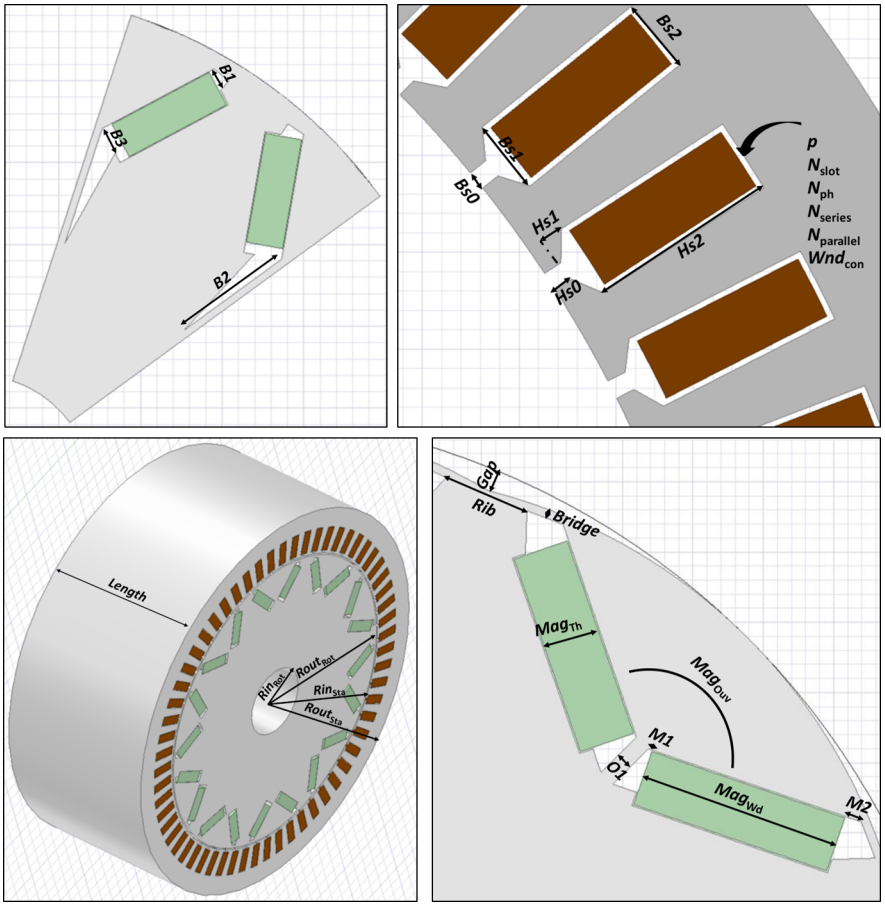

Figure 3.10: Machine design parameters

The materials used for the different machine parts are imposed. Copper is adopted as a winding conductor, while steel sheets are applied for the stator and rotor cores [135], and high performance NdFeB magnets are used to generate the rotor field.

Finite Element model

The electromagnetic phenomena occurring inside the EM is described using Maxwell's equations [136], expressed as:

$$\nabla \cdot \vec{E} = \frac{\rho}{\varepsilon} \tag{3.22a}$$

$$\nabla \cdot \vec{B} = 0 \tag{3.22b}$$

$$\nabla \times \vec{E} = -\frac{\partial \vec{B}}{\partial t} \tag{3.22c}$$

$$\nabla \times \vec{B} = \mu(\vec{J} + \varepsilon \frac{\partial \vec{E}}{\partial t}) \tag{3.22d}$$

where E is the electric field in V/m, B the magnetic flux density in Wb/m^2, ρ the electric charge density in C/m^3, J the electric current density in A/m^3 and ϵ and μ the permittivity in F/m and permeability in H/m of the material respectively.

FE simulation software, such as JMAG [137], solves these equations, by subdividing the PMSM components into smaller and simpler parts called finite elements, as shown in Figure 3.11. This space discretization, referred to as mesh, allows for the exact geometry of the machine to be considered when using the FE simulation software.

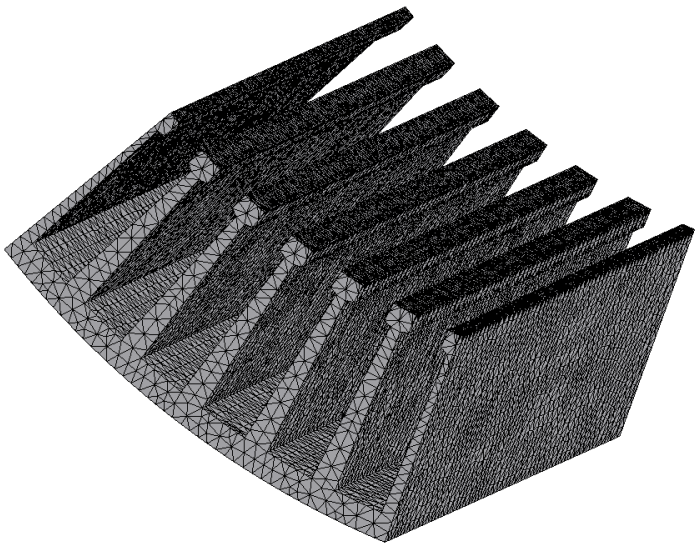

Figure 3.11: Mesh of a stator pole

Another advantage is that the FE software offers flexible and deep study parameters as well as the fact it considers the electrical circuit of the machine and the various material properties including magnetic saturation [138], leading to better results compared to other available solutions, such as reluctance networks and analytical models [54].

However, one of the main drawbacks when using FE software is the computation time, generally requiring several minutes for one operation point. In the case of radial flux machines such as the studied PMSM design, this can be greatly reduced through the use of 2D FE calculations on sections of the machine such as one pole or a pair of poles, as seen in Figures 3.12 and 3.13. With additionnal adjustments, these can provide similar results to 3D FE calculations of the whole machine.

A parametric FE model is then established. In the case of an on-load analysis, as displayed in Figure 3.14, the machine geometry, electrical circuit properties as well as the rest of the study parameters are defined in Matlab using the previously introduced parametric model and based on the values of $\boldsymbol{d}$, I, ϕ and ω_{EM}. This is then sent to JMAG via a .VBS script. Once the FE calculations have converged, the results are stored as .CSV outputs and are processed by Matlab afterwards. The requested quantities are then available as outputs of the model. The described model is also used for no-load and short circuit scenarios, providing the short-circuit current in the latter case for example.

The model's results are validated by selecting an existing Valeo machine, and comparing the parametric FE model's results to those of the more detailed 3D computer aided

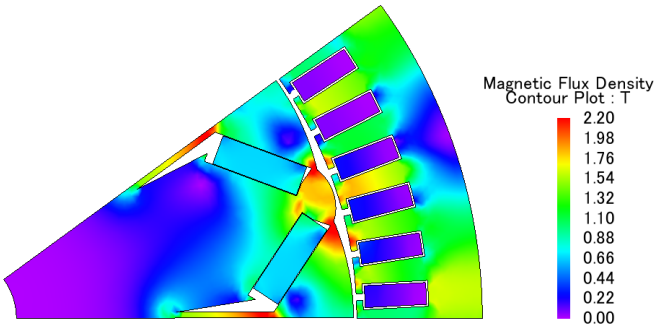

Figure 3.12: Contour plot of the magnetic flux density on a PMSM pole generated with a 2D simulation on JMAG, during on-load operation

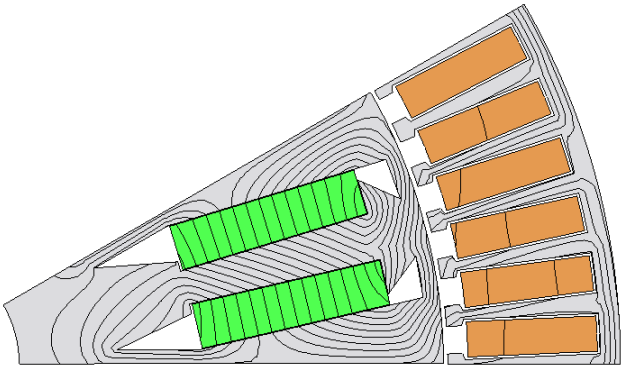

Figure 3.13: Flux lines on a PMSM pole generated with a 2D simulation on JMAG, during on-load operation

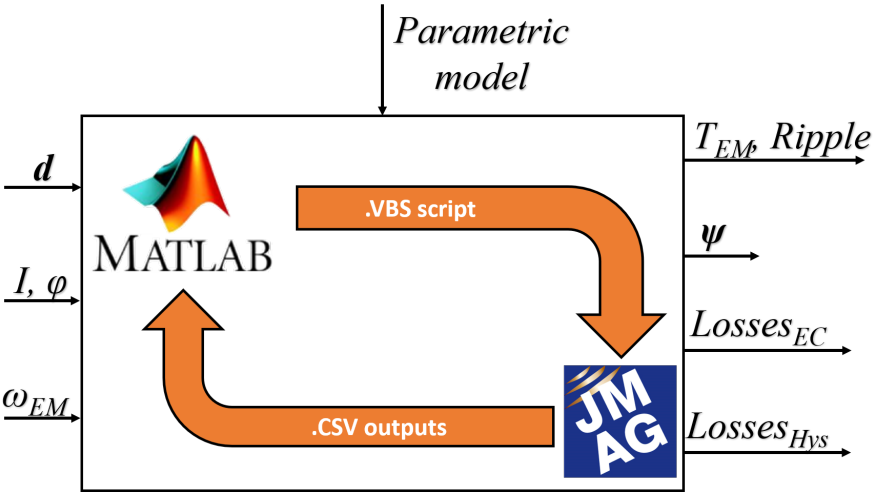

Figure 3.14: On load calculation using the FE model. *Ripple* refers to the torque ripple calculated at the studied operation point

design (CAD) FE calculations and the experimental bench test results. Acceptable devia-

tions of less than 2% with the bench test results have been found, as detailed in Appendix A.

However, besides a desirable level of precision, the model implemented to determine the machine's performance should require reasonably short calculation times. Even with the additionnal adjustments, the proposed 2D section model still requires one minute to analyze a machine's single operation point, as opposed to one hour initially for a complete 3D model[1]. Thus, other possibilities should be explored to develop a more suitable model that can be used for the optimization study.

Circuit model

The PMSM operation at different rotational speeds can be assessed using Park's representation, which converts the a-b-c variables expressed in Equation 3.17 into d-q-o (direct-quadrature-homopolar) variables as follows [139]:

$$\begin{bmatrix} Q_d \\ Q_q \\ Q_o \end{bmatrix} = \frac{2}{3} \begin{bmatrix} cos(\Theta_r) & cos(\Theta_r - \frac{2\Pi}{3}) & cos(\Theta_r + \frac{2\Pi}{3}) \\ sin(\Theta_r) & sin(\Theta_r - \frac{2\Pi}{3}) & sin(\Theta_r + \frac{2\Pi}{3}) \\ \frac{1}{2} & \frac{1}{2} & \frac{1}{2} \end{bmatrix} \begin{bmatrix} Q_a \\ Q_b \\ Q_c \end{bmatrix} \tag{3.23}$$

where $\boldsymbol{Q}$ can refer to the injected current $\boldsymbol{i}$ in A for example, as well as the phase-neutral voltage $\boldsymbol{v}$ in V and the flux-linkage $\boldsymbol{\psi}$ in Wb while Θ_r is the angular displacement of the rotor's d-axis, which is aligned with the stator's a-phase.

Through this transformation, the different AC wave forms are simplified into DC signals. Furthermore, when studying a balanced three-phase system, the homopolar component is equal to zero and the main outputs of the machine at steady state are expressed as [139]:

$$\omega = p\frac{2\Pi}{60}\omega_{\mathrm{EM}} = 2\Pi f \tag{3.24}$$

$$v_\mathrm{d} = R_\mathrm{s} i_\mathrm{d} - \omega\psi_\mathrm{q} \tag{3.25}$$

$$v_\mathrm{q} = R_\mathrm{s} i_\mathrm{q} + \omega\psi_\mathrm{d} \tag{3.26}$$

$$V = \sqrt{{v_\mathrm{d}}^2 + {v_\mathrm{q}}^2} \tag{3.27}$$

$$I = \sqrt{{i_\mathrm{d}}^2 + {i_\mathrm{q}}^2} \tag{3.28}$$

$$T_{\mathrm{El}} = \frac{N_{\mathrm{ph}}}{2} p(\psi_\mathrm{d} i_\mathrm{q} - \psi_\mathrm{q} i_\mathrm{d}) \tag{3.29}$$

[1]Comparison on the same work station equipped with an i7-6820HQ processor at 2.7 GHz and 31.8 GB of RAM, and using the Windows 10 Pro operating system

where ω is the magnetic field speed in rad/s, V the phase-neutral voltage amplitude in V and T_{El} the electromagnetic torque in N.m.

The above equations are valid for a 3-phase Wye connection machine configuration, and can be easily adjusted and extended for other studied configurations as well. The circuit model, shown in Figure 3.15, is then deduced and can be used to describe the machine.

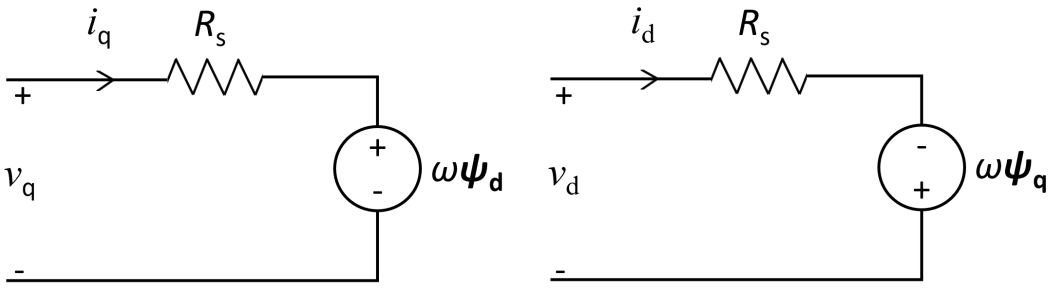

Figure 3.15: Steady state circuit model of the electric machine

In this work, for a fixed machine design, the flux linkage component values ψ_{d} and ψ_{q} are dependant on the values of i_{d} and i_{q}. The expressions for different machine losses are applied and $Losses_{\mathrm{Iron}}$ can be expressed as:

$$Losses_{\mathrm{Hys}} = k_{\mathrm{Hys}}\omega \tag{3.30a}$$

$$Losses_{\mathrm{EC}} = k_{\mathrm{EC}}\omega^2 \tag{3.30b}$$

$$Losses_{\mathrm{Exc}} = 0 \tag{3.30c}$$

where k_{Hys} and k_{EC} are the hysteresis losses coefficient in W.s/rad and the eddy current losses coefficient in W.s^2/rad^2 respectively, and are supposed to vary, similarly to the flux linkage components, only with respect to both the direct and quadrature values of the injected currents.

Response surfaces are used for these functions, based on the results from the previously introduced parametric FE model. Simulations are launched at a selected rotation speed for different values of (i_{d}, i_{q}), as seen in Figure 3.16 to determine the loss coefficient and flux linkage models. Based on the stated assumptions, these values can be used as well for other revolution speeds.

If more values for i_{d} and i_{q} are considered when establishing the response surfaces, the accuracy of the circuit model will be improved. However, the required time increases even if parallel computing has helped accelerate this process. The number of required values to select for (i_{d},i_{q}) to achieve acceptable accuracy and complete the circuit model depends on the value of I_{max} and the machine geometry.

Afterwards, the model will allow for the quick assessment of $Losses_{\mathrm{EM}}$, V as well as T_{El} for different values of (I, ϕ, ω_{EM}). T_{EM} is then deduced by the following equations:

$$T_{\mathrm{EM}} = T_{\mathrm{El}} \qquad ,\omega_{\mathrm{EM}} = 0 \tag{3.31a}$$

$$T_{\mathrm{EM}} = T_{\mathrm{El}} - \frac{Losses_{\mathrm{Mech}}}{\frac{2\Pi}{60}\omega_{\mathrm{EM}}} - \frac{Losses_{\mathrm{Iron}}}{\frac{2\Pi}{60}\omega_{\mathrm{EM}}} \quad ,\omega_{\mathrm{EM}} > 0 \tag{3.31b}$$

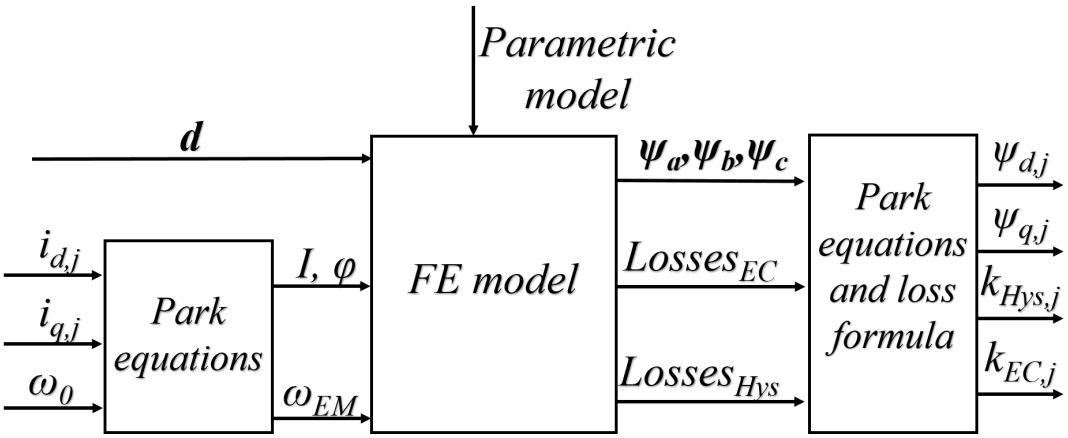

Figure 3.16: Calculation of values ($\psi_{\mathrm{d,j}}$, $\psi_{\mathrm{q,j}}$, $k_{\mathrm{Hys,j}}$, $k_{\mathrm{EC,j}}$) for values ($i_{\mathrm{d,j}}$, $i_{\mathrm{q,j}}$) at imposed speed ω_0

Losses mapping model

Once the circuit model is established for a set of design variables $\boldsymbol{d}$, a losses mapping model is calculated: first of all, the rotation speed range of the EM is discretized into discrete values ω_{i}. Afterwards, the maximum torque provided by the machine in motor mode $\boldsymbol{T_{\mathrm{EM,max}}}$ in N.m is calculated for each value of ω_{i} as followed:

$$T_{\mathrm{EM,max}}(\boldsymbol{d}, \omega_{\mathrm{i}}) = \max_{\phi} \; T_{\mathrm{EM}}(I_{\max}, \phi, \boldsymbol{d}, \omega_{\mathrm{i}}) \tag{3.32a}$$

$$\text{subject to} \quad V(I_{\max}, \phi, \boldsymbol{d}, \omega_{\mathrm{i}}) \leq V_{\max}(\boldsymbol{d}) \tag{3.32b}$$

$$\phi \in [\frac{\Pi}{2}, \Pi] \tag{3.32c}$$

where $V_{\max}$ is the maximum voltage threshold which depends on the power supply, winding configuration and inverter switching strategy. The different values for the torque and voltage are expressed using the circuit model. The minimum torque values of the machine $\boldsymbol{T_{\mathrm{EM,min}}}$ in generator mode in N.m are also calculated by solving the following optimization problem for:

$$T_{\mathrm{EM,min}}(\boldsymbol{d}, \omega_{\mathrm{i}}) = \min_{\phi} \; T_{\mathrm{EM}}(I_{\max}, \phi, \boldsymbol{d}, \omega_{\mathrm{i}}) \tag{3.33a}$$

$$\text{subject to} \quad V(I_{\max}, \phi, \boldsymbol{d}, \omega_{\mathrm{i}}) \leq V_{\max}(\boldsymbol{d}) \tag{3.33b}$$

$$\phi \in [\Pi, \frac{3\Pi}{2}] \tag{3.33c}$$

As a result, the envelope of the operation region is defined, as shown in Figure 3.17 and the machine's mechanical torque range is known. The latter is discretized into discrete values T_{j} for each value of ω_{i}.

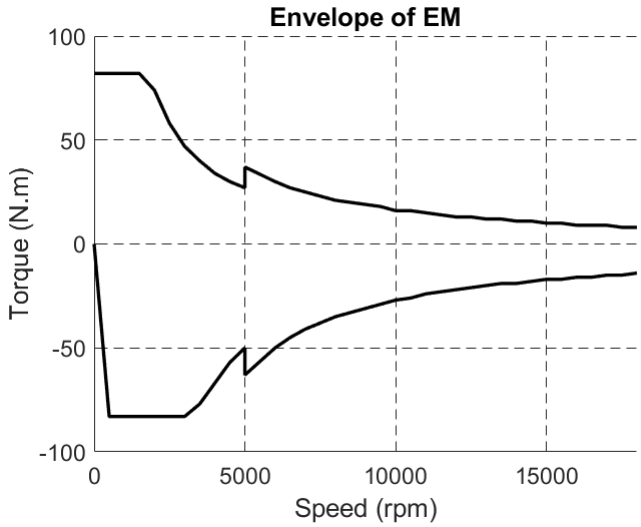

Figure 3.17: Example of EM operation envelope. The maximum torque region can be identified, as well as the maximum power region. The torque peak in the maximum power region corresponds to a change in the inverter's switching strategy ($Speed_{\mathrm{FWM}} = 5000$ rpm)

The optimal machine control for different values of $(\omega_{\mathrm{i}}, T_{\mathrm{j}})$ inside the machine operation range needs to be calculated afterwards. This is defined as values for the current supply that minimize the machine's losses at each operation point, which is expressed as:

$$\min_{I,\phi} \quad Losses_{\mathrm{EM}}(I, \phi, \omega_{\mathrm{i}}, \boldsymbol{d}) \tag{3.34a}$$

$$\text{subject to} \quad V(I, \phi, \omega_{\mathrm{i}}, \boldsymbol{d}) \leq V_{\max}(\boldsymbol{d}) \tag{3.34b}$$

$$T_{\mathrm{EM}}(I, \phi, \omega_{\mathrm{i}}, \boldsymbol{d}) = T_{\mathrm{j}} \tag{3.34c}$$

$$I \in [0, I_{\max}] \tag{3.34d}$$

$$\phi \in [\frac{\Pi}{2}, \frac{3\Pi}{2}] \tag{3.34e}$$

The losses mapping of the selected machine, delimited by its envelope is then defined, as seen in Figure 3.18. Hence, this model allows for the quick and direct assessment of the machine's optimal losses at any operation point defined by T_{EM} and ω_{EM} without additionnal time required to determine the optimal command, and are used for the hybrid powertrain's power management.

Furthermore, this losses model is better suited than the more commonly used efficiency mapping model, since it accurately assesses the machine's electrical power consumption at low power values, especially when $T_{\mathrm{EM}} = 0$ or $\omega_{\mathrm{EM}} = 0$, compared to the latter.

The electrical power consumption P_{E} of the electric machine component, which consists of the PMSM and the inverter, is expressed as:

$$P_{\mathrm{E}} = Losses_{\mathrm{EM}}(T_{\mathrm{EM}}, \omega_{\mathrm{EM}}, \boldsymbol{d}) + \frac{2\Pi}{60} T_{\mathrm{EM}} \omega_{\mathrm{EM}} \tag{3.35}$$

For imposed values of ω_{EM} and $\boldsymbol{d}$, P_{E} is a bijective function of T_{EM}, as it is strictly monotonous with respect to the latter. As a result, for any set of values (ω_{EM},$\boldsymbol{d}$, P_{E}), T_{EM}

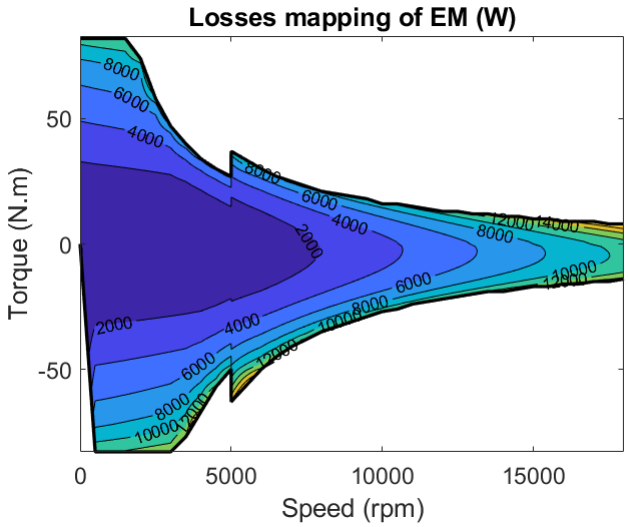

Figure 3.18: Example of EM losses mapping

can be deduced in return as well.

T_{EM}, along with ω_{EM}, need to verify the following command constraints, deduced from the same model:

$$\omega_{\mathrm{EM}}(\boldsymbol{d}, \boldsymbol{x}(t), \boldsymbol{u}(t)) - \omega_{\mathrm{EM,max}}(\boldsymbol{d}) \leq 0 \tag{3.36a}$$

$$T_{\mathrm{EM}}(\boldsymbol{d}, \boldsymbol{x}(t), \boldsymbol{u}(t)) - T_{\mathrm{EM,max}}(\boldsymbol{d}, \omega_{\mathrm{EM}}(\boldsymbol{d}, \boldsymbol{x}(t), \boldsymbol{u}(t))) \leq 0 \tag{3.36b}$$

$$T_{\mathrm{EM,min}}(\boldsymbol{d}, \omega_{\mathrm{EM}}(\boldsymbol{d}, \boldsymbol{x}(t), \boldsymbol{u}(t))) - T_{\mathrm{EM}}(\boldsymbol{d}, \boldsymbol{x}(t), \boldsymbol{u}(t)) \leq 0 \tag{3.36c}$$

3.3.4 Transmission

Having previously determined the required traction torque at the wheels, a model of the drive train is used to estimate the torque to be provided by both motors of the adopted hybrid architecture. This type of process is called "inverse" vehicle modelling, since from the desired effect, in this case the vehicle's target speed throughout the cycle, the source is defined, which is the torque to be supplied. The following reasoning is only valid in the case of positive power flow from the power converters to the wheels.

As shown in Figure 3.1, a gear connection is used to connect the EM to the engine shaft. The ratio of this torque coupler R_{GC} is a design variable that is considered during the optimization process. The torque delivered to the drive shaft is equal to:

$$T_{\mathrm{GC}}(t) = \eta_{\mathrm{GC}} R_{\mathrm{GC}} (T_{\mathrm{EM}}(t) - \Gamma_{\mathrm{EM}} \frac{\omega_{\mathrm{EM}}(t + \Delta t) - \omega_{\mathrm{EM}}(t)}{\Delta t}) \tag{3.37}$$

with η_{GC} the efficiency of the torque coupler and Γ_{EM} the inertia of the electric machine in kg.m^2. Γ_{EM} is negligible in this study, the previous equation is then simplified as:

$$T_{\mathrm{GC}}(t) = \eta_{\mathrm{GC}} R_{\mathrm{GC}} T_{\mathrm{EM}}(t) \tag{3.38}$$

The relation between both rotation speeds of the EM and ICE is also deduced:

$$\omega_{\mathrm{EM}}(t) = R_{\mathrm{GC}}\omega_{\mathrm{ICE}}(t) \tag{3.39}$$

Γ_{ICE} is introduced, which not only encompasses the engine's specific inertia, but that of the starter as well, in kg.m^2. The torque at the input of the gearbox, when the clutch is connected, is then expressed as:

$$T_{\mathrm{IGB}}(t) = T_{\mathrm{ICE}}(t) + T_{\mathrm{GC}}(t) - \Gamma_{\mathrm{ICE}}\frac{\omega_{\mathrm{ICE}}(t+\Delta t) - \omega_{\mathrm{ICE}}(t)}{\Delta t} \tag{3.40}$$

When the clutch is disconnected however, the input torque of the gearbox is simply defined as:

$$T_{\mathrm{IGB}}(t) = T_{\mathrm{GC}}(t) \tag{3.41}$$

In this work, a 5-gear ratio dual-clutch transmission (DCT) gearbox equips the powertrain. This gearbox allows for better efficiency and faster switching between the different gears. The gearbox's ratio R_{GB} and inertia Γ_{GB} naturally depends on the gear number while its efficiency η_{GB} depends on the selected gear, as well as the rotational speed and torque delivered through the drive shaft. The output torque is then equal to:

$$T_{\mathrm{GB}}(t) = R_{\mathrm{GB}}(x_2(t))\eta_{\mathrm{GB}}(\omega_{\mathrm{GB}}(t), T_{\mathrm{GB}}(t), x_2(t))(T_{\mathrm{IGB}}(t) - \Gamma_{\mathrm{GB}}\frac{\omega_{\mathrm{ICE}}(t+\Delta t) - \omega_{\mathrm{ICE}}(t)}{\Delta t}) \tag{3.42}$$

with the secondary shaft speed ω_{GB} defined as:

$$\omega_{\mathrm{ICE}}(t) = R_{\mathrm{GB}}(x_2(t))\omega_{\mathrm{GB}}(t) \tag{3.43}$$

If DCT allows for fast gear shifting, the latter is not instantaneous and leads to energy loss in the two clutches of the gearbox. This is considered afterwards on the ICE and EM models to assess its impact on fuel and electrical energy consumption. Gear switching is also limited to one upshift or downshift per time step. This is translated to the following condition on $\boldsymbol{u}$:

$$-1 \leq u_2(t) \leq 1 \tag{3.44}$$

By considering the transmission inertia Γ_{T} in kg.m^2 and the differential's gear ratio R_{D} afterwards, the torque delivered to the vehicle's wheels is equal to:

$$T_{\mathrm{D}}(t) = R_{\mathrm{D}}(T_{\mathrm{GB}}(t) - \Gamma_{\mathrm{T}}\frac{\omega_{\mathrm{GB}}(t+\Delta t) - \omega_{\mathrm{GB}}(t)}{\Delta t}) \tag{3.45}$$

Finally, the relation between the torque required by the wheels and that delivered by the powertrain, as well as the speed relation between the wheels and powertrain shaft, are deduced:

$$T_{\mathrm{w}}(t) = T_{\mathrm{D}}(t) - \Gamma_{\mathrm{w}} \frac{\omega_{\mathrm{w}}(t+\Delta t) - \omega_{\mathrm{w}}(t)}{\Delta t} \tag{3.46a}$$

$$\omega_{\mathrm{GB}}(t) = R_{\mathrm{D}} \omega_{\mathrm{w}}(t) \tag{3.46b}$$

where Γ_{w} is the combined inertia of the four wheels. The speed transmission model is directly expressed in this case as followed:

$$\omega_{\mathrm{ICE}}(t) = R_{\mathrm{D}} R_{\mathrm{GB}}(x_2(t)) \omega_{\mathrm{w}}(t) \tag{3.47a}$$

$$\omega_{\mathrm{EM}}(t) = R_{\mathrm{D}} R_{\mathrm{GB}}(x_2(t)) R_{\mathrm{GC}} \omega_{\mathrm{w}}(t) \tag{3.47b}$$

The torque transmission model is deduced as well by replacing the different torque related terms with their respective expressions in equation 3.46. A relation between $\boldsymbol{T_{\mathrm{EM}}}$, $\boldsymbol{T_{\mathrm{ICE}}}$ and $\boldsymbol{T_{\mathrm{w}}}$ is then found. Special attention is given when negative power flow is considered, as the different efficiencies values should be replaced with their inverse values.

3.3.5 Internal combustion engine

After determining both the torque and speed of the ICE, the instantaneous fuel consumption L is calculated using a torque/speed dependent consumption mapping, shown in Figure 3.19. This consumption model is adopted instead of the widely used efficiency mapping model since it assesses the losses of the engine at low power values more accurately.

On the other hand, it is important to mention that, when at low speed, the ICE only runs at a specific idle speed ω_{Idle} in order to operate smoothly. The ICE model also sets the maximum speed as well as the upper torque limit that can be delivered, depending on its rotation speed.

As such, the following expressions must be verified when the engine is on at every time step:

$$\omega_{\mathrm{ICE}}(\boldsymbol{d}, \boldsymbol{x}(t), \boldsymbol{u}(t)) - \omega_{\mathrm{ICE,max}} \leq 0 \tag{3.48a}$$

$$T_{\mathrm{ICE}}(\boldsymbol{d}, \boldsymbol{x}(t), \boldsymbol{u}(t)) - T_{\mathrm{ICE,max}}(\omega_{\mathrm{ICE}}(\boldsymbol{d}, \boldsymbol{x}(t), \boldsymbol{u}(t))) \leq 0 \tag{3.48b}$$

Energy loss during gear shifting is considered as well when calculating the fuel consumption of the engine. As explained earlier, gear shifting is not instantaneous and since the engine is characterized by slower dynamics compared to the EM, the engine's output power is higher than the requested power, leading to considerable losses. This is studied in Appendix B and the following expression is found for the fuel consumption in this case:

$$L(\boldsymbol{d}, \boldsymbol{x}(t), \boldsymbol{u}(t)) = \frac{L_{\mathrm{req}}(\boldsymbol{d}, \boldsymbol{x}(t), \boldsymbol{u}(t))}{\Delta t} \left(\left| \frac{R_{\mathrm{GB}}(x_2(t))}{R_{\mathrm{GB}}(x_2(t+\Delta t))} - 1 \right| \frac{t_{\mathrm{gs}}}{2} + \Delta t \right) \tag{3.49}$$

where L_{req} is the engine's fuel consumption at the required operation point in g/s and t_{gs} is the required time for the shift procedure in s.

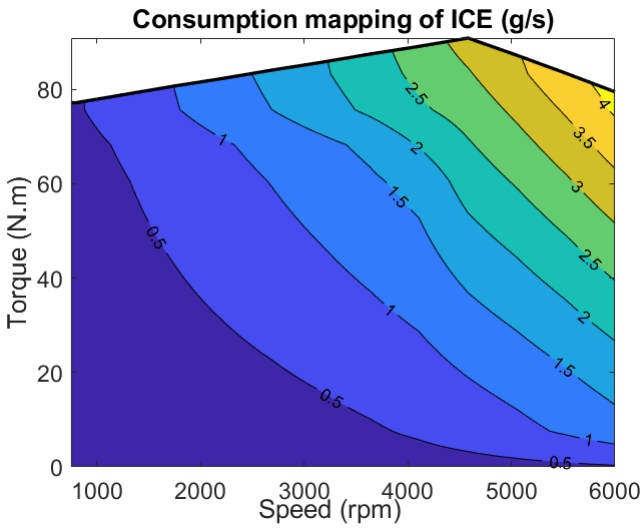

Figure 3.19: ICE consumption mapping with iso-consumption and peak torque lines. Data retrieved from [74]

3.3.6 Starter

When restarted, it is assumed that the ICE needs to be cranked to its idle speed before operation under its own power. The ICE's inertia Γ_{ICE}, is used to calculate the starter's electrical energy consumption during the ICE's restart after being turned off as well, expressed as:

$$P_{\text{St}}(t) = \frac{1}{\eta_{\text{DC}}\eta_{\text{St}}}(\frac{1}{2}\Gamma_{\text{ICE}}{\omega_{\text{Idle}}}^2)(1 - x_3(t))u_3(t)\frac{1 + u_3(t)}{2} \tag{3.50}$$

where η_{St} is the efficiency of the starter. η_{DC} is considered here as well since the starter is powered through the on-board 12 V network.

3.4 Optimization constraints

The command constraints, linked to both the command and state variables, have been presented earlier when discussing the component models and are expressed in Equations 3.10, 3.11, 3.36 and 3.48. Aside from these conditions, design considerations are also introduced in this study.

The design constraints are related to the electric machine as it is the sole component whose design is modified in this application. These are deduced by analyzing the machine specifications, illustrated in Figure 3.20, while considering the company's standards as well as additionnal design restrictions to guarantee a coherent design.

The different design considerations are detailed afterwards and are classified into:

- Geometric constraints
- Performance constraints
- Process constraints

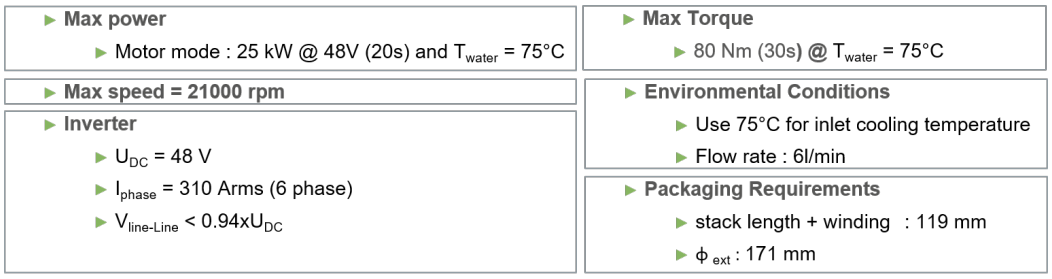

Figure 3.20: Example of machine requirements

- Mechanical constraints
- Thermal constraints
- Demagnetization constraints
- Torque ripple constraints
- Inverter constraints

3.4.1 Geometric constraints

The geometric constraints need to be verified for each machine design and ensures the machine's mechanical integrity and the ability of the parametric model to provide a consistent machine geometry. These constraints are expressed in the form of analytical equations $\boldsymbol{k_{\mathbf{Geom}}}$, which are enumerated and illustrated in Appendix C. For a design to be valid, the following needs to be satisfied:

$$-\boldsymbol{k_{\mathbf{Geom}}}(\boldsymbol{d}) \leq 0 \tag{3.51}$$

It is also worth mentioning that the air gap value Gap_{Air} is fixed afterwards. Thus, only the rotor's external radius $Rout_{\mathrm{Rot}}$ is considered while the value of the stator's internal radius Rin_{Sta} is deduced from the latter.

3.4.2 Performance constraints

The performance constraints are related to the peak torque $T_{\max}$ in N.m and peak power $P_{\max}$ in W that the machine should be able to produce in motor mode. For a given machine design, these values are deduced from the losses mapping model envelope as follows:

$$T_{\max}(\boldsymbol{d}) = \max_{\omega_{\mathrm{EM}} \in [0, \omega_{\mathrm{EM,max}}]} T_{\mathrm{EM,max}}(\boldsymbol{d}, \omega_{\mathrm{EM}}) \tag{3.52a}$$

$$P_{\max}(\boldsymbol{d}) = \max_{\omega_{\mathrm{EM}} \in [0, \omega_{\mathrm{EM,max}}]} \frac{2\Pi}{60} T_{\mathrm{EM,max}}(\boldsymbol{d}, \omega_{\mathrm{EM}}) \omega_{\mathrm{EM}} \tag{3.52b}$$

Their required values $P_{\mathrm{max,req}}$ and $T_{\mathrm{max,req}}$ are given in the machine specifications, as seen for example in Figure 3.20. Performance constraints are expressed as:

$$T_{\mathrm{max,req}} - T_{\max}(\boldsymbol{d}) \leq 0 \tag{3.53a}$$

$$P_{\mathrm{max,req}} - P_{\max}(\boldsymbol{d}) \leq 0 \tag{3.53b}$$

3.4.3 Process constraints

The only process considerations taken into account in this work are those related to the packaging requirements of the machine, mentioned in Figure 3.20. The latter introduce limitations on the machine's external diameter D_{Ext} in mm and its total length L_{Tot} in mm expressed as:

$$D_{\text{Ext}}(\boldsymbol{d}) = 2Rout_{\text{Sta}} \tag{3.54a}$$
$$L_{\text{Tot}}(\boldsymbol{d}) = Length + L_{\text{Winding}}(\boldsymbol{d}) \tag{3.54b}$$

where $Rout_{\text{Sta}}$ is the external stator radius in mm and $Length$ is the stack length in mm. L_{Winding} refers to the end-windings length in mm, which depends on the winding technology as well as multiple machine parameters.

This then leads to the following conditions to be satisfied during the optimization process:

$$D_{\text{Ext}}(\boldsymbol{d}) - D_{\max} \leq 0 \tag{3.55a}$$
$$L_{\text{Tot}}(\boldsymbol{d}) - L_{\max} \leq 0 \tag{3.55b}$$

where $D_{\max}$ and $L_{\max}$ define the maximum envelope of the machine volume in mm.

3.4.4 Mechanical constraints

During the design process, the mechanical integrity of the machine rotor under stress needs to be evaluated as well, specially at high speeds. In this work, mechanical simulations are launched at overspeed in steady state conditions for the proposed designs, as seen in Figure 3.21. The overspeed value is defined as:

$$\omega_{\text{overspeed}} = 1.2\omega_{\text{Em,max}} \tag{3.56a}$$

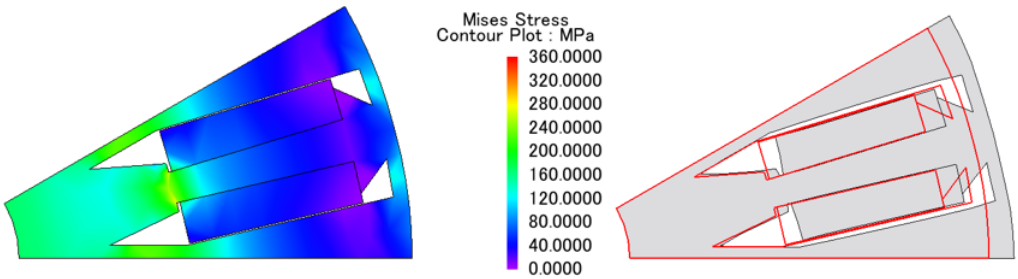

Figure 3.21: Mechanical simulation of rotor core at overspeed in JMAG. Left: Levels of Stress- Right: Deformation of rotor amplified at 100 times

The maximum value of the von Mises stress, referred to as k_{VMS} in MPa is calculated and should be lower than the steel sheet's elastic limit Lim_{El}, above which any deformation is irreversible [140]. Also the rotor's deformation in the radial direction k_{D} in mm should be lower than the airgap value, in order to avoid contact with the stator.

Thus, the mechanical constraints are defined as:

$$k_{\mathrm{VMS}}(\boldsymbol{d}) - Lim_{\mathrm{El}} \leq 0 \tag{3.57a}$$
$$k_{\mathrm{D}}(\boldsymbol{d}) - Gap_{\mathrm{Air}} \leq 0 \tag{3.57b}$$

3.4.5 Thermal constraints

Furthermore, the cooling efficiency of the machine needs to be assessed at demanding scenarios. For this study, a short-circuit at high speed is selected. Figure 3.22 shows the proposed thermal model of the machine. Thermal resistances are deduced from previous test campaign results and adjusted for each machine design while losses are adjusted using the FE model [141].

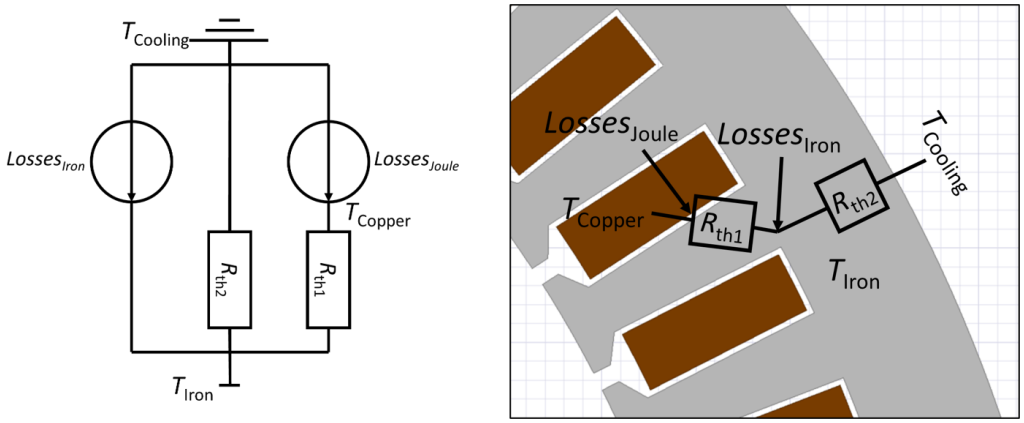

Figure 3.22: Thermal model of the EM. R_{th1} and R_{th2} are thermal resistances in K/W while T_{Cooling}, T_{Copper} and T_{Iron} are the cooling water, winding and stator core temperatures respectively in °C

As the losses values depend on the copper and iron temperatures, the MDF strategy presented in Chapter 1, is applied to accelerate the convergence of the thermal model.

The aim of the thermal study is to ensure that the winding temperature T_{Copper} does not exceed the melting temperature of the conductor coating T_{Coating}, leading to the following formulation for the thermal constraint:

$$T_{\mathrm{Copper}}(\boldsymbol{d}) - T_{\mathrm{Coating}} < 0 \tag{3.58}$$

3.4.6 Demagnetization constraints

The short-circuit scenario at high speed is also used to evaluate its impact on the magnet's characteristics. In this case, the stator's magnetic field is exactly opposite to the rotor's field, leading to the magnet's partial demagnetization.

JMAG allows for the possibility to reuse the demagnetized magnets. The proposed criteria for the validity of a machine design is to verify if there is no significant performance loss in this case. This means the peak torque using the demagnetized magnets satisfies the following condition:

$$0.95T_{\max} - T_{\text{Dem,max}}(\boldsymbol{d}) \leq 0 \tag{3.59}$$

3.4.7 Torque ripple constraints

During the design process, the torque ripple *Ripple* of the machine needs to be monitored. It is defined as undesirable variations in the machine's output torque during its revolution and is a result of many factors such as mechanical imbalances and flux harmonics.

In the case of PMSMs and the perimeter of this work, it is mainly due to the interaction between the magnetic field of the rotor magnets and the stator slots, also known as cogging torque, and can be estimated using the FE model.

The torque ripple should remain at acceptable levels, especially when providing its peak torque, in order to ensure driver comfort, prevent premature wear of the drivetrain components and reduce acoustic noise. This then translates to the following condition:

$$\mathit{Ripple}(\boldsymbol{d}) - \mathit{Ripple}_{\max} \leq 0 \tag{3.60}$$

where $\mathit{Ripple}_{\max}$ is the maximum torque ripple value.

3.4.8 Inverter constraints

When selecting either the PWM or FW strategy, the limitations of the embedded electronics need to be considered. In fact, the PWM strategy requires at least 10 switches per electrical period compared to the FW mode which only requires a single commutation instead. This then defines $f_{\text{PWM,max}}$ and $f_{\text{FW,max}}$ which refer to the maximum commutation frequency that should be achieved by the inverter components in PWM and FW modes respectively in Hz and are expressed as:

$$f_{\text{PWM,max}}(\boldsymbol{d}) = 10p\frac{\mathit{Speed}_{\text{FWM}}}{60} \tag{3.61a}$$

$$f_{\text{FW,max}}(\boldsymbol{d}) = p\frac{\omega_{\text{EM,max}}}{60} \tag{3.61b}$$

Since the inverter components have a maximum switching frequency $f_{\max}$, the following inverter conditions are introduced:

$$f_{\text{PWM,max}}(\boldsymbol{d}) - f_{\max} \leq 0 \tag{3.62a}$$

$$f_{\text{FW,max}}(\boldsymbol{d}) - f_{\max} \leq 0 \tag{3.62b}$$

Thus, the various design constraints are defined. Afterwards, depending on the degree of precision desired, an *a posteriori* approach can be adopted as well: the constraints that require long computation times, such as the demagnetization and mechanical constraints, are simplified for faster optimization iterations, using analytical formulations instead, and are reverified once a solution is found.

3.5 Problem definition

Different objectives can be studied when optimizing the hybrid powertrain such as the minimization of various types of emissions, improving the vehicle's fuel economy over a specific drive-cycle or reducing the powertrain's total cost. In this work, both of the latter objectives are considered and the hybrid powertrain optimization problem is formulated as:

$$\underset{\boldsymbol{d},\boldsymbol{u}}{\text{minimize}} \quad J(\boldsymbol{d},\boldsymbol{u}) = \alpha Inv(\boldsymbol{d}) + \beta \sum_{t_0}^{t_f-\Delta t} L(\boldsymbol{d},\boldsymbol{x}(t),\boldsymbol{u}(t),t)\Delta t \tag{3.63a}$$

$$\text{subject to} \quad \boldsymbol{x}(t+\Delta t) = \boldsymbol{f}(\boldsymbol{x}(t),\boldsymbol{u}(t),t)\Delta t + \boldsymbol{x}(t) \tag{3.63b}$$

$$x_1(t_0) = x_0 \tag{3.63c}$$

$$x_1(t_f) = x_f \tag{3.63d}$$

$$\boldsymbol{g}(\boldsymbol{d},\boldsymbol{x}(t),\boldsymbol{u}(t),t) \leq 0 \tag{3.63e}$$

$$\boldsymbol{k}(\boldsymbol{d}) \leq 0 \tag{3.63f}$$

$$\boldsymbol{x}(t) \in [\boldsymbol{x_{\min}}(t), \boldsymbol{x_{\max}}(t)] \tag{3.63g}$$

$$\boldsymbol{u}(t) \in [\boldsymbol{u_{\min}}(t), \boldsymbol{u_{\max}}(t)] \tag{3.63h}$$

$$\boldsymbol{d} \in [\boldsymbol{d_{\min}}, \boldsymbol{d_{\max}}] \tag{3.63i}$$

where L is the instantaneous fuel consumption in g/s which is calculated using the system model described earlier and Inv is the powertrain cost in €. Since the EM is the only powertrain component being modified while the rest of the drivetrain remains static during the optimization process, only the cost of the EM is considered as a function of its peak power and the following expression is proposed [142, 143, 144]:

$$Inv(\boldsymbol{d}) = 1000 + 0.02 P_{\max}(\boldsymbol{d}) \tag{3.64}$$

This proposition is valid for the selected machine topology and application power range, as well as the fact that the active part materials are imposed. Detailed functions separating the material and manufacturing costs could have been applied here as well. The values for α and β are selected to bring both terms of the cost function together. For this work, α is equal to 1 and the following expression is proposed for β, which considers the penalty payment for CO_2 emissions target exceedance:

$$\beta = \frac{Pen\ Conv_{\text{lgasoline-gCO}_2}}{\rho_{\text{gasoline}}\ Dist_{\text{cycle}}} \tag{3.65}$$

where Pen is the emissions target exceedance penalty value, equal to 95 €/(gCO_2/km) in Europe since 2019 while $Conv_{\text{lgasoline-gCO}_2}$ converts liters of gasoline consumption into grams of CO_2 emissions. ρ_{gasoline} is the gasoline's density in g/l and $Dist_{\text{cycle}}$ is the selected drive-cycle's distance in km.

The different design variables, shown in Figure 3.10, are enumerated afterwards in Table 3.1, as well as the command and state variables.

The charge sustaining condition, also called iso-SoC condition, is considered in this application as well and is expressed in Equation 3.66. It is an important criterion for HEV homologation, as it imposes that the energy used during the driving cycle only comes from

Type	Component	Name	Values
Design variables $\boldsymbol{d}$	Machine	p	{3;4;5;6}
		N_{slot}	{3;6}
		Length	[30 mm, 110 mm]
		$Rout_{\text{Sta}}$	[55 mm, 80.5 mm]
		Hs0	[0.5 mm, 2 mm]
		Hs1	[0 mm, 2 mm]
		Hs2	[6 mm, 8 mm]
		Bs0	[0.1 mm, 10 mm]
		Bs1	[3 mm, 6 mm]
		Bs2	[0.65 mm, 6 mm]
		Rin_{Rot}	[10 mm, 40 mm]
		$Rout_{\text{Rot}}$	[40 mm, 80 mm]
		R_1	[0 mm, 10 mm]
		R_2	[0 mm, 10 mm]
		Gap	[0 mm, 5 mm]
		Rib	[5 mm, 15 mm]
		Bridge	[0.1 mm, 6 mm]
		B1	[0.1 mm, 10 mm]
		B2	[0.1 mm, 30 mm]
		B3	[1 mm, 7 mm]
		M1	[0 mm, 4 mm]
		M2	[2 mm, 5 mm]
		O1	[0.2 mm, 5 mm]
		Ouv_{Mag}	[0, Π]
		Mag_{Th}	[2 mm, 7 mm]
		Mag_{Wd}	[6 mm, 20 mm]
		Wnd_{con}	{Delta; Wye}
		N_{ph}	{3;6}
		N_{series}	{3;4;5}
		N_{parallel}	{1;2}
	Inverter	$Speed_{\text{FWM}}$	[2000 rpm, 10000 rpm]
	Gear connection	R_{GC}	[1, 3.5]
Command variables $\boldsymbol{u}$	Battery	Battery's charge/discharge	$[\frac{-100I_{\max}\Delta t}{C_{\text{Batt}}}, \frac{100I_{\max}\Delta t}{C_{\text{Batt}}}]$
	Transmission	Gear shift	{-1;0;1}
	Starter	Engine stop/start	{0;1}
State variables $\boldsymbol{x}$	Battery	State of charge	[30 %, 70 %]
	Transmission	Selected gear	{1;2;3;4;5}
	ICE	Engine state	{-1;0;1}

Table 3.1: Optimization variables

the fuel tank. This in turn means that the energy stored in the battery at t_0 should be found by the end of the driving cycle at t_{f}.

$$x_0{=}x_{\text{f}} \tag{3.66}$$

Meanwhile, the inequality command constraints mainly refer to the use of the EM and ICE, as presented in Table 3.2. As it can be noticed from the problem's definition, no equality command constraints are considered as they are implicitly satisfied within the system model. The various design constraints, linked to the electric machine and explored in the previous section, are enumerated here as well in Table 3.3.

Component	Number	Nature	Reference
EM	3	black-box	3.36
ICE	2	black-box	3.48

Table 3.2: Command constraints

Discipline	Number	Nature	Reference
Geometric	25	analytic	3.51
Performance	2	black-box	3.53
Process	2	analytic	3.55
Mechanical	2	black-box	3.57
Thermal	1	black-box	3.58
Demagnetization	1	black-box	3.59
Torque ripple	1	black-box	3.60
Inverter	2	analytic	3.62

Table 3.3: Command constraints

Hence, the optimization problem adopts the same formulation as in Chapter 2. Thus, the different systemic design approaches studied previously can be applied here as well to find the optimal hybrid powertrain design. Using the same term definitions, the HEV power management problem is deduced as well:

$$\underset{\boldsymbol{u}}{\text{minimize}} \quad J(\boldsymbol{u}) = \sum_{t_0}^{t_f-\Delta t} L(\boldsymbol{d}, \boldsymbol{x}(t), \boldsymbol{u}(t), t)\Delta t \tag{3.67a}$$

$$\text{subject to} \quad \boldsymbol{x}(t+\Delta t) = \boldsymbol{f}(\boldsymbol{x}(t), \boldsymbol{u}(t), t)\Delta t + \boldsymbol{x}(t) \tag{3.67b}$$

$$x_1(t_0) = x_0 \tag{3.67c}$$

$$x_1(t_f) = x_f \tag{3.67d}$$

$$\boldsymbol{g}(\boldsymbol{x}(t), \boldsymbol{u}(t), t) \leq 0 \tag{3.67e}$$

$$\boldsymbol{x}(t) \in [\boldsymbol{x}_{\mathbf{min}}(t), \boldsymbol{x}_{\mathbf{max}}(t)] \tag{3.67f}$$

$$\boldsymbol{u}(t) \in [\boldsymbol{u}_{\mathbf{min}}(t), \boldsymbol{u}_{\mathbf{max}}(t)] \tag{3.67g}$$

Conclusion

An extended hybrid vehicle model is presented, which considers the impact of the battery's SoC variation, gear shifting and engine stop/restart with an iso-granularity representation for all the powertrain components.

In order to quickly and accurately estimate the EM's performance, a losses mapping model, based on parallel finite element simulations and Park's PMSM representation, is used. When modifying the machine parameters, this model can be recalculated in a few minutes and guarantee deviations of less than 2 % when confronted to prototype tests is found.

Different command and design constraints are enumerated afterwards, which consider the powertrain limitations and the machine requirements. Finally, the complete hybrid powertrain optimization problem as well as the power management problem are defined.

The next step, as it was the case for the HRPS application, is to be able to compare between different powertrains using efficient control strategies, before implementing systemic design strategies.

Chapter 4

Hybrid Electric Vehicle optimization

Contents

Introduction

In this chapter, different hybrid powertrain systemic design strategies are implemented, applied and compared. At first, the bi-level approach $\mathcal{BL}$, the iterative approach $\mathcal{IT}$ and alternative systemic design approaches $\mathcal{A}_1$, $\mathcal{A}_2$ and $\mathcal{A}_3$, introduced in Chapter 2, are adapted for the hybrid powertrain application. However, before proceeding to their application, it is crucial to be able to compare between several vehicle powertrains based on an efficient

control strategy.

Thus, different control methods are assessed: DPAM, PMP and a new rule-based strategy. They are compared in terms of fuel consumption and calculation times. The optimal command is analyzed further, as well as the impact of powertrain characteristics on fuel efficiency and hybrid mode selection.

The third section focuses on cycle reduction techniques, introduced in Chapter 1. These methods are investigated further and compared to quickly evaluate the machine performance over the drive-cycle and accelerate the design optimization process.

Afterwards, the selected hybrid vehicle case study is presented. The vehicle parameters, required for the vehicle model presented in the previous chapter, are listed, as well as the different requirements that the optimal machine design has to satisfy.

The fifth part of this chapter is devoted to the screening study that was carried out to identify the impact of the decision variables over the optimization process. This will then allow for the selection of the most influential parameters to relieve the calculation burden of the optimization algorithms and accelerate their convergence.

The assessment of the different optimization approaches considers key metrics such as the number of evaluations, the final cost of the powertrain and deviation from the initial design, as well as the impact of the number of decision variables and design constraints.

Finally, the robustness of the optimal solution is evaluated. This is deemed necessary since the HEV design problem is solved without considering its inherent uncertainties and it is conducted based on both local and global sensitivity analysis studies.

4.1 Systemic design approaches

Hybrid powertrain design optimization is conducted by applying the various strategies defined in Chapter 2: the bi-level approach $\mathcal{BL}$ and the iterative approach $\mathcal{IT}$ as well as alternative approaches $\mathcal{A}_1$, $\mathcal{A}_2$ and $\mathcal{A}_3$, based on the simultaneous, bi-level and iterative schemes respectively.

When using the $\mathcal{BL}$ approach, the design parameters are optimized with the SQP algorithm, described in Section 2.3. To consider the impact of the new parameters over the performance of the machine, a new losses mapping model is recalculated for the design geometry, as explained in Section 3.3.

The power management problem is then solved using an optimal control strategy, allowing for the calculation of the optimal powertrain cost, as shown in Figure 4.1. Selection of the most adequate control strategy is detailed in Section 4.2.

Approach $\mathcal{IT}$ starts by solving the power management problem of the initial powertrain design using an optimal command strategy, and then imposes these operation points to optimize the design variables of the powertrain using SQP.

During the design optimization process, the total energy used during the driving cycle, which is directly linked to the vehicle's fuel consumption can be expressed as:

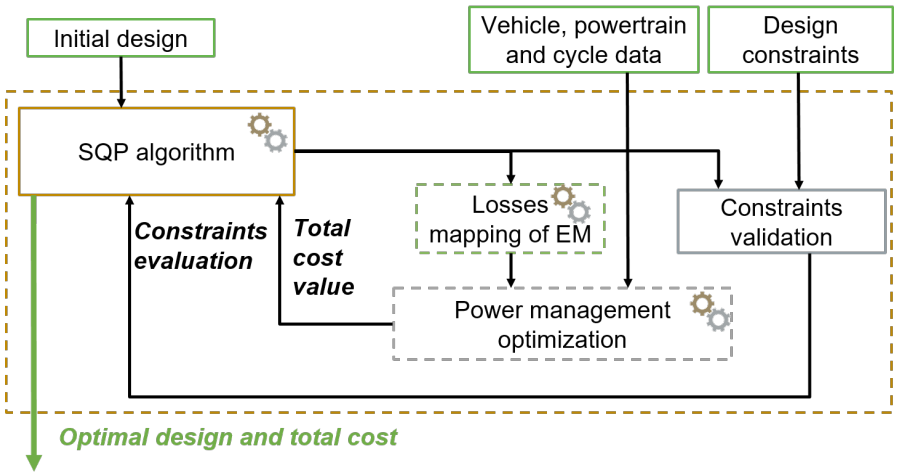

Figure 4.1: $\mathcal{BL}$ approach

$$E_{\text{tot}}{=}E_{\text{u}} + E_{\text{L,EM}} + E_{\text{L,Pow}} \tag{4.1}$$

where E_{u} is the useful energy in J, and $E_{\text{L,EM}}$ and $E_{\text{L,Pow}}$ are the total energy losses of the EM and the rest of the powertrain components respectively during the driving cycle in J.

Since all of the vehicle's energy comes from the fuel tank when imposing the charge sustaining condition, the total energy used during the driving cycle can also be expressed as:

$$E_{\text{tot}} = HV_{\text{gasoline}}\bar{\eta}_{\text{ICE}} \sum_{t_0}^{t_f-\Delta t} L(\boldsymbol{d}, \boldsymbol{x}(t), \boldsymbol{u}(t), t)\Delta t \tag{4.2}$$

where HV_{gasoline} is the heat value of gasoline in J/g and $\bar{\eta}_{\text{ICE}}$ is the mean efficiency of the engine.

When adopting the previously mentioned approach, fixing the operation points during design optimization means E_{u} is constant when varying the design parameters, as well as $E_{\text{L,Pow}}$, since the characteristics and operation of the other powertrain components are not modified. This means that minimizing E_{tot} is equivalent to minimizing $\text{E}_{\text{L,EM}}$ in this case. The design cost function to minimize becomes equivalent to:

$$J(\boldsymbol{d}) = \alpha Inv(\boldsymbol{d}) + \frac{\beta}{HV_{\text{gasoline}}\bar{\eta}_{\text{ICE}}} E_{\text{L,EM}} \tag{4.3}$$

Once an optimal design is found, the optimal command is recalculated and the total cost of the powertrain is evaluated. The described process is then repeated as long as the total cost difference remains greater than a selected tolerance ϵ. The iterative approach and the powertrain design optimization process are shown in Figure 4.2.

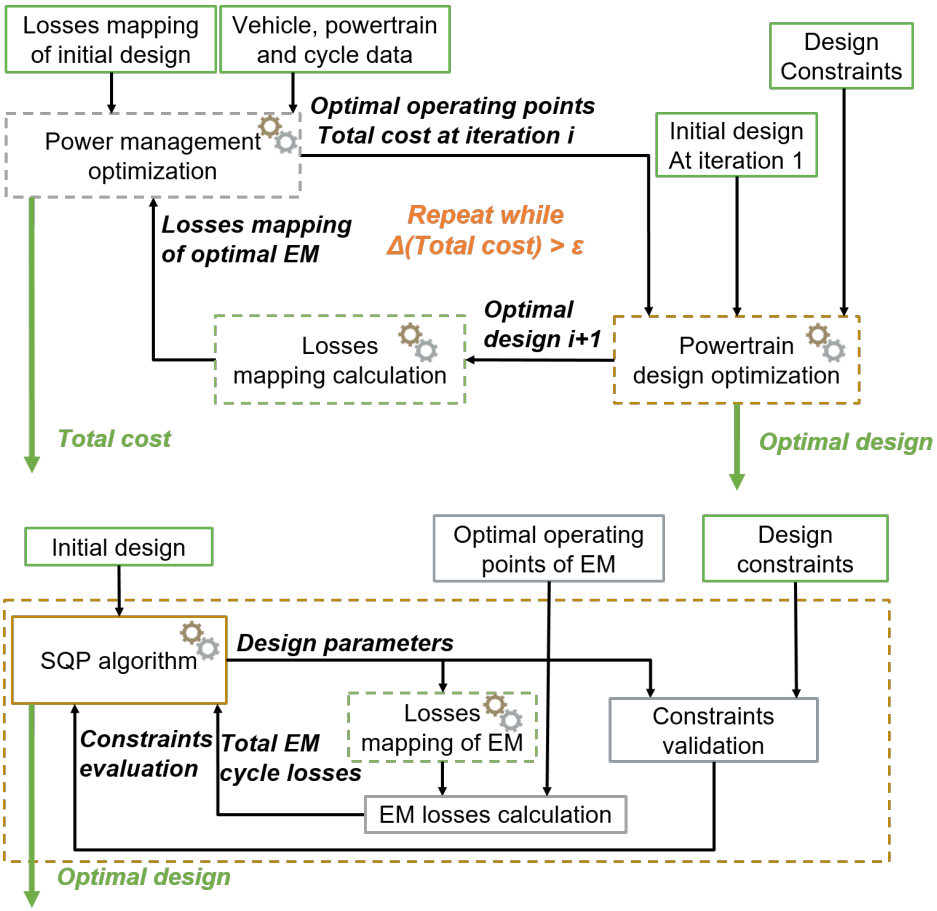

Figure 4.2: Above: $\mathcal{IT}$ approach - Below: Design optimization block of $\mathcal{IT}$ approach

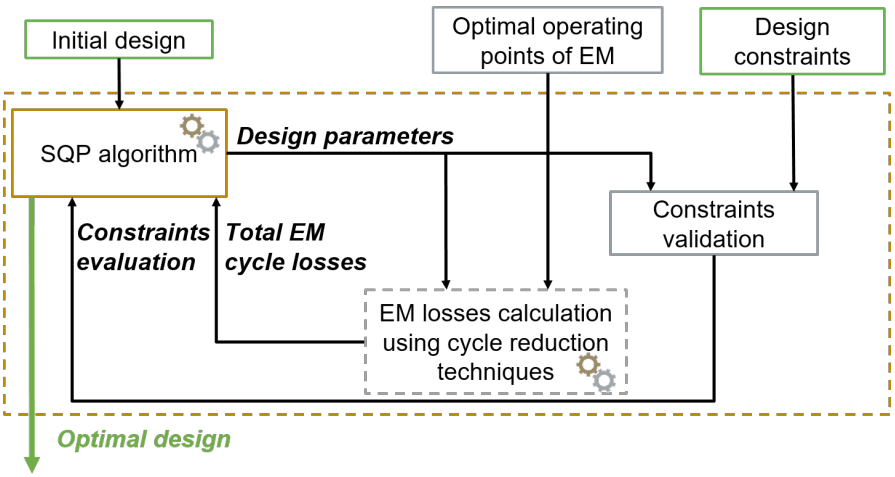

Figure 4.3: Design optimization block of $\mathcal{A}_3$ approach

Design strategy $\mathcal{A}_3$, presented in Figure 4.3, follows a similar scheme to the iterative approach $\mathcal{IT}$. The only difference lies within the design cost calculation. This approach will rely on cycle reduction techniques and the machine circuit model to estimate the machine losses, as explained in Section 4.3. This alternative approach to evaluate the design cost is expected to increase the calculation speed of the model compared to the iterative approach.

Meanwhile, systemic design strategy $\mathcal{A}_1$ relies on the SQP algorithm to adjust both the design variables and parameters of a rule-based strategy. This command strategy should allow for the calculation of the powertrain's fuel consumption as well as estimate the final state of charge of the battery. The charge sustaining is not guaranteed to be fulfilled using this strategy. This then requires adding the following condition to the other optimization constraints that are considered:

$$|x_1(t_\mathrm{f}) - x_\mathrm{f}| \leq 5\% \tag{4.4}$$

The process for this approach is shown in Figure 4.4. After the approach converges, the total cost of the provided solution is recalculated using the same optimal control strategy as approaches $\mathcal{BL}$ and $\mathcal{IT}$ to establish a common reference.

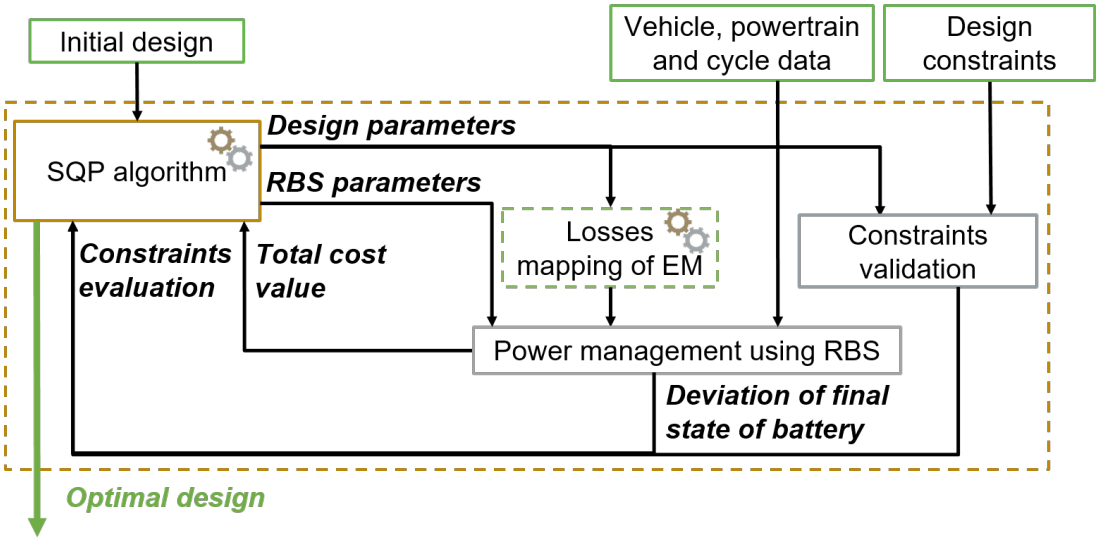

Figure 4.4: $\mathcal{A}_1$ approach

Finally, the proposed $\mathcal{A}_2$ method approximates the design cost function as well as the design constraints functions which require long calculation times using polynomial regression over the design search space. The following second order polynomial model is used:

$$y = b_0 + \sum_{i=1}^{k} b_\mathrm{i} d_\mathrm{i} + \sum_{i=1}^{k} \sum_{j=1}^{k} b_\mathrm{ij} d_\mathrm{i} d_\mathrm{j} \tag{4.6}$$

where y refers to the highly time-consuming models, whether for constraint or cost calculation, and k represents the number of considered design variables. $\boldsymbol{b}$ are the model coefficients. The process of calculating these coefficients is explained afterwards in Section 4.5. Once a

solution is found, the powertrain cost is recalculated and constraints are validated based on the models presented in Section 3.3.

4.2 HEV power management

The previous systemic design approaches rely on efficient control strategies to solve the HEV power management problem and compare the proposed powertrains. Thus, different control methods are investigated afterwards and assessed in terms of fuel economy and computation times.

4.2.1 Optimal control strategies

DPAM and PMP, explored in Chapter 2, are applied for hybrid vehicle control as well. These two strategies are extended in this study to consider the three components of the command and state variables.

This is done in the case of DPAM by accessing the SoC mesh at each instant for different combinations of gears and engine states. This has led to the creation of 10 parallel and connected SoC meshes in this application.

PMP also allows for the calculation of the optimal gear shift and stop/start command of the starter by calculating and minimizing the hamiltonian for all possible values of $\boldsymbol{u}$.

In addition to DPAM and PMP, a rule-based strategy (RBS) is also developed. Its implementation is based on the main guidelines for exploiting the advantages of hybridization [21]: the battery's state of charge is balanced by controlling the charge and discharge phases. Meanwhile, the engine is used at its highest efficiency at higher power request values and should be turned off the longest time possible to avoid fuel waste.

Hybrid modes are then selected as follows: Regenerative braking is used in order to store otherwise wasted energy, exploiting the electrical machine's reversibility. Full electric mode is applied at low-medium loads to be used for longer periods of time, leading to longer shutdown of the ICE. Boost mode is selected at higher loads, either to assist the engine or optimize its use. Finally, Generation mode is chosen when the battery is being depleted below its lower limit or when the ICE is running efficiently, providing enough electrical energy for future EM use.

The selection of these hybrid modes is summed up in the state machine shown in Figure 4.5, where transitions between them are made if certain conditions are fulfilled. The latter are linked to the values of ω_{ICE}, the battery's SoC and the requested torque and power at the clutch T_{IGB} and P_{IGB} at each instant.

Parameters SoC_{inf}, SoC_{sup}, T_{s} and P_{s}, are introduced as threshold values. They depend on the powertrain components and the driving cycle and are optimized to minimize the fuel consumption and reduce the gap between the initial SoC of the battery and its final value as much as possible.

Additionally, the ICE is automatically turned off when not used to cut pumping losses and simplify the strategy while gear selection is made based on the powertrain's overall efficiency, which means the selected gear should minimize the total powertrain losses. This

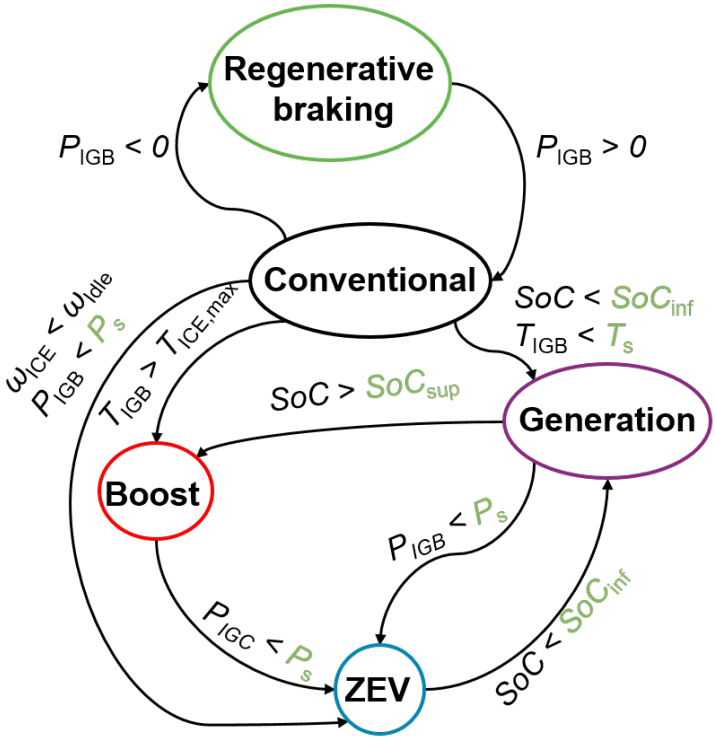

Figure 4.5: Hybrid mode selection. Green: parameters to be optimized

is seen as the best compromise and has offered better fuel gains when compared to directly minimizing the fuel consumption by gear selection for example, which leads the EM to operate at lower efficiency, resulting in much faster battery depletion and more frequent necessity to recharge it after at a higher fuel cost.

4.2.2 Application and comparison

To compare between the proposed strategies in terms of accuracy, fuel consumption gains and calculation time, the following application is set up: a C-segment vehicle weighing approximately 1 t and equipped with a 1.2-liter gasoline ICE (81 kW, ω_{idle} equal to 750 rpm), a 13 kW EM, a 48 V battery (C_{batt}: 15 A.h, I_{max}: 300 A, usable energy: 600 W.h) and a 5 DCT transmission, is selected.

Three driving cycles of varying time horizons and characteristics are then tested: the Urban Driving Cycle's (ECE-15) medium speed portion, the NEDC and WLTC 3-b cycles. Δt is equal to 1 s. The road is considered flat and dry and the battery is initially charged at 50% of its total capacity. No auxiliary consumption is considered for this application.

Table 4.1 sums up the results. *FC* refers to the fuel consumption in l/100 km, *FS* is the final value of the SoC in relative value and *TS* is the time required by each method in s.

The performances of the proposed strategies are close in terms of fuel consumption. However, the most efficient strategy remains DPAM, as it was the case for the HRPS application studied in Chapter 2. All the constraints, especially the iso-SoC condition, are satisfied for all the methods, with DPAM by concept ranking as the most precise as well.

Method	Cycle	*FC*	*FS*	*TS*
DPAM	ECE-15	1.88	50.0	63
PMP		1.93	50.1	73
RBS		1.99	49.8	36
DPAM	NEDC	2.92	50.0	1382
PMP		2.96	50.0	600
RBS		2.96	49.6	373
DPAM	WLTC 3-b	3.52	50.0	2320
PMP		3.59	50.0	962
RBS		3.63	49.7	617

Table 4.1: Comparison of HEV optimal control methods

Thus, DPAM is used to solve the optimal control problem when implementing the studied powertrain systemic design strategies.

On the other hand, RBS requires much less computation time than DPAM or PMP. This makes RBS a more adequate solution for fast optimal powertrain sizing. The overall calculation time is marginally reduced if the optimization algorithm recalculates the optimal control with each iteration. When using RBS, the biggest portion of the calculation time is spent on optimizing the strategy parameters. In Table 4.1, *TS* represents the total time required to find the most adequate parameters for RBS.

Table 4.2 presents the optimal values found for each one of the 3 driving cycles. The symbol "$\leq$" indicates that lower threshold values lead to similar results. Another optimization aimed at finding the optimal parameters for efficient power management of all three driving cycles combined is also conducted. These parameters, labeled general in the table below, minimize fuel consumption for the three driving cycles simultaneously. RBS's performance with these general parameters is close to DPAM's optimized results, with less than 5 % deviation found for each cycle separately.

Parameters	ECE-15	NEDC	WLTC 3-b	General
P_{s}	3700 W	1300 W	1700 W	3700 W
T_{s}	$\leq$ 40 N.m	$\leq$ 31 N.m	$\leq$ 35 N.m	30.5 N.m
SoC_{inf}	$\leq$ 44 %	31 %	$\leq$ 37 %	34 %
SoC_{sup}	$\leq$ 45 %	33 %	$\leq$ 38 %	40 %

Table 4.2: Comparison of HEV optimal control methods

This strategy is extended to other applications such as efficient real time control. More importantly, it is incorporated within systemic design strategy $\mathcal{A}_1$.

4.2.3 Analysis of optimal command

Figure 4.6 sums up the different outputs of the optimal command by DPAM, the most efficient strategy implemented, on the WLTC 3-b driving cycle. For better clarity, only the last portion of the cycle (extra-high speed section) is shown. The hybrid mode selection is also shown in the same figure.

The choice of a specific hybrid mode is justified based on the requested power values, leading to similar reasoning behind the establishment of the state machine for RBS is found. At

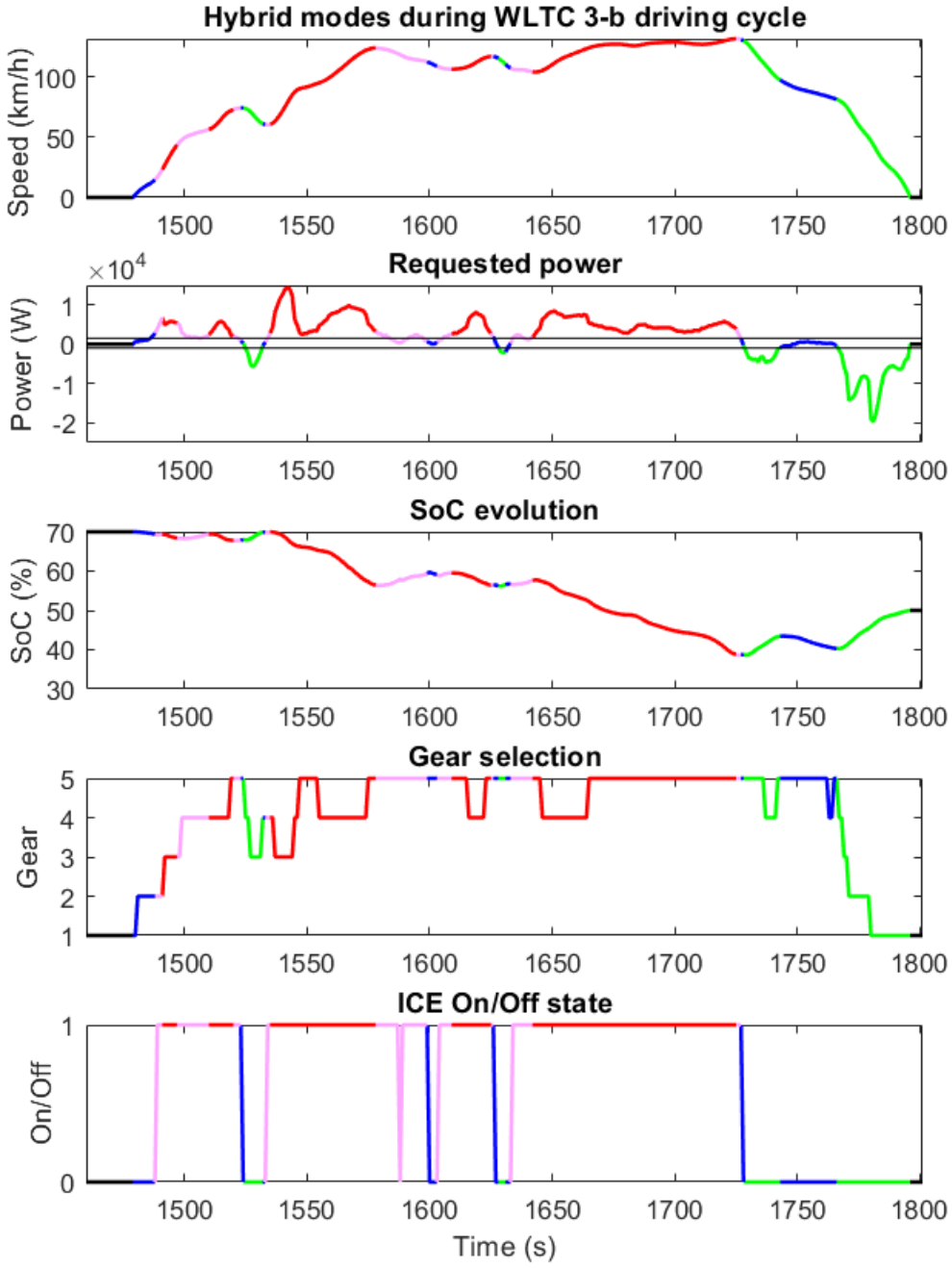

Figure 4.6: Optimal control results. Black: full stop, blue: ZEV mode - Red: Boost mode - Green: Regenerative Braking - Magenta: Generation mode

negative power request, the reversibility of the EM is exploited and the battery is recharged (regenerative braking). The restored energy is maximized by switching between high efficiency region or maximum power region through gear selection. This is represented over the EM's efficiency mapping in Figure 4.7.

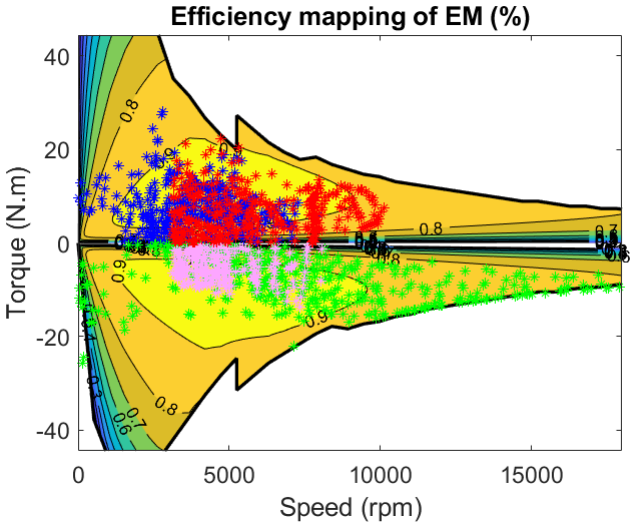

Figure 4.7: Optimal use of EM. Black: full stop - Blue: ZEV mode - Red: Boost mode - Green: Regenerative Braking - Magenta: Generation mode

Full electric mode (ZEV) is mainly selected when the power request is low, as displayed in Figure 4.6. This corresponds to the high efficiency operation region for the electrical machine as well. Using ZEV allows for longer engine shutdown which leads to higher gains in fuel consumption. ZEV is also used for takeoff from standstill or the vehicle's complete stop, due to the engine's limitations at low speed.

Generation is used at high power request when the ICE is at its high efficiency region. This enables battery recharging at a lower fuel cost, allowing for extended use of ZEV and Boost in the future afterwards when the engine is much less efficient. Generation is also selected when the battery's SoC reaches the minimum imposed value (30 %). For higher loads, Boost mode is selected to use the ICE more efficiently, as seen in Figure 4.8.

The SoC evolution is a consequence of the use of electrical energy: the battery is discharged when the EM is used during ZEV and torque assist phases and during the ICE's restart, while it is recharged by generation and regenerative braking. DPAM satisfies the iso-SoC condition, with the final value of SoC equal to its initial value set at 50 %.

The gear selection allows for higher efficiency use of the powertrain, even if it is limited by only one upshift or downshift per time step. 266 gear switches are recorded during the 30-minute driving cycle, which comes to 1 gear switch each 7 seconds.

4.2.4 Comparison with simulation platform

Command calculated using DPAM and the proposed vehicle backward model has been compared with the results provided by Valeo's simulation platform. This platform is based on

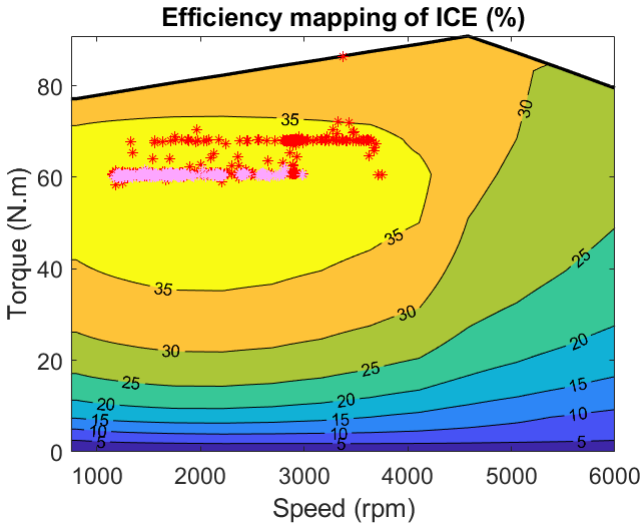

Figure 4.8: Optimal use of ICE. Red: Boost mode - Magenta: Generation mode

a forward vehicle model of the powertrain implemented on Amesim [145], controlled by a driver model and uses an equivalent consumption minimization strategy (ECMS) for power management.

This strategy is based on the PMP paradigm and uses a prediction horizon of 50 s at every time step to determine a value for λ. The cycle on the other hand is discretized to 0.02 s to take into account various dynamic phenomena that has been simplified in this study such as gear shifting and determine the best values for the command parameters.

Similar command is found for short cycles, as seen on Figure 4.9, and close consumption values are found for different driving cycles, validating the proposed powertrain model.

4.2.5 Application on different powertrains

3 EMs and 3 ICEs with varying characteristics (peak power, peak torque, inertia, mass and efficiency mappings) have been selected to equip the same hybrid vehicle as before. Fuel consumption values are then calculated using DPAM and are summed up in Table 4.3.

EM \ ICE		A	B	C
		43 kW	50 kW	63 kW
I	10 kW	3.14	3.09	3.89
II	13 kW	3.04	3.00	3.74
III	16 kW	3.24	3.21	3.95

Table 4.3: Comparison of fuel consumption values in l/100 km of different powertrains

It can be seen that configuration B-II has the lowest fuel consumption value and is thus the most adequate between the studied propositions for this application. Besides fuel gains, powertrain characteristics have an important impact over optimal command. Figure **??** shows the optimal hybrid mode distribution between the studied powertrain configurations.

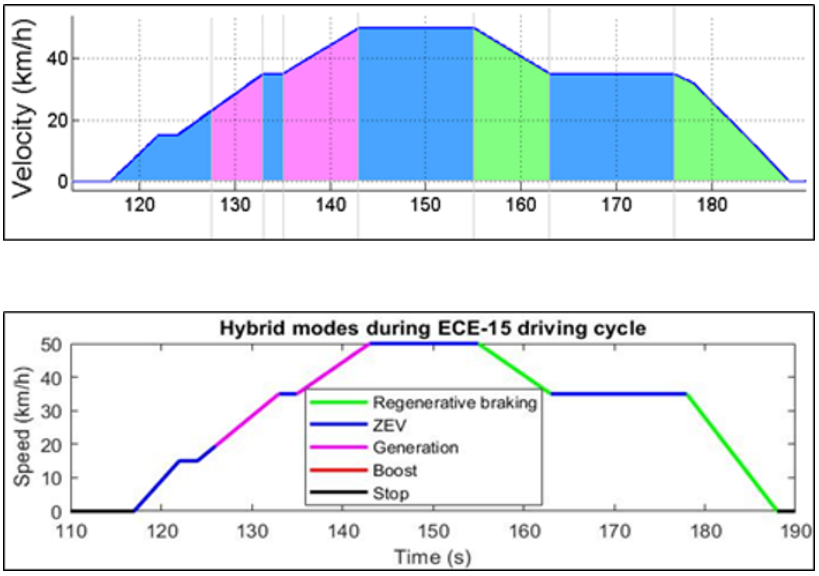

Figure 4.9: power management results. Above: simulation platform results - Below: proposed model results

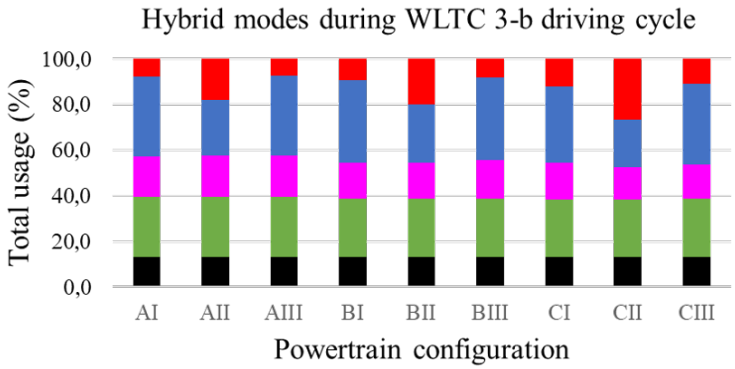

Figure 4.10: Optimal hybrid mode allocation between the studied powertrain, listed as in Table 4.3. Black: full stop, blue: ZEV mode - Red: Boost mode - Green: regenerative braking - Magenta: generation mode

It is concluded that the command greatly varies from one powertrain configuration to the other. For this reason, it is crucial to integrate the optimization of the control strategy when optimizing the design of the hybrid powertrain.

4.3 HEV cycle reduction

Once the optimal command of an HEV is defined, the optimal operation points of the different powertrain components can be determined. Cycle reduction techniques, presented in Chapter 1, are investigated afterwards to greatly reduce the number of the EM's operation points that are considered. This allows for faster assessment of the machine performance

over the driving cycle and can be used in conjunction with the proposed design approach $\mathcal{A}_3$.

4.3.1 Studied cycle reduction techniques

Four cycle reduction methods are implemented: Random sampling, histogram, barycenter and clustering methods. These methods vary first of all in the way they define the points of interest based on the thousands of operation points found for the EM during a specific driving cycle, as seen in Figure 4.11.

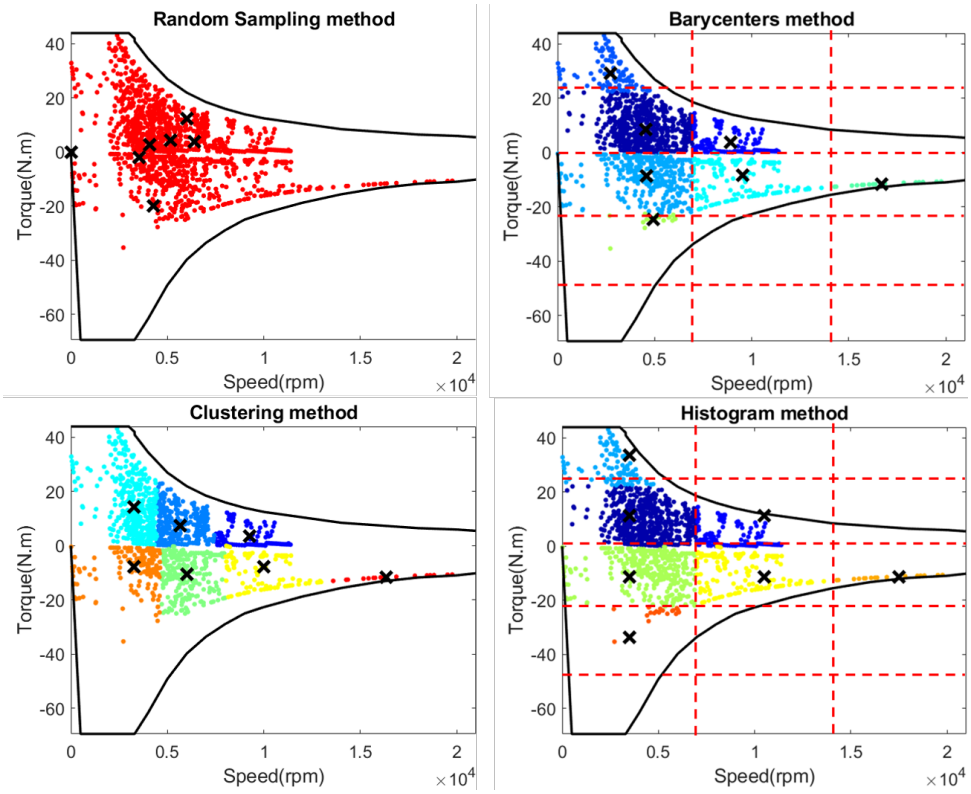

Figure 4.11: Application of different cycle reduction techniques

The random sampling method arbitrarily selects a reduced number of operation points, while the histogram and barycenter techniques divide the operation range of the machine into multiple regions before selecting their centers or barycenters respectively. In contrast, the clustering method uses the k-means approach to form homogeneous groups of operation points called clusters, from which the barycenter is selected afterwards.

Two variants are explored afterwards to evaluate the machine losses over the driving cycle using the selected interest points. The first variant introduces an equivalency factor between the losses calculated over the interest points and the total losses over the operations points in the corresponding segment, which is expressed as:

$$k_{\mathrm{eq,i}} = \frac{\sum_{j=1}^{N_{\mathrm{pt,i}}} T_{\mathrm{EM,(i,j)}} \omega_{\mathrm{EM,(i,j)}}}{T_{\mathrm{EM,i}} \omega_{\mathrm{EM,i}}} \tag{4.6}$$

where $N_{\mathrm{pt,i}}$ is the number of points in group i, $T_{\mathrm{EM,(i,j)}}$ and $\omega_{\mathrm{EM,(i,j)}}$ are the torque in N.m and rotation speed values in rpm respectively for operation point j in segment i, while $T_{\mathrm{EM,i}}$ and $\omega_{\mathrm{EM,i}}$ are the torque in N.m and rotation speed in rpm respectively of interest point i.

Meanwhile, the second variant is based on employing different expressions for the different types of machine losses enumerated in Section 3.3, as they evolve differently with respect to the torque and rotational speed values.

The following expressions are given instead:

$$Ene_{\mathrm{Joule,cycle}} = \sum_{i=1}^{N_{\mathrm{pt}}} N_{\mathrm{pt,i}} \frac{\sum_{j=1}^{N_{\mathrm{pt,i}}} T_{\mathrm{EM,(i,j)}}{}^2}{(\sum_{j=1}^{N_{\mathrm{pt,i}}} T_{\mathrm{EM,(i,j)}})^2} Losses_{\mathrm{Joule,i}} \Delta t \tag{4.7a}$$

$$Ene_{\mathrm{Iron\text{-}Hys,cycle}} = \sum_{i=1}^{N_{\mathrm{pt}}} N_{\mathrm{pt,i}} Losses_{\mathrm{Iron\text{-}Hys,i}} \Delta t \tag{4.7b}$$

$$Ene_{\mathrm{Iron\text{-}EC,cycle}} = \sum_{i=1}^{N_{\mathrm{pt}}} N_{\mathrm{pt,i}} \frac{\sum_{j=1}^{N_{\mathrm{pt,i}}} \omega_{\mathrm{EM,(i,j)}}{}^2}{(\sum_{j=1}^{N_{\mathrm{pt,i}}} \omega_{\mathrm{EM,(i,j)}})^2} Losses_{\mathrm{Iron\text{-}EC,i}} \Delta t \tag{4.7c}$$

$$Ene_{\mathrm{Mech,cycle}} = \sum_{i=1}^{N_{\mathrm{pt}}} N_{\mathrm{pt,i}} Losses_{\mathrm{Mech,i}} \Delta t \tag{4.7d}$$

$$Ene_{\mathrm{Inverter\text{-}Cond,cycle}} = \sum_{i=1}^{N_{\mathrm{pt}}} N_{\mathrm{pt,i}} \frac{\sum_{j=1}^{N_{\mathrm{pt,i}}} T_{\mathrm{EM,(i,j)}}{}^2}{(\sum_{j=1}^{N_{\mathrm{pt,i}}} T_{\mathrm{EM,(i,j)}})^2} Losses_{\mathrm{Inverter\text{-}Cond,i}} \Delta t \tag{4.7e}$$

$$Ene_{\mathrm{Inverter\text{-}Comm,cycle}} = \sum_{i=1}^{N_{\mathrm{pt}}} N_{\mathrm{pt,i}} Losses_{\mathrm{Inverter\text{-}Comm,i}} \Delta t \tag{4.7f}$$

The machine's total losses over the cycle are then estimated as the sum of the previously calculated values for each type of losses.

For the random sampling technique however, as no divisions are defined when applying said method, the following expression is proposed to estimate the cycle losses:

$$Ene_{\mathrm{cycle}} = \sum_{i=1}^{N_{\mathrm{pt}}} k_{\mathrm{eq,i}} Losses_{\mathrm{pt,i}} \Delta t \tag{4.8}$$

with:

$$k_{\mathrm{eq,i}} = \frac{N_{\mathrm{pt,tot}}}{N_{\mathrm{pt}}} \tag{4.9}$$

where N_{pt} is the number of interest points and $N_{\mathrm{pt,tot}}$ is the total number of operation points. $Losses_{\mathrm{pt,i}}$ are the machine losses calculated at the interest point i in W.

4.3.2 Comparison and analysis

The studied techniques with both alternatives for loss calculation are applied afterwards to estimate the losses of an electric machine over the WLTC 3-b driving cycle, while only

selecting 10 points of interest. Table 4.4 summarizes the results of the comparison, where deviations between the output values for each type of machine losses found when using cycle reduction methods and the real total cycle losses are presented in relative values.

	Joule (%)	Iron (Hys) (%)	Iron (EC) (%)	Mech (%)	Comm (%)	Cond (%)	Total losses (%)
Random sampling	20.72	5.61	23.13	11.73	11.63	15.81	**17.93**
Histogram (var. 1)	13.23	12.02	5.46	8.44	3.53	8.00	**7.61**
Histogram (var. 2)	13.23	9.14	2.11	4.92	3.53	8.00	**5.06**
Barycenters (var. 1)	17.07	0.64	7.77	3.94	10.63	13.60	**9.56**
Barycenters (var. 2)	17.07	2.08	0.28	0.27	10.63	13.60	**6.02**
Clustering (var. 1)	14.42	0.04	1.45	1.19	4.89	9.28	**5.29**
Clustering (var. 2)	14.43	1.04	0.45	0.00	4.92	9.30	**4.34**

Table 4.4: Deviation between the proposed cycle reduction techniques and real cycle losses

It can be understood that the second variant for each technique leads to better results. Furthermore, when considering the total machine losses, it can be deduced that the clustering method is the most accurate amongst the studied methods.

This can be enhanced by considering more interest points, as shown in Table 4.5. However, the required calculation time when implementing the selected method will also increase proportionally.

Number of clusters	5	10	15	20
Deviation (%)	6.15	4.34	3.95	3.33

Table 4.5: Evolution of clustering methods accuracy with respect to the number of interest points selected

4.3.3 Mirroring technique

A novel technique is proposed to improve the precision of the studied methods without increasing the number of interest points. This method, named Mirroring and shown in Figure 4.12, assumes that close loss values are found for two machine operation points of opposite electromagnetic torque values defined by (ω_{EM}, T_{El}) and (ω_{EM}, -T_{El}).

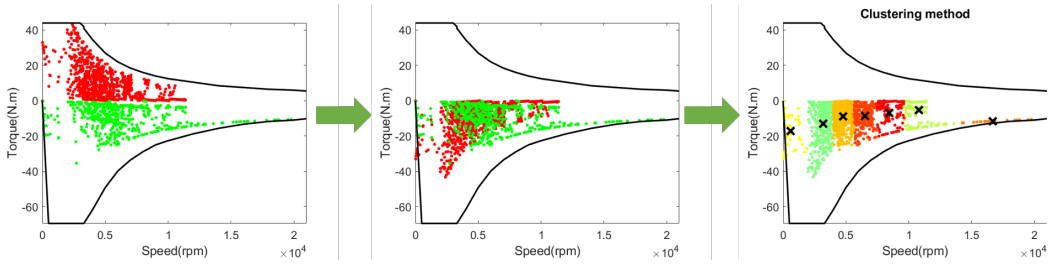

Figure 4.12: Mirroring technique principle applied using the clustering method

The technique then "mirrors" the operation points in motor mode into the generator operation range of the EM, before applying any of the previously mentioned cycle reduction methods.

This approach allows for a much more accurate division of one of the machine modes without modifying the total number of interest points selected. Table 4.6 presents the results

when applying this method using the second variant of the clustering technique for the same application described before.

	Joule + AC	Iron (Hysteresis)	Iron (EC)	Mechanical	Commutation	Conduction	Total losses
Original (%)	14.43	1.04	0.45	0.00	4.92	9.30	4.34
With Mirroring (%)	3.90	0.34	0.43	0.00	0.66	1.44	0.86

Table 4.6: Comparison between the proposed cycle reduction techniques. Deviations are calculated in relative value compared to cycle loss values

It can be seen that the accuracy of the technique has greatly improved in this case, with a general deviation in total losses of less than 1 %. This method is then selected for use with approach $\mathcal{A}_3$.

4.4 HEV case study

The powertrain design optimization applications conducted afterwards consider a similar setting to the one introduced in the previous chapter: a parallel hybrid compact car, whose characteristics as well as the features of the different powertrain components are presented in Table 4.7.

Component	Notation	Value
Vehicle	M	1470 kg
	C_{R}	4.57 10^{-3}
	k_{R}	1.79 10^{-4} s/m
	SC_{x}	0.6044 m^2
	r	0.2032 m
	Γ_{r}	3.76 $\mathrm{kg.m}^2$
Battery	C_{Batt}	54000 A.s
	I_{max}	310
	x_0	50 %
	x_{f}	50 %
	$MOCV$	45.31 V
	MIR	0.0118 Ω
Auxiliairies	$Cons$	0 W
	η_{DC}	90 %
Machine	Gap_{Air}	0.5 mm
	T_{Cooling}	75 °C
Transmission	R_{GB}	{3.45;1.86;1.11;0.76;0.57}
	Γ_{GB}	0.05 $\mathrm{kg.m}^2$
	R_{D}	4.29
	Γ_{T}	0 $\mathrm{kg.m}^2$
Engine	Γ_{ICE}	0.259 $\mathrm{kg.m}^2$
	$\omega_{\mathrm{ICE,max}}$	6250 rpm
	ω_{Idle}	750 rpm
	$P_{\mathrm{ICE,max}}$	81 kW
Starter	η_{St}	70 %

Table 4.7: Studied vehicle characteristics

The problem expressed in Chapter 3 is then solved, with the vehicle's fuel consumption evaluated over the WLTC 3-b cycle, with Δt equal to 1 s. This cycle is selected as it has been designed to be more representative of the real and modern driving conditions compared to previous homologation procedure, becoming the reference cycle for measuring CO_2 emissions. This measurement takes place in laboratory conditions on a flat and dry road.

The various constraints enumerated in the previous chapter are considered afterwards. Based on a given set of machine and project requirements, key values necessary to validate the machine design are deduced. These parameters are listed in Table 4.8.

Parameter	Value
$P_{\text{max,req}}$	25 kW
$T_{\text{max,req}}$	70 N.m
$\omega_{\text{EM,max}}$	21000 rpm
D_{max}	161 mm
L_{max}	119 mm
Lim_{EL}	365 MPa
T_{Coating}	250 °C
$Ripple_{\text{max}}$	15 %
f_{max}	10 kHz

Table 4.8: Required values for the definition of EM design constraints

The large number of design variables present in the original optimization problem however should be reevaluated, as this will lead to longer optimizations as well as convergence difficulties afterwards. Different options should be assessed to restrain the number of variables considered and allow for an optimal machine design to be found in reasonable delays.

4.5 Screening study

The presence of 32 design variables has prompted the launch of screening experiments, in a bid to reduce the number of decision variables during optimization. This study is one of the main stages of the design of experiments (DoE), a widely used tool in engineering that maximises learning about a system or a process while using minimum resources [146, 147].

Screening designs are used to scout the search space when little is known about the mathematical models used for the optimization application. It is possible afterwards to deduce the impact of each studied parameter, but interactions between the latter are hard to interpret.

For this study, a reduced number of experiments are selected using Sobol's Quasirandom Sequence to achieve uniform distribution over the search space [112]. Possible configurations are limited by the ranges defined in Table 3.1. An initial pool sample of 346 designs, over 10 times the total number of design variables, is chosen to achieve acceptable accuracy.

The cost function is calculated using DPAM, while the various constraints adopt the models described previously. The impact of each factor is evaluated using Pearson's correlation coefficient [148], expressed as:

$$I_{\mathrm{d_i,y_j}} = \frac{|\sum_{k=1}^{n}(d_{\mathrm{i,k}} - \bar{d}_{\mathrm{i}})(y_{\mathrm{j,k}} - \bar{y}_{\mathrm{j}})|}{\sqrt{\sum_{k=1}^{n}(d_{\mathrm{i,k}} - \bar{d}_{\mathrm{i}})^2}\sqrt{\sum_{k=1}^{n}(y_{\mathrm{j,k}} - \bar{y}_{\mathrm{j}})^2}} \tag{4.10}$$

where $d_{\mathrm{i,k}}$ refers to the value of design variable d_{i} in experiment k, while $\bar{d}_{\mathrm{i}}$ corresponds to its mean value over the pool sample, defined by its size n. Similarly, $y_{\mathrm{j,k}}$ refers to the value of output y_{j} for evaluation k while $\bar{y}_{\mathrm{j}}$ refers to its mean value.

Figures 4.13, 4.14, 4.15 and 4.16 show the screening results found for the main outputs of the models used in this work that are crucial for the optimization process: fuel consumption J_{fuel}nomenclature[Z] T_{max}Fuel consumption over driving cycle [l] over the WLTC 3-b cycle, the machine's peak power P_{max}, its peak torque T_{max} and the stator winding's maximum temperature attained in a short-circuit scenario at high speed T_{Copper}.

The effect of the various parameters on the studied outputs can also be mostly deduced using the current understanding of the operation of the electrical machine. The screening helps confirm these initial hypothesis as well as select the most "vital" parameters.

Since constrained optimizations are conducted afterwards, this selection should be based on the impact of these factors on all of the outputs displayed above and not only the cost function by itself. Figure 4.17 shows the global impact of each design parameter. The global impact is a weighted sum of effects where the impact on fuel consumption is given a weight of 3, while all the other outputs discussed earlier are attributed a uniform weight of 1.

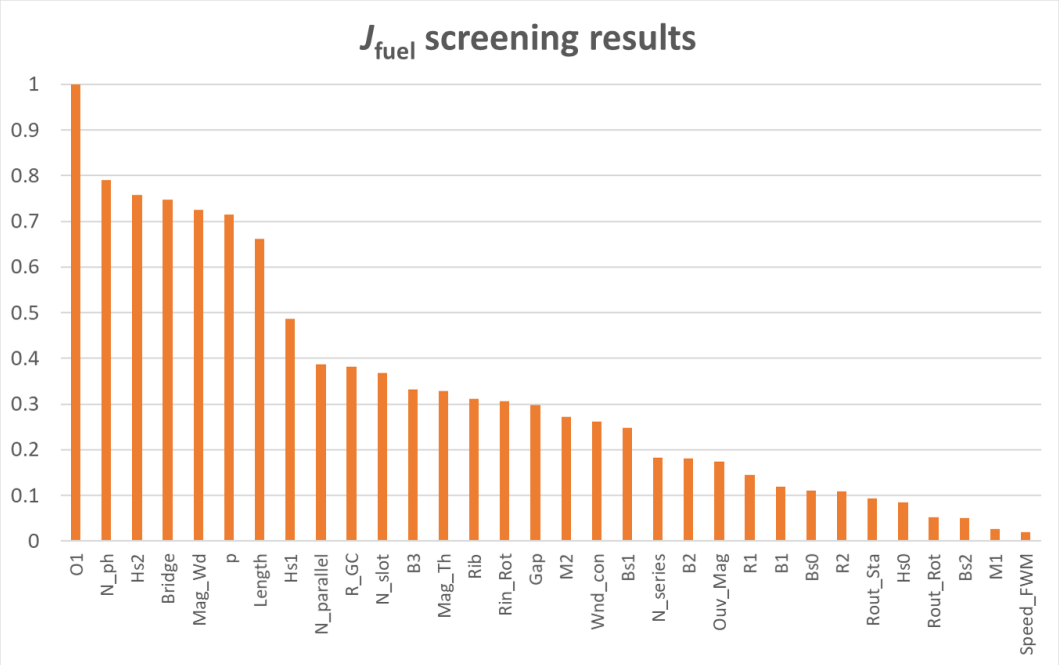

Figure 4.13: Normalized Pearson coefficients for J_{fuel} deduced from conducted screening experiments

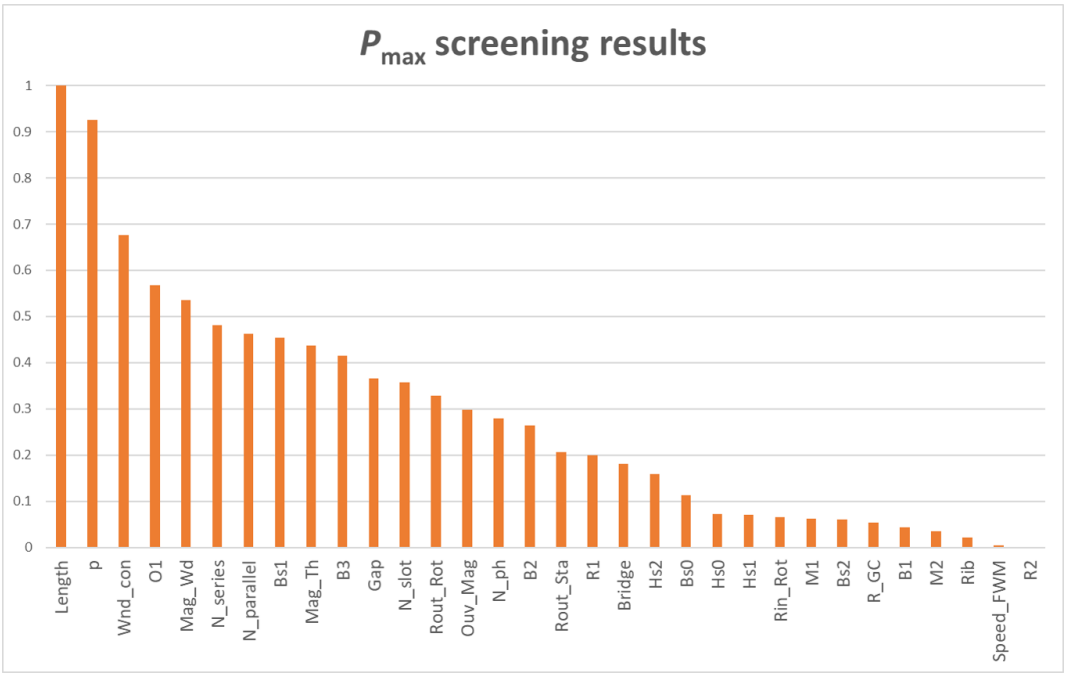

Figure 4.14: Normalized Pearson coefficients for $P_{\max}$ deduced from conducted screening experiments

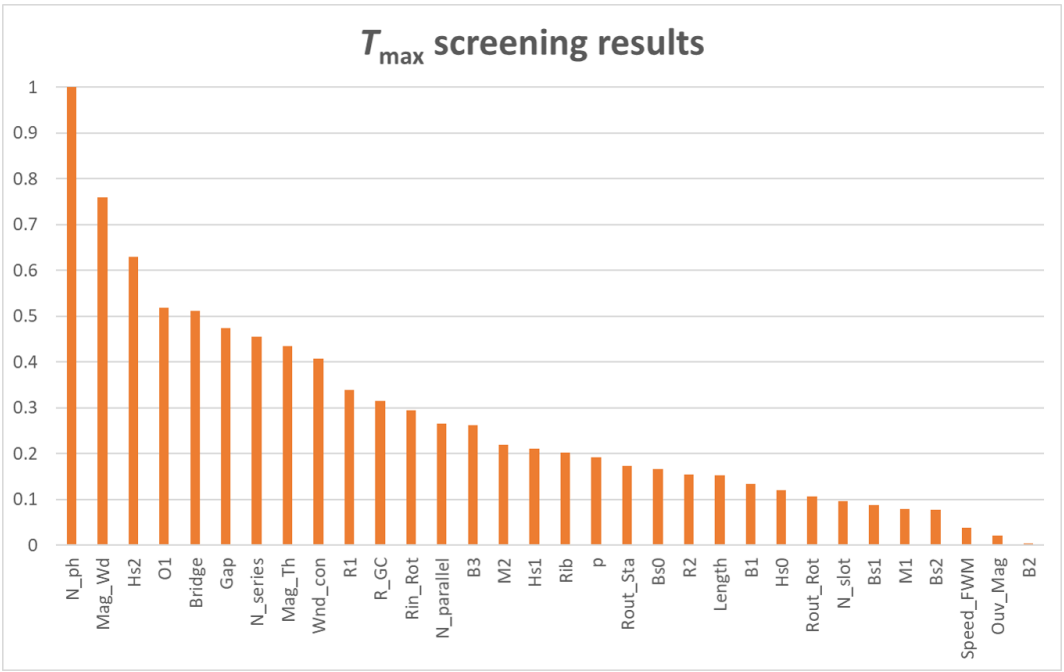

Figure 4.15: Normalized Pearson coefficients for $T_{\max}$ deduced from conducted screening experiments

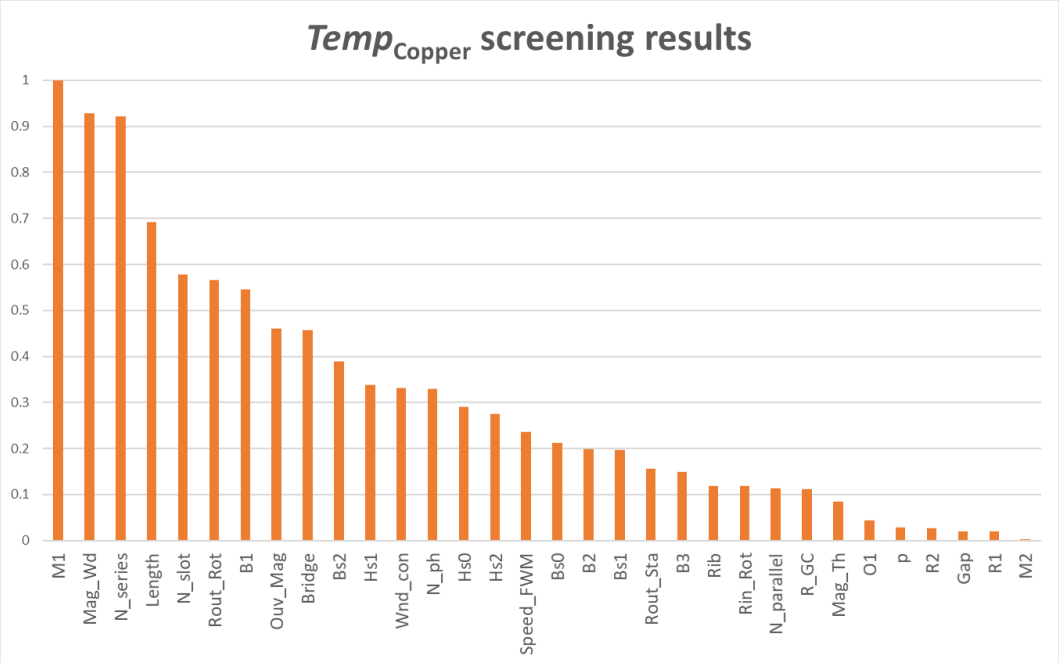

Figure 4.16: Normalized Pearson coefficients for $Temp_{\text{Copper}}$ deduced from conducted screening experiments

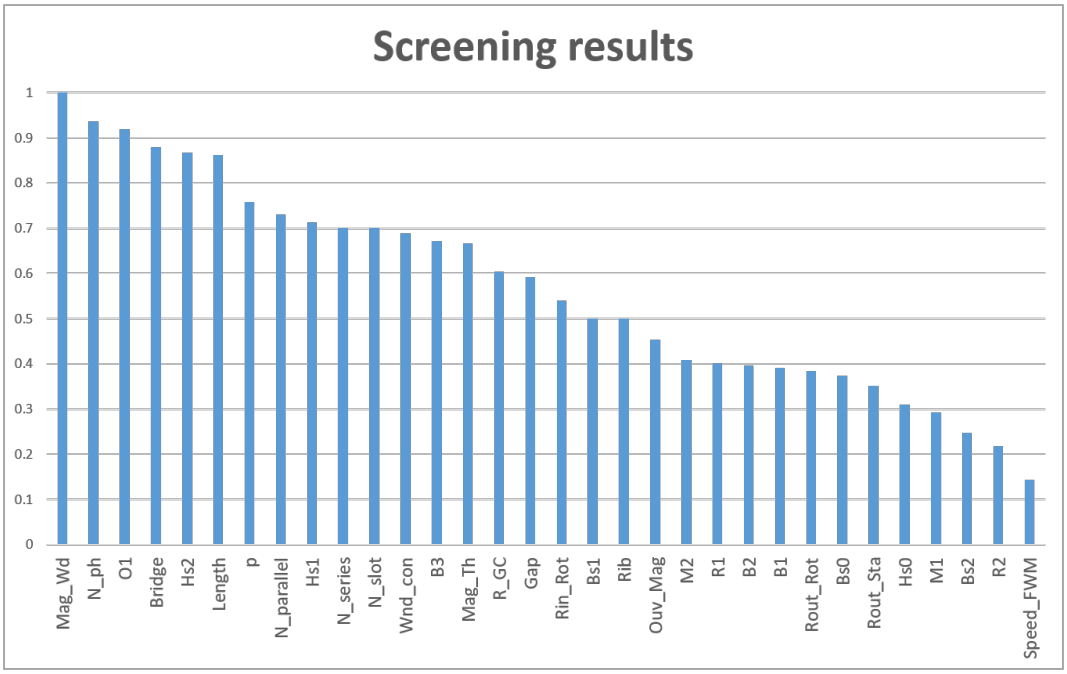

Figure 4.17: Normalized global impact of the design parameters deduced from conducted screening experiments

Aside from identifying the most influential design variables, the screening experiments are also used to calculate coefficients $\boldsymbol{b}$ of the analytical models used for approach $\mathcal{A}_2$, expressed in Equation 4.6. The resulting models lead to very low values of RMSD (Root-mean-square deviation), which is seen as a good measure for their "goodness-of-fit".

4.6 Optimization results

The proposed systemic design strategies are assessed over the parallel hybrid powertrain optimization problem. The solutions found by each approach are compared afterwards to an existing design referred to as REF. The machine in question satisfies the various requirements of the design application and was optimized for maximum efficiency at a single operation point: peak torque at 1000 rpm.

4.6.1 Optimization over 4 design variables

A first comparison is conducted based on the optimization of 4 continuous parameters. These are selected following the conclusions of the screening study (d_1: Mag_{Wd}, d_2: *O1*, d_3: *Bridge*, d_4: *Hs2*). The other design parameters are fixed and are equal to those of the reference design, which also serves to initialize the chosen optimization variables when using the different approaches. Since approach $\mathcal{A}_2$ allows for much faster model evaluations, Sobol's Quasirandom Sequence is used again to generate 100 additionnal initial guesses for the optimization algorithm to help it achieve better results.

The selection of the continuous parameters over the discrete parameters has been made to simplify the search process, as discrete variables only have two or three possible values. This then limits the use of mixed variable optimization algorithms such as Branch and Bound. Their recommended values, determined based on the previous screening process, have also been found to correspond to the initial design's values.

The average distance between the optimal parameters and their reference $dist_{\mathrm{Avg}}$ and the maximum distance to reference $dist_{\mathrm{Max}}$ are evaluated as well and calculated using the following expressions:

$$dist_{\mathrm{Avg}} = \frac{1}{N} \sum_{i=1}^{N} \frac{|d_{\mathrm{i,ref}} - d_{\mathrm{i}}{}^*|}{d_{\mathrm{i,max}} - d_{\mathrm{i,min}}} \tag{4.11a}$$

$$dist_{\mathrm{Max}} = \max_i \frac{|d_{\mathrm{i,ref}} - d_{\mathrm{i}}{}^*|}{d_{\mathrm{i,max}} - d_{\mathrm{i,min}}} \tag{4.11b}$$

where N is the number of optimization variables while $d_{\mathrm{i,min}}$ and $d_{\mathrm{i,max}}$ refer respectively to the lower and upper bounds for optimization variable d_{i}. $d_{\mathrm{i,ref}}$ and $d_{\mathrm{i}}{}^*$ correspond respectively to its reference and optimal values.

Table 4.9 compiles the optimization results. The total cost difference between the optimal designs and the reference machine in € is estimated, as well as the number of cost function evaluations and total calculation time in s.

The solutions provided by each approach satisfy the imposed constraints. High values of both $dist_{\mathrm{Avg}}$ and $dist_{\mathrm{Max}}$ demonstrate the ability of the different approaches to search for

Approach	$\mathcal{BL}$	$\mathcal{IT}$	$\mathcal{A}_1$	$\mathcal{A}_2$	$\mathcal{A}_3$
$dist_{\text{Avg}}$	0.1187	0.0906	0.0744	0.3191	0.1225
$dist_{\text{Max}}$	0.3243	0.2747	0.2053	0.8814	0.3333
Total cost reduction	370 €	377 €	340 €	122 €	253 €
EM cost reduction	81 €	87 €	63 €	40 €	60 €
CO_2 emissions reduction	3.04 gCO_2/km	3.05 gCO_2/km	2.92 gCO_2/km	0.86 gCO_2/km	2.03 gCO_2/km
Number of cost function evaluations	29	252	19	5900	331
Calculation time	24273 s	125019 s	5341 s	822 s	128536 s

Table 4.9: Comparison of systemic design approaches based on 4 optimization variables

the optimal solution outside the immediate vicinity of the initial design.

In terms of total cost reduction, approaches $\mathcal{BL}$, $\mathcal{IT}$ and $\mathcal{A}_1$ have led to close performance. The best solution for this first application, labeled OD1, is the one proposed by approach $\mathcal{IT}$. However, important disparity is found between these three approaches in terms of calculation times.

$\mathcal{A}_1$ finds an optimal solution 25 times faster than the iterative approach, since a much higher number of total function evaluations is needed for approach $\mathcal{IT}$, as a result of multiple outer loop iterations when using the latter. This then leads to important computation times, and makes it even slower than the $\mathcal{BL}$ approach, which requires the longest function evaluation times between the implemented strategies. This can be improved for example by relaxing tolerances of the iterative loop, set at 0.1 € for this application. Thus, it can be concluded that $\mathcal{A}_1$ represents the best compromise in this initial comparison.

The remaining approaches also manage to reduce costs, but fail to reach the same level of gains as the previously mentioned strategies. This means that the necessary conditions stated in Chapter 2 to achieve system optimality have not been met. It is understood that to achieve higher cost reduction, the accuracy of the adopted models needs to be improved as well when using either approaches.

On one hand, for approach $\mathcal{A}_2$, improving the model's precision could rely on increasing the number of sample experiments. Approach $\mathcal{A}_3$ on the other hand, which is based on cycle reduction techniques, should consider additionnal clusters in order to find similar solutions to those found by the iterative approach. On a different note, computation times for approaches $\mathcal{IT}$, $\mathcal{A}_1$ and $\mathcal{A}_3$ can be easily divided by 5 folds when launching even more FE simulations in parallel. This has not been possible during this study as a consequence of hardware and software license limitations.

4.6.2 Optimization over 10 design variables

A second comparison is launched afterwards for an increased number of optimization variables, identified based on the findings in Table 4.3 as well: machine design parameters Mag_{Wd}, *O1*, *Bridge*, *Hs2*, *Length*, *Hs1*, *B3*, Mag_{Th}, *Gap* and gear connection ratio R_{GC}. Table 4.10 summarizes the comparison results.

As expected, adding more optimization variables leads to better cost reductions when using the various systemic design approaches, while significantly increasing calculation times. This justifies once more the importance of limiting the number of decision variables to obtain optimization results in reasonable delays.

The bi-level approach has led to better cost reduction compared to approaches $\mathcal{IT}$ and

Approach	$\mathcal{BL}$	$\mathcal{IT}$	$\mathcal{A}_1$	$\mathcal{A}_2$	$\mathcal{A}_3$
$dist_{\text{Avg}}$	0.0940	0.0952	0.0505	0.1863	0.0550
$dist_{\text{Max}}$	0.6438	0.5861	0.3601	1	0.3784
Total cost reduction	806 €	661 €	597 €	151 €	424 €
EM cost reduction	87 €	85 €	86 €	71 €	71 €
CO_2 emissions reduction	7.57 gCO_2/km	6.06 gCO_2/km	5.38 gCO_2/km	0.84 gCO_2/km	3.72 gCO_2/km
Number of cost function evaluations	164	681	365	8600	459
Calculation time	137268 s	336087 s	102617 s	891 s	177841 s

Table 4.10: Comparison of systemic design approaches based on 10 optimization variables

$\mathcal{A}_1$ for this application. This can be explained in part by comparing values of $dist_{\text{Max}}$. Similar conclusions to those found in Chapter 2 are outlined: approaches $\mathcal{IT}$ and $\mathcal{A}_1$ are more sensitive to the selected design initialization. Increasing the number of initial guesses will improve the quality of their solutions. OD2, the solution found by approach $\mathcal{BL}$ leads to the best total cost reduction.

In terms of computation time, similar findings to those of the previous application are observed in here as well, with approach $\mathcal{A}_2$ logically remaining the fastest approach. The previous recommendations made for both $\mathcal{A}_2$ and $\mathcal{A}_3$ to improve the quality of their proposed solution and approaches $\mathcal{IT}$, $\mathcal{A}_1$ and $\mathcal{A}_3$ to drastically reduce their calculation times are also valid for this application.

4.6.3 Design optimization without considering performance constraints

A study is conducted afterwards to evaluate the impact of design constraints and their role in altering the optimization's results. If most of the design conditions considered in the previous applications, such as the cooling efficiency and mechanical integrity of the machine, need to be satisfied since they impact the product's quality, its lifespan and are necessary to comply with the company's standards, others are seen as not critical when designing an EM.

One of these conditions are the performance constraints, linked to the machine's peak power P_{max} and peak torque T_{max}. These requirements are system design guidelines that should allow for near-optimal use of the powertrain, as opposed for pure EV applications in contrast, where these quantities have direct impact on the vehicle's specifications such as acceleration and torque at standstill.

Approach $\mathcal{BL}$ is used afterwards to find a new solution OD3 for the previous application without considering the aforementioned performance constraints. The results are compiled in Table 4.11.

$dist_{\text{Avg}}$	0.1095
$dist_{\text{Max}}$	0.6672
Total cost reduction	846 €
EM cost reduction	163 €
CO_2 emissions reduction	7.18 gCO_2/km
Number of evaluations	88
Calculation time	73656 s

Table 4.11: Powertrain optimization results over 10 variables without considering design constraints

As expected, the overall cost is improved, leading to a further 40 € cost reduction. The systemic design process is much faster as well, converging nearly twice as fast when compared to the previous application. The proposed approach is used to challenge design guidelines and can be applied further as a pre-design tool as well.

4.7 Comparison of optimal designs

The 2D pole geometries of REF, OD1, OD2 and OD3 are displayed in Figure 4.18 while their efficiency mappings are shown in Figure 4.19. Their characteristics are listed in Table 4.12.

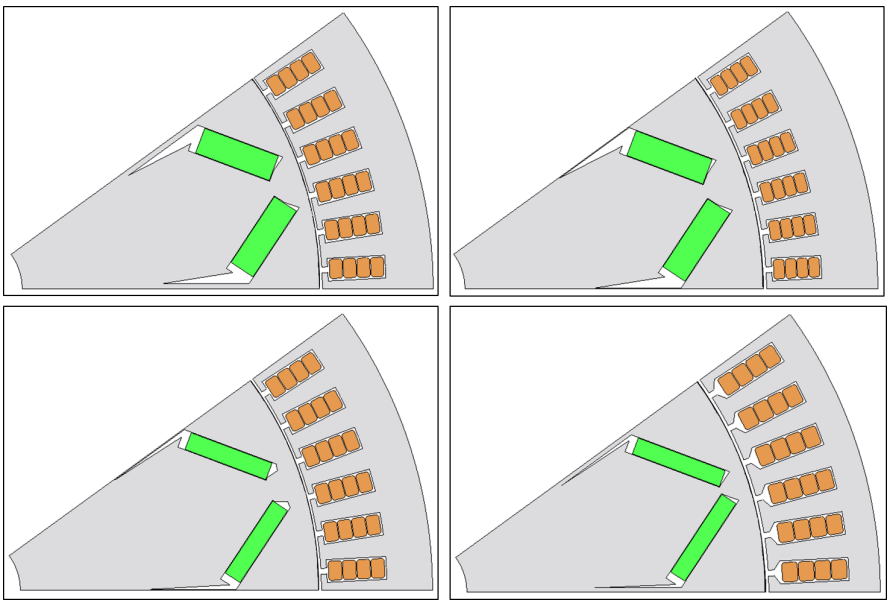

Figure 4.18: 2D pole geometry of the proposed designs. From top left to bottom right: REF - OD1 - OD2 - OD3

Characteristics	REF	OD1	OD2	OD3
Peak power	29.37 kW	25.29 kW	25.02 kW	21.19 kW
Peak torque	88.86 N.m	79.19 N.m	72.52 N.m	56.30 N.m
Maximum speed	21000 rpm	21000 rpm	21000 rpm	21000 rpm
Torque ripple	9.12 %	8.07 %	13.29 %	14.39 %
Peak copper temperature	235 °C	152 °C	170 °C	138 °C
Total length	110.23 mm	115 mm	109 mm	111 mm
External diameter	155 mm	161 mm	161 mm	161 mm

Table 4.12: Characteristics of the proposed designs

The main difference between REF and OD1 lies in the enhanced efficiency in the high speed and maximum power regions. This then enables much lower electrical energy consumption, which improves the vehicle's fuel efficiency.

Meanwhile, at similar peak power, OD2's design provides more efficient traction throughout all of the machine's operation range, which then leads to lower fuel consumption com-

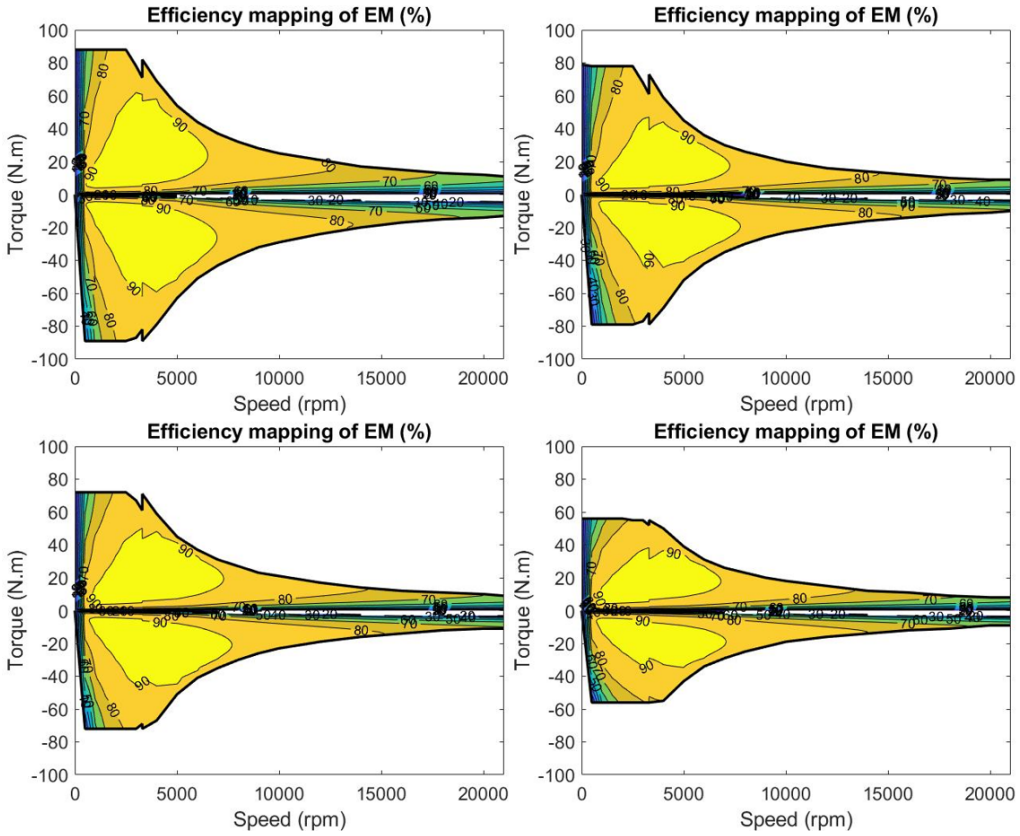

Figure 4.19: Efficiency mappings of the proposed designs. From top left to bottom right: REF - OD1 - OD2 - OD3

pared to OD1. The gear connection ratio was also optimized to allow better use of the powertrain.

Finally, OD3's efficiency is close to that of OD2. However, the total cost reduction is largely attributed to a lower machine cost, since the machine's peak power has greatly decreased. This means the initial design requirements led to the unnecessary oversizing of the EM for this type of application. A powertrain equipped with a 21 kW machine is able to achieve to similar levels of fuel economy as another drivetrain using 25 kW machine.

Lower peak temperatures observed for all three optimal designs compared to the reference machine are also a direct consequence of their improved efficiency, as this translates to lower losses in a short-circuit scenario.

4.8 Sensitivity analysis

In the previous sections, the optimization problem is solved in a deterministic way. However, when industrial processes are involved, the different design variables add in a certain degree of uncertainty into their values. It is then recommended to assess the robustness of the optimal solution that is provided. For the scope of this study, a solution is considered robust if the cost reduction does not degrade by over 5 % when integrating said uncertainties, while

all the design requirements are satisfied.

A local sensitivity analysis can for example be conducted where the impact of adding small perturbations to the nominal variables over the quality of the solution is quantified [149, 150]. Mathematically, this sensitivity index, referred to as ***SI***, is equal to the partial derivative of the total cost function with respect to these variables. The term local means all derivatives are taken at the optimal solution. The optimization requirements need to be fulfilled as well when considering these design variations.

In this work, the values of ***SI*** are calculated using finite differences, as detailed in the following expression:

$$SI_{\mathrm{i}}=J(\boldsymbol{d}^*_{\mathrm{i}}, \boldsymbol{u}^*) - J(\boldsymbol{d}^*, \boldsymbol{u}^*) \tag{4.12}$$

where $\boldsymbol{d}^*_{\mathrm{i}}$ is a configuration which differs from optimal set $\boldsymbol{d}^*$ by design variable d_{i}, whose value is displaced by step Δ_{i}. The step values is deduced from the study of manufacturing tolerances for the different geometric parameters, and are listed in Table 4.13.

Δ_{Length}	Δ_{Hs1}	Δ_{Hs2}	Δ_{Gap}	Δ_{Bridge}	Δ_{B3}	Δ_{O1}	$\Delta_{Mag_{Th}}$	$\Delta_{Mag_{Wd}}$	$\Delta_{\mathrm{R_{GC}}}$
0.50 mm	0.2 mm	0.2 mm	0.1 mm	0.1 mm	0.1 mm	0.1 mm	0.05 mm	0.05 mm	0.01

Table 4.13: Step values for the selected design variables

The values for SI_{i} with regards to the selected optimization variables are summarized in Table 4.14.

SI_{Length}	SI_{Hs1}	SI_{Hs2}	SI_{Gap}	SI_{Bridge}	SI_{B3}	SI_{O1}	$SI_{Mag_{Th}}$	$SI_{Mag_{Wd}}$	$SI_{\mathrm{R_{GC}}}$
0.90 €	0.85 €	0.25 €	1.12 €	3.36 €	1.36 €	4.76 €	4.21 €	1.71 €	1.48 €

Table 4.14: Values of sensitivity index ***SI***

Low values for indexes ***SI*** have been found. The maximum deviation calculated represents less than 1 % of the total cost reduction. In addition to this, the different designs satisfy the imposed design constraints. Thus, it can be concluded that the solution is not sensitive to local variations into the values of the chosen design parameters.

However, this method is a one-at-a-time (OAT) technique, which means the effect of only one parameter on the cost function is analyzed at a time, while the other parameters are fixed. This then leads to the exploration of a small restrained portion of the design space, in addition to the fact that the interactions between variables on the cost function and constraints are neglected as well.

Another sensitivity analysis method which can be used is based of multiple simulations in the optimal solution neighborhood, delimited by the tolerances listed earlier [149]. For the scope of this study, 100 configurations are selected and assessed using Sobol's Quasirandom sequence.

It has been found that the studied configurations have all respected the imposed constraints. Thus, the proposed optimal solution remains feasible even while including uncertainties and has managed to respect the machine requirements as well. A maximum

deviation of around 20 € is found as well. This value is equal to 2.5 % of the total cost reduction and the optimal solution is considered robust.

Conclusion

In this chapter, three optimal control strategies have been tested: DPAM, PMP and RBS. Fuel gains and computation time are used as the main criteria for comparison. Similarly to the HRPS case study, DPAM provides the minimum values for fuel consumption in here as well, while the proposed RBS is much faster. RBS is applied for the quick assessment of fuel consumption for coupled systemic design strategies and is directly incorporated in approach $\mathcal{A}_1$ afterwards.

Cycle reduction techniques are assessed afterwards, with the losses pondering variant of the clustering method ranking as the most precise. When coupled with the mirroring method, a deviation of less than 1 % is achieved. This method allows for faster design optimization of the electric machine over drive-cycle and enables the direct use of the circuit model or even the FE model to improve the precision of the results.

Once the hybrid powertrain optimization application has been defined, it was necessary to launch a screening study to identify the most vital factors. Approaches $\mathcal{BL}$, $\mathcal{IT}$, $\mathcal{A}_1$, $\mathcal{A}_2$ and $\mathcal{A}_3$, are then implemented to optimize these variables and improve the cost of the hybrid powertrain.

Important cost reduction is then achieved, which translates in part into improved fuel efficiency. This also cements the importance of systemic design in exploiting the hybrid powertrain to its fullest and leading to much better fuel economy as compared to focusing on the optimization of a single component, which is the case of the reference machine.

These cost gains logically increase with the number of the decision variables considered. However, the required calculation times rise exponentially as well, limiting the maximum number of design parameters that can be considered. These applications were also an opportunity to assess the performance of each method separately and confront them to the analysis initiated in Chapter 2.

Approach $\mathcal{BL}$ still manages to lead to the best cost reduction values among the studied strategies. However, since the optimal command is recalculated for each new proposed machine, the required calculation time remains high as well.

Design optimization method $\mathcal{IT}$, based on the iterative scheme, proves to be another efficient strategy. It manages to find close values of the total cost when confronted to $\mathcal{BL}$. The gap between both solutions increases however with the number of decision variables, since it is more impacted with the algorithm's initialization, as it has been found previously for the HRPS application. Nevertheless, in contrast with the findings of Chapter 2, $\mathcal{IT}$ requires the most calculation time since design cost calculation is based on heavy-model evaluations. Significant computation time reduction can be expected when relaxing the outer loop tolerances, which will reduce the number of function calls, as well as accelerating the design cost evaluations by increasing the number of parallel FE simulations.

Systemic design strategy $\mathcal{A}_1$, based on the co-optimization of the design and RBS parameters, manages to offer the best compromise between accuracy and calculation time. However, it is also sensitive to the initial guess of the decision variables and better results

can be found when combined with a multi-start technique.

Meanwhile, approach $\mathcal{A}_2$ ranks as the fastest approach since it uses analytical models to estimate the powertrain's total cost and evaluate the design constraints. For this reason as well, lower cost reduction values are found compared to the results of other approaches. One perspective is to improve the accuracy of these models, which can be achieved by increasing the sample pool of the screening experiments. This approach can also be used as means to propose better initializations for the other strategies.

The fifth approach, referred to as $\mathcal{A}_3$ and proposed as an alternative to the iterative design strategy, is based on estimating the machine losses by applying cycle reduction techniques. This approach is faster however compared to $\mathcal{IT}$, with much quicker iterations expected once more FE evaluations are launched in parallel. On the other hand, it does not reach the same level of cost reduction. This can be improved when adopting a more precise model, based on an increased number of interest points for example.

A study aimed at challenging system guidelines over the performance requirements of the machine is carried out afterwards. Optimization based on the $\mathcal{BL}$ approach without considering these constraints is launched and further cost reduction is obtained. Thus, it can be understood that this approach can be used to accurately define the machine specifications as well for future applications, which will allow for better use of the powertrain.

Finally, local and global sensitivity analysis studies were conducted to evaluate the robustness of the most efficient design "a posteriori". The solution is then seen as robust since integrating the various industrial uncertainties does not degrade its quality.

Conclusion

During this thesis work, we were interested in the optimal design of complex systems over drive-cycle. We have demonstrated that focusing on isolated components, without an outlook on all physical behaviors and their usage does not lead to a system optimum. A global vision of the system is required to find the best solution possible. However, this remains difficult to achieve in a classic company structure with limited exchanges between the various teams involved in the project. The main objective was then to propose design methodologies which consider, the components, the system, the control and the environment while meeting project deadlines and requirements.

Hybrid powertrains are seen as a great fit for the premise of this work, as strong coupling exists between their different components, their use and the power management strategy. There is also a growing need for more energy efficient propulsion systems as a response to the current environmental and health concerns. Thus, systemic design approaches that are developed are assessed over the case of a C-segment vehicle equipped with a parallel hybrid powertrain. However, the proposed methodologies can be easily adapted for other applications as well.

In Chapter 1, we have presented the state of the art in the optimization of complex systems. The most popular strategies fall mainly into two categories: multidisciplinary design optimization methods and Plant/Controller frameworks used in conjunction with optimal control strategies. The balance tipped more in favor of the second option due to the use of time consuming and strongly non-linear black-box models and the presence of a large number of decision variables.

The use of optimal control strategies afterwards instead of online power management methods is made to remove any bias related to the quality of the control strategy when comparing different possible solutions. Thus, non-linear programming (NLP), Collaborative Optimization (CO), Dynamic Programming (DP) and Pontryagin's Minimum Principle (PMP) are investigated afterwards to solve the optimal control problem. The most adequate control strategy can then be applied for systemic design optimization by adopting either the nested approach $\mathcal{BL}$ where an external design optimization process calculates the best possible cost at each iteration by solving the optimal control problem, or approach $\mathcal{IT}$ where the design and command problem are solved iteratively. These frameworks are expected to achieve better results compared to using an all-at-once approach such as $\mathcal{SM}$, especially for long design cycles.

Chapter 2 presents the hybrid railway power substation (HRPS) benchmark which is chosen as a first benchmark to compare the previous methods for both power management and design optimization. The HRPS model is much faster to analyse, and the related optimization problem can be linearized afterwards providing a global optimum as a reference

solution for different cycle lengths as opposed to the hybrid vehicle case study.

When solving the optimal control problem, NLP and CO were only adequate for short cycles of a few hundred time steps. PMP ranked as the fastest but failed to find satisfying results. This is due to the fact that optimal command is found at its boundaries, which then restricts its use in this case. Finally, DP provided optimal results in reasonable calculation times. DPAM, an improved version of this method based on the adaptive meshing process, manages to find precise results in faster calculation times and is integrated in both $\mathcal{BL}$ and $\mathcal{IT}$.

The HRPS design problem is tackled afterwards. As expected, the simultaneous approach $\mathcal{SM}$ fails to find an optimal solution when thousands of optimization variables are involved. Meanwhile, $\mathcal{BL}$ leads to precise results and has a high convergence rate but requires long calculation times. In contrast, $\mathcal{IT}$ is 10 times faster but leads to sub-optimal results and lower convergence rates. Relaxing the command constraints leads to similar results as those found by $\mathcal{BL}$. Approaches $\mathcal{BL}$ and $\mathcal{IT}$ are then used for hybrid powertrain optimization.

Chapter 3 starts by describing the hybrid vehicle model. An iso-granularity representation at fixed temperature is selected for all the various components. The decision variables are also listed, with the electric machine being the core component to be modified during the following optimization applications. The machine model was based on the combined use of FE simulations and Park's representation to accurately consider the machine's design variations, achieving less than 2 % deviation with bench-test results, and generate component data for system simulation in a couple of minutes.

The powertrain limitations as well as the requirements and specifications of the product are translated into command and design constraints, evaluated by analytic and simulation-based functions. The hybrid powertrain optimization problem is defined afterwards, with the cost function incorporating both the design cost and fuel consumption calculated over the Worldwide harmonized Light vehicles Test Cycles (WLTC).

Chapter 4 then focuses on the comparison of the most promising strategies. Three optimal control strategies have been tested: DPAM, PMP and an optimal rule-based strategy (RBS). Fuel gains and computation time are used as the main criteria for comparison. The performances of the three proposed strategies are close. Similarly to the HRPS case study, DPAM provides the minimum values for fuel consumption. The proposed RBS is much faster and is instantaneous once the strategy parameters are imposed. The optimal command is analyzed further and it is concluded that it follows all the hybrid vehicle use recommendations, allowing efficient exploitation of the powertrain. Simulation platform results confirm these findings as well.

Different cycle reduction techniques are compared afterwards. They are developed to quickly assess the machine cycle losses using only a dozen of interest points. The clustering technique is the most precise, with the loss pondering variant incorporating the new Mirroring method achieving small deviations of less than 1 % with the real loss values.

Once the hybrid powertrain design optimization application is defined, a screening study allowed for the identification of the most influent decision variables in a bid to greatly improve the convergence of the systemic design approaches. A machine design optimized over a singular operation point is used for both algorithm initialization and as a reference design.

Five systemic design approaches are applied: the previously mentioned $\mathcal{BL}$ and $\mathcal{IT}$, as well as alternative approaches $\mathcal{A}_1$, $\mathcal{A}_2$ and $\mathcal{A}_3$. $\mathcal{A}_1$ is based on the simultaneous optimization of the design and RBS parameters to overcome the difficulties encountered by $\mathcal{SM}$. $\mathcal{A}_2$ uses meta-models to evaluate the cost and constraint functions while $\mathcal{A}_3$ is another variant to $\mathcal{IT}$ applying cycle reduction techniques for faster design cost evaluations.

$\mathcal{BL}$, $\mathcal{IT}$ and $\mathcal{A}_1$ lead to close cost reduction values when considering a small number of design variables. However, $\mathcal{BL}$ finds better solutions for increased parameters, as $\mathcal{IT}$ and $\mathcal{A}_1$ are more sensitive to design initialization. A multi-start strategy can then be used to achieve better results. Meanwhile, design approaches $\mathcal{A}_2$ and $\mathcal{A}_3$ led to lower cost reduction, which can be improved by enhancing the accuracy of their models.

In terms of computation time, $\mathcal{A}_2$ logically ranked as the fastest. $\mathcal{BL}$, $\mathcal{IT}$ and $\mathcal{A}_3$, followed by $\mathcal{A}_1$, required long computation times which increased substantially with the number of variables. In the case of $\mathcal{A}_1$ and both alternatives of the iterative scheme, their respective calculation time can be greatly reduced by stronger parallelization.

Besides leading to significant cost reduction, the solution found by the bi-level design strategy is deemed robust as a result of the sensitivity studies conducted afterwards. Finally, $\mathcal{BL}$ is also used to challenge the performance requirements used generally as design guidelines in the company environment and propose a more efficient powertrain over the WLTC 3-b cycle at a much lower cost.

Perspectives

This work can open up to multiple research perspectives and can serve as an entry point for future developments at various fronts.

From an application point of view, the proposed design strategies can easily be extended to the sizing of other components of the hybrid powertrain. However, this will require using models for the engine, the battery and the transmission that consider the impact of their design parameters.

The implemented approaches should also allow for the comparison between various hybrid architectures with different component technologies. Integrating these parameters as discrete variables during the optimization process will help define the most adequate traction solution for a specific application, although additional design constraints are required when considering other powertrain architectures.

In this study, an iso-granularity representation based mostly on interpolation models established at fixed temperature is selected. The use of higher fidelity models considering the dynamic thermal behaviour's impact on performance over the cycle will certainly improve the accuracy of system simulation and the validity of the solution when manufactured. The expected increase in calculation time can be limited by applying the Individual Discipline Feasible (IDF) framework in this case.

Robust optimization which propagates the various uncertainties resulting from manufacturing processes during the decision-making process will lead to a robust solution when the design methodology converges. This is seen as a more rigorous approach as opposed to the adopted "a posteriori" approach where the robustness of the solution is only verified but a more robust solution may exist.

Regarding the optimization process, the total cost can be developed further to better estimate the cost of the powertrain. The materials price and manufacturing costs can be added separately for example to achieve this feat.

In addition to this, fuel economy can be evaluated over other cycles such as homologation cycles from other countries. The impact of the selected cycle over the final solution can then be studied.

Finally, other optimization targets can be set as well such as particle emissions reduction, minimization of fuel consumption over separate drive-cycles and component ageing. A mono-objective optimization approach such as the one undertaken in this work can be applied as well by adding different weights for each objective. A multi-objective optimization approach can also be suggested to give better insight to decision makers.

Appendices

Appendix A

Validation of FE parametric model

After selecting an existing machine and identifying the machine parameters $\boldsymbol{d}$, the parametric FE model's accuracy is assessed based on the experimental results of said machine and the 3D FE CAD calculations of the same machine.

The different results are summarized in the following tables, with deviations determined between the bench-test values and calculations of the parametric FE model. BT refers to the bench test results, while CAD and PM are correspondingly the 3D CAD model and parametric FE model results and the compared quantities are the mainly used outputs in the optimization study.

The no load results are compiled in Table A.1. They mainly focus on the root mean square (rms) value of the back EMF voltage (EMF) and its first harmonic (EMF-h1) at different magnet temperatures and rotational speeds.

	BT (Vrms)	CAD (Vrms)	PM (Vrms)	Deviation (%)
EMf at 25 °C/1000 rpm	9.72	9.71	9.77	-0.51
EMF-h1 at 25 °C/1000 rpm	9.70	9.76	9.68	-0.20
EMf at 80 °C/1000 rpm	9.38	9.38	9.40	-0.21
EMF-h1 at 80 °C/1000 rpm	9.33	9.33	9.33	0.00
EMf at 110 °C/1000 rpm	9.21	9.18	9.08	1.41
EMF-h1 at 100 °C/1000 rpm	9.16	9.13	9.00	1.75

Table A.1: Comparison results for no load scenarios

Table A.2 on the other hand shows the obtained rms value of the steady state short-circuit current for the three cases at high speed (6000 rpm).

BT (Arms)	CAD (Arms)	PM (Arms)	Deviation (%)
220.7	227.1	224.1	-1.50

Table A.2: Comparison results on a short-circuit scenario

Finally, Table A.3 compares the average mechanical torque values obtained at multiple operation points of the machine, in both generator and motor modes. The current phase is calculated as to minimize the losses in the machine.

	BT (N.m)	CAD (N.m)	PM (N.m)	Deviation (%)
Motor mode at 355 Arms/0 rpm	95.0	94.9	95.0	0.00
Motor mode at 234 Arms/1000 rpm	70.0	68.8	68.8	1.65
Motor mode at 195 Arms/2000 rpm	60.0	59.0	58.9	1.83
Motor mode at 217 Arms/3000 rpm	60.0	60.6	61.1	-1.80
Generator mode at 193 Arms/3000 rpm	-60.0	-58.6	-58.3	-2.83
Motor mode at 164 Arms/5000 rpm	40.0	40.2	40.0	-0.01
Generator mode at 131 Arms/6000 rpm	-30.0	-30.1	-30.0	0.12

Table A.3: Comparison results for on-load scenarios

The different results presented in the three tables show acceptable deviations, of around 2%, for the measured quantities.

Appendix B

Energy losses during gear-shifting

Gear shifting is not instantaneous and since the engine suffers from slower dynamics compared to the EM, its output power is not constant during the transition period. In the case of an upshift for example, the engine switches between constant speed and constant torque, as shown in Figure B.1.

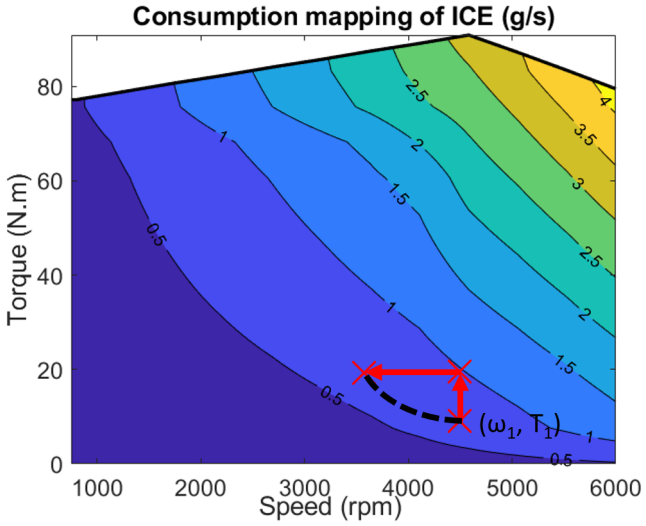

Figure B.1: Upshift procedure using a DCT with the iso-power line. Data retrieved from [74]

Let t_{gs} be the time required for completing a gear shift in s, ω_{req} the rotational speed of the engine in rpm and T_{req} and P_{req} the torque in N.m and power in W to be provided by the engine respectively during the selected time step. R_1 and R_2 refer correspondingly to the ratios of the current and selected gears.

By assuming the torque delivered by the engine varies linearly during gear shifting, the following expression can be given to the produced torque's evolution:

$$T_{\text{ICE}}(t) = \frac{T_{\text{req}}}{R_2}(R_2 + (R_1 - R_2)\frac{2t}{t_{\text{gs}}}), \qquad t \in [0, \frac{t_{\text{gs}}}{2}] \tag{B.1a}$$

$$T_{\mathrm{ICE}}(t) = \frac{R_1}{R_2} T_{\mathrm{req}} \quad , \quad t \in [\frac{t_{\mathrm{gs}}}{2}, \Delta t] \tag{B.1b}$$

The engine's rotational speed on the other hand can also be expressed as:

$$\omega_{\mathrm{ICE}}(t) = \omega_{\mathrm{req}} \quad , \quad t \in [0, \frac{t_{\mathrm{gs}}}{2}] \tag{B.2a}$$

$$\omega_{\mathrm{ICE}}(t) = \frac{\omega_{\mathrm{req}}}{R_1}(R_1 + (R_2 - R_1)\frac{2t - t_{\mathrm{gs}}}{t_{\mathrm{gs}}}), \quad t \in [\frac{t_{\mathrm{gs}}}{2}, t_{\mathrm{gs}}] \tag{B.2b}$$

$$\omega_{\mathrm{ICE}}(t) = \frac{R_2}{R_1}\omega_{\mathrm{req}} \quad , \quad t \in [t_{\mathrm{gs}}, \Delta t] \tag{B.2c}$$

The power delivered by the engine can then be deduced:

$$P_{\mathrm{ICE}}(t) = \frac{P_{\mathrm{req}}}{R_2}(R_2 + (R_1 - R_2)\frac{2t}{t_{\mathrm{gs}}}), \quad t \in [0, \frac{t_{\mathrm{gs}}}{2}] \tag{B.3a}$$

$$P_{\mathrm{ICE}}(t) = \frac{P_{\mathrm{req}}}{R_2}(R_1 + (R_2 - R_1)\frac{2t - t_{\mathrm{gs}}}{t_{\mathrm{gs}}}), \quad t \in [\frac{t_{\mathrm{gs}}}{2}, t_{\mathrm{gs}}] \tag{B.3b}$$

$$P_{\mathrm{ICE}}(t) = P_{\mathrm{req}}, \quad t \in [t_{\mathrm{gs}}, \Delta t] \tag{B.3c}$$

Thus, the average power delivered by the ICE during the selected time step can be calculated using the following equation:

$$P_{\mathrm{ICE}}(t) = \frac{P_{\mathrm{req}}}{\Delta t}(\frac{t_{\mathrm{gs}}}{2} + (\frac{R_1}{R_2} - 1)\frac{t_{\mathrm{gs}}}{4} + \frac{R_1}{R_2}\frac{t_{\mathrm{gs}}}{2} + (1 - \frac{R_1}{R_2})\frac{t_{\mathrm{gs}}}{4} + \Delta t - t_{\mathrm{gs}}) \tag{B.4a}$$

$$= \frac{P_{\mathrm{req}}}{\Delta t}((\frac{R_1}{R_2} - 1)\frac{t_{\mathrm{gs}}}{2} + \Delta t) \tag{B.4b}$$

Finally, and based on the assumption that the engine's consumption varies linearly close to its operation point with respect to the delivered power, a simple expression for the fuel consumption during gear shifting is proposed:

$$L = \frac{L_{\mathrm{req}}}{\Delta t}((\frac{R_1}{R_2} - 1)\frac{t_{\mathrm{gs}}}{2} + \Delta t) \tag{B.5a}$$

where L_{req} is the engine's fuel consumption at the operating point (ω_{req}, T_{req}). Using similar reasoning, the following expression is deduced when downshifting:

$$L = \frac{L_{\mathrm{req}}}{\Delta t}((1 - \frac{R_1}{R_2})\frac{t_{\mathrm{gs}}}{2} + \Delta t) \tag{B.6a}$$

And a generalized expression, valid for both downshifting and upshifting can be given:

$$L = \frac{L_{\mathrm{req}}}{\Delta t}(|\frac{R_1}{R_2} - 1|\frac{t_{\mathrm{gs}}}{2} + \Delta t) \tag{B.7a}$$

Appendix C

Machine geometric constraints

Using the same designations for the design variables as in the parametric model definition, $\boldsymbol{k_{Geom}}$ is expressed as:

$$k_{\mathrm{Geom},1}(\boldsymbol{d}) = N_{\mathrm{ph}} - N_{\mathrm{slot}} + 1 \tag{C.1a}$$
$$k_{\mathrm{Geom},2}(\boldsymbol{d}) = y_{\mathrm{st3}} - y_{\mathrm{st2}} \tag{C.1b}$$
$$k_{\mathrm{Geom},3}(\boldsymbol{d}) = Hs0 + Hs1 + Hs2 + 0.5 - Rout_{\mathrm{Sta}} + Rin_{\mathrm{Sta}} \tag{C.1c}$$
$$k_{\mathrm{Geom},4}(\boldsymbol{d}) = Bs0 - 0.9Rin_{\mathrm{Sta}}\frac{\Pi}{pN_{\mathrm{slot}}} \tag{C.1d}$$
$$k_{\mathrm{Geom},5}(\boldsymbol{d}) = Bs1 - 0.9(Rin_{\mathrm{Sta}} + Hs0 + Hs1)\frac{\Pi}{pN_{\mathrm{slot}}} \tag{C.1e}$$
$$k_{\mathrm{Geom},6}(\boldsymbol{d}) = \frac{Bs0}{Rin_{\mathrm{Sta}}} - \frac{Bs1}{Rin_{\mathrm{Sta}} + Hs0 + Hs1} \tag{C.1f}$$
$$k_{\mathrm{Geom},7}(\boldsymbol{d}) = B1 - Mag_{\mathrm{Th}} \tag{C.1g}$$
$$k_{\mathrm{Geom},8}(\boldsymbol{d}) = B3 - Mag_{\mathrm{Th}} \tag{C.1h}$$
$$k_{\mathrm{Geom},9}(\boldsymbol{d}) = R_2 - R_1 \tag{C.1i}$$
$$k_{\mathrm{Geom},10}(\boldsymbol{d}) = Rout_{\mathrm{Rot}} - \sqrt{{x_{\mathrm{rt10}}}^2 + {y_{\mathrm{rt10}}}^2} - 2R_2 + R_1 \tag{C.1j}$$
$$k_{\mathrm{Geom},11}(\boldsymbol{d}) = Rin_{\mathrm{Rot}} - \sqrt{{x_{\mathrm{rt1}}}^2 + {y_{\mathrm{rt1}}}^2} \tag{C.1k}$$
$$k_{\mathrm{Geom},12}(\boldsymbol{d}) = Rin_{\mathrm{Rot}} - \sqrt{{x_{\mathrm{rt2}}}^2 + {y_{\mathrm{rt2}}}^2} \tag{C.1l}$$
$$k_{\mathrm{Geom},13}(\boldsymbol{d}) = -x_{\mathrm{rt2}} \tag{C.1m}$$
$$k_{\mathrm{Geom},14}(\boldsymbol{d}) = Rin_{\mathrm{Rot}} - \sqrt{{x_{\mathrm{rt4}}}^2 + {y_{\mathrm{rt4}}}^2} \tag{C.1n}$$
$$k_{\mathrm{Geom},15}(\boldsymbol{d}) = Rin_{\mathrm{Rot}} - \sqrt{{x_{\mathrm{rt5}}}^2 + {y_{\mathrm{rt5}}}^2} \tag{C.1o}$$
$$k_{\mathrm{Geom},16}(\boldsymbol{d}) = Rin_{\mathrm{Rot}} - \sqrt{{x_{\mathrm{rt6}}}^2 + {y_{\mathrm{rt6}}}^2} \tag{C.1p}$$
$$k_{\mathrm{Geom},17}(\boldsymbol{d}) = (y_{\mathrm{rt9}} - y_{\mathrm{rt3}})(x_{\mathrm{rt7}} - x_{\mathrm{rt3}}) - (x_{\mathrm{rt9}} - x_{\mathrm{rt3}})(y_{\mathrm{rt7}} - y_{\mathrm{rt3}}) \tag{C.1q}$$
$$k_{\mathrm{Geom},18}(\boldsymbol{d}) = (y_{\mathrm{rt9}} - y_{\mathrm{rt7}})(x_{\mathrm{rt6}} - x_{\mathrm{rt7}}) - (x_{\mathrm{rt9}} - x_{\mathrm{rt7}})(y_{\mathrm{rt6}} - y_{\mathrm{rt7}}) \tag{C.1r}$$
$$k_{\mathrm{Geom},19}(\boldsymbol{d}) = atan(\frac{y_{\mathrm{rt2}}}{x_{\mathrm{rt2}}}) - \frac{\Pi}{2p} \tag{C.1s}$$
$$k_{\mathrm{Geom},20}(\boldsymbol{d}) = atan(\frac{y_{\mathrm{rt4}}}{x_{\mathrm{rt4}}}) - \frac{\Pi}{2p} \tag{C.1t}$$
$$k_{\mathrm{Geom},21}(\boldsymbol{d}) = atan(\frac{y_{\mathrm{rt5}}}{x_{\mathrm{rt5}}}) - \frac{\Pi}{2p} \tag{C.1u}$$

$$k_{\text{Geom},22}(\boldsymbol{d}) = atan(\frac{y_{\text{rt6}}}{x_{\text{rt6}}}) - \frac{\Pi}{2p} \tag{C.1v}$$

$$k_{\text{Geom},23}(\boldsymbol{d}) = atan(\frac{y_{\text{rt7}}}{x_{\text{rt7}}}) - \frac{\Pi}{2p} \tag{C.1w}$$

$$k_{\text{Geom},24}(\boldsymbol{d}) = atan(\frac{y_{\text{rt9}}}{x_{\text{rt9}}}) - \frac{\Pi}{2p} \tag{C.1x}$$

$$k_{\text{Geom},25}(\boldsymbol{d}) = Exc - Rout_{\text{Rot}} \tag{C.1y}$$

with:

$$x_{\text{st1}} = Rin_{\text{Sta}} - \frac{(Rin_{\text{Sta}}\frac{3\Pi}{N_{\text{slot}}} - 0.5Bs0)^2}{2Rin_{\text{Sta}}} \tag{C.2a}$$

$$y_{\text{st1}} = \sqrt{Rin_{\text{Sta}}{}^2 - x_{\text{st1}}{}^2} \tag{C.2b}$$

$$x_{\text{st2}} = x_{\text{st1}} + Hs0cos(\frac{\Pi}{2pN_{\text{slot}}}) \tag{C.2c}$$

$$y_{\text{st2}} = y_{\text{st1}} + Hs0cos(\frac{\Pi}{2pN_{\text{slot}}}) \tag{C.2d}$$

$$Rprime1 = \sqrt{x_{\text{st2}}{}^2 + y_{\text{st2}}{}^2} + Hs1 \tag{C.2e}$$

$$x_{\text{st3}} = Rprime1 - \frac{(\frac{Rprime1\Pi}{2pN_{\text{slot}}} - 0.5Bs1)^2}{2Rprime1} \tag{C.2f}$$

$$y_{\text{st3}} = \sqrt{Rprime1^2 - x_{\text{st3}}{}^2} \tag{C.2g}$$

$$Exc = Gap\frac{Rout_{\text{Rot}} - 0.5Gap}{Rout_{\text{Rot}} - (Rout_{\text{Rot}} - Gap)cos(\frac{\Pi}{2p})} \tag{C.2h}$$

$$Kexc = Rout_{\text{Rot}} - Gap \tag{C.2i}$$

$$T = Mag_{\text{Th}} + M1 + M2 \tag{C.2j}$$

$$Ri = Rout_{\text{Rot}} - Exc - Bridge \tag{C.2k}$$

$$xi = \frac{0.5O1 + Tsin(Ouv_{\text{Mag}})}{Ri} \tag{C.2l}$$

$$x_{\text{rt1}} = Exc + Ricos(asin(xi)) - Tcos(Ouv_{\text{Mag}}) \tag{C.2m}$$

$$y_{\text{rt1}} = 0.5O1 \tag{C.2n}$$

$$x_{\text{rt2}} = x_{\text{rt1}} - B2 \tag{C.2o}$$

$$y_{\text{rt2}} = y_{\text{rt1}} \tag{C.2p}$$

$$x_{\text{rt3}} = x_{\text{rt1}} + Tcos(Ouv_{\text{Mag}}) \tag{C.2q}$$

$$y_{\text{rt3}} = y_{\text{rt1}} + Tsin(Ouv_{\text{Mag}}) \tag{C.2r}$$

$$x_{\text{rt4}} = x_{\text{rt1}} - B3sin(Ouv_{\text{Mag}}) \tag{C.2s}$$

$$y_{\text{rt4}} = y_{\text{rt1}} - B3cos(Ouv_{\text{Mag}}) \tag{C.2t}$$

$$x_{\text{rt5}} = x_{\text{rt1}} - (Mag_{\text{Th}} + 2Mag_{\text{Insulation}})sin(Ouv_{\text{Mag}}) \tag{C.2u}$$

$$y_{\text{rt5}} = y_{\text{rt1}} + (Mag_{\text{Th}} + 2Mag_{\text{Insulation}})cos(Ouv_{\text{Mag}}) \tag{C.2v}$$

$$x_{\text{rt6}} = x_{\text{rt5}} + (Mag_{\text{Th}} + 2Mag_{\text{Insulation}} + M1)cos(Ouv_{\text{Mag}}) \tag{C.2w}$$

$$y_{\text{rt6}} = y_{\text{rt5}} + (Mag_{\text{Th}} + 2Mag_{\text{Insulation}} + M1)sin(Ouv_{\text{Mag}}) \tag{C.2x}$$

$$x_{\text{rt7}} = x_{\text{rt6}} + (Mag_{\text{Th}} + 2Mag_{\text{Insulation}} - B1)sin(Ouv_{\text{Mag}}) \tag{C.2y}$$

$$y_{\text{rt7}} = y_{\text{rt6}} - (Mag_{\text{Th}} + 2Mag_{\text{Insulation}} - B1)cos(Ouv_{\text{Mag}}) \tag{C.2z}$$

$$a_{\text{Rot}} = 1 + tan(\frac{\Pi}{2p})^2 \tag{C.2aa}$$

$$b_{\text{Rot}} = -2Exc \tag{C.2ab}$$

$$c_{\text{Rot}} = (0.5Rib\ sin(\frac{\Pi}{2p}) - Exc)^2 + (0.5Rib\ cos(\frac{\Pi}{2p}))^2 - Ri^2 \tag{C.2ac}$$

$$x_{\text{rt8}} = (-b_{\text{Rot}} + \sqrt{{b_{\text{Rot}}}^2 - 4a_{\text{Rot}}c_{\text{Rot}}})/(2a_{\text{Rot}}) \tag{C.2ad}$$

$$y_{\text{rt8}} = x_{\text{rt8}} tan(\frac{\Pi}{2p}) \tag{C.2ae}$$

$$x_{\text{rt9}} = x_{\text{rt8}} + 0.5Rib\ sin(\frac{\Pi}{2p}) \tag{C.2af}$$

$$y_{\text{rt9}} = y_{\text{rt8}} - 0.5Rib\ cos(\frac{\Pi}{2p}) \tag{C.2ag}$$

$$x_{\text{rt10}} = Exc + (Rout_{\text{Rot}} - Exc)cos(atan(\frac{Kexc\ sin(\frac{\Pi}{2p})}{Kexc\ cos(\frac{\Pi}{2p}) - Exc})) \tag{C.2ah}$$

$$y_{\text{rt10}} = (Rout_{\text{Rot}} - Exc)sin(atan(\frac{Kexc\ sin(\frac{\Pi}{2p})}{Kexc\ cos(\frac{\Pi}{2p}) - Exc})) \tag{C.2ai}$$

with $Mag_{\text{Insulation}}$ the thickness of the magnet's insulating paper in mm.

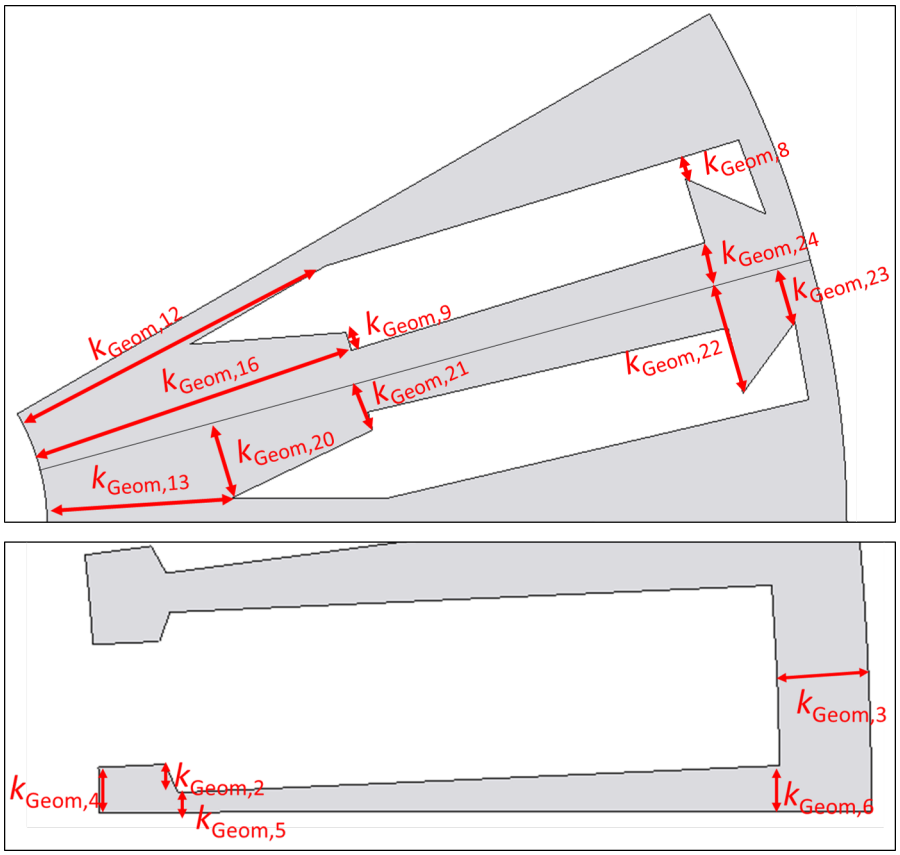

Figure C.1: Above: Rotor geometric constraints - Below: Stator geometric constraints

List of Abbreviations

μHEV	Micro-hybrid vehicle
AAO	All-At-Once
AC	Alernative current
ATC	Analytical Target Cascading
BLISS	Bi-Level Integrated System Synthesis
CAD	Computer aided design
CO	Collaborative Optimization
DC	Direct current
DP	Dynamic Programming
DPAM	Dynamic Programming with Adaptive Meshing
ECMS	Equivalent Consumption Minimization Strategy
EM	Electric motor
EV	Electric vehicle
FE	Finite element
FHEV	Full hybrid vehicle
FW	Full Wave
GCC	Global climate change
GWP	Global warming potential
HCU	Hybrid control unit
HEV	Hybrid electric vehicle

HJB	Hamilton-Jacobi-Bellman equation
HRPS	Hybrid railway power substation
ICE	Internal combustion engine
IDF	Individual Discipline Feasible
LMS	Loss Minimization Strategy
MDF	MultiDisciplinary Feasible
MDO	Multidisciplinary Design Optimization
MDSDO	Multidisciplinary Dynamic System Design Optimization
MHEV	Mild hybrid vehicle
MOSFET	Metal–oxide–semiconductor field-effect transistor
NEDC	New European Driving Cycle
OEM	Original Equipment Manufacturer
PHEV	Plug-in hybrid vehicle
PMP	Pontryagin's Minimum Principle
PMSM	Permanent magnet synchronous machine
PWM	Pulse Width Modulation
RBS	Rule-based strategy
RCP	Representative Concentration Pathways
RDE	Real Driving Emissions
RMSD	Root-mean-square deviation
SAND	Simultaneous Analysis and Design
SDP	Stochastic Dynamic Programming
SQP	Sequential Quadratic Programming
STT	Stop-Start
VI-PMSM	V-shape inserted permanent magnet synchronous machine
WLTC	World Harmonized Light Vehicles Test cycles

ZEV	Zero Emissions Vehicle

List of Symbols

Chapter 1

ϵ_{R}	Response tolerance
ϵ_{y}	Shared variable tolerance
F	Global cost function
f	Objective function
N_{ss}	Number of subsystems
$\boldsymbol{g_{\mathrm{sys}}}$	System inequality constraints
$\boldsymbol{G}$	Consistency constraints function
$\boldsymbol{g}$	Inequality constraints function
$\boldsymbol{g_{\mathrm{com,k}}}$	Component inequality constraints function
$\boldsymbol{g_{\mathrm{i}}}$	Subproblem inequality constraints function
$\boldsymbol{g_{\mathrm{ss,j}}}$	Subsystem inequality constraints function
$\boldsymbol{h_{\mathrm{sys}}}$	System equality constraints
$\boldsymbol{h}$	Equality constraints function
$\boldsymbol{h_{\mathrm{com,k}}}$	Component equality constraints function
$\boldsymbol{h_{\mathrm{i}}}$	Subproblem equality constraints function
$\boldsymbol{h_{\mathrm{ss,j}}}$	Subsystem equality constraints function
$\boldsymbol{N_{\mathrm{com,j}}}$	Number of components of the considered subsystem
$\boldsymbol{R^L}$	Output feedback
$\boldsymbol{R^U}$	Target values
$\boldsymbol{R_{\mathrm{ss}}}$	Subsystem response values
$\boldsymbol{R_{\mathrm{sys}}}$	System response values
$\boldsymbol{R_{\mathrm{com}}}$	Components response
$\boldsymbol{T_{\mathrm{sys}}}$	System target values
$\boldsymbol{x_{\mathrm{sys}}}$	Local system design variables

$\boldsymbol{x}$	Vector of optimization variables
$\boldsymbol{x_{\mathbf{com,k}}}$	Local component design variables
$\boldsymbol{x_{\mathbf{ss,j}}}$	Local subsystem design variables
$\boldsymbol{y'}$	Added variables
$\boldsymbol{y^U}$	New values for shared variables
$\boldsymbol{y^U}$	Shared variables
$\boldsymbol{y_{\mathbf{ss}}}$	Subsystem shared variables
$\boldsymbol{y}$	Vector of model outputs
$\boldsymbol{y_{\mathbf{com}}}$	Components shared variables
$\boldsymbol{z^*}$	Imposed values at the subproblem level
$\boldsymbol{z}$	Optimization variables

Chapter 2

α	Weight of plant's cost
β	Weight of controller's cost
$\boldsymbol{\lambda}$	Inequality Lagrange multipliers
$\boldsymbol{\mu}$	Equality Lagrange multipliers
Δt	Time step
C	Optimal controller cost
C_{grid}	Energy cost function
C_{PV}	Cost related to S_{PV}
C_{W}	Cost related to S_{W}
$C^{\mathrm{E}}{}_{\mathrm{sto}}$	Cost related to $E_{\max}$
$C^{\mathrm{P}}{}_{\mathrm{sto}}$	Cost related to $P_{\max}$
E_{ini}	Energy initially stored in batteries [J]
$E_{\max}$	Energy storage capacity [J]
f	Evolution function
g	Inequality command constraints function
g_{s}	Simplified inequality constraints function
H	Hamiltonian function
h	Equality command constraints function
h_{s}	Simplified equality constraints function

Inv	Plant's cost function
J	Total cost function
J_{e}	Equivalent cost function
J_{s}	Simplified cost function
$P_{\max}$	Maximum input/output power to the batteries [W]
S_{PV}	Surface of solar panels [m^2]
S_{W}	Swept surface of the wind turbines [m^2]
t	Current time step
t_0	Initial time step
t_{f}	Final time step
u	Cost functional
V	Cost-to-go function
$\boldsymbol{d*}$	Optimal design values
$\boldsymbol{d*}$	Optimal solution
$\boldsymbol{D}$	Feasible domain
$\boldsymbol{d}$	Design variables
$\boldsymbol{d_{\mathrm{ini}}}$	Initial values for the design variables
$\boldsymbol{D_{\mathrm{x}}}$	Dynamic programming grid
$\boldsymbol{eq}$	All equality constraints function
$\boldsymbol{E_{\mathrm{sto}}}$	Energy stored in batteries [J]
$\boldsymbol{ineq}$	All inequality constraints function
$\boldsymbol{k}$	Inequality design constraints function
$\boldsymbol{l}$	Equality design constraints function
$\boldsymbol{N}$	Solution neighborhood
$\boldsymbol{p}$	Parameters of control strategy
$\boldsymbol{P_{\mathrm{grid}}}$	Power flow from the grid [W]
$\boldsymbol{P_{\mathrm{grid}}}^{+}$	Power received from the grid [W]
$\boldsymbol{P_{\mathrm{grid}}}^{-}$	Power sent to the grid [W]
$\boldsymbol{P_{\mathrm{irr}}}$	Solar irradiance [$\mathrm{W/m}^2$]
$\boldsymbol{P_{\mathrm{load}}}$	Consumed power [W]
$\boldsymbol{P_{\mathrm{PV}}}$	Power flow from the installed solar panels [W]

$\boldsymbol{P_{sto}}$	Power flow from the batteries [W]
$\boldsymbol{P_{wind}}$	Available wind power [W/m^2]
$\boldsymbol{P_W}$	Power flow from the installed wind turbines [W]
$\boldsymbol{R}$	Control strategy
$\boldsymbol{u*}$	Optimal command values
$\boldsymbol{u}$	Command variables
$\boldsymbol{u}$	State variables
$\boldsymbol{x_0}$	State variables values at initial time step
$\boldsymbol{x_f}$	State variables values at final time step

Chapter 3

ω	Magnetic field speed [rad/s]
ϕ	Winding current phase [rad]
ψ_{d}	Direct component of the flux linkage [Wb]
ψ_{q}	Quadrature component of the flux linkage [Wb]
B1	Rotor parameter 1 [mm]
B2	Rotor parameter 2 [mm]
B3	Rotor parameter 3 [mm]
Bridge	Rotor parameter 4 [mm]
Bs0	Stator tooth parameter 1 [mm]
Bs1	Stator tooth parameter 2 [mm]
Bs2	Stator tooth parameter 3 [mm]
Gap	Rotor external shape parameter 1 [mm]
Hs0	Stator tooth parameter 4 [mm]
Hs1	Stator tooth parameter 5 [mm]
Hs2	Stator tooth parameter 6 [mm]
M1	Rotor parameter 5 [mm]
M2	Rotor parameter 6 [mm]
Mag_{Th}	Magnet thickness [mm]
Mag_{Wd}	Magnet width [mm]
N_{parallel}	Number of parallel conductors
N_{ph}	Number of phases

N_{series}	Number of series conductors
N_{slot}	Number of slots per pole
$O1$	Rotor parameter 7 [mm]
Ouv_{Mag}	Magnet opening angle [rad]
Rib	Distance between magnets [mm]
R_1	Rotor external shape parameter 2 [mm]
R_2	Rotor external shape parameter 3 [mm]
$Speed_{\text{FWM}}$	Switching speed from PWM strategy to FW strategy [rpm]
Wnd_{con}	Winding connection
$\boldsymbol{\Theta}$	Slope angle [rad]
Δt	Discretization time step [T]
η_{DC}	DC-to-DC converter efficiency
η_{GC}	Efficiency of the torque coupler
η_{St}	Starter efficiency
Γ_{EM}	Inertia of the electric machine [kg.m^2]
Γ_{ICE}	Compounded inertia of the engine and starter [kg.m^2]
ω_{Idle}	Engine idle speed [rad/s]
ρ_{Air}	Air density [kg/m^3]
$Cons$	Fixed auxiliary consumption [W]
C_{Batt}	Battery capacity [A.s]
C_{R}	Rolling coefficient
C_{x}	Drag coefficient
D_{Ext}	Machine external diameter [mm]
D_{max}	Maximum machine diameter [mm]
f_{max}	Maximum switching frequency [Hz]
Gap_{Air}	Air gap value [mm]
i_{d}	Direct component of the current [A]
I_{max}	Maximum battery current [A]
i_{q}	Quadrature component of the current [A]
k_{R}	Tyre rolling characteristic [s/m]
$Length$	Stator stack length [mm]

Lim_{El}	Steel sheet elastic limit [Mpa]
$Losses_{\mathrm{EC}}$	Eddy current losses [W]
$Losses_{\mathrm{Exc}}$	Excess losses [W]
$Losses_{\mathrm{Hys}}$	Hysteresis losses [W]
$Losses_{\mathrm{Inverter}}$	Inverter losses [W]
$Losses_{\mathrm{Iron}}$	Iron losses [W]
$Losses_{\mathrm{Joule}}$	Joule losses [W]
$Losses_{\mathrm{Mech}}$	Mechanical losses [W]
$L_{\max}$	Maximum machine length [mm]
L_{Tot}	Machine total length [mm]
MIR	Mean value of the battery's internal resistance [Ω]
$MOCV$	Mean value of the battery's open circuit voltage [V]
M	Mass of the vehicle [kg]
$P_{\max}$	Machine peak power [W]
Rin_{Sta}	Stator internal radius [mm]
$Ripple_{\max}$	Maximum ripple value
$Rout_{\mathrm{Rot}}$	Rotor external radius [mm]
$Rout_{\mathrm{Sta}}$	Stator external radius [mm]
R_{GC}	Ratio of torque coupler
S	Projected frontal surface [m^2]
T_{Coating}	Copper coating melting temperature [°C]
T_{El}	Electromagnetic machine torque [W]
t_{gs}	Gear shifting duration [T]
$T_{\max}$	Machine peak torque [N.m]
$\boldsymbol{\omega_{\mathbf{EM}}}$	Electric machine rotation speed [rpm]
$\boldsymbol{\omega_{\mathbf{EM}}}$	Internal combustion engine rotation speed [rpm]
$\boldsymbol{\omega_{\mathbf{w}}}$	Wheel speed [rpm]
$\boldsymbol{Cons_{\mathbf{Aux}}}$	Auxiliary consumption power [W]
$\boldsymbol{d}$	Design variables
$\boldsymbol{F}$	Evolution function
$\boldsymbol{F_{\mathbf{A}}}$	Aerodynamic drag [N]

$\boldsymbol{F_B}$	Braking force [N]
$\boldsymbol{F_C}$	Contact force [N]
$\boldsymbol{F_P}$	Vehicle weight force [N]
$\boldsymbol{F_R}$	Rolling resistance [N]
$\boldsymbol{Id}$	Identity function
$\boldsymbol{IR}$	Battery internal resistance [Ω]
$\boldsymbol{L}$	Instantaneous fuel consumption [g/s]
$\boldsymbol{OCV}$	Battery open circuit voltage [V]
$\boldsymbol{P_{Batt}}$	Battery output power [W]
$\boldsymbol{P_E}$	Provided electric power [W]
$\boldsymbol{P_{St}}$	Starter consumption [W]
$\boldsymbol{T_{EM}}$	Electric machine torque [N.m]
$\boldsymbol{T_w}$	Required torque at the wheels [N.m]
$\boldsymbol{u}$	Command variables
$\boldsymbol{v}$	Driving cycle speed [m/s]
$\boldsymbol{v_r}$	Relative speed of the wind [m/s]
$\boldsymbol{x}$	State variables

Chapter 4

$dist_{\mathrm{Avg}}$	Average distance between the optimal parameters and their reference values
$dist_{\mathrm{Max}}$	Maximum distance between the optimal parameters and their reference values
$E_{\mathrm{L,EM}}$	Total electric machine losses over driving cycle [J]
$E_{\mathrm{L,Pow}}$	Total powertrain losses over driving cycle excluding the losses of the EM block [J]
E_{u}	Useful energy over driving cycle [J]
HV_{gasoline}	Heat value of gasoline [J/g]
P_{max}	Electric machine's peak power [kW]
T_{Copper}	Stator winding's maximum temperature attained in a short-circuit scenario [°C]
T_{max}	Electric machine's peak torque [N.m]
$\boldsymbol{SI}$	Sensitivity index

List of Tables

List of Figures

Bibliography

[1] The World Bank. World Development Indicators, 2020. URL http://datatopics.worldbank.org/world-development-indicators/.

[2] The Intergovernmental Panel on Climate Change. The Intergovernmental Panel on Climate Change, 2020. URL https://www.ipcc.ch/.

[3] Environmental Protection Agency. About Urban Air Toxics, 2020. URL https://www.epa.gov/urban-air-toxics/about-urban-air-toxicshttps://www.epa.gov/urban-air-toxics.

[4] Anses. Particules de l'air ambiant extérieur. 2019.

[5] PublicHealth. CLIMATE CHANGE, 2020. URL https://www.publichealth.org/public-awareness/climate-change/.

[6] Environmental Protection Agency. Greenhouse Gas Emissions, 2018. URL https://www.epa.gov/ghgemissions/overview-greenhouse-gases.

[7] NASA. The Effects of Climate Change, 2020. URL https://climate.nasa.gov/effects/.

[8] NASA. Global Climate Change: Vital Signs of the Planet, 2020. URL https://climate.nasa.gov/vital-signs.

[9] National Oceanic and Atmospheric Organization. Global Climate Report - Annual 2019, 2020. URL https://www.ncdc.noaa.gov/sotc/global/201913.

[10] GIEC. *Rapport spécial du GIEC sur les conséquences d'un réchauffement planétaire de 1,5 degrés par rapport aux niveaux préindustriels et les trajectoires associées d'émissions mondiales de gaz.* 2018. ISBN 9789291692514.

[11] CSIRO. Sea Level : Understanding the past – Improving projections for the future, 2020. URL https://research.csiro.au/slrwavescoast/sea-level/.

[12] Commissariat Général au développement durable. Chiffres clés du climat - France, Europe et Monde - Édition 2020. Technical report, 2020.

[13] BloombergNEF. New energy outlook 2019, 2020. URL https://bnef.turtl.co/story/neo2019/page/1?teaser=true.

[14] European Commission. Average CO2 emissions from new light-duty vehicles registered in Europe increased in 2018, requiring significant future emission reductions to meet upcoming 2020 and 2021 targets, 2019. URL https://ec.europa.eu/clima/news/average-co2-emissions-new-light-duty-vehicles.

[15] European Commission. Reducing CO2 emissions from passenger cars - before 2020, 2019. URL https://ec.europa.eu/clima/policies/transport/vehicles/cars{_}en.

[16] European Environment Agency. Monitoring of CO2 emissions from passenger cars – Regulation (EC) No 443/2009, 2019. URL https://www.eea.europa.eu/data-and-maps/data/co2-cars-emission-16.

[17] Jos Dings. Mind the gap. *Transport and Environment*, pages 1–47, 2013.

[18] Detlev Mohr, Nicolai Müller, Alexander Krieg, Paul Gao, Hans-Werner Kaas, Axel Krieger, and Russell Hensley. The road to 2020 and beyond: What's driving the global automotive industry? *Advanced Industries*, 2013.

[19] Hans Kolff. The impact of WLTP, 2018. URL https://www.businesslease.com/wltp/.

[20] Car Emissions Testing Facts. Real Driving Emissions Test, 2018. URL https://www.caremissionstestingfacts.eu/rde-real-driving-emissions-test/.

[21] Lin Guzzella and Antonio Sciarretta. *Vehicle Propulsion Systems : Introduction to Modeling and Optimization*. Springer, 2013. ISBN 9783642359125.

[22] Statista. Vehicles & Road Traffic Statistics and Facts about Vehicles & Traffic, 2020. URL https://www.statista.com/markets/419/topic/487/vehicles-road-traffic/.

[23] H Wu, G Alberts, J Hopper, and B Walton. *New market. New entrants. New challenges. Battery Electric Vehicles*. Deloitte LLP, London, UK, 2019. URL https://www2.deloitte.com/content/dam/Deloitte/uk/Documents/manufacturing/deloitte-uk-battery-electric-vehicles.pdf.

[24] J.P.Morgan and J P Morgan. Driving into 2025: The Future of Electric Vehicles. Available online: https://www.jpmorgan.com/global/research/electric-vehicles (accessed on 1 October 2020), 2018. URL https://www.jpmorgan.com/global/research/electric-vehicles.

[25] Volvo Group. Volvo Cars' Electrification Strategy acknowledged by the United Nations, 2017. URL https://group.volvocars.com/news/electrification/2018/volvo-cars-electrification-strategy-acknowledged-by-the-united-nations.

[26] Bradley Berman. Honda CEO says 'There will be no dramatic increase in EV demand'. URL https://electrek.co/2019/12/26/honda-ceo-says-no-dramatic-increase-in-ev-demand/.

[27] Michaël Torregrossa. La voiture hybride a représenté 52 % des ventes de Toyota en 2019. URL https://www.automobile-propre.com/la-voiture-hybride-a-represente-52-des-ventes-toyota-en-2019/.

[28] Mark Kwilosz, Robert Bartell, Stephen Burt, David Althoff, Howard Johnson, Alexandre Pierantoni, Andreas Stoecklin, Klaus Pfulm, Paul Teuten, and David Lu. Market Share of Hybrid/Electric Vehicles (EVs) Poised to Increase, 2019. URL https://www.duffandphelps.com/insights/publications/m-and-a/millennials-and-auto-trends-report/market-share-of-hybrid-electric-vehicles-poised-to-increase.

[29] Francis Roy. Optimisation énergétique de chaînes de traction électrifiées. *Thèse de doctorat, Université Pierre et Marie Curie - Paris VI*, 2015.

[30] Jean-Louis Le Moigne. *Théorie du système général - Théorie de la modélisation.*

[31] Ludwig von Bertalanffy and Ludwig von Bertalanffy. *Théorie générale des systèmes.* 1973. ISBN 978-2-04-007504-0.

[32] George Braziller. *General System theory: Foundations, Development, Applications.* Revised ed edition, 1976. ISBN 0-8076-0453-4.

[33] H K Fathy, J A Reyer, P Y Papalambros, and A G Ulsoy. On the Coupling between the Plant and Controller Optimization Problems. *Proceedings of the American Control Conference*, pages 25–27, 2001.

[34] George P O Neal, Byung-kwon Min, Zbigniew J Pasek, and Yoram Koren. Integrated Structural / Control Design of Micro-Positioner for Boring Bar Tool Insert. *Journal of Intelligent Material Systems and Structures*, 2001. doi: 10.1177/10453890122145401.

[35] Vineet Sahasrabudhe, Roberto Celi, and André L Tits. Integrated Rotor-Flight Control System Optimization with Aeroelastic and Handling Qualities Constraints. *Journal of Guidance, Control and Dynamics*, 20(2), 1997.

[36] Julie A Reyer and Panos Y. Papalambros. Combined Optimal Design and Control With Application to an Electric DC Motor. *Journal of Mechanical Design, Transactions of the ASME*, 124(June 2002):183–191, 2002. doi: 10.1115/1.1460904.

[37] Eli Livne. Alternative Approximations for Integrated Control / Structure Aeroservoelastic Synthesis. *AIAA Journal*, 31(6), 1993.

[38] H. Asada, J Park, and S. Rai. A Control-Configured Flexible Arm : Integrated Structure/ Control Design. *Proceedings of the 1991 IEEE International Conference on Robotics and Automation*, pages 2356–2362, 1991.

[39] James T Allison and Daniel R Herber. Multidisciplinary Design Optimization of Dynamic Engineering Systems. pages 1–30, 2013.

[40] Richard Bellman. *Adaptive Control Processes: A Guided Tour.* 1961. ISBN 9780691652214.

[41] Sangkla Kreuawan. *Modelling and optimal design in railway applications.* PhD thesis, Ecole Centrale de Lille, 2008.

[42] Fouzia Moussouni. Méthodologie et algorithmes adaptés à l'optimisation multi-niveaux et multi-objectifs de systèmes complexes. *Thèse de doctorat, Ecole Centrale de Lille*, 072, 2009.

[43] Martin Cantegrel. *Vers une conception optimale des chaînes de traction ferroviaire.* PhD thesis, Ecole Centrale de Lille, 2012.

[44] Stephane Brisset and Maxime Ogier. Collaborative and multilevel optimizations of a hybrid railway power substation. *International Journal of Numerical Modelling: Electronic Networks, Devices and Fields*, 32(4):1–13, 2019. ISSN 10991204. doi: 10.1002/jnm.2289.

[45] Pierre Caillard. Conception par optimisation d'une chaine de traction électrique et de son contrôle par modélisation multi-physique. 2016.

[46] Alexandru Berbecea. *Multi-level approaches for optimal system design in railway applications*. PhD thesis, Ecole Centrale de Lille, 2012.

[47] Andrea Lackzo. *Optimisation du dimensionnement et de la commande sur cycle de fonctionnement d'un générateur à aimants permanents et auto-commutation pour applications micro-éoliennes*. PhD thesis, Ecole Centrale de Lille, 2016.

[48] Tuan Vu Tran. *Problèmes Combinatoires et Modèles Multi-Niveaux pour la Conception Optimale des Machines Électriques*. PhD thesis, Ecole Centrale de Lille, 2009.

[49] Antoine Pierquin. *Conception de systèmes électriques multidynamiques par optimisation multigranularité*. PhD thesis, Ecole Centrale de Lille, 2015.

[50] Gwenaëlle Souffran. *Dimensionnement de la chaîne de traction d'un véhicule électrique hybride basé sur une modélisation stochastique de ses profils de mission*. PhD thesis, 2013.

[51] Cédric Jaouen. *Méthodologie de dimensionnement sur cycle de vie d'une distribution en courant continu dans le bâtiment : applications aux câbles et convertisseurs statiques DC / DC*. PhD thesis, ENS Cachan, 2012.

[52] Remy RIGO-MARIANI. *Méthodes de conception intégrée "Dimensionnement-Gestion" par optimisation d'un micro-réseau avec stockage*. PhD thesis, INP Toulouse, 2014.

[53] Thibaut Kovaltchouk. *Contributions à la co-optimisation contrôle-dimensionnement sur cycle de vie sous contrainte réseau des houlogénérateurs directs*. PhD thesis, ENS Cachan, 2015.

[54] Vincent Reinbold. *Méthodologie de dimensionnement d'un moteur électrique pour véhicules hybrides : Optimisation conjointe des composants et de la gestion d'énergie*. PhD thesis, Université de Grenoble, 2015.

[55] M Jianning. *Design and Control Co-Optimization for Advanced Vehicle Propulsion Systems*. PhD thesis, CentraleSupelec, 2017.

[56] National Renewable Energy Laboratory. HOMER Energy. URL `https://www.homerenergy.com/`.

[57] Murdoch University Energy Research Institute. RAPSim - Microgrid Simulator. URL `https://sourceforge.net/projects/rapsim/`.

[58] University of Geneva. PVsyst. URL `https://www.pvsyst.com/`.

[59] Alparslan Emrah Bayrak, Namwoo Kang, and Panos Y. Papalambros. Decomposition-Based Design Optimization of Hybrid Electric Powertrain Architectures: Simultaneous Configuration and Sizing Design. *Journal of Mechanical Design, Transactions of the ASME*, 138(7):1–9, 2016. ISSN 10500472. doi: 10.1115/1.4033655.

[60] C Desai and S S Williamson. Optimal design of a parallel Hybrid Electric Vehicle using multi-objective genetic algorithms. *2009 IEEE Vehicle Power and Propulsion Conference*, pages 871–876, 2009. doi: 10.1109/VPPC.2009.5289754. URL `http://ieeexplore.ieee.org/document/5289754/`.

[61] Lincun Fang, Shiyin Qin, Gang Xu, Tianli Li, and Kemin Zhu. Simultaneous optimization for hybrid electric vehicle parameters based on multi-objective genetic algorithms. *Energies*, 4(3):532–544, 2011. ISSN 19961073. doi: 10.3390/en4030532.

[62] Olle Sundström. *Optimal control and design of hybrid-electric vehicles*. PhD thesis, 2009.

[63] Mohamed Yaich, Mohamed Radhouan Hachicha, and Moez Ghariani. Modeling and simulation of electric and hybrid vehicles for recreational vehicle. In *Proceedings of the 16th International Conference on Sciences and Techniques of Automatic Control and Computer Engineering (STA)*, pages 181–187. IEEE, 2015.

[64] R Fellini, N Michelena, P Papalambros, and M Sasena. Optimal design of automotive hybrid powertrain systems. *Proceedings - 1st International Symposium on Environmentally Conscious Design and Inverse Manufacturing, EcoDesign 1999*, pages 400–405, 1999. doi: 10.1109/ECODIM.1999.747645.

[65] Gao Wenzhong, Sachin Kumar Porandla, Wenzhong Gao, and Sachin Kumar Porandla. Design optimization of a parallel hybrid electric powertrain. In *Proceedings of the 2005 IEEE Vehicle Power and Propulsion Conference (VPPC)*, volume 2005, pages 530–535. IEEE, 2005. ISBN 0780392809. doi: 10.1109/VPPC.2005.1554609.

[66] Teresa Donateo, Lorenzo Serrao, and Giorgio Rizzoni. A two-step optimisation method for the preliminary design of a hybrid electric vehicle. *International Journal of Electric and Hybrid Vehicles*, 1(2):142–165, 2008. ISSN 17514088. doi: 10.1504/IJEHV.2008.017831.

[67] Sheldon S Williamson, Alireza Khaligh, Sung Chul Oh, and Ali Emadi. Impact of energy storage device selection on the overall drive Train efficiency and performance of heavy-duty hybrid vehicles. *2005 IEEE Vehicle Power and Propulsion Conference, VPPC*, 2005:381–390, 2005. doi: 10.1109/VPPC.2005.1554586.

[68] Tobias Nüesch, Tobias Ott, Soren Ebbesen, Lino Guzzella, Tobias Nuesch, Tobias Ott, Soren Ebbesen, and Lino Guzzella. Cost and fuel-optimal selection of HEV topologies using particle swarm optimization and dynamic programming. In *Proceedings of the 2012 American Control Conference (ACC)*, number 1, pages 1302–1307. IEEE, 2012. ISBN 9781457710957. doi: 10.1109/acc.2012.6314868.

[69] Theo Hofman, Sren Ebbesen, and Lino Guzzella. Topology optimization for hybrid electric vehicles with automated transmissions. *IEEE Transactions on Vehicular Technology*, 61(6):2442–2451, 2012. ISSN 00189545. doi: 10.1109/TVT.2012.2196299.

[70] Julien Scordia. *Approche systématique de l'optimisation du dimensionnement et de l'élaboration de lois de gestion d'énergie de véhicules hybrides*. PhD thesis, 2004.

[71] Messaoud Mohammedi. *Gestion de l'énergie pour une chaîne multi-sources*. PhD thesis, Université Mohamed Khider-Biskra, 2016.

[72] Maxime Debert. *Stratégies optimales multi-critères , prédictives, temps réel de gestion des flux d'énergie thermique et électrique dans un véhicule hybride*. PhD thesis, Université d'Orléans, 2013.

[73] Julien EYNARD. *Gestion optimale de l'énergie dans un procédé multi-source pour le chauffage de bâtiments*. PhD thesis, Université de Perpignan, 2010.

[74] National Renewable Energy Laboratory. Advanced Vehicle Simulator (ADVISOR), 2019. URL `https://sourceforge.net/projects/adv-vehicle-sim/`.

[75] Ruijun Liu, Dapai Shi, and Chao Ma. Real-time control strategy of Elman neural network for the parallel hybrid electric vehicle. *Journal of Applied Mathematics*, 2014, 2014. ISSN 16870042. doi: 10.1155/2014/596326.

[76] Carla Majed, Sami H. Karaki, and Rabih Jabr. Neural network technique for hybrid electric vehicle optimization. *Proceedings of the 18th Mediterranean Electrotechnical Conference: Intelligent and Efficient Technologies and Services for the Citizen, MELECON 2016*, (April):18–20, 2016. doi: 10.1109/MELCON.2016.7495327.

[77] Tobias Nüesch, Philipp Elbert, Michael Flankl, Christopher Onder, and Lino Guzzella. Convex optimization for the energy management of hybrid electric vehicles considering engine start and gearshift costs. *Energies*, 7(2):834–856, 2014. ISSN 19961073. doi: 10.3390/en7020834.

[78] Saida Kermani, Rochdi Trigui, Sebastien Delprat, Bruno Jeanneret, and Thierry Marie Guerra. PHIL implementation of energy management optimization for a parallel HEV on a predefined route. *IEEE Transactions on Vehicular Technology*, 60(3):782–792, 2011. ISSN 00189545. doi: 10.1109/TVT.2011.2107534.

[79] Dominik Karbowski, Namwook Kim, and Aymeric Rousseau. Route-based online energy management of a PHEV and sensitivity to trip prediction. *2014 IEEE Vehicle Power and Propulsion Conference, VPPC 2014*, 2014. doi: 10.1109/VPPC.2014.7007126.

[80] Grégory Rousseau. *Véhicule hybride et commande optimale.* PhD thesis, Ecole Nationale Supérieure des Mines de Paris, 2009.

[81] Meisam Amiri, Mohsen Esfahanian, Mohammad Reza Hairi-Yazdi, and Vahid Esfahanian. Minimization of power losses in hybrid electric vehicles in view of the prolonging of battery life. *Journal of Power Sources*, 190(2):372–379, 2009. ISSN 03787753. doi: 10.1016/j.jpowsour.2009.01.072.

[82] Qi Jiang, Florence Ossart, and Claude Marchand. Comparative study of real-time HEV energy management strategies. *IEEE Transactions on Vehicular Technology*, 66 (12):10875–10888, 2017. ISSN 00189545. doi: 10.1109/TVT.2017.2727069.

[83] Tae Soo Kim, Chris Manzie, and Rahul Sharma. Optimal control of a parallel hybrid vehicle with a traffic preview. *Proceedings of the Institution of Mechanical Engineers, Part D: Journal of Automobile Engineering*, 228(7):719–733, 2014. ISSN 09544070. doi: 10.1177/0954407013506567.

[84] Sébastien Delprat. *Evaluation de stratégies de commande pour véhicules hybride parallèles.* PhD thesis, Université de Valenciennes, 2005. URL `http://tel.archives-ouvertes.fr/docs/00/04/75/45/PDF/tel-00007966.pdf{#}page=1{&}zoom=auto,0,778`.

[85] J WU, C.-H. ZHANG, and N.-X. CUI. PSO algorithm-based parameter optimization for HEV powertrain and its control strategy. *International Journal of Automotive Technology*, 9(2):53–69, 2008.

[86] Julien Scordia, Rochdi Trigui, Matthieu Desbois-renaudin, Bruno Jeanneret, and François Badin. Global Approach for Hybrid Vehicle Optimal Control. *Journal of Asian Electric Vehicles*, 7(1):1221–1230, 2009.

[87] Zou Yuan, Liu Teng, Sun Fengchun, and Huei Peng. Comparative study of dynamic programming and pontryagin's minimum principle on energy management for a parallel hybrid electric vehicle. *Energies*, 6(4):2305–2318, 2013. ISSN 19961073. doi: 10.3390/en6042305.

[88] Heinz Schättler and Urszula Ledzewicz. *Synthesis of optimal controlled trajectories with chattering arcs*, volume 19. 2012. ISBN 9781461438342. doi: 10.1007/978-1-4614-3834-2.

[89] Stephan Uebel, Nikolce Murgovski, Conny Tempelhahn, and B Bernard. Optimal Energy Management and Velocity Control. *IEEE Transactions on Vehicular Technology*, 67(1):327–337, 2018.

[90] Olle Sundström and Lino Guzzella. A generic dynamic programming Matlab function. *Proceedings of the IEEE International Conference on Control Applications*, (7):1625–1630, 2009. doi: 10.1109/CCA.2009.5281131.

[91] O. Sundström, D. Ambühl, and L. Guzzella. On Implementation of Dynamic Programming for Optimal Control Problems with Final State Constraints. *Oil & Gas Science and Technology – Revue de l'Institut Français du Pétrole*, 65(1):91–102, 2010. ISSN 1294-4475. doi: 10.2516/ogst/2009020.

[92] Emmanuel Vinot. Time reduction of the Dynamic Programming computation in the case of hybrid vehicle. *International Journal of Applied Electromagnetics and Mechanics*, 53(S2):S213—-S227, 2017. ISSN 13835416. doi: 10.3233/JAE-140163.

[93] E Hoang, M Lécrivain, S Hlioui, and M Gabsi. Hybrid excitation synchronous permanent magnets synchronous machines optimally designed for hybrid and full electrical vehicle. *8th International Conference on Power Electronics - ECCE Asia: "Green World with Power Electronics", ICPE 2011-ECCE Asia*, pages 153–160, 2011. ISSN 2150-6078. doi: 10.1109/ICPE.2011.5944569.

[94] P Lazari, J Wang, and L Chen. A computationally efficient design technique for electric vehicle traction machines. *IEEE Transactions on Industry Applications*, 50(5):2596–2602, 2014. doi: 10.1109/ICElMach.2012.6350251. URL `http://ieeexplore.ieee.org/xpls/abs{_}all.jsp?arnumber=6350251{%}5Cnhttp://ieeexplore.ieee.org/lpdocs/epic03/wrapper.htm?arnumber=6350251`.

[95] G. Krebs, E. De Cecco, and C. Marchand. Design approach of an axial flux motor for electrical powertrain vehicle. *Proceedings - 2012 20th International Conference on Electrical Machines, ICEM 2012*, pages 2812–2817, 2012. doi: 10.1109/ICElMach.2012.6350285.

[96] Maya HAGE-Hassan. Méthodologies de conception optimale de systèmes de conversion électromécanique. *Thèse de doctorat, Université Paris Sud - Paris XI*, 2014.

[97] Tufféry Stéphane. *Data Mining and Statistics for Decision Making*. Wiley, 2011. ISBN 9780470688298.

[98] H K Fathy, Panos Y. Papalambros, and A G Ulsoy. On combined Plant and Control optimization.

[99] Ramzi Ben Ayed. *Eco-conception d'une chaine de traction ferroviaire*. PhD thesis, Ecole Centrale de Lille, 2013.

[100] Nestor Michelena, Hyungju Park, and Panos Papalambros. Convergence properties of analytical target cascading. *9th AIAA/ISSMO Symposium on Multidisciplinary Analysis and Optimization*, 41(5), 2002. doi: 10.2514/6.2002-5506.

[101] Natalia M Alexandrov and Robert Michael Lewis. Analytical and Computational Aspects of Collaborative Optimization for Multidisciplinary Design. *AIAA Journal*, 40(2):301–309, 2002. ISSN 0001-1452. doi: 10.2514/2.1646. URL `http://arc.aiaa.org/doi/10.2514/2.1646`.

[102] Natalia M Alexandrov. Comparative Properties of Collaborative Optimization and Other Approaches to MDO. *1st ASMO UK/ISSMO Conference on Engineering Design Optimization*, 1999.

[103] Jaroslaw Sobieszczanski-Sobieski. Bi-Level (BLISS) Integrated System Synthesis. *NASAM-1998-208715*, 1998.

[104] Michel Minoux. *Programmation mathématique: théorie et algorithmes, Volume 1.* Dunod, 1983. ISBN 2040154876, 9782040154875.

[105] Daniel Tabak and Benjamin C. Kuo. *Optimal Control by Mathematical Programming.* S R L Publishing Company, 1971. ISBN 978-0-13-638106-8.

[106] Sean Luke. *Essentials of metaheuristics*, volume 12. 2011. ISBN 9781300549628. doi: 10.1007/s10710-011-9139-0.

[107] K Schittkowski. NLPQL: A fortran subroutine solving constrained nonlinear programming problems. *Annals of Operations Research*, 5(1-4):485–500, 1986. ISSN 02545330. doi: 10.1007/BF02739235.

[108] Benoit Chachuat. *Nonlinear and Dynamic Optimization: From Theory to Practice.* Automatic Control Laboratory, EPFL, 2007.

[109] Lev Pontryagin, V Boltyanski, R Gamkrelidze, and E Mischenko. *The Mathematical Theory of Optimal Processes.* 1962.

[110] MathWorks. Constrained Nonlinear Optimization Algorithms. Available online: https://fr.mathworks.com/help/optim/ug/constrained-nonlinear-optimization-algorithms.html (accessed on 1 October 2020). URL `https://fr.mathworks.com/help/optim/ug/constrained-nonlinear-optimization-algorithms.html`.

[111] Jitendra R. Raol and Ramakalyan Ayyagari. *Control Systems: Classical, Modern, and AI-Based Approaches.* CRC Press, 2019. ISBN 9780815346302.

[112] P. Bratley and B. L. Fox. Algorithm 659 Implementing Sobol's Quasirandom Sequence Generator. *ACM Transactions on Mathematical Software*, 14, 1988.

[113] I Alcalá, A Claudio, and G V Guerrero. Analysis of Propulsion Systems in Electric Vehicles. (Cie):309–313, 2005.

[114] Thomas Finken, Matthias Felden, and Kay Hameyer. Comparison and design of different electrical machine types regarding their applicability in hybrid electrical vehicles . pages 1–5, 2008.

[115] M Zeraoulia, Student Member, M E H Benbouzid, Senior Member, and D Diallo. Electric Motor Drive Selection Issues for HEV Propulsion Systems : A Comparative Study. pages 280–287, 2005.

[116] C C Chan. An Overview of Electric Vehicle Technology. 81(9), 1993.

[117] Quoc Huong Bui. *Étude numérique de l'influence de la texture de chaussée sur la résistance au roulement.* PhD thesis, Ecole des Ponts ParisTech, 2014.

[118] Yoann Eulalie. Etude aérodynamique et contrôle de la traînée sur un corps de Ahmed culot droit. *Thèse de doctorat, Université de Bordeaux*, 2014.

[119] Commission économique pour l'Europe. Proposition visant à élaborer un nouveau Règlement technique mondial relatif à la procédure d'essai mondiale harmonisée en ce qui concerne les émissions des voitures particulières et véhicules utilitaires légers (WLTP). Technical report, 2014.

[120] Hong Tu Luu. *Développement de méthodes de réduction de la consommation en carburant d'un véhicule dans un contexte de sécurité et de confort : un compromis entre économie et écologie.* PhD thesis, Université d'Evry-Val-d'Essonne, 2001.

[121] Maxime Montaru. *Contribution à l'évaluation du vieillissement des batteries de puissance utilisées dans les véhicules hybrides selon leurs usages.* PhD thesis, Institut Polytechnique de Grenoble, 2009.

[122] Jacques Saint-Michel. Bobinage des machines tournantes à courant alternatif. *Techniques de l'ingénieur*, 2001.

[123] Thomas Finken, Marco Hombitzer, and Kay Hameyer. Study and comparison of several permanent-magnet excited rotor types regarding their applicability in electric vehicles. *2010 Emobility - Electrical Power Train, EEPT 2010*, (c), 2010. doi: 10.1109/EMOBILITY.2010.5668074.

[124] Seung-Ki Sul. *Control of Electric Machine Drive Systems.* Wiley, 2011. ISBN 9780470590799.

[125] Phil Mellor, Rafal Wrobel, and Nick Simpson. AC losses in high frequency electrical machine windings formed from large section conductors. *2014 IEEE Energy Conversion Congress and Exposition, ECCE 2014*, (2):5563–5570, 2014. doi: 10.1109/ECCE.2014.6954163.

[126] Giuseppe Volpe. Accounting for AC Winding Losses in the Electric Machine Design Process. pages 1–4, 2018.

[127] Mircea Fratila. *Contribution à la prise en compte des pertes fer dans la modélisation des machines électriques par élements finis.* PhD thesis, Université Lille 1, 2012.

[128] Chas Proteus Steinmetz. On the law of hysteresis. *Proceedings of the IEEE*, 72(2): 197–221, 1984. ISSN 15582256. doi: 10.1109/PROC.1984.12842.

[129] Yicheng Chen and Pragasen Pillay. An improved formula for lamination core loss calculations in machines operating with high frequency and high flux density excitation. *Conference Record - IAS Annual Meeting (IEEE Industry Applications Society)*, 2: 759–766, 2002. ISSN 01972618. doi: 10.1109/IAS.2002.1042645.

[130] D. C. Jiles and D. L. Atherton. Theory of ferromagnetic hysteresis (invited). *Journal of Applied Physics*, 55(6):2115–2120, 1984. ISSN 00218979. doi: 10.1063/1.333582.

[131] F. Preisach. Uaber die magnetische Nachwirkung. *Annalen der Physik*, 1935. ISSN 15213889. doi: 10.1002/andp.18983010504.

[132] T. Chevalier, A. Kedous-Lebouc, B. Cornut, and C. Cester. A new dynamic hysteresis model for electrical steel sheet. *Physica B: Condensed Matter*, 275(1-3):197–201, 2000. ISSN 09214526. doi: 10.1016/S0921-4526(99)00768-1.

[133] Z. John Shen, Yali Xiong, Xu Cheng, Yue Fu, and Pavan Kumar. Power MOSFET switching loss analysis: A new insight. *Conference Record - IAS Annual Meeting (IEEE Industry Applications Society)*, 3(1):1438–1442, 2006. ISSN 01972618. doi: 10.1109/IAS.2006.256719.

[134] Jizhen Fu, Zhiliang Zhang, Yan Fei Liu, and Paresh C. Sen. MOSFET switching loss model and optimal design of a current source driver considering the current diversion problem. *IEEE Transactions on Power Electronics*, 27(2):998–1012, 2012. ISSN 08858993. doi: 10.1109/TPEL.2011.2138163.

[135] Arcelor Mittal. D20 - Fully processed standard grades, 2020. URL `https://industry.arcelormittal.com/catalogue/D20/EN`.

[136] Oliver Heaviside. *Electrical papers*. New York and London: MacMillan and Co., 1894.

[137] JSOL Corporation. JMAG, 2020. URL `https://www.jmag-international.com/`.

[138] E.Y.Tsymbal. Section 16 : Magnetic properties of materials (continued). *The University of Nebraska*, Physics 92(section 16):1–19.

[139] R. H. PARK. Two-Reaction Theory of Synchronous Machines: Generalized Method of Analysis-Part I. *Transactions of the American Institute of Electrical Engineers*, 48 (3):716–727, 1929. ISSN 00963860. doi: 10.1109/T-AIEE.1929.5055275.

[140] Robert M Jones. *DEFORMATION THEORY OF PLASTICITY*. Bull Ridge Publishing, 2009.

[141] Mamy Rakotovao. *Un modèle opérationnel complet pour l'alternateur à griffes dans le domaine automobile*. PhD thesis, Ecole Normale Supérieure de Cachan, 1996.

[142] Emilia Silvas, Erik Bergshoeff, Theo Hofman, and Maarten Steinbuch. Comparison of bi-level optimization frameworks for sizing and control of a hybrid electric vehicle. In *Proceedings of the 2014 IEEE Vehicle Power and Propulsion Conference (VPPC)*. IEEE, 2014.

[143] S. Ebbesen, P. Elbert, and L. Guzzella. Engine Downsizing and Electric Hybridization Under Consideration of Cost and Drivability. *Oil & Gas Science and Technology – Revue d'IFP Energies nouvelles*, 68(1):109–116, 2013. ISSN 1294-4475. doi: 10.2516/ogst/2012030.

[144] Mitra Pourabdollah, Nikolce Murgovski, Anders Grauers, and Bo Egardt. Optimal sizing of a parallel PHEV powertrain. *IEEE Transactions on Vehicular Technology*, 62(6):2469–2480, 2013. ISSN 00189545. doi: 10.1109/TVT.2013.2240326.

[145] Siemens. Simcenter Amesim, 2019. URL `https://www.plm.automation.siemens.com/global/en/products/simcenter/simcenter-amesim.html`.

[146] Maneesha Altekar, Carol A Homon, Mohammed A Kashem, Steven W Mason, Richard M Nelson, Lori A Patnaude, Jeffrey Yingling, and Paul B Taylor. Assay optimization: a statistical design of experiments approach. *Clinics in laboratory medicine*, 27(1):139–154, 2007.

[147] Roger Ghanem, David Higdon, and Houman Owhadi. *Handbook of Uncertainty Quantification*. Springer, 2017. ISBN 978-3-319-12385-1.

[148] Kent State University. SPSS TUTORIALS: PEARSON CORRELATION. Available online: https://libguides.library.kent.edu/SPSS/PearsonCorr (accessed on 1 October 2020). URL https://libguides.library.kent.edu/SPSS/PearsonCorr.

[149] José García and Alvaro Peña. Robust Optimization: Concepts and Applications. *Nature-inspired Methods for Stochastic, Robust and Dynamic Optimization*, 2018. doi: 10.5772/intechopen.75381.

[150] Virginie Gabrel, Cécile Murat, and Aurélie Thiele. Recent advances in robust optimization: An overview. *European Journal of Operational Research*, 235(3):471–483, 2014. ISSN 03772217. doi: 10.1016/j.ejor.2013.09.036. URL http://dx.doi.org/10.1016/j.ejor.2013.09.036.

Extended french abstract

Les travaux de thèse menés s'intéressent à la conception optimale des systèmes complexes sur cycles. En effet, il a été démontré que se concentrer sur l'optimisation isolée des composants, sans tenir compte de leur utilisation et de leur environnement, ne conduit pas à un système optimal. Une vision globale du système est donc requise afin de trouver la meilleure solution possible. Cependant, ceci reste difficile à réaliser dans une structure d'entreprise classique avec des échanges limités entre les différentes équipes impliquées dans le même projet. L'objectif principal de la thèse était alors de proposer des méthodologies de conception qui prennent en compte les composants, le système, le contrôle et l'environnement tout en respectant les délais et les exigences du projet.

L'optimisation des chaînes de traction hybrides est choisie comme l'application principale de ce projet de recherche, car il existe un fort couplage entre les différents composants de la chaîne, leur utilisation et la stratégie de gestion de l'énergie. Il existe également un besoin croissant pour des systèmes de propulsion plus efficaces et moins polluants, en réponse aux préoccupations actuelles en matière d'environnement et de santé. Ainsi, les approches de conception systémique développées sont évaluées sur le cas d'un véhicule compact équipé d'une chaîne de traction hybride parallèle. Cependant, les méthodologies proposées peuvent être facilement implémentées et réadaptées pour d'autres applicatifs.

Dans le chapitre 1, un état de l'art sur les approches d'optimisation des systèmes complexes est réalisé. Les stratégies les plus populaires se répartissent principalement en deux catégories : les méthodes d'optimisation multidisciplinaire (MDF) et les stratégies basées sur l'étude du couplage entre le système et sa commande (Plant/Controller optimization frameworks). La balance a davantage penché en faveur de la seconde option en raison de l'utilisation de modèles de boîte noire lourds et fortement non linéaires ainsi que la présence d'un grand nombre de variables de décision.

L'utilisation des stratégies de contrôle optimale par la suite au lieu des méthodes de gestion de l'énergie en temps réel a pour but d'éliminer tout biais lié à la qualité de la stratégie de contrôle lors de la comparaison des différentes solutions possibles. Ainsi, la programmation non linéaire (NLP), l'optimisation collaborative (CO), la programmation dynamique (DP) et le principe du minimum de Pontryagin (PMP) sont étudiés pour optimiser la répartition d'énergie du système. La stratégie de contrôle la plus adéquate est ensuite incorporée pour la conception optimale du système en se basant sur deux schémas possibles : l'approche imbriquée $\mathcal{BL}$ où un algorithme externe optimisant les variables de conception évalue le meilleur coût possible pour chaque design en déterminant sa commande optimale, ou l'approche itérative $\mathcal{IT}$ où le problème de conception et de commande sont résolus successivement. Ces cadres devraient permettre d'obtenir de meilleurs résultats que l'utilisation d'une approche simultanée telle que $\mathcal{SM}$, en particulier pour des cycles longs.

Le chapitre 2 présente le benchmark des sous-stations électriques ferroviaires hybrides (HRPS) qui est choisi comme premier cas d'étude afin de comparer les méthodes de gestion de l'énergie ainsi que d'optimisation systémique citées précédemment. Ce cas d'étude est beaucoup plus rapide à traiter vu qu'il est basé sur des modèles analytiques. Le problème d'optimisation de commande et de conception associés peuvent être linéarisés afin de déterminer l'optimum global sur différents cycles, ce qui n'est pas envisageable pour l'applicatif du véhicule hybride. Cet optimum peut donc servir de référence pour mieux comparer les méthodes d'optimisation non-linéaires implémentées.

On constate donc que NLP et CO n'étaient adéquats que sur des cycles courts de quelques centaines de pas de temps. La stratégie PMP est la plus rapide mais n'arrive pas à trouver des résultats satisfaisants. Ceci est dû au non-respect des conditions strictes de convexité pour ce cas d'étude, nécessaires à son application. Enfin, DP a fourni de très bons résultats dans des temps de calcul raisonnables. DPAM, une version améliorée de DP basée sur un processus de maillage adaptatif, parvient à trouver des résultats aussi précis dans des délais encore plus rapides et est donc implémentée pour optimiser la commande dans $\mathcal{BL}$ et $\mathcal{IT}$.

La conception optimale de l'HRPS est abordée par la suite. Comme prévu, l'approche simultanée $\mathcal{SM}$ ne permet pas de trouver une solution optimale lorsque des milliers de variables d'optimisation sont considérées à la fois. En revanche, $\mathcal{BL}$ donne des résultats très proches de la solution de référence et présente un taux de convergence élevé mais nécessite de longs temps de calcul. En revanche, $\mathcal{IT}$ est 10 fois plus rapide mais conduit à des résultats sous-optimaux et à des taux de convergence plus faibles. La relaxation des contraintes de commande conduit à des résultats similaires à ceux trouvés par $\mathcal{BL}$. Les approches $\mathcal{BL}$ et $\mathcal{IT}$ sont alors aussi utilisées pour l'optimisation de la chaîne hybride.

Le chapitre 3 commence par décrire le modèle du véhicule hybride. Une représentation à iso-granularités et à température fixe est choisie pour les différents composants de la chaîne de traction. Les variables de décision sont également énumérées. La machine électrique est définie comme le composant central à modifier au cours des applications d'optimisation. Le modèle de la machine a été basé sur l'utilisation combinée de simulations éléments finis et du modèle de Park de la machine synchrone afin de prendre en compte avec précision l'impact des paramètres de design. On arrive ainsi à obtenir un écart de moins de 2 % avec les résultats sur bancs d'essais, et de générer la cartographie de pertes de la machine, utilisée par la suite pour simuler la chaîne hybride, en quelques minutes seulement.

Les limitations de la chaîne de traction hybride ainsi que le cahier de charges de la machine sont traduits en contraintes de commande et de conception, évaluées par des fonctions analytiques et par simulations éléments finis. La fonction coût intègre à la fois le coût de la machine et la consommation de carburant calculés sur le cycle WLTC 3-b. Ainsi, le problème d'optimisation est entièrement défini.

Le chapitre 4 se concentre au début sur la comparaison des stratégies les plus prometteuses. Trois stratégies de contrôle optimales sont testées : DPAM, PMP et une nouvelle stratégie à base de règles (RBS). Les gains en consommation de carburant et le temps de calcul sont utilisés comme principaux critères pour cette comparaison. Les performances des trois stratégies proposées sont proches. Comme c'était le cas sur l'applicatif de l'HRPS, la DPAM fournit encore une fois les meilleures valeurs de consommation. Par ailleurs, RBS est beaucoup plus rapide et est instantanée une fois que les paramètres de la stratégie sont optimisés. La commande optimale proposée est analysée plus en détail après et on conclut qu'elle suit toutes les recommandations d'utilisation des véhicules hybrides, permettant ainsi

une exploitation efficace de la chaîne de traction hybride. Les résultats de la plateforme de simulation Amesim développée du côté de Valeo confirment également ces conclusions.

Différentes techniques de réduction de cycle sont ensuite comparées. Elles sont développées pour évaluer rapidement les pertes sur cycle de la machine en s'appuyant seulement sur une dizaine de points d'intérêt. La technique du Clustering à pondération des pertes est la plus précise. En la couplant avec la nouvelle méthode du Mirroring, on obtient des écarts plus faibles de moins d'1 % pour une estimation des pertes totales sur cycle basée sur 10 clusters seulement.

Une fois qu'un cas d'étude de conception optimale de la chaîne de traction hybride est défini, une étude de screening est menée afin d'identifier les variables de décision les plus influentes à optimiser. Cette démarche améliore considérablement la convergence des approches de conception systémique en réduisant le nombre de variables d'optimisation. Le design optimal trouvée par la suite à partir des approches est comparée à une machine de référence proposée par l'entreprise. Cette dernière a été optimisée sur un point unique de fonctionnement en adoptant l'approche de design classique. La machine de référence est aussi utilisée pour initialiser l'algorithme d'optimisation.

Cinq approches de conception systémique sont appliquées : les approches $\mathcal{BL}$ et $\mathcal{IT}$ mentionnées précédemment, ainsi que trois nouvelles approches alternatives : $\mathcal{A}_1$, $\mathcal{A}_2$ et $\mathcal{A}_3$. $\mathcal{A}_1$ est basée sur l'optimisation simultanée des variables de design et des paramètres de la stratégie RBS, ce qui permet de réduire la complexité d'optimisation de la commande. $\mathcal{A}_2$ s'appuie sur l'utilisation des méta-modèles pour évaluer les fonctions coût et de contraintes tandis que $\mathcal{A}_3$ est une nouvelle variante de la stratégie $\mathcal{IT}$, basé sur l'exploitation des techniques de réduction de cycle pour évaluer plus rapidement la fonction coût.

D'une part, $\mathcal{BL}$, $\mathcal{IT}$ et $\mathcal{A}_1$ conduisent à des réductions de coût assez proches lorsqu'on optimise un nombre réduit de variables de conception. Cependant, $\mathcal{BL}$ trouve de meilleures solutions pour un nombre de paramètres plus important. Ceci s'explique du fait que les approches $\mathcal{IT}$ et $\mathcal{A}_1$ sont plus sensibles à leurs initialisations. Une stratégie multi-start, ou multi-tirs, peut résoudre ceci et conduira à de meilleurs résultats. D'autre part, les approches de conception $\mathcal{A}_2$ et $\mathcal{A}_3$ ont mené à une réduction moindre des coûts. Accroître la précision de leurs modèles permettra de trouver de meilleures solutions.

En termes de délais, $\mathcal{A}_2$ est naturellement l'approche la plus rapide. $\mathcal{BL}$, $\mathcal{IT}$ et $\mathcal{A}_3$, suivi de $\mathcal{A}_1$, nécessitent de longs temps de calcul, qui ont tendance à augmenter exponentiellement avec le nombre de variables considérées. Les temps de calcul des approches $\mathcal{A}_1$ et des deux alternatives du schéma itératif pourront être considérablement réduits en lançant plus de simulations en parallèle.

En plus de conduire à une réduction significative des coûts, la solution trouvée par l'approche imbriquée $\mathcal{BL}$ est jugée robuste aussi d'après les conclusions des études de sensibilité qui sont menées. Enfin, $\mathcal{BL}$ est également exploitée pour remettre en question les exigences de performance imposées, généralement vues plutôt comme des lignes directrices de conception dans un contexte projet. On trouve ainsi une meilleure efficacité énergétique à moindre coût quand ces contraintes ne sont pas considérées au cours du processus d'optimisation.

Abstracts

Systemic design of hybrid and electric powertrains

Abstract Designing hybrid powertrains is a complex task, which calls for experts from various fields. In addition to this, finding the optimal solution requires a system overview. This can be, depending on the granularity of the models at the component level, highly time-consuming. This is even more true when the system's performance is determined by its control, as it is the case of the hybrid powertrain. In fact, various possibilities can be selected to deliver the required torque to the wheels during the driving cycle. Hence, the main obstacle is to achieve optimality while keeping the methodology fast and robust.

In this work, novel approaches to exploit the full potential of hybridization are proposed and compared. The first strategy is a bi-level approach consisting of two nested optimization blocks: an external design optimization process that calculates the best fuel consumption value at each iteration, found through control optimization using an improved version of dynamic programming. Two different systemic design strategies based on the iterative scheme are proposed as well. The first approach is based on model reduction while the second approach relies on precise cycle reduction techniques. The latter enables the use of high precision models without penalizing the calculation time. A co-optimization approach is implemented afterwards which adjusts both the design variables and parameters of a new efficient rule-based strategy. This allows for faster optimization as opposed to an all-at-once approach. Finally, a meta-model based technique is explored.

Keywords: plant/controller optimization, optimal design of complex systems, hybrid electric vehicle, optimal control, cycle reduction, model reduction, electric machines, powertrain simulation, electric propulsion, parallel hybrid powertrain

Conception de chaînes de traction hybrides et électriques par optimisation sur cycles routiers

Résumé La conception des chaînes de traction hybrides est une tâche complexe, qui fait appel à des experts de différents domaines s'appuyant sur des compétences et des outils distincts. En plus de cela, la recherche d'une solution optimale nécessite un retour système. Cela peut être, selon la granularité des modèles de composants, très coûteux en temps de calcul. Ceci est d'autant plus vrai lorsque la performance du système est déterminée par sa commande, comme c'est le cas du véhicule hybride. En fait, différentes possibilités peuvent être sélectionnées pour fournir le couple requis aux roues pendant le cycle de conduite. Ainsi, le principal obstacle est d'atteindre l'optimalité tout en conservant une méthodologie rapide et robuste.

Dans ces travaux de thèse, de nouvelles approches visant à exploiter le potentiel complet de l'hybridation sont proposées et comparées. La première stratégie est une approche bi-niveaux composée de deux blocs d'optimisation imbriqués: un processus d'optimisation des paramètres de design externe qui calcule la meilleure valeur de consommation de carburant à chaque itération en se basant sur une version améliorée de la programmation dynamique pour l'optimisation de la commande. Deux stratégies de conception systémique différentes basées sur le schéma itératif sont également proposées. La première approche est basée sur la réduction de modèle tandis que la seconde se repose sur des techniques précises de réduction de cycle. Cette dernière permet l'utilisation de modèles de haute précision sans pénaliser le temps de calcul. Une approche simultanée est ensuite mise en œuvre, qui optimise à la fois les variables de conception et les paramètres d'une nouvelle stratégie efficace à base de règles. Cette dernière permettra une optimisation plus rapide par rapport à l'optimisation directe de toutes les variables de décision. Enfin, une technique basée sur l'utilisation des méta-modèles est explorée.

Mots-clés: conception optimale de systèmes complexes, véhicule hybride, contrôle optimal, réduction de cycles, réduction de modèles, machines électriques, simulation de la chaîne de traction, propulsion électrique, chaîne de traction hybride parallèle